Vibrational Energy Flow in Structures

by J.D.Palmer, BEng.

Thesis submitted to The University of Nottingham
for the Degree of Doctor of Philosophy, May 1994

Acknowledgement

I would like to thank my supervisors, Dr.E.J.Williams and Dr.C.H.J.Fox, for their assistance, guidance and advice throughout the period of my study. I should also like to acknowledge the contribution made by the Noise and Vibration Group of Rolls-Royce and Associates Ltd, in terms of their financial and technical support for this project.

Contents

page

Appendices

Abstract

This investigation explores the use of an approximate energy flow approach to provide a global modelling tool capable of predicting the pattern and level of vibrational energy flow in complex structures. The modelling approach is based on a differential control volume formulation which, by virtue of its simplified nature, describes the flow of mechanical energy within a structural component in a manner analogous to the flow of thermal energy in heat conduction problems. For complex structures the approach can be implemented using existing finite element software through an analogy between the thermal and vibrational systems.

Energy flow predictions along simple beam structures, obtained using the energy flow approach, are compared to "exact" analytical solutions and experimental structural intensity measurements on real structures. This provides useful insight into the capabilities and requirements of the approach, such as the quality of model predictions at lower frequencies and the accuracy requirement for modelling parameters.

The task of modelling the transmission of vibrational energy in practical engineering structures is complicated by the partial reflection of incident wave energy at structural discontinuities. Methods to account for this effect are discussed and an approach is developed which can be incorporated into the finite element global modelling scheme. This is used to model a complex multiple transmission path structure which illustrates the ability of the approach to form an effective transmission path ranking tool.

Finally, the approach is used to build a representative energy flow model of a ribbed bulkhead structure typical of marine applications. A wavenumber measurement technique is used to assess the wave transmission characteristics of this structure which exhibit strong directional dependence. Predictions provided by the energy flow model are in good general agreement with energy flow measurements obtained from the real structure.

Throughout these modelling exercises particular attention is paid to the provision of suitable estimates of the parameters (damping, group velocity, power input and transmission efficiency) on which the accuracy of the model predictions rely.

This investigation represents a significant contribution to current knowledge regarding the use of the energy flow approach and its ability to provide representative models of real structures. Although further research is still required, considerable progress has been made and the work documented here provides the framework for a global modelling tool using existing finite element software.

Nomenclature

a	acceleration
c	phase velocity
c_b	phase velocity for flexural motion in a beam
c_g	group velocity
c_L	phase velocity for longitudinal motion in a rod
d_{el}	depth of a finite element
e	vibrational energy density
E	Young's modulus
f	frequency
F	force
h	plate thickness, convective heat transfer coefficient
I	second moment of area
k	wavenumber
K	thermal conductivity
l_{el}	length of a finite element
L	length
M	mass, moment
p	power
P	power input
q	vibrational energy flux
Q	thermal energy
r	reflection coefficient, radial distance
R	radius of gyration
s_{el}	surface area of a finite element
S	cross-sectional area
t	time
T	kinetic energy density, decay time, temperature

u,U	axial displacement
v	transverse velocity
V	strain energy density
V_{el}	volume of a finite element
w	transverse displacement
W	width
x	distance
X	cross-spectral quantity
z	mobility
η	hysteretic damping loss factor
β	reflection efficiency
γ	damping ratio
θ	heat per unit volume
λ	wavelength
ν	Poisson's ratio
ρ	mass density
σ	stress
ϕ	mode shape function, angular displacement
τ	transmission efficiency
ω	radian frequency
ω_r	natural frequency
Ω	angular velocity

Introduction

For many years engineers and scientists have been concerned with the control of unwanted structural vibration. The primary aims of this have been to avoid possible damage due to excessive and repeated motion, or to reduce acoustic radiation into areas surrounding the structure. The latter is of great importance in the design of automotive vehicles, ships, aircraft and buildings. One area where radiated noise levels are of extreme concern is in the design of warships. Here, the emission of acoustic radiation into the sea is generally undesirable because it provides a target for hostile sensors and may also interfere with the vessels own detection systems.

The major sources of vibration in ships are often attributed to running machinery within the vessel's engine spaces. This equipment generates noise which is transmitted through machinery mountings into the ship's structure. Ideally these vibrations should be reduced at source, although in many cases this can not easily be achieved. It is therefore inevitable that some vibrational energy will be carried through the ship's structure, via a number of structural or acoustic paths, resulting in the emission of unwanted noise into the sea. The ability to make some prediction of the levels of transmitted vibrational energy in marine structures, and in particular the ranking of potential vibration transmission paths, has been the driving force behind the research documented here.

Traditionally, the study of structural dynamics has focused on the evaluation of the response of a structure to dynamic force excitation. For engineering structures this is usually achieved by modal analysis techniques, either experimentally, or analytically using finite elements. These modal approaches are based on the assumption of linearity and that response is made up of contributions from a number of individual

responses which correspond to the structure's natural modes of vibration. The relative size of each contribution is dependent on the coupling between the mode shape and the distribution of excitation forces, together with the correlation between the natural frequency of the mode and the excitation frequency.

The use of modal analysis techniques has, in the main, been aimed at the study of the first few resonant modes of vibration because these usually dominate the response of the structure and often lead to the largest displacements. This is fortunate because, although modal analysis is not theoretically limited by frequency, in practice, both the experimental and analytical methods are restricted to use in the lower frequency ranges, covering perhaps the first fifty modes.

Experimental modal analysis relies on the ability to identify resonant peaks in measured frequency response data. Two factors affect the quality of this data at higher frequencies. Firstly, the resonant frequencies are closer together and the peaks in the spectra tend to overlap. Secondly, these peaks become rounded because of the increased effect of damping. The net result of these effects is that the higher frequency response data becomes blurred and the identification of individual modal peaks becomes difficult, if not impossible to achieve.

Analytical modal analysis using the finite element technique also suffers a drawback at higher frequencies, although in this case the problem is concerned with the cost of execution. As with all modal superposition techniques, in order to provide an accurate solution, the calculation requires information on all modes which contribute significantly to the response. At higher frequencies the number of these contributing modes must increase. This means that the detail of the finite element model needs to be increased to provide sufficient information to properly analyse the complex mode shapes attributed to the higher order modes. This process leads to rapidly increasing costs, both in terms of man hours and computer time, which normally limits the use of traditional finite element analysis to the lower frequency ranges.

The frequency limitation imposed on modal analysis techniques is of serious consequence in the case of the vibration transmission problem considered here. It is often the case that the frequency content of machinery induced excitation is beyond the lower order modal region of the structures concerned. It is also important to note that modal analysis provides information on the resonant behaviour of the structure, which is dominated by standing wave energy. For the task in hand, it would be more useful to identify the components of travelling wave energy which give rise to the transmission of vibration through the structure. This would also allow comparison between the ability of particular paths to transmit noise from a given source to the eventual sinks, giving rise to the concept of "transmission path ranking". These requirements lead to the idea of the evaluation of the vibrational energy flow through the structure in order to identify the more dominant energy flow paths. Given this information the engineer can address those paths which transmit the largest components of unwanted noise into the sea.

This study

The overall objective of this work has been to develop an analytical design tool which is capable of describing the way in which vibrational energy is transmitted through structures which are typical of marine construction. The major requirement of this tool is that it should be able to provide energy flow predictions at frequencies beyond the normal limits of the traditional modal analysis techniques at low computational cost. In addition to this, it is essential that the approach maintains a wide field of application.

In recent years an energy flow approach to vibration analysis has emerged which describes the flow of mechanical energy within common structural components in a simplified manner. The form of the equations governing this approach are analogous to those describing the flow of thermal energy in heat conduction problems. A primary aim of this research has been to assess the accuracy of the predictions provided by this approach and to investigate its use in the estimation of the levels of vibrational energy flow through a number of structural assemblies.

An important aspect in the development of a general modelling tool is the ability to assemble the analytical descriptions of the individual structural components to form a *global* model of the structure. The nature of the equations governing the energy flow approach makes it possible to draw an analogy between the vibrational and thermal cases and execute the analysis using a finite element technique. This property is seen to be a major advantage of the approach and one of the aims of this work has been to exploit this feature in the development of a general purpose design tool. In this form the analysis should be of most use to an engineer who requires predictive information about the vibration transmission characteristics of a structure during the early stages of its design.

For convenience, a finite element approach has been developed which can be executed using existing thermal finite element packages. In this way the properties of the general approach can be examined without the expense of developing a dedicated computational framework in which to carry out the analysis.

Throughout the modelling work particular attention has been paid to the provision of suitable estimates of the parameters required by the model. Where possible this information has been obtained experimentally from the real structures concerned ensuring that the parameters are representative of the real engineering situation. In a number of cases model predictions have been compared with experimental measurements of energy flow to assess the accuracy of the modelling approach.

Layout of the thesis

In all there are eight more chapters in this thesis.

Chapter 2 contains a literature review discussing previous work concerning the evaluation of vibrational energy flow through complex structures. This includes a discussion of the principles and previous applications of some well established modelling techniques, as well as some more recent work which leads up to the energy flow modelling approach considered here. The development and application of techniques for the measurement of vibrational energy flow are also discussed.

Chapter 3 describes the development and principles of the energy flow approach in more detail. The main purpose of this discussion is to point out certain assumptions made in the development of the technique and highlight their possible effects on model predictions.

Chapter 4 gives examples of the application of this technique to single beam structures to provide an insight into the capabilities and requirements of the approach. Model predictions are compared with measured energy flow in a beam to allow the accuracy requirements of some of the model parameters to be assessed.

Chapter 5 discusses the problem of representing the connection between individual components to form models of built-up structures. This is followed by an example of the application of the energy flow approach to provide a model of a real connected beam structure. Experimental measurements are used to validate the model predictions.

Chapter 6 presents an analogy between the equations governing the energy flow model and those relating to thermal energy flow. This allows an existing finite element package to be used to assemble the individual modelling expressions to form a global modelling tool. The use of this finite element approach is illustrated by creating a model of a multiple transmission path structure. This analysis highlights the transmission path ranking capabilities of the modelling approach.

Chapter 7 describes an experimental study into the energy transmission characteristics of a section of ribbed bulkhead which is typical of marine construction. This includes an experimental assessment of the wavenumber characteristics of this structure and the measurement of vibrational energy flow levels across the bulkhead plate.

Chapter 8 describes the creation of two energy flow models which are representative of the real bulkhead structure. The parameters used in these models are based on the findings of the experimental work presented in Chapter 7. Model predictions are once again compared to experimental results.

Finally, Chapter 9 discusses some of the more general aspects of the approach including a review of some very recent literature. This allows recommendations to be made concerning aspects of the approach requiring further attention and the direction which the future development of the technique might take. This discussion is followed by some concluding remarks.

Chapter 2

Literature review

2.1 Introduction

This chapter presents a review of previous work aimed at quantifying the process of vibrational energy transmission in structures. The purpose of this review is to outline existing approaches at the outset of this project and to assess their potential to provide a suitable solution to the problem presented in Chapter 1.

In Chapter 1 it was suggested that the principal task of the design tool should be to predict the general level of vibrational energy flow through a structure, rather than provide a detailed description of its structural response. Consequently this review concentrates on techniques within which vibrational energy is the primary quantity of interest. It was established at an early stage that an important part of this project would be involved with the validation of model predictions against experimental measurements. It is appropriate therefore, that this review covers the development of both modelling and experimental techniques.

The aim of the review is to provide a brief description of each approach and indicate the key stages in its development. Where possible this will be accompanied by an assessment of the technique's scope of application and level of accuracy, with particular reference to real engineering structures.

2.2 Modelling methods

An important feature of the required design tool is that it should provide an analytical framework within which one can create global models of a wide variety of structural configurations. The review of modelling methods will therefore focus on approaches which have the potential to model relatively complex structural geometries. These

include finite element analysis, statistical energy analysis and a number of approaches which can be gathered under the general heading of energy flow approaches.

2.2.1 Traditional finite element analysis

Finite element analysis (FEA) is now accepted as a standard engineering tool able to provide a detailed analysis of complex structures. There are currently a wide variety of well developed and tested commercial finite element codes readily available to the engineering community. Within these packages dynamic analysis is normally carried out as a two stage process. The first stage is to carry out a modal analysis calculation to determine natural frequency and mode shape information for the model. If response predictions are required, these are obtained in the second stage by a modal superposition technique. The resulting response information can be expressed in terms of displacement, velocity, acceleration, stress etc. Although in general, commercial packages only provide response predictions, the availability of this very extensive and well developed tool has prompted some investigators to post-process response data to calculate vibrational energy flow.

Hambric (1990) used response predictions provided by the NASTRAN finite element code to calculate vibrational energy flow through beam and plate finite elements. Having obtained the natural frequency and mode shape information from the modal analysis, energy flow was determined on a frequency by frequency basis using stress and velocity values calculated at the nodes of the finite element mesh. Because of the detailed nature of the FEA calculation this approach was able to account for energy transmission due to flexural, longitudinal and torsional motion.

Garvic et al (1990a, 1990b) presented two companion papers based on a similar approach, except in this case the energy flow was determined directly from modal parameters. The results of this analysis highlighted the importance of the higher order modes on the evaluation of vibrational energy flow, even at low frequencies. Modal truncation of the calculation was shown to significantly disturb the predicted energy flow pattern, sometimes providing misleading results.

This type of approach has advantages in that it is able to provide a very detailed description of the energy flow characteristics of a structure and be applied to a wide variety of structural geometries. Because the approach is based on a modal calculation it is also able to account for resonant behaviour. This is a useful feature because levels of vibrational energy flow often increase significantly around resonances, particularly in the lower frequency ranges.

In the context of this project however, a major drawback of this approach stems from the fact that the results are obtained using the output of a standard dynamic FEA calculation. This means that in practice, this type of analysis would probably be limited to use in the lower frequency ranges due to the high computational costs involved in applying traditional FEA at higher frequencies.

2.2.2 Statistical energy analysis

Statistical energy analysis (SEA) is an analytical technique aimed at providing estimates of the vibrational response of complex structures at high frequencies. The development of SEA began in the 1960's because of the increase in large, lightweight aerospace structures, excited by high frequency broad-band loads. This resulted in a need for a higher order modal analysis technique which did not incur the high computational costs of the more deterministic techniques like FEA.

In developing this approach it was recognised that the response of structures at high frequencies is highly sensitive to small details of geometry and construction. SEA modelling, as the name suggests, is therefore based on the assembly of statistical information about groups of similar modes or sub-systems. Within the SEA framework connected sub-systems are compared to temperature baths because, on a frequency-averaged basis when many modes of the sub-systems are excited, the energy flow between them is proportional to the difference in their total modal energy levels. This behaviour is similar to that of two connected heat conductors.

To create an SEA model one considers an energy balance for each sub-system which accounts for external power inputs, energy dissipated due to damping and the energy

transferred to and from other sub-systems in the model. These individual energy balances are then assembled to provide a global model of the structure. This global model takes the form of a set of simultaneous linear equations which can be solved to provide the individual sub-system energies. The total energy in each sub-system can then be converted into space and time-averaged estimates of response in terms of displacements, velocities, accelerations etc. Having obtained the sub-system energies it is also possible to determine the power transfer between sub-systems which allows the more dominant energy transmission paths to be identified.

Lyon (1975) carried out much of the early research into the use of this approach and his book still stands as one of the most complete records of the development and principles of SEA. This text also includes a description of the parameters required by the SEA model and some approaches to calculate these parameters for a number of common structural components.

The parameters required by an SEA model consist of loss factors and modal densities for each of the sub-systems, and coupling loss factors between each sub-system. The evaluation of these parameters is an area which has probably attracted the most attention over subsequent years. Clarkson and Pope (1981) described an approach to experimentally determine the modal densities and loss factors for plate and shell structures. Norton and Greenhalgh (1986) discussed several methods for the estimation of loss factors in lightly damped pipeline structures.

Probably the most difficult aspect of the SEA procedure is the determination of the so called coupling loss factor which governs the amount of energy transferred between sub-systems. In many cases these coupling loss factors have been derived analytically from impedance or transmission efficiency information. Because of the complexity of these calculations simplifications are often made by representing finite structures by similar structures of infinite extent. Pinnington and White (1981) showed that this approach could be justified at higher frequencies.

In many applications the coupling arrangements are too complicated to be treated analytically and coupling parameters must be determined experimentally. There have been numerous publications concerning this area over recent years. Some of the more notable, which address representative engineering situations, are those by Bies and Hamid (1980), Clarkson and Ranky (1984) and Langley (1990).

Several applications of SEA to design problems have also been reported. Ghering and Raj (1987) compared SEA predictions with experimental measurements for a structure comprising a combination of plates, beams and a cylinder. They concluded that SEA was very effective at predicting trends in the response data, but reliable absolute levels of response could only be achieved by "benchmarking" model predictions against experimental results. This allowed model parameters determined for individual structural components to be adjusted to take account of the effects of their assembly into the complete structure. Rockwood et al (1987) applied SEA to the analysis of a number of marine structures. These structures included a fabricated beam structure, a marine gearbox and a steam turbine. This work highlighted the need to account for all the important mode types within the system if reliable predictions are to be obtained from an SEA model. As expected, the results of these analyses showed that the SEA predictions compared better with experimental measurements at higher, rather than lower frequencies.

The generalised nature of the SEA model makes it ideally suited to providing a tool to estimate the vibrational characteristics of a complex structure at an early stage of the design process. The fact that it requires only a coarse representation of the physical system means that the analysis can be carried out before the details of the design have been finalised. It also employs relatively few parameters per sub-system which means that computational costs are relatively low compared to FEA. These features make SEA a useful analytical framework within which to carry out parametric studies to assess the effects of design changes on the global behaviour of the system.

A major drawback of SEA is that the confidence limits of the predicted results are difficult to assess. The accuracy of the SEA model is dependent on the ability of the

analysis to satisfy a number of assumptions concerning the properties of the structure and the nature of the excitation. These assumptions are necessary so that the physical system can be represented in a simplified manner. For example the analysis requires that each sub-system exhibits many resonant modes within the frequency range of interest. This condition is easily satisfied in the case of acoustic problems, but is often difficult to satisfy for many structural components except at very high frequencies. These difficulties have lead to some scepticism of the approach within the engineering community and as a result, its use has mainly been limited to analysis at very high frequencies where the SEA assumptions are more readily satisfied.

2.2.3 Energy flow approaches

In many cases engineers are presented with problems where analysis by dynamic FEA would prove too expensive and the frequency range of interest is such that the requirements of SEA are difficult to satisfy. To tackle this type of problem a number of alternative approaches have been proposed which provide a description of the energy flow characteristics of the structure in a simplified manner.

Early energy flow models

Some of the earliest examples of this type of approach can be found in Russian literature. This work was prompted by the desire to model the energy transmission characteristics of complex ship structures in a relatively simple analytical form. Belov et al (1977) proposed an approach to estimate the transmission of vibrational energy through periodically ribbed plate structures in the direction perpendicular to the ribs. By assuming that the wave field within the plate was diffuse in nature they created an energy balance for a section of plate between two ribs. This energy balance contained a number of reflection and transmission coefficients which determined the proportion of energy crossing the ribs and the level of mode conversion between flexural and longitudinal motion. Belov et al then showed that after assembling the energy balance expressions for each section, the system of equations could be reduced to a second-order differential form, similar to that governing heat conduction. These equations were solved analytically to carry out a parametric study to determine the optimum thickness of a layer of damping material required to minimise energy levels

in the plate.

Nikiforov (1975, 1990) provided a two-dimensional model for predicting vibrational energy flow through plate structures reinforced by ribs attached in the form of a grid. This analysis was aimed at higher frequency ranges, typically above 200-300 Hz for real ship structures, where the energy field could once again be assumed to be diffuse. The model was based on the hypothesis that under these conditions the structure could be represented by an "equivalent plate" having directionally dependent transmission properties which account for the attenuating effects of the ribs. Using this simplified approach Nikiforov proposed that the energy flow through the structure could be described by a two-dimensional second-order differential equation of the heat conduction type. The parameters which determine the "conductive" properties of the model were related to the rib spacing, the transmission coefficient across a rib and the group velocity of waves travelling across the plate. This model was used to provide predictions of the vibrational energy levels across a ship's deck at distances from a vibration source. These predictions compared well with measured results.

Buvailo and Ionov (1989) implemented Nikiforov's equations numerically using an algorithm designed for thermal finite element analysis. This technique provided a more versatile tool which could also be used to model the effects of local variations in structural properties, like the application of localised damping treatments. This approach was used to build a finite element model of a reinforced raft structure which provided predictions which were in good agreement with measured results from the real structure, over a 200-2500 Hz frequency range.

Nefske and Sung

Up until this point simplified energy approaches had been used to provide models of large composite structures for which a more detailed analysis would prove too expensive or difficult to implement. Nefske and Sung (1987) were the first to employ this type of approach to the analysis of finite beam structures. Their approach was based on an energy balance equation for an elemental volume of material which was analogous to the treatment of an individual sub-system in SEA. In order to fully

define this energy balance Nefske and Sung made two assumptions based on the analogy with SEA. The first was to assume that the dissipation of energy due to damping is proportional to the local energy density of the system. The second, and perhaps the more important, was to assume that the flow of vibrational energy through the structure is proportional to the gradient of energy density. It can be argued that these assumptions were arrived at by simply applying the basic principles of SEA on a continuum basis. Having made these assumptions Nefske and Sung were able to express the energy balance in the form of a second-order differential equation analogous to the one governing heat conduction.

The key issue in the development of this approach is the constitutive relationship between the power flux and the gradient of vibrational energy density. Nefske and Sung derived a constant of proportionality linking these quantities in a beam structure by considering far-field components of the wave motion. The use of this approach was then illustrated by the analysis of single and connected beam structures.

The energy flow models used to carry out these analyses were created by modifying the properties of a NASTRAN structural finite element model. It was also suggested that a similar analysis could be implemented using a thermal finite element analysis via the analogy with the heat conduction equation. The finite element models provided smooth predictions for the structural response along the beams which were shown to agree well with the results of a classical model solution at very high frequencies. There were however, significant differences between the two solutions at the point of excitation and at the ends of the beams, although these were not commented upon in the publication.

Nefske and Sung's finite element models were also used to show that this simplified approach was able to predict the response of a beam at frequencies where a traditional FEA model, with the same mesh density, provided poor results. It was also noted that these analyses could be carried out at a significantly reduced level of computational cost as compared to traditional FEA.

Another important feature illustrated by these examples was that the analysis was able to provide an indication of the spatial variation of energy and power along the beam structure which represented a significant improvement over the single mean value provided by SEA. This potential advantage, together with the ability to provide a low cost, high frequency finite element analysis, sparked off a wave of interest in this type of approach.

Lase and Jezequel

Lase and Jezequel (1990) introduced an approach which provides a complete description of the dynamics of a single rod structure purely in terms of energy quantities. The first of these quantities was the total local vibrational energy density used in Nefske and Sung's approach. Unlike Nefske and Sung however, they also included a "Lagrangian term" which represented the difference in the local kinetic and potential energy densities. The inclusion of the Lagrangian meant that the solution could incorporate resonant behaviour and satisfy various boundary conditions at the ends of the rod eg. free-free, free-fixed etc. In effect, it meant that both active and reactive power components were accounted for in the solution which provided an accurate model at low, as well as high, frequencies everywhere in the rod. The final form of the model was shown to be a pair of coupled second-order differential equations linking active and reactive quantities. The solution to these equations was shown to be identical to the results obtained by a modal displacement solution.

Lase and Jezequel showed that it was also possible to introduce a "smoothing function" into the solution which suppressed the resonant nature of the model to give a smoothed frequency-averaged estimate of the response. This approach therefore has the potential to provide accurate predictions at low frequencies, and in the interest of saving on computational cost, a simplified estimate of response at high frequencies.

Burrell

Burrell et al (1990) reformulated Nefske and Sung's expressions in a two-dimensional polar form and applied them to the analysis of a thin circular plate excited by a dynamic point force at its centre. An energy flow model of the structure was created by modifying the properties of the thermal analysis provided by the ANSYS finite

element package. The response predictions provided by this model were compared to those obtained by an analytical modal solution and traditional dynamic FEA. These results show that the energy flow solution compared well with the more "exact" analysis except in the region of the point excitation. Some improvement was obtained by including more elements close to the point of excitation, although the reasons for this was never really explained.

Wohlever, Bouthier, Bernhard and Cho

The work by Nefske and Sung (1987) and later by Burrell et al (1900) showed that a simplified energy formulation could provide results which compared well with classical modal solutions. They also suggested a finite element implementation of the approach which could be developed into a very versatile design tool. It must be noted however, that the examples provided in these publications showed results for a very limited number of cases at very high frequencies and under rather extreme conditions of damping.

The central issue in developing this approach is the proportional relationship between the power flux and the gradient of energy density. In these publications this relationship was developed in a rather heuristic manner and was never proven explicitly. It is therefore impossible to assess the conditions under which this relationship holds and the nature of the solutions at frequencies other than those presented by the above authors. With these thoughts in mind, Wohlever (1988) looked more closely at the relationship between power flux and local energy in one-dimensional structures to determine the validity of the relationships assumed by Nefske and Sung.

In this work Wohlever was the first to derive constitutive relationships between power and energy density in a way which is consistent with classical mechanics. He showed that for low levels of damping, the time-averaged power flux in a rod was indeed proportional to the gradient of the time-averaged energy density. He also showed that a similar relationship could be developed for beams if near-field terms were neglected and a form of space-averaging was carried out on the classical energy expressions.

These simplifications explained the smoothed nature of previous results presented by Nefske and Sung, and the failure of the approach to accurately predict energy levels near discontinuities. This work later formed part of a paper presented by Wohlever, Bernhard and Bouthier (1990) and again by Wohlever and Bernhard (1992). The latter also included some results relating to coupled rod and beam models.

At the same time, Bouthier (1992) began work on developing similar relationships for two-dimensional membrane and plate structures. He showed that a constitutive relationship could be developed for membrane structures under conditions of space- and time-averaging, and similarly for plates, if near-field components are omitted from the analysis. This work also formed part of the earlier publication by Wohlever, Bernhard and Bouthier (1990) and a later paper by Bouthier and Bernhard (1992). The latter included a description of a finite element formulation dedicated solely to this type of analysis.

The work by Wohlever on one-dimensional structures was continued by Cho and Bernhard (1990). They provided a dedicated finite element formulation for the development of rod models. This work also included further research into the problem of modelling the coupling conditions between dissimilar rod structures. This problem of coupling was once again addressed by Cho and Bernhard (1992) who provided an analytical solution, based on the energy flow approach, for the response of an angled beam model. Because of the angled nature of the beam this solution required the inclusion of both flexural and longitudinal wave energy quantities, as well as the necessary transmission and reflection coefficients which describe the partial reflection and mode conversion characteristics of the joint. Model predictions were in good agreement with an "exact" calculation obtained by a classical modal approach.

2.3 Measurement techniques

It has been established that in parallel with the development of a modelling tool it will be necessary to employ experimental measurement techniques to determine the levels of vibrational energy flow in real structures. The purpose of this part of the review is to describe the development of these experimental techniques since work began on

them over two decades ago.

Time domain measurement

Noiseux (1970) was one of the first investigators to recognise the value of quantifying the travelling component of vibrational energy as a means of identifying the more dominant vibration transmission paths in structures. This paper introduced the quantity "structural intensity" which was defined as the vibrational power per unit width or area of cross-section. Noiseux's analysis showed that the structural intensity in a plate in flexure comprises both shear force and moment contributions. These components are obtained from the product of the force or moment vectors at some cross-section of the structure with their corresponding velocity vectors. In regions far from boundaries and discontinuities these two power components were shown to be equal. This allowed Noiseux to determine the total intensity in a plate by measurement of the moment component only.

Noiseux also showed that in the far-field of plate and beam structures the internal moment could be related to the translational motion at their surface. This relationship allowed Noiseux to make measurements of the structural intensity in a plate using two accelerometers mounted at right angles on a block attached to the its surface. One accelerometer provided a measure of the translational motion of the plate and the second a measure of the rotational motion at the point of attachment, by virtue of the displacement of its axis from the plate's centre line. Using this simple combination of transducers, together with an analogue integrating circuit, Noiseux was able to measure structural intensity in the two in-plane directions across the plate. This information was processed to give a vector representation of energy flow which clearly identified the location of the source of excitation and the flow of energy towards a sink.

Pavic (1976) derived a general expression for structural intensity through a section of plate experiencing flexure. The important feature of this expression was that intensity was expressed entirely in terms of spatial derivatives of the surface motion of the plate. Pavic showed that these spatial derivatives could be estimated by a finite

difference approach which required an array of accelerometer measurements around the point of interest. This finite difference approach effectively removed the need for the accelerometer mounting block employed earlier by Noiseux.

This general expression for plate intensity is valid everywhere in the plate, including areas which are influenced by near-field effects. It does however, require the use of an eight accelerometer array to evaluate all the spatial derivatives contained in the expression. Pavic showed that in certain circumstances, such as far-field conditions or if measurements are made on a beam, the number of accelerometers in the array could be reduced. For example, the measurement of far-field intensity in a beam could be achieved using just two accelerometers.

Frequency domain measurement

The increased availability of FFT signal processing equipment encouraged Verheij (1980) to investigate methods for the measurement of structural intensity using frequency domain techniques. He showed that the expressions developed earlier by Pavic could be implemented in the frequency domain using cross-spectral quantities. This allowed greater flexibility with respect to frequency resolution and eliminated the need to develop specialised signal processing circuitry to evaluate structural intensity. Verheij's interest centred on beam and pipe structures and he proposed a number of two-accelerometer techniques to measure structural intensity in these one-dimensional structures experiencing flexural, longitudinal and torsional motion. This work represented a major breakthrough in the area of structural intensity measurement because it provided techniques which could be implemented using tools which were already available to the engineering community.

Following these early papers interest in the evaluation of structural intensity grew, although the basic principles laid down by Pavic and Verheij remained virtually unchanged. There were a number of publications on the subject over the next decade, mostly relating to detailed aspects of the approach or reporting its successful application to engineering problems. Some examples of these were provided by Pinnington et al (1981), Redman-White (1984), Zhao (1987), Sato and Honda (1988)

and Carrol and Clark (1989). A useful summary of the progress made in the field up to the late 1980's was provided by Linjama and Lahti (1989). This included a description of a set of experiments carried out to study the practical application of various measurement techniques to the evaluation of structural intensity in beam structures.

Wavenumber measurement

Up to this point the majority of work in the area of structural intensity measurement was still based on the original proposals by Pavic and Verheij. There were however, a few techniques which moved away from these original formulations. Meyer et al (1990) developed a technique for measurement of the far-field structural intensity in a plate in flexure which involved the measurement of wavenumber. It was shown that wavenumber measurements in any one direction could be obtained using a linear array of three accelerometers. In order to measure wavenumber, and hence structural intensity, in both in-plane directions of the plate, Meyer et al used a five-accelerometer array in a cross configuration.

A similar approach was used by Wagstaff et al (1990) to measure the flexural wavenumber in a beam. In this paper Wagstaff et al also proposed a novel technique which involved the evaluation of structural intensity from signals referenced to a measurement made close to the source of excitation. The aims of this technique were to eliminate the effects of unwanted noise and to identify components of intensity associated with multiple source excitation. These techniques were also identified as being more appropriate for the measurement of structural intensity in lightly damped structures.

Laser vibrometry

All the techniques described above rely on the use of accelerometers attached to the surface of the structure. In recent years there has been a rapid increase in the application of laser technology to the study of structural vibration. Laser vibrometry has an advantage over the use of contacting transducers in that it does not interfere with the dynamics of the structure. This is particularly important in the case of light-

weight structures where the added mass of accelerometers may have significant effects. Laser techniques also have the potential to make measurements on structures which are hot, rotating or have limited accessibility.

Hayek et al (1990) showed that Pavic's finite difference expressions could be adapted to accommodate velocity measurements obtained by a scanning laser vibrometer. Baker et al (1990) showed that the need for finite difference approximations could be eliminated altogether by employing an optical technique which is able to provide a measurement of the gradient of the surface velocity. These techniques reduce the level of approximation and eliminate some of the difficulties inherent in the accelerometer methods. They do however, require the use of very expensive and often cumbersome equipment. It remains to be seen how well further development of these techniques can reduce these limitations in future years.

Practical limitations

The major drawback of structural intensity measurement is that its use is limited to cases where mechanical quantities within the structure such as shear force and moment, can be directly and simply related to the motion at the surface. Such structures include beams, plates, and shells which allow wave propagation only in the direction parallel to their surface in the frequency ranges of interest. This feature has been, and still is, a major obstacle to the development of generally applicable measurement techniques.

There are also a number of practical problems associated with the use of accelerometers which require special attention in order to achieve reliable measurements. One of these is related to transducer phase mismatch. The expressions for structural intensity require a measurement of the phase differences between the motion at a closely spaced array of points on the surface of the structure. In some cases, particularly when damping levels are low, these phase differences are comparable with the phase tolerances of the accelerometers and signal conditioning equipment which can lead to large errors in the results.

These errors can be reduced using calibration techniques to account for phase differences in the signals which are not related to the motion of the structure. The idea of calibration seems very straightforward in principle, but is often very difficult to achieve in practice. This is because of the difficulty in providing both accelerometers with exactly the same excitation during the calibration process. In the case of a two-transducer technique, phase mismatch can be removed quite conveniently by "switching" the accelerometers during the measurement process and averaging the two signals. In doing this, any phase bias due to accelerometer mismatch is effectively cancelled out. This approach cannot however, be employed if more than two accelerometers are involved. In general it can be concluded that the greater the number of accelerometers used to make the measurements, the more difficult it is to eliminate the effects of these phase mismatch problems.

These measurement techniques also suffer from errors introduced by finite difference approximations. Again, these can be accounted for in the case of two-accelerometer measurements, but are more difficult to remove as the number of transducers in the array increases.

It is apparent that some of the above problems are being addressed by the introduction of laser based techniques. The use of lasers should also enable data to be collected with greater precision and speed than can be achieved using the traditional accelerometer methods. It is still unclear however, if the increase in hardware costs will make this avenue prohibitively expensive to the general user.

Because of the practical problems involved in structural intensity measurement its development has progressed rather slowly over the past 20 years. For the majority of this time measurements have been confined to the laboratory and restricted to use on simple beam and plate structures. Recently however, there have been a few very good examples of the use of structural intensity measurement in the real engineering environment. Verheij (1993a, 1993b) presented two such examples relating to the transmission of vibrational energy along propeller shafts in ships. It remains to be seen whether this type of work will result in an increased recognition of the value of

structural intensity measurement to the wider engineering community.

2.4 Summary

In this chapter the work by previous investigators to provide a means of measuring or predicting vibrational energy flow in structures has been outlined. The main points relating to this area are as follows:

1. The adaptation of traditional finite element analysis to provide energy flow predictions results in a very detailed and complete description of the wave transmission characteristics of a structure. This technique is however, limited to use at lower frequencies due to rapidly increasing computational costs.

2. Statistical energy analysis provides a good global model for the analysis of structures at high frequencies if the model parameters are known. Over the years the evaluation of these parameters has proved the most difficult aspect of SEA, although a number of analytical and experimental techniques are available. The major limitation of SEA is the ability of the structure to satisfy the statistical nature of the assumptions used in its development in the low to medium frequency ranges.

3. The simplified continuum energy flow approaches have the potential to bridge the frequency gap between traditional finite element analysis and SEA. After a number of approximations are made, the energy governing equations reduce to a second-order differential form, analogous to that of the heat conduction equation. The ability to solve this equation using finite element techniques indicates a potential for this approach to provide energy flow estimates through relatively complex structures over a wide frequency range.

4. The development of structural intensity measurement techniques has been limited by the difficulty in obtaining information about internal shear forces and moments of a structure from measurements of the motion at its surface. There are also significant errors induced due to transducer phase mismatch and

the use of finite difference approximations in the analysis. As a result, previous applications of this technique have been mainly limited to simple structural geometries and carried out under laboratory conditions. Very recently however, there have been a few good examples of the application of these techniques to real engineering applications.

Chapter 3

Theoretical development

3.1 Introduction

In this chapter the theoretical basis of the energy flow approach will be presented in more detail. It will be shown that by considering the conservation of energy in an enclosed volume of material and applying steady state conditions, a second-order differential equation can be developed which governs the flow of vibrational energy within a general structural component. The exact form of this equation is determined by the relationship between vibrational power flux and energy density, which in turn is dependent on the type of structure under consideration. These relationships have been developed by Wohlever (1988) for rods and beams and Bouthier (1992) for membranes and plates. Although these expressions will not be derived fully here, their development will be described in some detail to highlight the impact of certain assumptions made in simplifying the relationships.

3.2 The energy balance equation

Consider the elemental volume of material shown in Fig.3.2.1, which possesses some form of vibrational energy quantified by energy density, e. The power dissipated by damping is denoted p_{diss} and q represents a power flux crossing the boundary. Using the principle of the conservation of energy, the rate of change of energy within the system must be equal to the algebraic sum of the net power crossing the boundary and the power dissipated by damping. This leads to an instantaneous energy balance governing the conduction and dissipation of vibrational energy within the system, given by:

$$\frac{\partial e}{\partial t} = - \nabla . q - p_{diss} \qquad (3.2.1)$$

For steady state conditions, the time derivative is zero and the energy balance becomes:

$$- \nabla.q - p_{diss} = 0 \tag{3.2.2}$$

An expression to determine the value of the dissipated power p_{diss} due to material damping has been developed in a number of ways. Wohlever (1988) developed an expression through a detailed study of the damping mechanisms within a rod model. Bouthier (1992) provided a more general analysis based on the classical hysteretic damping model described by Cremer (1973). Nefske and Sung (1987) simply borrowed an expression from SEA and applied it to the energy flow model in a continuum manner. In all cases it was concluded that the time-averaged effects of damping in a general structural element can be effectively modelled using the expression:

$$p_{diss} = \omega \eta e \tag{3.2.3}$$

where η represents the hysteretic damping loss factor for the material and ω is the radian frequency of vibration.

The fundamental principles behind the energy flow approach is to assume that the energy flows from regions of high energy density to regions of lower energy density and that the rate of energy flow is proportional to the energy gradient between those points. These assumptions can be expressed in equation form as:

$$q \propto - \nabla e \tag{3.2.4}$$

Substituting (3.2.3) and (3.2.4) into (3.2.2) gives:

$$C \nabla^2 e - \omega \eta e = 0 \tag{3.2.5}$$

which is the general form of the differential equation providing a simplified description of the conduction and dissipation of vibrational energy within a structural component.

The constant of proportionality, C, is dependent on the nature of the component concerned, ie whether it can be considered as a rod, beam or plate. The form of this parameter in each of these cases has been determined by Wohlever (1988) and Bouthier (1992) by developing a relationship between power flux and the gradient of energy density similar in form to (3.2.4), from classical wave theory. In each of these cases the proposed relationship is of the general form:

$$q = - \frac{c_g^2}{\omega\eta} \nabla e \qquad (3.2.6)$$

where c_g is the group velocity of waves which is dependent on the type of structure and the nature of the wave motion involved.

It should be noted that in the case of rod structures q and e are time-averaged quantities. In the cases of beam and plate structures, the above relationship can only be formed if q and e are both space- and time-averaged and relate only to far-field conditions. These simplifications will be explained in more detail in the following sections.

The relationship between vibrational power flux and energy density (3.2.4) forms the central core of the energy flow approach. As mentioned earlier, this relationship has been developed for common structural components from basic wave theory. An understanding of the development of these expressions is vital in order to appreciate the limitations and applicability of the energy flow approach to the analysis of real structures. The development of the expressions relating to rod, beam and plate structures will be looked at in some detail here so that the impact of the assumptions made to simplify the analysis are fully understood.

Before embarking on this discussion it is necessary to point out some differences in nomenclature between the expressions used here and those appearing in earlier work. The analysis for rods and beams presented here is based on the work by Wohlever (1988), although the expressions used are slightly different from those which appear in Wohlever's original text. Here, the quantity *energy density, e,* is interpreted as

energy per unit volume in units of [J/m^3]. In keeping with expression (3.2.6), q must represent a *power flux* defined as *the rate of energy flow per unit area* having units of [W/m^2]. Wohlever's expressions for energy density were expressed in terms of *energy per unit length*, although a relationship of the same form as (3.2.6) was still obtained because his power quantity, q, was expressed in units of *watts*.

3.3 Theoretical development for rod structures

Before focusing on the relationship between power flux and energy density it is appropriate to introduce the solution to the wave equation for a rod structure experiencing longitudinal harmonic motion. This solution, together with its counterpart relating to flexural motion in a beam, will feature regularly throughout this thesis.

3.3.1 The wave equation of motion for a rod

Consider the section of rod shown in Fig.3.3.1. Assuming that sections of the rod remain plane during motion and that the stress over these sections is uniform, the equation of motion for a section of length δx, given by Newton's second law, is:

$$\rho S \delta x \frac{\partial^2 U}{\partial t^2} = S \frac{\partial \sigma}{\partial x} \delta x \qquad (3.3.1)$$

where U represents the displacement of the rod section, S denotes its cross-sectional area and ρ the mass density of the rod material.

The stress, σ, is related to the strain in the rod $\partial U/\partial x$ by:

$$\sigma = E \frac{\partial U}{\partial x} \qquad (3.3.2)$$

where E represents the Young's modulus for the rod material. Using this relationship the equation of motion becomes:

$$\rho \frac{\partial^2 U}{\partial t^2} = E \frac{\partial U^2}{\partial x^2} \qquad (3.3.3)$$

For steady state harmonic motion, the longitudinal displacement, U, is a function of both space and time and can be expressed as:

$$U(x,t) = u(x)\, e^{i\omega t} \tag{3.3.4}$$

Substituting (3.3.4) into (3.3.3) gives:

$$\frac{\partial^2 u(x)}{\partial x^2} + \frac{\rho\omega^2}{E}\, u(x) = 0 \tag{3.3.5}$$

At this point it is necessary to introduce some well established quantities relating to wave motion. These are wavenumber, k, and phase speed, c, which are described in some detail by Cremer (1973) and Fahy (1985).

Wavenumber, k, is given by:

$$k = \frac{\omega}{c} \tag{3.3.6}$$

and the phase speed for longitudinal motion, c_L, is given by:

$$c_L = \sqrt{\frac{E}{\rho}} \tag{3.3.7}$$

Using (3.3.6) and (3.3.7) above, (3.3.5) reduces to:

$$\frac{\partial^2 u(x)}{\partial x^2} + k^2 u(x) = 0 \tag{3.3.8}$$

which has the general solution:

$$u(x) = Ae^{-ikx} + Be^{ikx} \tag{3.3.9}$$

The complete solution for longitudinal motion, as a function of space and time, from (3.3.4) is:

$$U(x,t) = \left(Ae^{-ikx} + Be^{ikx} \right) e^{i\omega t} \tag{3.3.10}$$

where A and B are dependent on boundary conditions and represent complex wave amplitudes which correspond to waves propagating in the positive and negative x

directions respectively. This expression will be used extensively throughout this thesis to describe harmonic longitudinal wave motion in one-dimensional structures.

3.3.2 Damping

Damping can be introduced into the equation of motion by replacing the modulus of elasticity, E, by a complex modulus defined by $E_c = E(1+i\eta)$, where η is the hysteretic damping loss factor. In doing this the wavenumber also becomes complex and is given by:

$$k^2 = \frac{\omega^2}{c_L^2} \frac{\left(1 - i\eta \right)}{\left(1 + \eta^2 \right)} \tag{3.3.11}$$

In most practical cases $\eta<<1$ and it can be shown that:

$$k_c = \frac{\omega}{c_L} \left(1 - i\frac{\eta}{2} \right) \approx k_1 + i k_2 \tag{3.3.12}$$

The significance of this complex wavenumber becomes apparent when it replaces k in the wave solution (3.3.10), so that:

$$U(x,t) = \left(Ae^{(-ik_1x + k_2x)} + Be^{(ik_1x - k_2x)} \right) e^{i\omega t} \tag{3.3.13}$$

This expression indicates that the introduction of damping causes the wave amplitudes to decay exponentially with distance at a rate of $\exp(-\omega\eta x/2c_L)$.

3.3.3 Power flux and energy density relationship for rods

The vibrational power flux at any point in the rod is given by the product of axial force per unit area and axial velocity. Expressing these quantities in terms of the axial displacement yields:

$$q = - E \frac{\partial U}{\partial x} \frac{\partial U}{\partial t} \tag{3.3.14}$$

Goyder and White (1980) showed that under harmonic conditions, a time-averaged power quantity can be obtained from:

$$< p > = < \text{(force)(velocity)} > = \frac{1}{2} \text{Re} \left[\text{(force)(velocity)}^* \right] \quad (3.3.15)$$

where < > indicates time-averaging and * denotes a complex conjugate.

Using (3.3.13), (3.3.14) and (3.3.15) the time-averaged power flux, $< q >$, can be expressed as:

$$\begin{aligned} < q > = & \frac{1}{2} \omega E k_1 \left[|A|^2 e^{2k_1 x} - |B|^2 e^{-2k_1 x} \right] \\ & - \omega E k_2 \left[\text{Im}(AB^*) \cos 2k_1 x - \text{Re}(AB^*) \sin 2k_1 x \right] \end{aligned} \quad (3.3.16)$$

The total energy density is given by the sum of the strain and kinetic energy densities, denoted by V and T respectively. In the case of a rod:

$$V = \frac{1}{2} E \left(\frac{\partial U}{\partial x} \right)^2 \quad (3.3.17)$$

and

$$T = \frac{1}{2} \rho \left(\frac{\partial U}{\partial t} \right)^2 \quad (3.3.18)$$

Following the procedure used to derive the time-averaged power flux and summing the two energy components, the total energy density is given by:

$$\begin{aligned} < e > = & \frac{1}{4} \left\{ |A|^2 e^{2k_1 x} + |B|^2 e^{-2k_1 x} \right\} \left\{ E|k|^2 + \rho\omega^2 \right\} \\ & - \frac{1}{2} \left\{ \text{Re}(AB^*) \cos 2k_1 x + \text{Im}(AB^*) \sin 2k_1 x \right\} \left\{ E|k|^2 - \rho\omega^2 \right\} \end{aligned} \quad (3.3.19)$$

At present there seems to be no simple relationship between equations (3.3.16) and (3.3.19). However, if the assumption is made that the damping in the structure is light ie. $\eta << 1$, then $|k_1| >> |k_2|$ and the expression for power flux, equation (3.3.16), reduces to:

$$< q > \approx \frac{1}{2} \omega E k_1 \left[\, |A|^2 e^{2k_2 x} - |B|^2 e^{-2k_2 x} \, \right] \tag{3.3.20}$$

This assumption also means the expression for wavenumber, equation (3.3.11), reduces to:

$$|k|^2 \approx \frac{\omega^2}{c_L^2} \tag{3.3.21}$$

and hence

$$E|k|^2 \approx E \frac{\omega^2}{c_L^2} = E \frac{\omega^2 \rho}{E} = \rho \omega^2 \tag{3.3.22}$$

Substituting (3.3.22) into (3.3.19) provides an approximate time-averaged total energy density given by:

$$< e > \approx \frac{1}{2} \rho \omega^2 \left\{ \, |A|^2 e^{2k_2 x} + |B|^2 e^{-2k_2 x} \, \right\} \tag{3.3.23}$$

Differentiating (3.3.23) with respect to x and dividing (3.3.20) by this differential results in the relationship:

$$< q > = - \frac{c_L^2}{\eta \omega} \frac{d<e>}{dx} \tag{3.3.24}$$

This shows that if damping is assumed to be light, the time-averaged power flux in a rod is proportional to the gradient of the time-averaged energy density as assumed in (3.2.4). Noting that for longitudinal waves $c_g = c_L$ then (3.3.24) compares directly with the more general expression (3.2.6).

3.4 Theoretical development for beam structures

The treatment of the theory relating to beam structures will be carried out in a similar manner to that for rods. The expressions describing the relationships between mechanical quantities in a beam are more complicated than those relating to a rod because of the increased complexity of the motion involved. As a consequence, a simple relationship between power flux and energy density is more difficult to establish. It is possible however, to develop a relationship of the same form as (3.2.4) if certain components of the expressions relating to flexural motion are neglected. These simplifications will be described in some detail in the following sections.

Before looking at the development of the relationship between power flux and energy density, the solution to the wave equation of motion for a beam will be introduced. As with the case of the rod solution this expression will feature regularly throughout this thesis.

3.4.1 The wave equation of motion for a beam

Using a similar approach to the one employed earlier in the rod analysis, Fahy (1985) showed that the equation of motion for a small section of beam experiencing harmonic flexural motion is a fourth-order relationship of the form:

$$EI \frac{\partial^4 w(x)}{\partial x^4} + \rho S \frac{\partial^2 w(x)}{\partial t^2} = 0 \qquad (3.4.1)$$

where $w(x)$ represents the transverse displacement of the beam section. By following similar steps to those described in section 3.3.1, the complete solution to this equation under harmonic conditions is:

$$W(x,t) = (Ae^{-ikx} + Be^{ikx} + Ce^{-kx} + De^{kx}) e^{i\omega t} \qquad (3.4.2)$$

where wavenumber, k, is given by:

$$k^4 = \omega^2 \frac{\rho S}{EI} \qquad (3.4.3)$$

and the constants A,B,C and D are dependent on boundary conditions.

3.4.2 Near-field and far-field effects

It is evident from the above expressions that the fourth-order nature of the equation of motion results in a solution which contains four terms. The first pair of terms represent flexural waves propagating in the positive and negative x directions, with wave amplitudes A and B respectively. These terms are similar to those appearing in the solution for longitudinal motion in a rod. The remaining terms, containing C and D, represent non-propagating fields with amplitudes which decay exponentially with distance. Cremer (1973) explained that these terms are required to satisfy equilibrium and continuity conditions at a structural discontinuity. In this context, a discontinuity could take the form of an end condition, the coupling point between two beams or the location of the driving force.

The displacement solution (3.4.2) shows that these terms decay with distance at a rate of $\exp(-kx)$. This decay function can also be expressed in terms of the wavelength of vibration. Since:

$$k = \frac{2\pi}{\lambda} \tag{3.4.4}$$

the decay function becomes:

$$f(x) = \exp\left(-\frac{2\pi x}{\lambda}\right) \tag{3.4.5}$$

Fig.3.4.1 shows this function plotted against distance from a discontinuity expressed in terms of wavelength. It can be seen that $f(x)$ decays almost completely within the distance of one wavelength. For this reason the terms containing C and D in (3.4.2) are normally considered negligible at distances greater than one half of a wavelength from a discontinuity. Because these terms are only important close to discontinuities they have become known as the "near-field" part of the solution. In contrast, the terms containing A and B describe propagating waves which are important everywhere in the beam. These terms have subsequently become known as the "far-field" part of the solution.

3.4.3 Power flux and energy density relationship for beams

The strain and kinetic energy densities, V and T, for a transversely vibrating beam are given by:

$$V = \frac{1}{2}\frac{EI}{S}\left(\frac{\partial^2 W}{\partial x^2}\right)^2 \tag{3.4.6}$$

and

$$T = \frac{1}{2}\rho\left(\frac{\partial W}{\partial t}\right)^2 \tag{3.4.7}$$

Using the displacement solution (3.4.2) and carrying out time-averaging in a similar manner to that applied to rods, these quantities can be expressed as:

$$\begin{aligned} \langle V \rangle = \frac{1}{4}\frac{EI|k^2|^2}{S}\ \mathrm{Re}\Big[&\left(Ae^{-ikx} + Be^{ikx} - Ce^{-kx} - De^{kx} \right) \\ &\left(Ae^{-ikx} + Be^{ikx} - Ce^{-kx} - De^{kx} \right)^* \Big] \end{aligned} \tag{3.4.8}$$

and

$$\begin{aligned} \langle T \rangle = \frac{1}{4}\rho\omega^2\ \mathrm{Re}\Big[&\left(Ae^{-ikx} + Be^{ikx} + Ce^{-kx} + De^{kx} \right) \\ &\left(Ae^{-ikx} + Be^{ikx} + Ce^{-kx} + De^{kx} \right)^* \Big] \end{aligned} \tag{3.4.9}$$

When these expressions are evaluated they result in relationships which are considerably more complicated than the ones obtained during the rod analysis presented earlier. Using the assumption of low damping, Wohlever (1988) showed that the total energy density, given by the sum of the above expressions, can be reduced to:

$$\begin{aligned} \langle e \rangle = \frac{1}{2}\rho\omega^2 \Big[&|A|^2 e^{2k_1 x} + |B|^2 e^{-2k_1 x} + |C|^2 e^{-2k_2 x} + |D|^2 e^{2k_2 x} \Big] \\ &+ \rho\omega^2 \Big[\mathrm{Re}(AB^*)\cos 2k_1 x + \mathrm{Im}(AB^*)\sin 2k_1 x \Big] \\ &+ \rho\omega^2 \Big[\mathrm{Re}(CD^*)\cos 2k_2 x + \mathrm{Im}(CD^*)\sin 2k_2 x \Big] \end{aligned} \tag{3.4.10}$$

where the real and imaginary components of wavenumber, k_1 and k_2, result from the

introduction of damping using the complex modulus of elasticity.

There are several differences between this equation and the equivalent expression for rods. Firstly, there are near-field terms containing C and D which are only important close to the discontinuities. There is also a harmonic far-field component:

$$\rho\omega^2 \left[\mathrm{Re}(AB^*) \cos 2k_1 x + \mathrm{Im}(AB^*) \sin 2k_1 x \right] \qquad (3.4.11)$$

Wohlever (1988) showed that this part of the function could be removed if a space-averaged energy density is obtained by integrating (3.4.10) over one wavelength.

If in addition near-field components are neglected, the space- and time-averaged energy density in the far-field of the beam becomes:

$$< \bar{e} >_{ff} = \frac{1}{2} \frac{EIk_1^4}{S} \left(|A|^2 e^{2k_1 x} + |B|^2 e^{-2k_1 x} \right) \qquad (3.4.12)$$

where $\bar{e}$ is the space-averaged energy density, $< >$ indicates time-averaging and the suffix *ff* shows that only far-field components are retained in the analysis.

Vibrational power in a beam is transmitted by two separate mechanisms, one related to shear force and the other to bending moment. The time-averaged power flux associated with the shear force component is:

$$< q >_s = \frac{1}{2} \mathrm{Re} \left[\left(\frac{EI}{S} \frac{\partial^3 W}{\partial x^3} \right) \left(\frac{\partial W}{\partial t} \right)^* \right] \qquad (3.4.13)$$

and similarly, for the moment component:

$$< q >_m = \frac{1}{2} \mathrm{Re} \left[\left(\frac{EI}{S} \frac{\partial^2 W}{\partial x^2} \right) \left(- \frac{\partial^2 W}{\partial x \partial t} \right)^* \right] \qquad (3.4.14)$$

Using the displacement expression (3.4.2), neglecting near-field terms and carrying out space-averaging, Wohlever showed that the far-field space- and time-averaged power flux in a beam can be expressed as:

$$< \bar{q} >_{ff} = \frac{EI\omega k_1^3}{S} \left(|A|^2 e^{2k_x x} - |B|^2 e^{-2k_x x} \right) \qquad (3.4.15)$$

Differentiating (3.4.12) with respect to x and dividing (3.4.15) by this differential gives:

$$< \bar{q} >_{ff} = - \frac{4c_b^2}{\eta\omega} \frac{d<\bar{e}>_{ff}}{dx} \qquad (3.4.16)$$

which is the assumed relationship given by equation (3.2.4). Noting that for flexural wave motion in a beam $c_g = 2c_b$, (3.4.16) becomes identical to the more general relationship (3.2.6).

3.5 Theoretical development for plate structures

The analysis developed by Bouthier (1992) for the relationship between vibrational power flux and energy density in a finite thin plate follows a similar procedure to that for rods and beams presented by Wohlever (1988). With the inclusion of damping, the equation of motion for a thin uniform plate is of the form:

$$D(1+i\eta)\ \nabla^4 w + \rho h \frac{\partial^2 w}{\partial t^2} = 0 \qquad (3.5.1)$$

where η represents the damping loss factor for the plate material and D is the bending stiffness of the plate section given by:

$$D = \frac{Eh^3}{12(1-\nu^2)} \qquad (3.5.2)$$

Bouthier explained that due to its biharmonic nature (3.5.1) is not separable and a general solution cannot be obtained in closed form. To overcome this difficulty he made use of an approximate expression for the wave motion in a plate structure which consists of the superposition of two far-field plane waves.

Using this approach the wave solution for the transverse displacement of the plate is given by:

$$w_{ff}(x,t) = \left(A_x e^{-ik_x x} + B_x e^{ik_x x} \right) . \left(A_y e^{-ik_y y} + B_y e^{ik_y y} \right) e^{i\omega t} \qquad (3.5.3)$$

where the suffix *ff* shows that this expression is only valid in the far-field.

Bouthier substituted this expression into those for power flux and energy density in a thin plate provided by Timoshenko (1955). After time-averaging and neglecting terms containing sinusoidal functions of wavenumber (equivalent to space-averaging), he showed that:

$$< \bar{q} >_{ff} = - \frac{c_g^2}{\eta\omega} \nabla < \bar{e} >_{ff} \qquad (3.5.4)$$

This expression is of course, only valid far from discontinuities because the far-field components of the wave equation were neglected at the outset of the analysis.

3.6 Discussion

In developing the simplified energy balance governing the flow of mechanical energy through a structural component, it was assumed that vibrational power flux is proportional to the gradient of the energy density between points in the structure. If the level of material damping is low, it has been shown that for the case of a rod experiencing longitudinal motion, this direct relationship can be obtained . For beams and plates however, this proportional relationship can only be obtained by carrying out some form of space-averaging and neglecting near-field components.

The assumption that damping is low can be justified for most engineering structures because the majority of marine, aerospace and automotive structures, where this technique is potentially most useful, are constructed from steel or aluminium. The damping loss factors for these materials are typically less than 0.01.

In the case of plate and beam structures a necessary simplification to the analysis was achieved by neglecting near-field components of the displacement solutions. This simplification should only be detrimental to the solution for parts of the structure within a distance of one half of a wavelength from a structural discontinuity. In most cases it will be possible to make some judgement of the proportion of the structure which is affected by this simplification at a given frequency. This information will be important when assessing the applicability of this modelling technique to the particular structure concerned.

In developing the relationships for plate and beam structures, it was necessary to remove the sinusoidal variation of the far-field power flux and energy density expressions by a space-averaging technique. As a result, the analysis provided by this approach will lack some of the detail present in the exact solutions, although the general level of power and energy density will be provided in the form of a space-averaged estimate. This greatly reduces the numerical complexity of the solution at the cost of introducing some level of approximation into the result. This trade off is in keeping with the requirements of the modelling tool set out in Chapter 1.

3.7 Summary

This chapter outlined the theoretical basis of the energy flow approach proposed by Nefske and Sung (1987), Wohlever (1988) and Bouthier (1992). The key points concerning this analysis are as follows:

1. The equation governing the flow of vibrational energy within a structural component is developed by considering the steady state energy balance for an elemental volume of material which is capable of both dissipation and transmission of vibrational energy.

   By assuming that the dissipated energy is related to the local level of energy density and that the transmission of energy is proportional to the energy gradient, this governing equation becomes a second-order differential equation

of the form:

$$C \nabla^2 e - \omega \eta e = 0 \tag{3.7.1}$$

2. By considering the expressions for the energy and power in a rod structure Wohlever (1988) showed that if damping levels are low:

$$\langle q \rangle = \frac{c_g^2}{\omega \eta} \frac{d\langle e \rangle}{dx} \tag{3.7.2}$$

where < > indicates a time-averaged quantity.

3. Wohlever (1988) and Bouthier (1992) showed that similar relationships could be developed for beam and plate structures in flexure if, in addition to the condition of low damping, the expressions involved are space-averaged and near-field terms are omitted from the analysis.

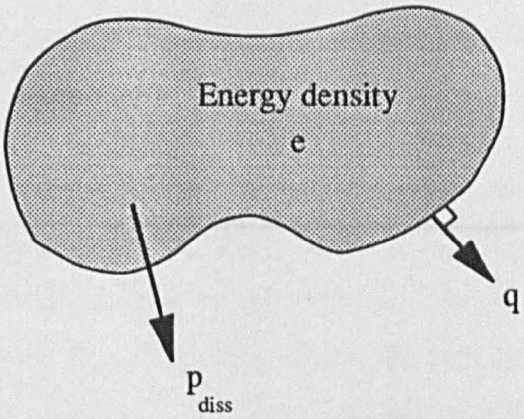

Fig.3.2.1 Elemental volume of material

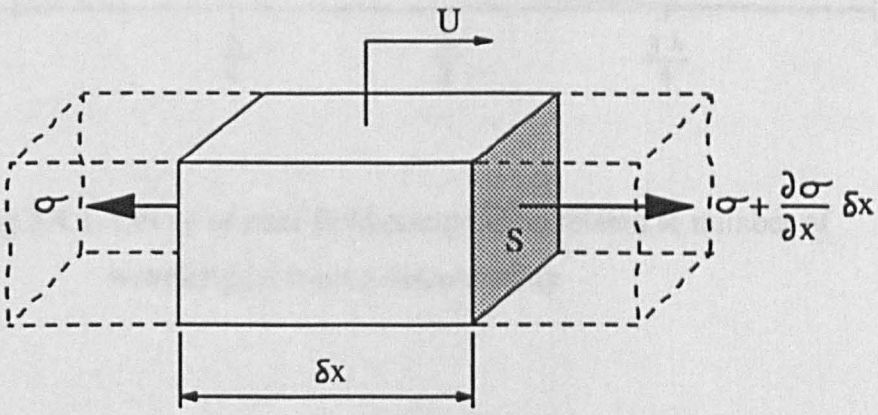

Fig.3.3.1 Forces acting on an element of rod experiencing longitudinal motion

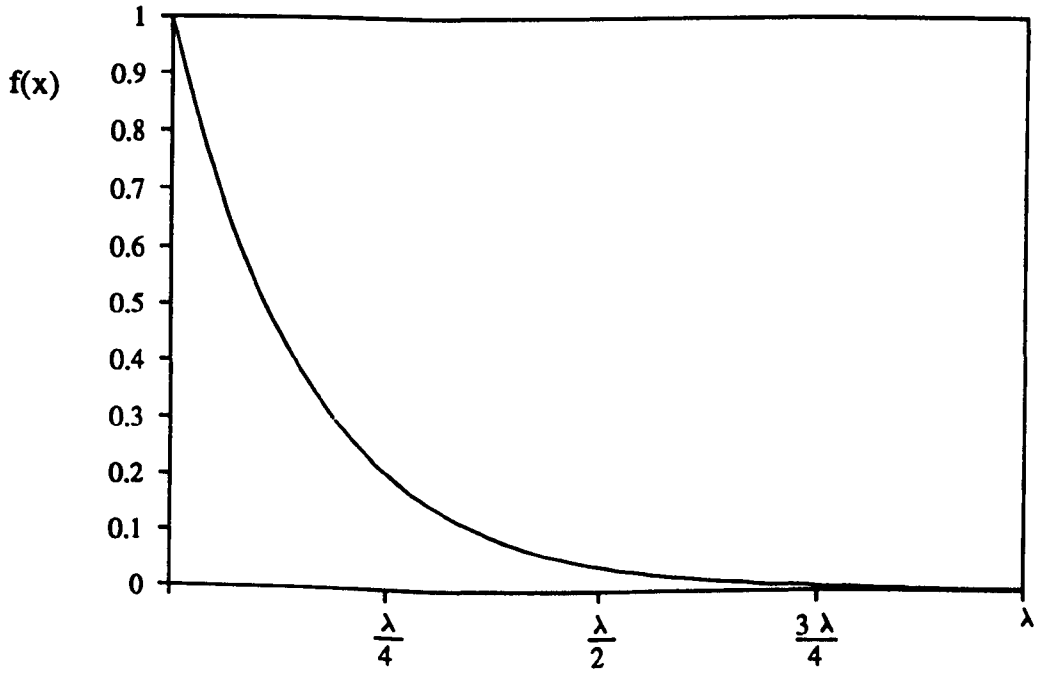

Fig.3.4.1 Decay of near-field components related to number of wavelengths from a discontinuity

Chapter 4

Application to beam structures

4.1 Introduction

In this chapter the energy flow approach is applied to the analysis of beam structures. The first study describes the development of an energy flow model to provide an estimate of the response of a simply supported beam structure experiencing harmonic force excitation applied at its mid-section. This work provides useful insight into the nature of the predictions obtained from the energy flow approach which are influenced by the simplifications outlined in the previous chapter. The quality of the model predictions is assessed by comparison with a modal response solution for this type of structure.

The second study describes the use of the energy flow approach to build a representative model of a real beam structure. This structure consists of a freely supported perspex beam with shaker excitation at one end. Energy flow predictions from the model are compared with measured values obtained along the length of the beam using a far-field structural intensity technique. This work serves to determine the quality of energy flow predictions obtained from the model and allows the accuracy requirement of modelling parameters (eg. power input and damping) to be assessed.

4.2 Energy flow analysis for a simply supported beam structure

Fig.4.2.1 shows a simply supported beam structure excited by a point harmonic force at its mid-section. An energy flow model of this structure will be developed to provide some insight into the nature of the predictions obtained by the energy flow approach. This information will also be useful in assessing how this technique might best be applied to the analysis of real structures.

4.2.1 The energy flow solution

The energy flow model used to represent the simply supported beam structure is shown in Fig.4.2.2. In this model, the supply of vibrational energy provided by the excitation is represented by a power input, P, applied at the centre of the beam. It is assumed that energy does not flow into the simple supports, which gives rise to boundary conditions such that the power flux, q, at each end of the beam is equal to zero.

It was shown in Chapter 3 that the differential equation governing the steady state flow of vibrational energy within a structural component is:

$$C \nabla^2 e - \omega \eta e = 0 \tag{4.2.1}$$

Equation (3.4.16) shows that for a beam structure in flexure:

$$C = \frac{4c_b^2}{\eta \omega} \tag{4.2.2}$$

Combining (4.2.1) and (4.2.2) gives:

$$\frac{4 c_b^2}{\eta \omega} \frac{d^2 e}{dx^2} - \omega \eta e = 0 \tag{4.2.3}$$

This is the governing equation for flexural energy conduction and dissipation within the beam model. It should be remembered that due to the assumptions described in Chapter 3, the energy density value, e, is a space- and time-averaged quantity and related only to far-field conditions.

Rearranging (4.2.3) gives:

$$\frac{d^2 e}{dx^2} - \alpha^2 e = 0 \tag{4.2.4}$$

where,

$$\alpha = \frac{\omega \eta}{2 c_b} \tag{4.2.5}$$

Equation (4.2.4) has a general solution of the form:

$$e(x) = A \cosh(\alpha x) + B \sinh(\alpha x) \tag{4.2.6}$$

where the constants A and B can be found from the boundary conditions applied to the model.

The symmetry of the energy flow model allows the solution (4.2.6) to be obtained for each symmetric half of the structure in turn. The energy flow solution for the left-hand half of the beam, defined by $0 \leq x \leq L/2$, is obtained by considering the boundary conditions at each end of this section. These are related to the power flux values defined by:

$$q(x) = - \frac{4 c_b^2}{\eta \omega} \frac{de}{dx} \tag{4.2.7}$$

Using (4.2.6) this equation becomes:

$$q(x) = - 2 c_b \left[A \sinh(\alpha x) + B \cosh(\alpha x) \right] \tag{4.2.8}$$

At the left-hand end of model, $x = 0$, the power flux, q, is zero. Applying this condition to (4.2.8) shows that in this case $B = 0$.

At the point of excitation, $x = L/2$, the power flux is:

$$q(L/2) = - \frac{P}{2S} \tag{4.2.9}$$

where S represents the cross-sectional area of the beam.

Applying this condition to (4.2.8) yields:

$$A = \frac{P}{4c_b S \sinh(\alpha L/2)} \tag{4.2.10}$$

Substituting these values for A and B into the general solution (4.2.6) gives:

$$e(0 \le x \le L/2) = \frac{P}{4c_b S} \frac{\cosh(\alpha x)}{\sinh(\alpha L/2)} \tag{4.2.11}$$

A similar analysis for the right-hand half of the beam gives:

$$e(L/2 \le x \le L) = \frac{P}{4c_b S} \left\{ \frac{\sinh(\alpha x - \alpha L)}{\sinh(-\alpha L/2)} \right\} \tag{4.2.12}$$

In this analysis comparisons between the energy flow and modal solutions will be made in terms of displacement response. Cremer (1973) showed that the potential and kinetic energy density values in the far-field region of a beam are equal. It follows that the total energy density can therefore be expressed as twice the kinetic energy density, thus:

$$e(x) = \rho v^2(x) \tag{4.2.13}$$

where v represents the transverse velocity of the beam.

For harmonic conditions displacement is related to velocity by:

$$v^2(x) = \omega^2 w^2(x) \tag{4.2.14}$$

hence the displacement response along the beam can be calculated from:

$$w(x) = \sqrt{\frac{e(x)}{\rho \omega^2}} \tag{4.2.15}$$

where $e(x)$ is the energy density value obtained by either (4.2.11) or (4.2.12) above.

4.2.2 The modal solution

For comparison with the energy flow solution the displacement response for a simply supported beam excited at its centre has been obtained by a classical modal superposition calculation. The derivation of this modal solution is described fully in Appendix A and for brevity only the final expressions will be provided here.

The analysis shows that the rms value of the displacement response at a distance x from the left-hand end of the beam is given by:

$$w(x)_{rms} = \frac{1}{\sqrt{2}} \left| \frac{2F}{\rho S L} \sum_{r=1}^{\infty} \phi_r(a)\, \phi_r(x)\, Z_r^* \right| \qquad (4.2.16)$$

where $\phi_r(x)$ is the mode shape function for a simply supported beam, given by:

$$\phi_r(x) = \sin \frac{r\pi x}{L} \qquad (4.2.17)$$

and Z_r^* is a complex quantity which takes account of the presence of damping and is given by:

$$Z_r^* = \frac{\omega_r^2 - \omega^2(1+\eta^2) + i(\eta\,\omega_r^2)}{(\omega_r^2 - \omega^2)^2 + \eta^2\omega^4} \qquad (4.2.18)$$

Here F is the magnitude of the sinusoidal force applied at a distance a from the end of the beam, ω_r is the eigen frequency of the r^{th} mode, ρ is mass density of the beam material and L is the length of the beam.

4.2.3 Results and discussion

For the purposes of this analysis the properties and dimensions of the beam structure are as follows:

Length = 1.2 m	Mass density = 7800 kg/m^3
Depth = 10.3 mm	Young's modulus = 209 GN/m^2
Width = 10 mm	

The value for the loss factor will initially be set at 0.2. This rather high value contradicts the assumption of low damping required to develop the governing expressions for this approach, but allows direct comparison with the earlier results presented by Nefske and Sung (1987).

In order to evaluate the energy flow solutions (4.2.11) and (4.2.12) one requires a value for the mechanical power input to the beam, P. This can be obtained using the driving point impedance of the structure which is defined as the ratio of excitation force to the resulting velocity at the point of excitation. Using this definition Cremer (1973) showed that the rms power imparted to a structure by a harmonic force of magnitude F is:

$$P_{rms} = \frac{1}{2} |F|^2 \, \mathrm{Re}\left(\frac{1}{z}\right) \tag{4.2.19}$$

where z is the driving point impedance.

Pinnington and White (1981) showed that at higher frequencies, the point impedance of a finite structure approximates to that calculated for an equivalent infinite structure. This property was employed by Nefske and Sung (1987), who obtained a value of z for their beam model using:

$$z = 2\rho S c_b (1 + i) \tag{4.2.20}$$

which corresponds to the point impedance of an infinite beam, derived by Cremer (1973).

Mean displacement values for the beam calculated by the modal approach over a frequency range of 0-10 kHz are shown in Fig.4.2.3. The corresponding response estimates provided by the energy flow solution using the infinite beam approximation for power input are also shown in this figure by a dotted line. This line agrees well with the modal values above 1 kHz, but does not reflect the variation in response around resonances in the lower frequency region. As a consequence, significant discrepancies are evident between the two results. These differences stem from the fact that equation (4.2.20) relates to an infinite structure which does not possess modal behaviour. Moreover, equation (4.2.20) takes no account of the level of damping in the structure and further investigation has shown that good agreement between the two solutions is only obtained for loss factors of around 0.2. For example, when the damping factor is reduced to 0.02, which is more representative of steel structures, the comparison between the two solutions becomes very poor indeed, see Fig 4.2.4.

For this analysis it is more representative to obtain the value for the driving point impedance of the beam from the modal solution, which is more representative of the behaviour of the structure, particularly at lower frequencies. This value of impedance can be determined from:

$$z = \frac{F}{i\omega w} \tag{4.2.21}$$

where w represents the displacement response of the beam at the point of excitation given by the modal solution described in section 4.2.2.

Using this improved value for the point impedance, the power input parameter used in energy flow solution is able to reflect the resonant behaviour of the structure and include the effects of damping. As a result there is significant improvement in the response estimates provided by the energy flow approach over the full frequency range, see Figs.4.2.3 and 4.2.4. This exercise highlights the fact that the quality of the predictions obtained by this approach is critically dependent on the power input parameter, P. If reliable estimates are to be obtained from an energy flow model, then a realistic value for this parameter must be provided.

So far only mean response at a particular frequency has been considered. Another aspect to be investigated is the ability of the model to predict the response profile along the length of the structure. Nefske and Sung (1987) showed that at a frequency of 10 kHz and with a damping loss factor of 0.2, the energy flow approach is able to predict the general shape of the response profile calculated by the modal technique. The corresponding result using the analysis presented here is shown in Fig.4.2.5 and compares well with the one published earlier by Nefske and Sung. It can be seen that the profile provided by the energy flow approach does indeed reflect the general pattern of the modal response over the majority of the beam. There are differences however, near to the supports and in the region of the excitation. These differences are due to the fact that the near-field components of the wave expressions, which become important near discontinuities, have been neglected in developing the energy flow modelling expressions. For this particular structure at a frequency of 10 kHz, near-field effects are only important in regions within 50 mm from a discontinuity. This explains the close agreement between the two solutions over the majority of the length of the beam.

The effects of this simplification become more evident at lower frequencies. Fig.4.2.6 shows a comparison between the energy flow and modal solutions at a frequency of 159 Hz. At this frequency near-field effects are important over the entire length of the beam and in the absence of this part of the solution, the energy flow approach cannot be expected to provide a close match to the modal response solution. Nevertheless the energy flow solution does provide a good estimate of the level of response. This explains the good general agreement between the mean response values obtained by the two solutions which is evident in Figs.4.2.3 and 4.2.4.

This investigation has shown that the energy flow solution provides a good indication of the mean energy level along the length of a beam structure over a wide frequency range. The ability of the approach to predict the shape of the response profile along the structure is dependent on the proportion of the beam which is strongly influenced by near-field effects. This proportion is reduced at higher frequencies leading to a subsequent improvement in results.

Despite the neglect of near-field effects this approach does provide a good estimate of the mean response of a structural component, even at low frequencies. This feature represents a potential advantage over SEA which can become very difficult to apply in the lower frequency regions.

4.3 Energy flow model of a real beam structure

In the previous section the energy flow approach was used to provide response predictions which compared well with those obtained from a modal superposition calculation. Confidence in the use of the energy flow approach would be further increased by comparing predictions from an energy flow model with measured levels of energy flow in a real beam structure. This would also enable the accuracy requirement for the parameters used as input to the model to be determined. With this in mind, energy flow measurements made along the length of a freely suspended perspex beam, shown schematically in Fig.4.3.1, will be compared with predictions provided by a representative energy flow model of this structure.

A beam was chosen for these comparisons because the nature of vibrational energy transmission in this type of structure is well understood. It is also possible to measure structural intensity in beams with confidence using well established accelerometer array techniques. Perspex was chosen as the beam material because of its relatively high level of material damping. This property serves to:

a) reduce reverberation in the structure which increases the reliability of the measurement technique.

b) ensure a marked reduction in the level of power flux along the length of the beam which will aid in assessing the ability of the model to accurately predict the effects of damping.

4.3.1 The energy flow model

The energy flow model used to represent the perspex beam is shown in Fig.4.3.2. In this model the energy provided by the shaker is represented by a power input, P, applied at the left hand-end of the beam. The boundary conditions for the model are expressed in terms of power flux, q. At the point of excitation, x=0, the power flux

entering the beam has a value of P/S, where S represents the cross-sectional area of the beam. At $x=L$, the fact that energy cannot flow away from a free end means that the power flux, q, must be equal to zero.

Earlier work has shown that the general solution for the energy density profile along the length of the beam is given by:

$$e(x) = A \cosh(\alpha x) + B \sinh(\alpha x) \tag{4.3.1}$$

where,

$$\alpha = \frac{\omega\eta}{2c_b} \tag{4.3.2}$$

Using the boundary conditions given in Fig.4.3.2 and the expression for power flux in the beam:

$$q(x) = - \frac{4c_b^2}{\eta\omega} \frac{de}{dx} \tag{4.3.3}$$

the unknowns A and B can be shown to be:

$$A = \frac{P\eta\omega}{4c_b^2\alpha S} \frac{\cosh(\alpha L)}{\sinh(\alpha L)} \tag{4.3.4}$$

and

$$B = - \frac{P\eta\omega}{4c_b^2\alpha S} \tag{4.3.5}$$

Substituting (4.3.4) and (4.3.5) into (4.3.1) gives:

$$e(x) = \frac{P\eta\omega}{4c_b^2\alpha S} \left\{ \frac{\cosh(\alpha x - \alpha L)}{\sinh(\alpha L)} \right\} \tag{4.3.6}$$

and using (4.3.3):

$$q(x) = -\frac{P}{S}\left\{\frac{\sinh(\alpha x - \alpha L)}{\sinh(\alpha L)}\right\} \qquad (4.3.7)$$

It can be seen that three parameters are required to evaluate the energy density and power flux profiles along the length of the beam, namely power input, P, damping loss factor, η, and phase velocity, c_b. In order to provide a representative model of this structure these quantities will be determined by experimental measurement.

4.3.2 Experimental arrangement

A schematic of the experimental setup is shown in Fig.4.3.3. The perspex beam is freely supported on flexible elastic cords to approximate free-free conditions. Excitation is provided by a shaker attached to the left-hand end of the beam. A force gauge and accelerometer are located at the shaker connection to measure the power input to the structure. Pairs of accelerometer mounting studs are located at 5 positions along the beam, marked A to E, to facilitate structural intensity measurements using an FFT-based frequency domain technique.

4.3.3 Power input measurement

In the frequency domain mechanical power at a point in the structure is given by the conjugate product (or cross-spectrum) of the Fourier transformed force and velocity values, ie:

$$p(f) = \{\, u(f) \,.\, F(f)^* \,\} \qquad (4.3.8)$$

where u and F are complex quantities and * indicates a complex conjugate.

Verheij (1980) showed that if mechanical power due to a point force is measured by a combination of a force gauge and an accelerometer, (4.3.8) becomes:

$$P(f) = \frac{1}{\omega}\,\mathrm{Im}\,\{X_{FA}\} \qquad (4.3.9)$$

where Im $\{X_{FA}\}$ represents the imaginary part of the cross-spectrum between the force gauge and accelerometer outputs. The measured power input is represented by P in keeping with the expressions obtained for the energy flow model described in section 4.3.1.

4.3.4 Damping loss factor measurement

The second parameter required by the energy flow model is a measure of the structure's ability to dissipate energy by damping. In previous chapters the damping parameter, η, has been defined to as the "hysteretic" or "material" damping loss factor. This quantity is purely a material property which characterises the energy loss within a volume of material due to the hysteretic relationship between stress and strain (see Cremer et al (1973) p.177).

If one considers the dissipation of energy within a structural component, as well as hysteretic effects, energy is also dissipated by other mechanisms such as friction and radiation. Moreover, these effects are often dependent on the nature of the response which may lead to some frequency dependence.

For practical purposes in most modelling work one generally considers the total dissipation of energy within a structural component due to the combined effects of the various damping mechanisms. A similar approach will also be adopted here for the development of an energy flow model to represent the perspex beam. For the purposes of this particular study the "structural" damping loss factor will be estimated using two experimental techniques, modal analysis and decay time measurement.

Modal analysis

Experimental modal analysis is a widely used technique for determining the natural frequencies and mode shapes of real structures. Most modal analysis software also provides an estimate of the modal damping loss factor at each natural frequency. De Clerk et al (1992) showed that a frequency dependent loss factor obtained by a power flow approach formed a smooth curve through the values obtained by modal analysis. It should therefore be possible to estimate loss factor over a frequency range by interpolation between modal values.

Modal analysis software was used to analyse measured frequency response data obtained at ten points along the perspex beam. This software provides an estimate of the modal damping loss factor, η_r , directly from its curve fitting algorithm. Excitation was provided using an impact hammer, rather than a shaker, to avoid any sources of damping which are external to the beam. The natural frequencies and modal loss factors obtained over a 0-2 kHz range are shown in Table 4.3.1 overleaf.

Bending mode number	Natural frequency (Hz)	Modal loss factor
1	15.5	0.088
2	*	*
3	93.2	0.067
4	152.0	0.054
5	226.4	0.050
6	319.3	0.048
7	422.7	0.049
8	539.4	0.058
9	680.2	0.050
10	822.0	0.046
11	977.5	0.045
12	1158.5	0.052
13	1340.0	0.040
14	1531.8	0.043
15	1737.0	0.035
16	1960.4	0.033

* not analyzed due to poor quality of measured data in this region.

TABLE 4.3.1

Decay time measurement

Norton and Greenhalgh (1986) discussed several methods for the estimation of frequency band averaged loss factors in lightly damped pipeline systems for use in SEA. One of these methods is the measurement of the time taken for band-filtered response to decay by 60 dB. Lyon (1976) showed that this 60 dB decay time, T_{60}, is related to the loss factor by:

$$\eta = \frac{2.2}{T_{60} f_i} \tag{4.3.9}$$

where f_i is the central frequency of the band of interest in Hz. Both texts suggest that this technique is more reliable in regions of high modal density and that a minimum of 5 modes should be present within the frequency band of interest.

Excitation was applied to the beam over a wide range of frequencies by a sharp hammer tap applied close to its mid-section. A high- and low-pass filter set was used

to obtain band-pass-filtered response data from accelerometers mounted at a number of positions along the beam. These filters were set up for the 7 frequency ranges listed in Table 4.3.2 below. These frequency ranges were chosen so that they each contain 5 modes, in line with the recommendations made by Norton and Greenhalgh (1986). Plots showing the decay of time domain response data were used to estimate a value of T_{60} in each frequency range of interest. The average loss factors obtained using equation (4.3.9), for each of the 7 frequency bands, are given in Table 4.3.2 below.

Frequency Band (Hz)	Centre Frequency (Hz)	Loss factor
0-250	125	0.028
100-500	300	0.031
200-700	450	0.017
400-1000	700	0.040
600-1400	1000	0.038
900-1800	1350	0.032
1100-2000	1550	0.039

TABLE 4.3.2

The values for η obtained by the two measurement techniques are compared in Fig.4.3.4. It can be seen that above 400 Hz the two sets of data compare well. At lower frequencies however, the comparison is not so good, although it should be noted that the time decay measurement technique was suggested for use with SEA which is normally employed in the higher frequency ranges.

The results of these measurements suggest that a reasonable estimate for a structural damping loss factor for this beam would be between 0.035 and 0.055 over most of the frequency range. A blanket value of 0.045 will be used as an initial estimate for the energy flow model.

4.3.5 Phase velocity

The phase velocity for a beam in flexure is given by:

$$c_b = \sqrt[4]{\frac{EI\omega^2}{\rho S}} \tag{4.3.10}$$

Density, ρ, for perspex is given as 1200 kg/m^3 in the material data supplied by the manufacturer. Values for the Young's modulus, E, are not so readily available. For the purposes of this analysis E can be obtained by matching analytical modal solutions, giving the natural bending frequencies of a beam, to the results obtained by the experimental modal analysis.

Bishop and Johnson (1960) showed that the natural frequencies of a free-free beam can be calculated from:

$$\omega_r = \left(\frac{\lambda_r L}{L}\right)^2 \left(\frac{EI}{\rho S}\right)^{1/2} \tag{4.3.11}$$

where

$\lambda_1 L = 4.730$ $\quad$ $\lambda_4 L = 14.137$

$\lambda_2 L = 7.853$ $\quad$ $\lambda_5 L = 17.279$

$\lambda_3 L = 10.996$ $\quad$ $\lambda_{>5} L = (r+½)\pi$

Using the measured natural frequencies of modes 3 to 8 and equation (4.3.11) above, the calculated values of E for the perspex beam are given in Table 4.3.3 below.

Mode Number	Frequency (Hz)	E (GN/m^2)
3	93.2	5.39
4	152.0	5.31
5	226.4	5.25
6	319.3	5.42
7	422.7	5.36
8	539.4	5.29

TABLE 4.3.3

The average of these E values is 5.34 GN/m^2 and will be used for the energy flow model.

4.3.6 Structural intensity measurements

Predictions provided by the energy flow model will be compared with measured energy flow obtained by a structural intensity measurement technique. Pavic (1976) showed that structural intensity in the far-field of a beam can be measured using two accelerometers mounted a small distance apart on its surface. This approach employs a finite difference approximation which allows rotational components of the motion to be estimated by translational measurements on either side of the point of interest.

This technique is only accurate when measurements are made at locations far enough away from discontinuities for near-field effects to be neglected. This is because a two-accelerometer technique can only provide a measure of the moment component of vibrational power. In the far-field however, the total power can be evaluated from this single component because the shear and moment components are equal.

Verheij (1980) showed that for frequency domain measurements the structural intensity in the far-field of a beam can be obtained from:

$$p(f) = - \frac{2\sqrt{EI\rho S}}{\Delta\omega^2} \, \mathrm{Im}\{X_{21}\} \qquad (4.3.12)$$

where Im $\{X_{21}\}$ represents the imaginary part of the cross-spectrum between the outputs of two accelerometers fixed a small distance Δ apart on the beam.

It is evident from equation (4.3.12) that structural intensity is related to the phase difference between the two accelerometer signals which is quantified by the imaginary part of the cross-spectrum. Measurement of this imaginary component has been a source of difficulty for practitioners employing this technique, particularly for lightly

damped structures. This is because when damping levels are low the phase difference between motion at two closely spaced points on a beam may be comparable with the phase tolerance of the transducers and signal conditioning equipment. As a result, accurate measurement of the imaginary part of the cross-spectrum becomes very difficult.

A number of techniques have been proposed to overcome this inherent phase error, some of which are described in detail by Linjama and Lahti (1989). The most straightforward of these, when only two accelerometers are involved, is known as "switching". This method consists of obtaining the cross-spectrum between the two accelerometers and then switching their position to obtain a second measurement. Averaging these results eliminates the effects of inherent phase differences between the two transducers. Care must be taken to ensure that the accelerometers are located at exactly the same positions on the beam during the two measurements. For this reason stud-mounted accelerometers were employed in these experiments.

A second source of error inherent in these measurements is due to the finite difference approximation used to derive equation (4.3.12). Troshin et al (1990) showed that the error involved in the measurement of the moment component of intensity, ε_M, is:

$$\varepsilon_M = 1 - \frac{\sin(k\Delta)}{k\Delta}\left[\frac{\sin(k\Delta/2)}{k\Delta/2}\right]^2 \qquad (4.3.13)$$

where k represents the bending wavenumber for the beam and Δ is the accelerometer spacing. For a given structure and accelerometer spacing, this error increases quite dramatically with frequency.

Structural intensity measurements were made at 300 mm intervals along the beam, at locations marked A to E on Fig.4.3.3. The accelerometer spacing, Δ, was chosen as 30 mm which gives rise to a 9% finite difference error at 1000 Hz. Phase errors in the cross-spectrum were removed using the switching technique described earlier.

Because these measurements are to be used as a datum for comparison with model predictions, measurements were limited to the 0-1 kHz frequency range so that finite difference errors remain below 10%.

4.3.7 Results and discussion

The objective of this exercise is to match predicted levels of vibrational power to those obtained experimentally. Before doing this however, it would be useful to look at the experimental results to check that they are of a sensible nature. Fig.4.3.5 shows the power input and structural intensity measurements obtained along the beam. It can be seen that each measurement downstream of the power input indicates a general reduction in power level caused by the dissipation of energy by damping. This type of result is to be expected and suggests that the structural intensity measurements obtained here should provide a good datum against which to compare model predictions.

Figs.4.3.6 to 4.3.10 show comparisons between the structural intensity measurement at positions A to E and the prediction for vibrational power at these points given by the energy flow model. It can be seen that throughout this series of results the model gives predictions which are very close to the measured results over the majority of the frequency range.

Some differences in the form of the spectra can be observed below about 100 Hz. This can be explained by the fact that the two-accelerometer structural intensity technique is only accurate at points in the beam where near-field effects can be neglected. It was shown in section 3.4.2 that the distance required for near-field effects to decay is dependent on the wavelength of the motion, which in turn is related to frequency. At lower frequencies the near-field region requires a greater distance to decay and a smaller proportion of the beam is subject to true far-field conditions. This effect leads to some fluctuation in the structural intensity measurements at lower frequencies which is particularly evident in these results below 100 Hz. The form of the energy flow spectra provided by the model is the same at all points along the beam because these are related to the power input measurement which is not affected

by the far-field assumption.

It has generally been accepted that accurate measurements of the damping level within a structure are difficult to obtain. It is evident from Fig.4.3.5 that there is a significant reduction in power flowing along the beam due to structural damping. The fact that the model predictions are able to reflect this reduction accurately at each point shows that the model is able to represent this behaviour adequately and that the loss factor estimate used here is of sufficient accuracy to give a representative prediction. To get an idea of the degree of accuracy required for this damping factor, energy flow predictions have been calculated for different values of η. Fig.4.3.11 shows that variation of the value of η between 0.01 and 0.1 does not cause the result to deviate much from the one obtained using the estimated value of 0.045. The effects of greater variation are shown in Fig.4.3.12. At these relatively low levels of damping, a gross underestimation of η (by a factor of 10), does not greatly affect the energy flow prediction when plotted on a log scale. However, if the loss factor is set to a very high value, eg. 0.45, the energy flow model provides a very poor prediction. This exercise suggests that for this particular structure, with the levels of damping present, an order of magnitude estimate of the damping level is adequate. This level of accuracy is well within the capability of the two damping measurement techniques employed here.

Although a relatively simple structure was chosen for this piece of work it must be remembered that the main object of this exercise was to assess the ability of the modelling approach to predict the level of vibrational energy flow in a real structure. Excellent agreement has been obtained between measurement and prediction which provides confidence for the extension of this approach to the analysis of more complex structures. It is important to note however, that good model predictions can only be obtained if the model is provided with representative values for the modelling parameters, in this case power input and damping loss factor. It is also worth noting that the upper frequency limit for these comparisons was dictated by the limitations of the measurement technique rather than the validity of the model. Previous work suggests that at higher frequencies this type of model should provide an even better

representation of the dynamics of a structure.

4.4 Summary

This chapter describes the application of the continuum energy flow approach to provide representative models of beam structures. The main points arising from these investigations are as follows.

1. The simplified nature of the energy flow approach gives rise to a smoothed estimate of the energy profile along the length of the beam structure. At high frequencies this profile compares well with response profiles predicted by exact solutions. At lower frequencies the response estimate represents a good mean value of response. The analysis is unable to describe the response of the structure close to boundaries and other discontinuities because near-field effects have been neglected in the development of the equations governing the approach .

2. The far-field structural intensity technique provides sensible measurements of the vibrational power levels at points along a beam structure. In order to interpret these measurements correctly the problems of transducer phase mismatch and frequency limitations imposed by the finite difference approximations must be fully understood.

3. An energy flow model was able to provide very good predictions of the power levels at a number of points in the beam provided that good estimates of power input and beam properties were supplied to the model. In particular this analysis showed that the model was able to accurately reflect the effects of damping on energy flow levels along the beam.

4. A sensitivity study on the accuracy requirement of the damping parameter showed that experimental modal analysis can provide damping estimates of sufficient accuracy for use with this modelling technique.

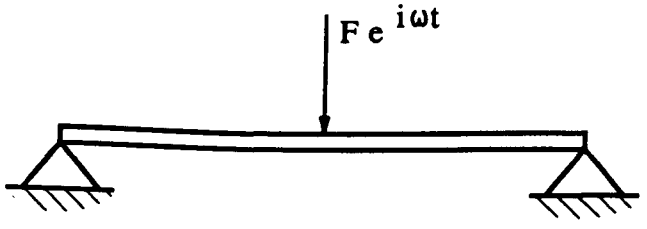

Length = 1.2 m
Depth = 10.3 mm
Width = 10 mm

Young's modulus = 209 x 10^9 N/m ^{2}
Density = 7800 kg/m ^{3}

Fig.4.2.1 Simply supported beam structure

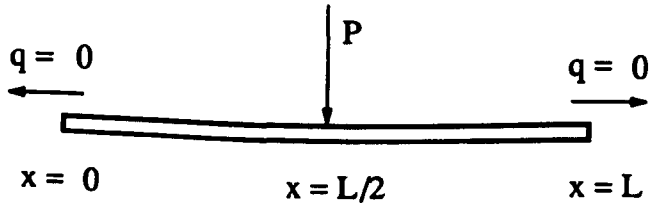

Fig.4.2.2 Energy flow model

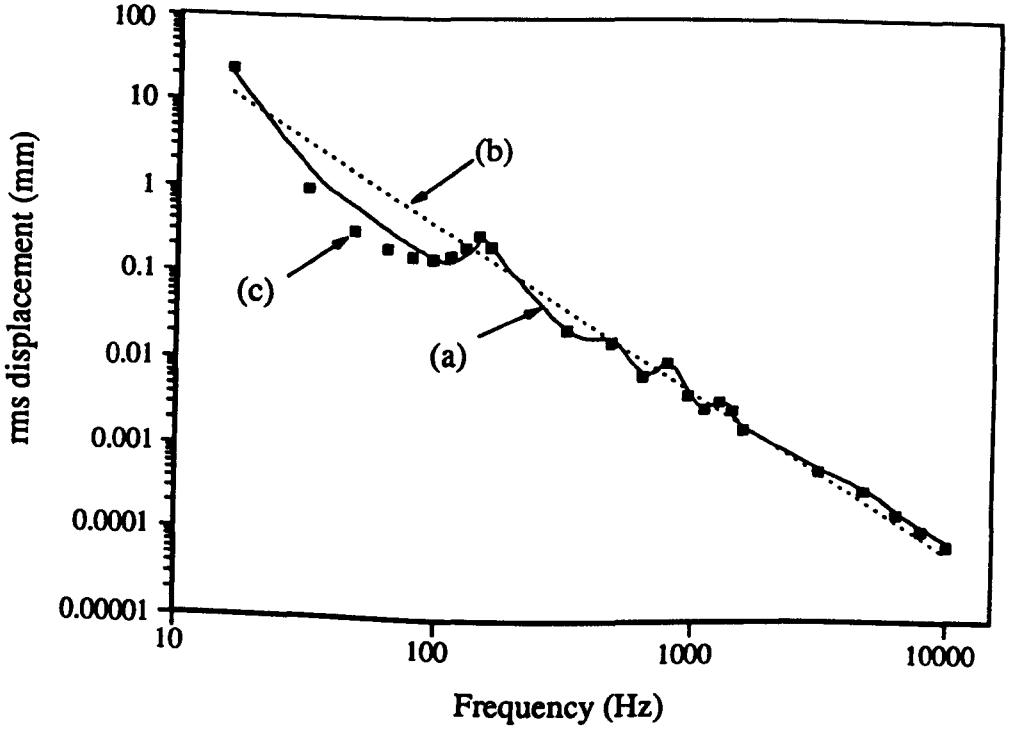

Fig.4.2.3 Mean displacement values for the beam with a loss factor of 0.2

a) modal solution

b) energy flow solution using the infinite beam impedance value

c) energy flow solution using impedance obtained from the modal solution

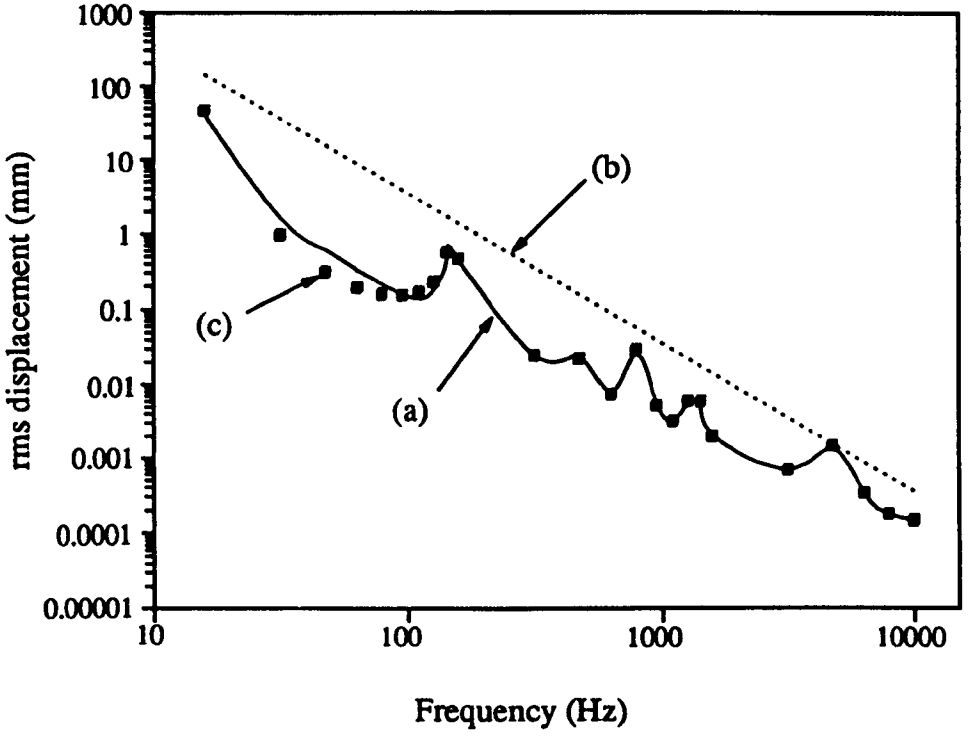

Fig.4.2.4 Mean displacement values for the beam with a loss factor of 0.02

a) modal solution

b) energy flow solution using the infinite beam impedance value

c) energy flow solution using impedance obtained from the modal solution

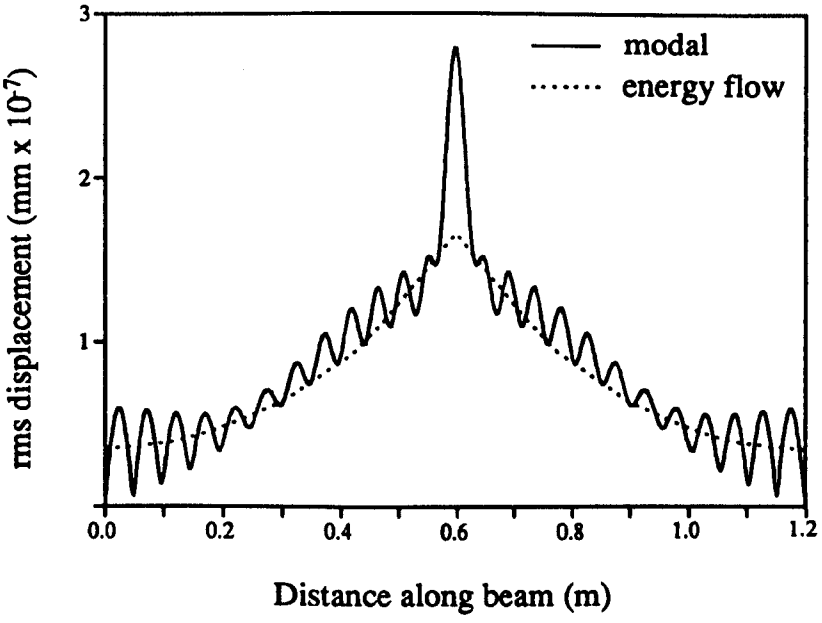

Fig.4.2.5 Rms displacement profile along the beam at 10 kHz (between modes 23 and 24) with a loss factor of 0.2

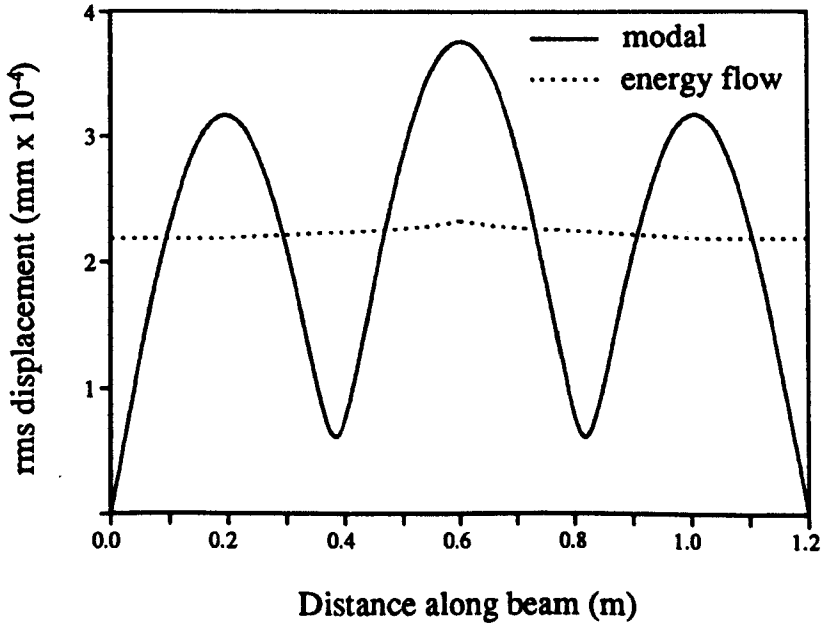

Fig.4.2.6 Rms displacement profile along the beam at 159 Hz (close to mode 3) with a loss factor of 0.2

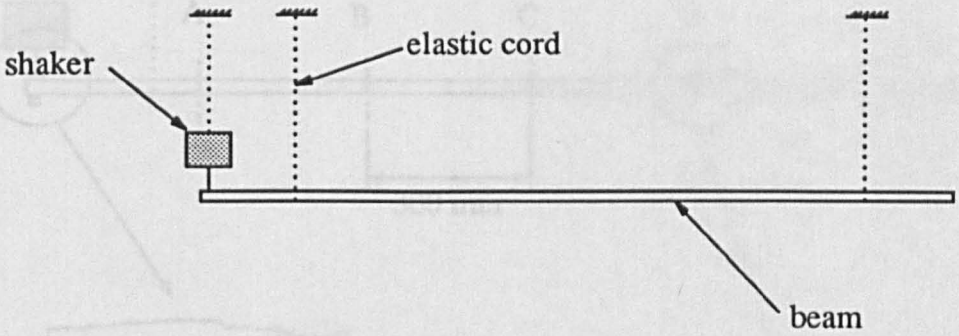

Fig.4.3.1 Perspex beam arrangement

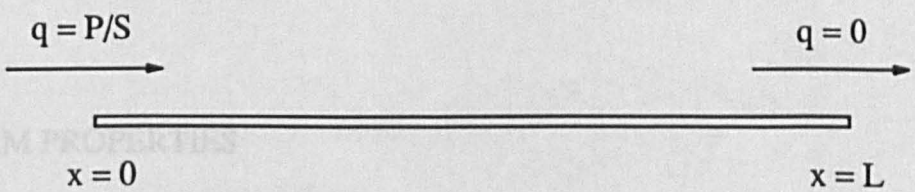

Fig.4.3.2 Energy flow model for the suspended beam structure

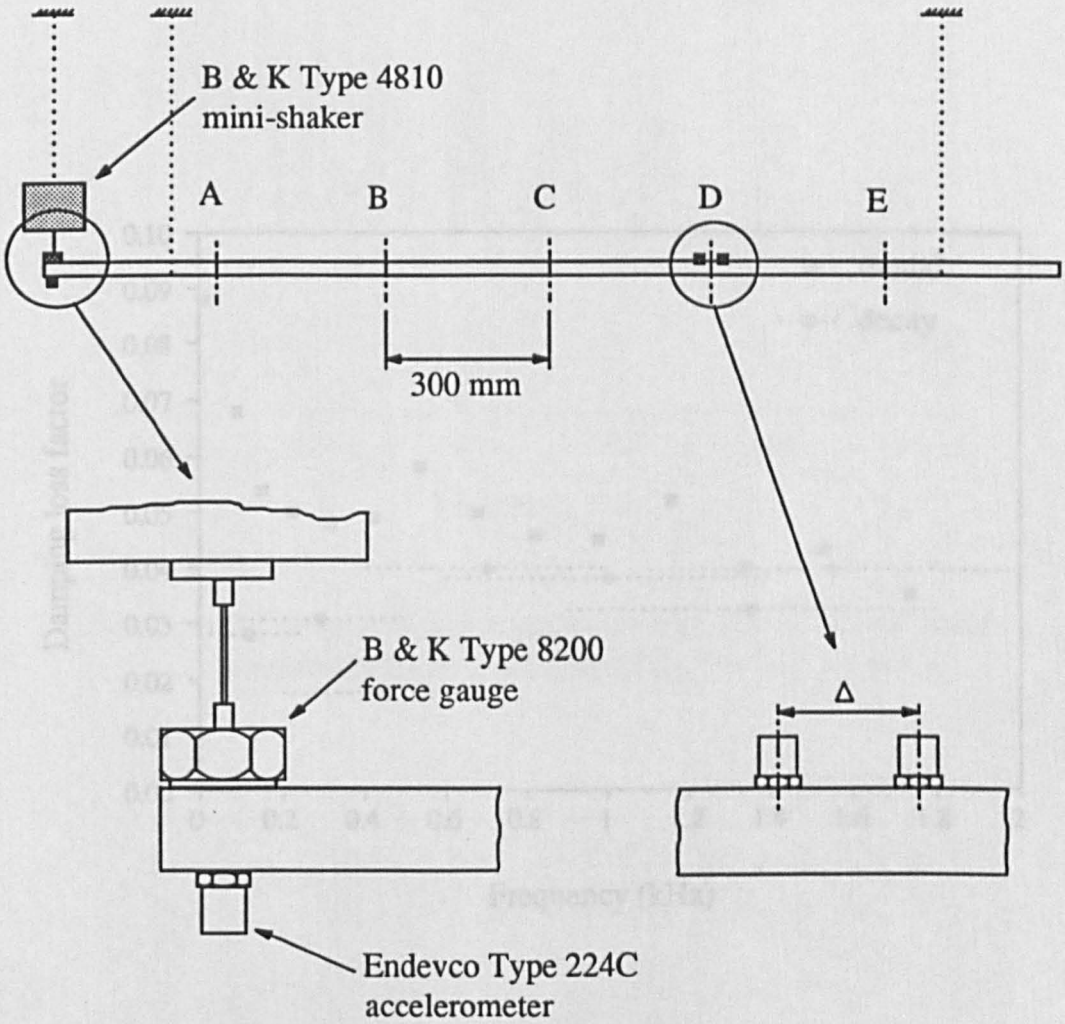

BEAM PROPERTIES

length = 1.8 m

section = 25.4 mm x 25.4 mm

density = 1200 kg/m ^{3}

Δ = 30 mm (nominal)

Fig.4.3.3 Transducer arrangement and beam properties

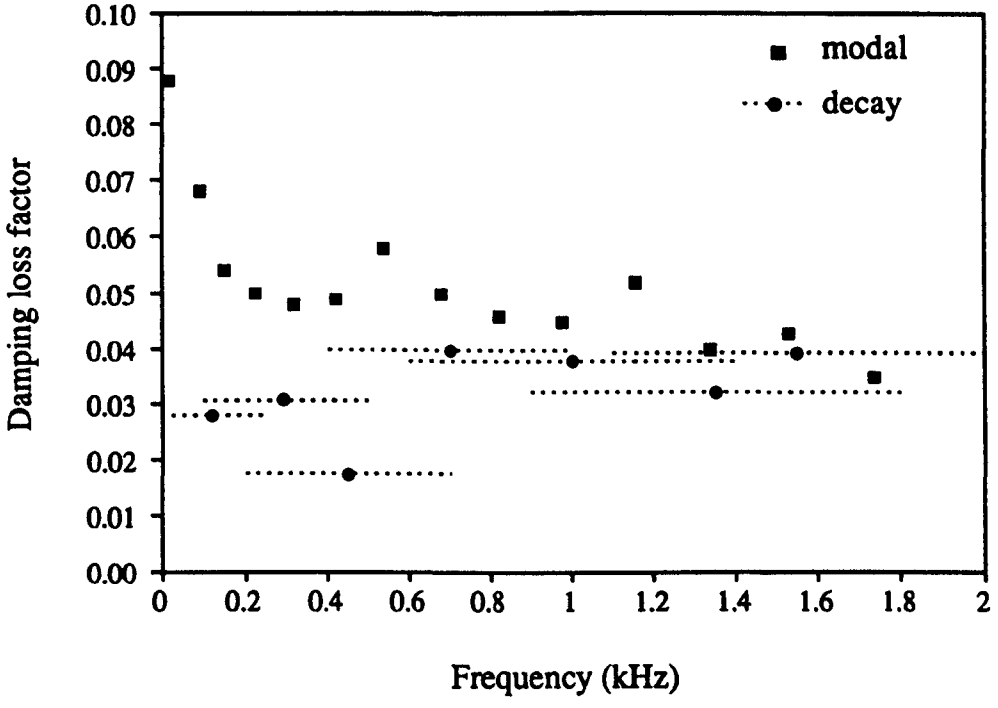

Fig4.3.4 Comparison between measured damping loss factors for the perspex beam obtained by:

a) modal analysis

b) decay time measurement

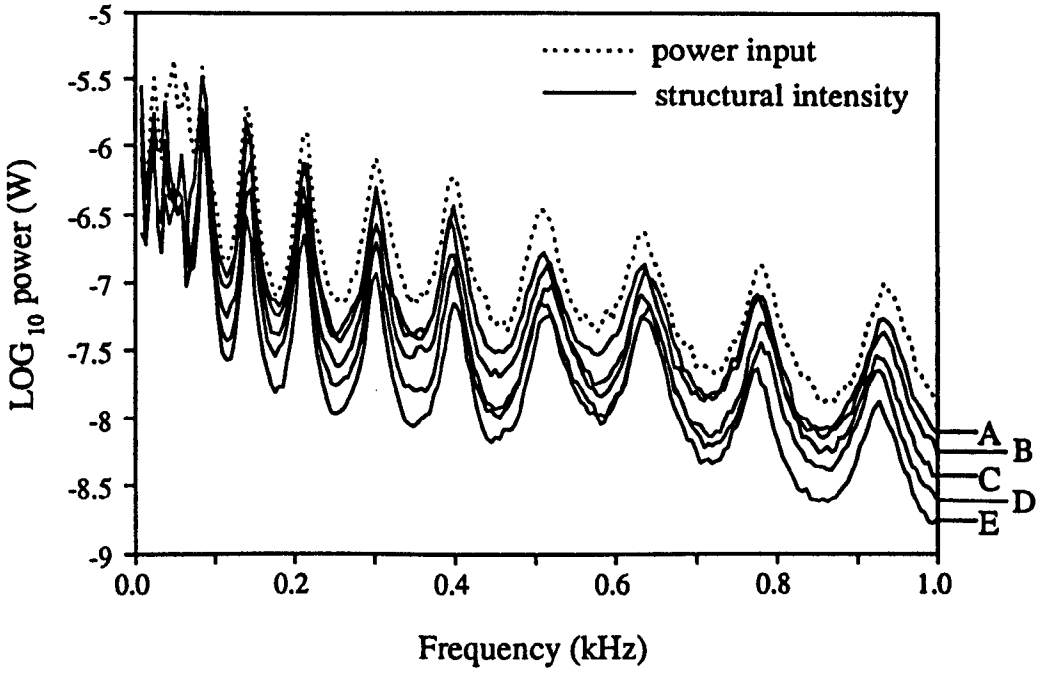

Fig.4.3.5 Comparison between power input and successive structural intensity measurements made along the perspex beam

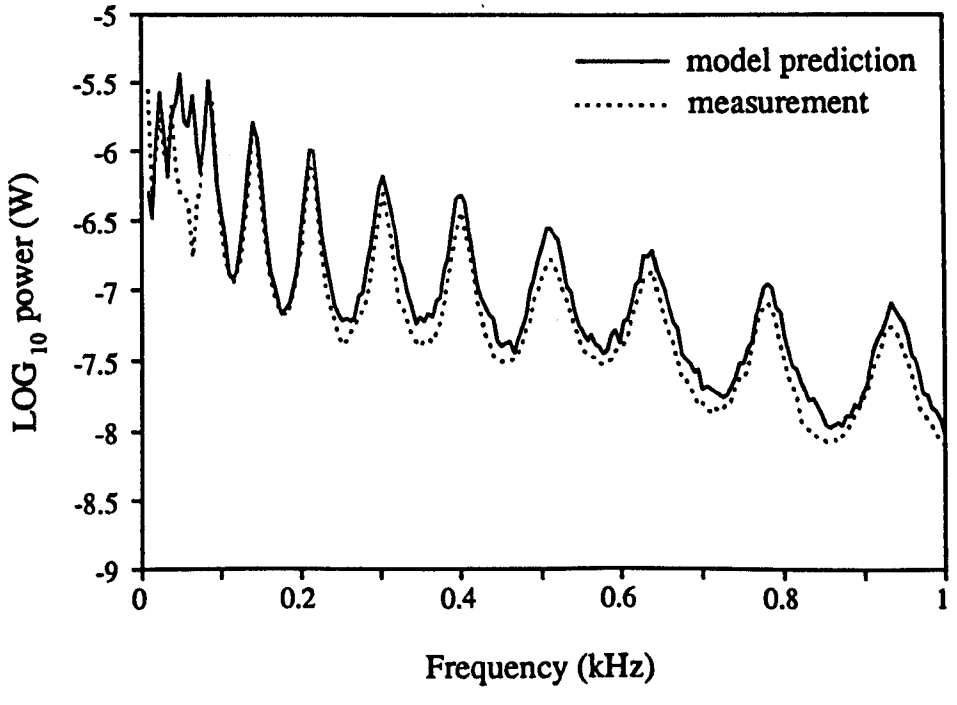

Fig.4.3.6 Comparison between structural intensity measurement and model prediction at point A

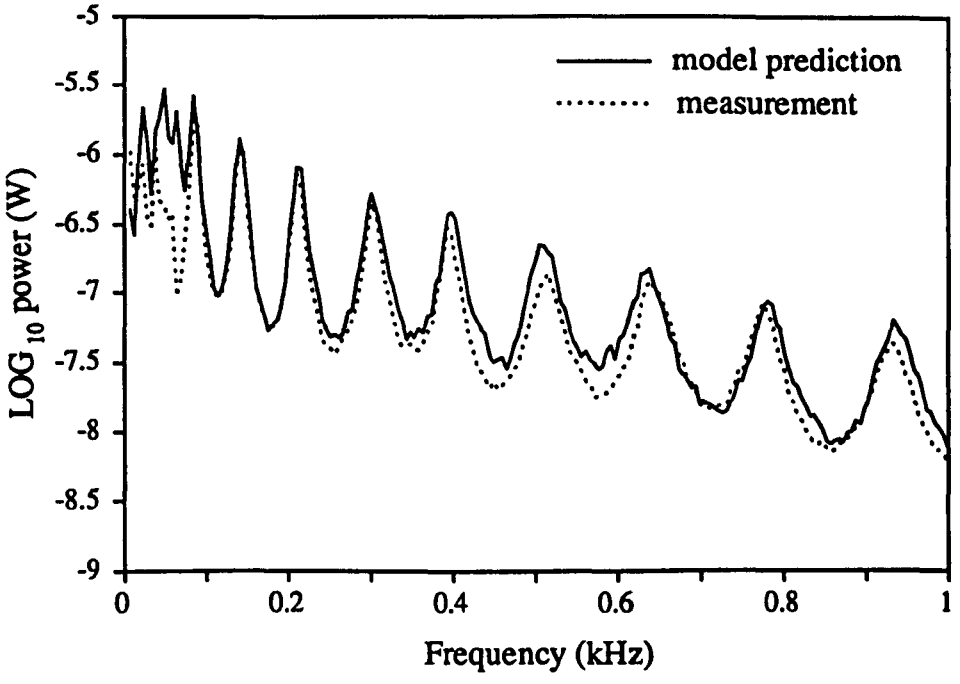

Fig.4.3.7 Comparison between structural intensity measurement and model prediction at point B

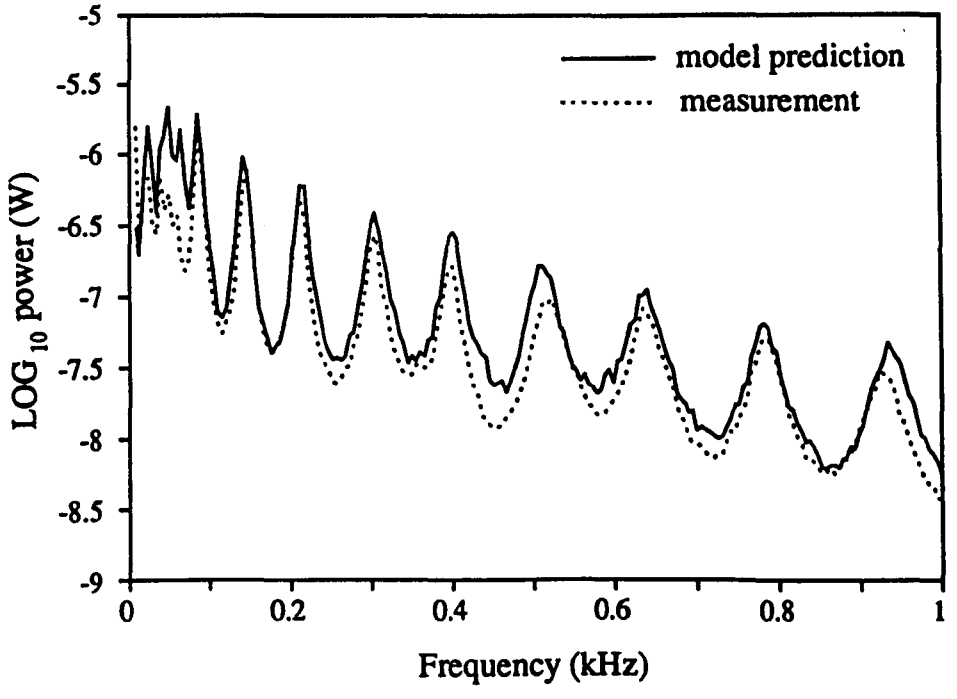

Fig.4.3.8 Comparison between structural intensity measurement and model prediction at point C

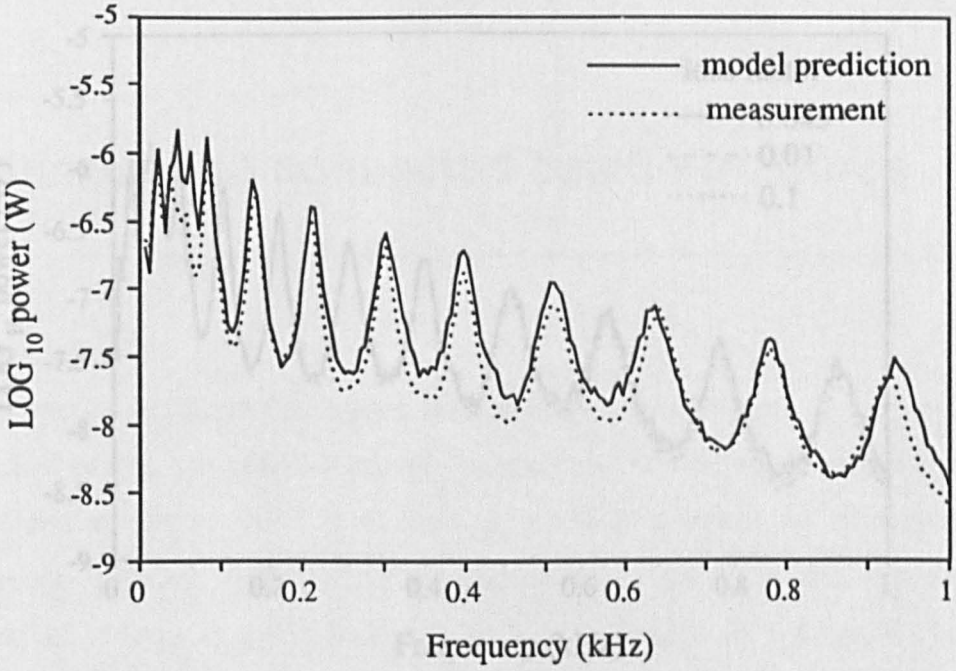

Fig.4.3.9 Comparison between structural intensity measurement and model prediction at point D

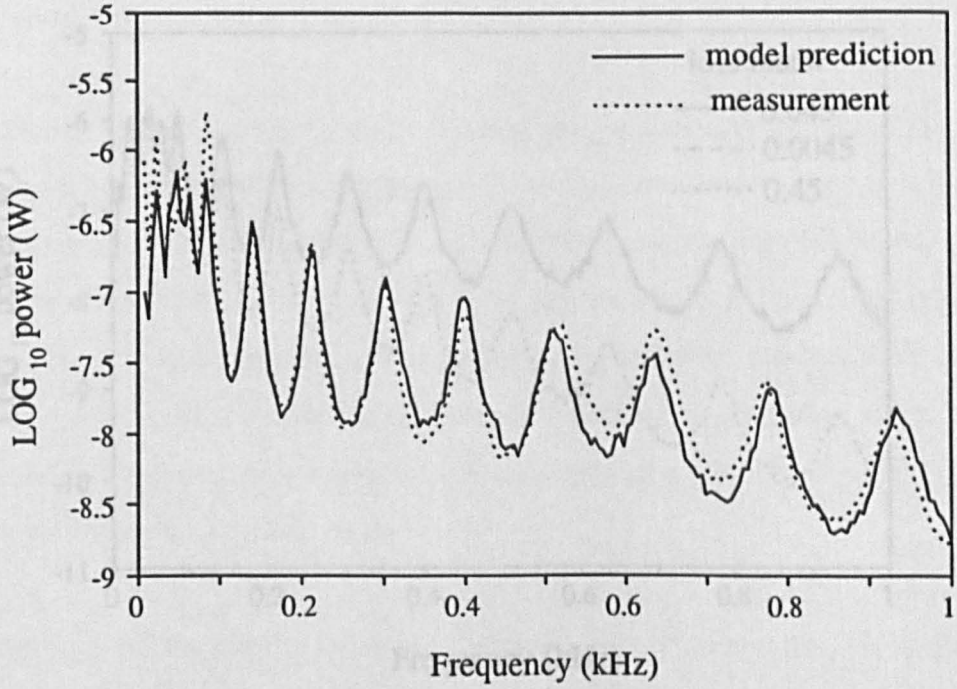

Fig.4.3.10 Comparison between structural intensity measurement and model prediction at point E

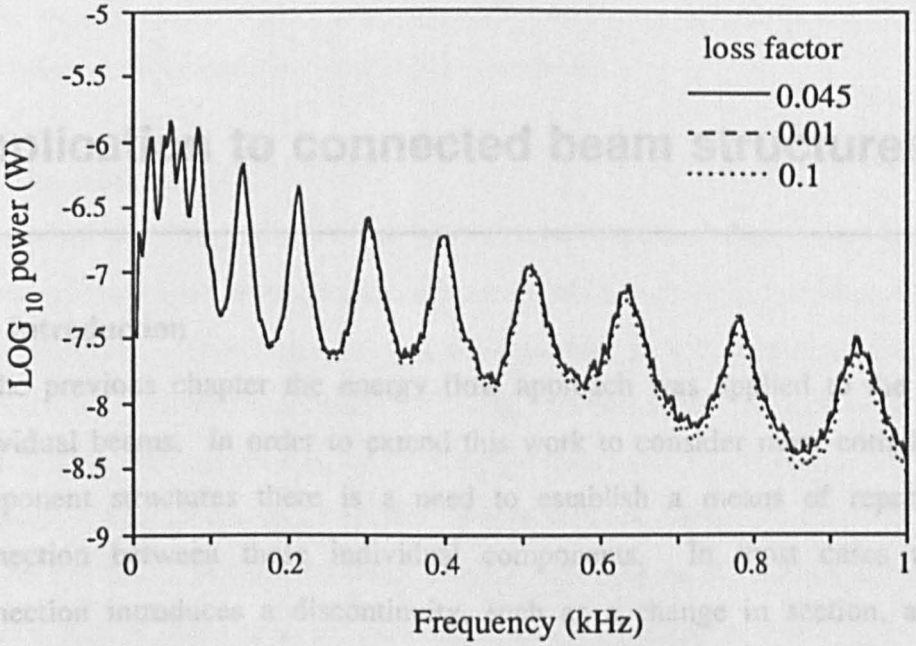

Fig.4.3.11 Effect of small variation in loss factor value on model prediction at point E

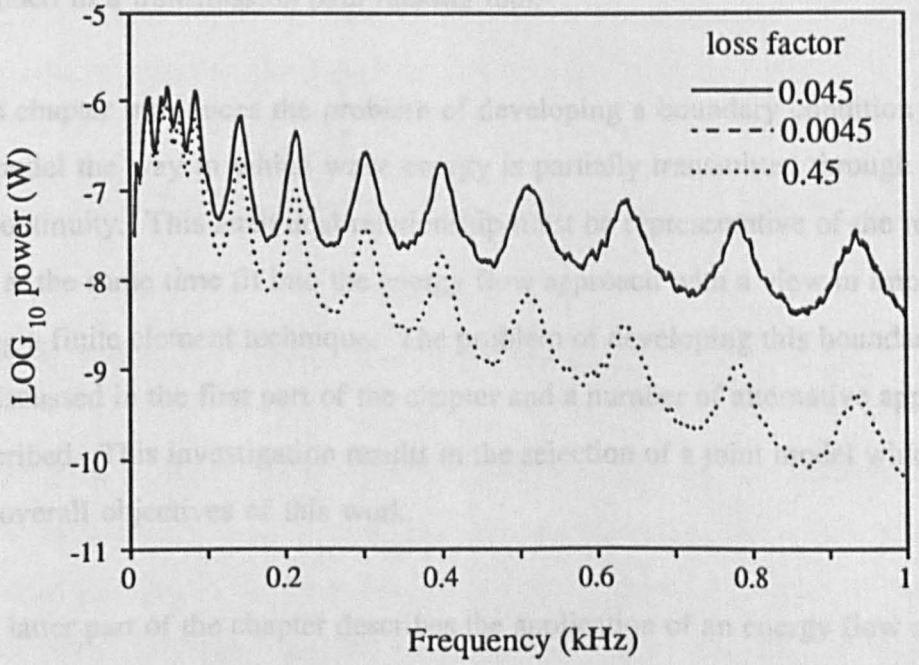

Fig.4.3.12 Effect of large variation in loss factor value on model prediction at point E

Chapter 5

Application to connected beam structures

5.1 Introduction

In the previous chapter the energy flow approach was applied to the analysis of individual beams. In order to extend this work to consider more complex multiple component structures there is a need to establish a means of representing the connection between these individual components. In most cases a structural connection introduces a discontinuity, such as a change in section, a change in material properties, the presence of a flange or a bend. These discontinuities often give rise to partial reflection of incident wave energy which leads to a reduction in *net* energy flow through the structure. These partial transmission characteristics are an important feature of the *global* transmission properties of the structure and must be included in a transmission path ranking tool.

This chapter introduces the problem of developing a boundary condition that is able to model the way in which wave energy is partially transmitted through a structural discontinuity. This analytical relationship must be representative of the real situation and at the same time fit into the energy flow approach with a view to implementation using a finite element technique. The problem of developing this boundary condition is discussed in the first part of the chapter and a number of alternative approaches are described. This investigation results in the selection of a joint model which best suits the overall objectives of this work.

The latter part of the chapter describes the application of an energy flow model to the analysis of a structure consisting of two beams connected by a flanged joint. A major component of this work is the experimental determination of the transmission efficiency across the flange using a wave decomposition approach. This case study

serves to assess the ability of the energy flow approach to provide a representative model of a real connected beam structure and provides further examples of the evaluation of representative modelling parameters.

5.2 The joint model

The overall objective of this work is to develop a general design tool which utilises the energy flow approach and takes advantage of its potential to be implemented using finite elements. This criterion will be important in the selection of a scheme to represent the connection between individual sub-structures. A number of approaches have already been proposed by previous investigators to provide a joint boundary condition for inclusion in an energy flow model. A discussion of these approaches will be presented in the following section, resulting in the development of a joint model which is best suited for adaptation into finite element form.

5.2.1 The joint boundary condition

The analysis of connected structures and the nature of the required joint boundary condition can be illustrated using the simple two beam energy flow model shown in Fig.5.2.1. According to the analysis for a single beam described in section 4.2.1, the energy density profile along each section of beam is of the form:

$$e_m(x) = A_m \cosh(\alpha_m x) + B_m \sinh(\alpha_m x) \qquad m = 1,2 \qquad (5.2.1)$$

where A_m and B_m are unknowns and α_m is given by equation (4.2.5).

The solution to this problem requires the determination of four unknowns which can be obtained using boundary conditions prescribing power flux values at each end of the beam sections, as shown in Fig.5.2.2. For this model it is assumed that the values for the power flux entering beam 1, $q_{1\,in}$, and leaving beam 2, $q_{2\,out}$, are known. These provide the first two boundary conditions.

The third boundary condition can be developed by assuming conservation of energy across the joint. Assuming that no energy is lost in the joint, an energy balance across it becomes:

$$p_{joint} = q_{1\ out}\ S_1 = q_{2\ in}\ S_2 \qquad (5.2.2)$$

where S_1 and S_2 are the cross-sectional areas of beams 1 and 2 respectively.

To establish the fourth boundary condition it is necessary to determine the rate of energy flow across the joint, denoted p_{joint}. Previous investigators have approached this problem in a number of ways. Some of these will be described in the following sections.

Wohlever

Wohlever (1988) described two approaches for the determination of the rate of energy transfer across a joint in connected rod and beam structures. The first required the use of mobility expressions which are dependent on the nature of the structural components and the type of connection concerned. Using these mobilities it is possible to establish an expression for the flux crossing the joint in terms of the power input to the structure. This approach has the advantage that it is able to take account of the modal behaviour of the structure which has an effect on the level of energy flow across the joint. The form of the expressions developed using this approach however, were too complex for adaptation into finite element form.

A second approach employed by Wohlever involved the development of an SEA model of the structure which provided the energy flow between sub-systems given knowledge of the coupling loss factor at the joint. Under these circumstances, the use of an SEA model seems rather contrary to the aim of the development of a model based on the energy flow approach. It is also evident that, like the previous method, this approach does not provide a boundary condition which is suitable for implementation using a finite element technique.

Nefske and Sung

In their earlier work Nefske and Sung (1987) proposed an alternative expression for the boundary condition at the joint which fits more readily into a finite element formulation. In this approach they considered the *net power* transfer across the joint as the algebraic sum of the power entering from each side, see Fig.5.2.3. Using this approach they showed that:

$$p_{joint} = p_{12} - p_{21} \tag{5.2.3}$$

The transmissive properties of a structural discontinuity are often described using its transmission efficiency, τ. This quantity is defined as the ratio of the wave power transmitted through a discontinuity to the wave power incident to it. Cremer (1973) showed that in an infinite structure, local energy density can be related to vibrational power by:

$$p = c_g \, S \, e \tag{5.2.4}$$

Using this expression, together with the definition of transmission efficiency, Nefske and Sung proposed that the energy flow across the joint could be obtained from:

$$p_{joint} = \tau_{12} \, c_{g1} \, S_1 \, e_1 - \tau_{21} \, c_{g2} \, S_2 \, e_2 \tag{5.2.5}$$

and assuming reciprocity at the joint, ie. $\tau_{12} = \tau_{21} = \tau$, (5.2.5) becomes:

$$p_{joint} = \tau \, (\, c_{g1} \, S_1 \, e_1 - c_{g2} \, S_2 \, e_2 \,) \tag{5.2.6}$$

Cho and Bernhard

A similar analysis was carried out by Cho and Bernhard (1992), although in this case they considered the conditions in the beam sections on either side of the joint. This analysis also employed equation (5.2.4) which relates local energy density and power flux. In this case however, they justified the use of this relationship because, on a frequency-averaged basis, the response of a finite structure approaches that of a similar structure of infinite extent.

In this approach one considers the connection between two semi-infinite beams where the incident waves approaching from each side of the joint are both partially reflected and partially transmitted across it, see Fig.5.2.4. Using the definition of transmission efficiency and assuming reciprocity at the joint, the *net* vibrational energy flow away from the joint in each direction can be shown to be:

$$q_1^- = (1-\tau)\, q_1^+ + \tau\, q_2^- \tag{5.2.7}$$

and

$$q_2^+ = \tau\, q_1^+ + (1-\tau)\, q_2^- \tag{5.2.8}$$

It is important to note the $(1-\tau)q$ terms which represent a proportion of the incident energy which is reflected back by the discontinuity. This aspect was not properly dealt with in Nefske and Sung's earlier model.

From this point Cho and Bernhard went on to establish relationships required for the analysis of an angled beam structure, which included the effects of conversion between flexural and longitudinal motion. Here, equations (5.2.7) and (5.2.8) will be used as the starting point for the development of a more general boundary condition to describe the power transfer across the joint, similar in form to equation (5.2.6). The important feature of this expression is that it lends itself to inclusion in a finite element formulation.

This study

It follows from (5.2.7) and (5.2.8) that the *net* vibrational power transmitted away from the joint in each direction is:

$$p_1^- = (1-\tau)\, S_1\, q_1^+ + \tau\, S_2\, q_2^- \tag{5.2.9}$$

and

$$p_2^+ = \tau\, S_1\, q_1^+ + (1-\tau)\, S_2\, q_2^- \tag{5.2.10}$$

The total power at a point in beam 1, close to the joint, is:

$$p_1 = p_1^+ - p_1^- \tag{5.2.11}$$

and similarly

$$p_2 = p_2^+ - p_2^- \tag{5.2.12}$$

Assuming that the relationship between the local energy density and power flux given in equation (5.2.4) holds for the power flux in each direction, it follows that:

$$q^+ = c_g e^+ \qquad \text{and} \qquad q^- = c_g e^- \tag{5.2.13}$$

Using (5.2.9), (5.2.10) and (5.2.13), expressions (5.2.11) and (5.2.12) become:

$$p_1 = p_2 = \tau (S_1 c_{g1} e_1^+ - S_2 c_{g2} e_2^-) \tag{5.2.14}$$

By definition

$$e_1 = e_1^+ + e_1^- \tag{5.2.15}$$

and

$$e_2 = e_2^+ + e_2^- \tag{5.2.16}$$

Using (5.2.7), (5.2.8) and (5.2.13) these can be expressed as:

$$e_1 = (2-\tau)\, e_1^+ + \frac{\tau S_2 c_{g2}}{S_1 c_{g1}} e_2^- \tag{5.2.17}$$

and

$$e_2 = \frac{\tau S_1 c_{g1}}{S_2 c_{g2}} e_1^+ + (2-\tau)\, e_2^- \tag{5.2.18}$$

Solving (5.2.14), (5.2.17) and (5.2.18) simultaneously gives:

$$p_{joint} = p_1 = p_2 = \frac{\tau}{2(1-\tau)} \left(S_1 c_{g1} e_1 - S_2 c_{g2} e_2 \right) \qquad (5.2.19)$$

This relationship has the same general form as Nefske and Sung's boundary condition (5.2.6), but differs by the denominator term $2(1-\tau)$. This difference occurs because the reflected component of power at the joint was not properly included in the earlier formulation by Nefske and Sung. The consequences of this omission will be illustrated in the following section.

5.2.2 Connected beam energy flow model

The solution to the boundary condition problem related to a two beam energy flow model is provided in Appendix B. This solution will be used to illustrate the consequences of adopting Nefske and Sung's joint boundary condition for use in an energy flow model. The form of the energy flow model, together with the beam dimensions and material properties are shown in Fig.5.2.5.

The fundamental problem with expression (5.2.6) is that it implies that there must always be an energy difference across the joint to sustain power transmission, even if $\tau=1$. This is intuitively incorrect because a total transmission condition across the joint implies that the beam should be effectively continuous and that a step in the energy level across it should not exist. The magnitude of this error can be examined by comparing the results of the two beam model, with τ set to unity, to those obtained from a continuous beam model of identical dimensions. Fig.5.2.6 shows this comparison at a frequency of 1000 Hz and damping loss factor of 0.01. The remaining parameters for this analysis are given in Fig.5.2.5. Here the energy step at the joint is clearly illustrated, together with the magnitude of the error in both the energy density and power flux profiles. Although these errors are relatively small under these conditions the difference between the two solutions becomes larger with an increase of either frequency or damping, as illustrated in Figs.5.2.7 and 5.2.8.

This error is eliminated if (5.2.19) is used as the boundary condition across the joint. In this expression, as τ tends towards unity the quotient in front of the brackets tends to infinity and in the limit, the energy difference across the joint becomes infinitesimally small. The solution thus approaches that for a continuous beam. This has been proved using the solution to the connected beam problem provided in Appendix B with a τ value set to 0.999. Under these conditions the jointed model provides results which are indiscernible from those obtained from the continuous beam solution.

This discussion has outlined a number of approaches used by previous investigators to model the effects of structural discontinuities within the energy flow approach. The earlier approaches which rely on mobility expressions or the development of an SEA model cannot be easily incorporated into a finite element technique. The alternative approaches which relate the power transmission across the joint to the difference in energy density between the connected sections provide simpler expressions which can be more readily adapted into a finite element form. Of these, the original proposal by Nefske and Sung fails to satisfy the physics of the problem which is highlighted when the transmission efficiency value is close to unity. The improved expression, based on the work by Cho and Bernhard, is intuitively correct and although still relatively simplified, incorporates the general effects of partial reflection at the joint. This model will therefore be adopted for use within this work.

5.3 Energy flow model for a real connected beam structure

The previous section developed an energy flow model for a general connected beam structure. In order to test this approach the predictions obtained from this type of model will be compared with measured results obtained from a real structure.

The structure chosen for this study consists of two beams, one steel the other aluminium, connected by a bolted flange joint, see Fig.5.3.1. Each beam is 1.5 m long and has a cross-section of 16.5 mm x 16.5 mm. Excitation is provided by a shaker sited at the free end of the steel beam. The free end of the aluminum beam is buried in sand to provide an energy sink. This sand termination results in an

increase in the level of vibrational energy flow along the beam and reduces reverberation. Both these factors lead to improvement in the quality of structural intensity measurements.

5.3.1 The energy flow model

The energy flow model used to represent the connected structure described above is shown in Fig.5.3.2. In accordance with the theory for a single beam structure developed in Chapter 4, the energy density and power flux profiles along each beam are given by:

$$e_m(x) = A_m \cosh(\alpha_m x) + B_m \sinh(\alpha_m x) \tag{5.3.1}$$

and

$$p_m(x) = - \frac{4\, c_{b\,m}^2 S_m \alpha_m}{\eta_m \omega} \left\{ A_m \sinh(\alpha_m x) + B_m \cosh(\alpha_m x) \right\} \tag{5.3.2}$$

where m=1,2 and refers to beams 1 and 2 respectively. The quantity α_m was defined earlier by equation (4.2.5).

The boundary conditions which provide solutions for the unknowns A_m and B_m are obtained given knowledge of the flux values at the ends of the beams and the boundary condition at the joint. In this case $q_{1\,in}$ is obtained from the measured power input at the shaker, P_i. At the other end, $q_{2\,out}$ is obtained from a structural intensity measurement made at point 3, just before the sand termination, see Fig.5.3.1. The flux values at either side of the joint are determined using the joint modelling expression (5.2.19) described earlier. A full description of the energy flow solution for this model is provided in Appendix C.

In order to obtain realistic energy flow predictions from this model, representative values for five modelling parameters must be determined. These parameters can be summarised as follows:

a) the power input measured at shaker, P_i.

b) the rate of energy flow out of the structure into the sand termination, p_o.

c) the phase velocity for the beam sections, c_b.

d) the structural damping loss factors for each beam, η.

e) the transmission efficiency at the flanged joint, τ.

For this model, the values for P_i and p_o have been obtained using the measurement techniques already described in sections (4.3.3) and (4.3.5) respectively. The phase velocities, c_b, can be calculated from:

$$c_b = \left(\frac{EI}{\rho S}\right)^{\frac{1}{4}} \omega^{\frac{1}{2}} \qquad (5.3.3)$$

using the dimensions and material properties given in Fig.5.3.1. The experimental determination of the remaining parameters, η and τ, will be discussed in the following sections.

5.3.2 Damping loss factor measurement

It was shown in Chapter 4 that a reasonable estimate of the damping loss factor parameter for an energy flow model can be obtained using modal analysis. Consequently, this approach has been used to establish the modal damping loss factors for each of the beams which make up this structure. For this purpose, the beams were separated and tested individually using a modal analysis technique identical to that described earlier for the perspex beam.

In contrast to the case of the perspex beam however, the lower levels of damping present in these materials necessitate the application of exponential windowing to the measured response data to avoid leakage error in the FFT analysis. This windowing has the effect of appearing to introduce additional damping into the modal analysis

calculation. In order to estimate the true values of the damping loss factors of the beams, the modal analysis results were corrected using the technique described in Appendix F which removes the effects of windowing.

The natural frequencies and corrected loss factors for the steel and aluminium beams are given in Tables 5.3.1 and 5.3.2 below.

Mode Number	Natural Frequency (Hz)	Corrected Loss Factor
1	99.3	0.0040
2	194.0	0.0023
3	321.2	0.0030
4	479.0	0.0050
5	667.5	0.0040
6	888.6	0.0041
7	1142.5	0.0029
8	1421.6	0.0028
9	1735.3	0.0024

TABLE 5.3.1 Modal loss factors for the steel beam

Mode Number	Natural frequency (Hz)	Corrected Loss Factor
1	98.2	0.0027
2	192.8	0.0018
3	318.3	0.0051
4	474.5	0.0097
5	662.2	0.0067
6	880.6	0.0060
7	1131.3	0.0030
8	1410.8	0.0028
9	1714.8	0.0040

TABLE 5.3.2 Modal loss factors for the aluminium beam

It was shown in section 4.3.6 that the model predictions are relatively insensitive to small changes in damping parameter. It was therefore decided that the mean values of the aforementioned adjusted loss factors would be used as representative values in the energy flow model over the entire 0-2 kHz frequency range. These values are 0.0034 and 0.0046 for the steel and aluminium beams respectively.

5.3.3 Transmission efficiency measurement using wave decomposition

The transmission efficiency parameter, τ, has been introduced into the joint boundary condition (5.2.19) to include the effects of partial reflection of incident wave energy. In a number of simple cases a value for the transmission efficiency at the joint can be derived analytically given knowledge of the boundary conditions at the discontinuity. A number of examples of this type of calculation have been provided by Cremer (1973). In many practical cases however, these boundary conditions are difficult to determine exactly and an experimental study may provide more realistic information.

David-Taylor (1990) provided the basis for a technique which is able to determine the amplitudes of the near- and far-field wave components in a beam from measurements made using four closely spaced accelerometers. This approach is referred to as the "wave decomposition technique" and was illustrated using a terminated beam structure, like the one shown in Fig.5.3.3. In this diagram A and B represent the amplitudes of the rightward and leftward travelling far-field waves and C and D are the amplitudes of the decaying near-field effects associated with the discontinuities. In his paper David-Taylor used this approach to determine the reflection coefficient and impedance of a real beam termination from the decomposed wave amplitudes A, B, C and D.

The reflection coefficient, r, of a termination is defined as the ratio of the reflected to incident wave amplitudes. In the case of the beam structure illustrated in Fig.5.3.3, if the effects of damping are neglected, then r is given by the ratio B/A.

Given knowledge of this reflection coefficient it is also possible to calculate the transmission efficiency using:

$$\tau = 1 - |r|^2 \tag{5.3.11}$$

It should be noted that to determine r, one only requires knowledge of the far-field wave amplitudes, A and B, which can be obtained by making measurements at two, rather than four, accelerometer locations.

A full derivation of the analysis required to determine the reflection coefficient of the termination is given in Appendix D. This shows that the auto-spectra of the decomposed wave amplitudes, X_{AA} and X_{BB}, can be extracted from the measured auto- and cross-spectral values obtained using accelerometers placed at distances x_1 and x_2 from the termination.

These decomposed auto-spectra can then be used to calculate the reflection coefficient, r, using:

$$r = \left(\frac{X_{BB}}{X_{AA}} \right)^{\frac{1}{2}} \tag{5.3.12}$$

If required, the decomposed wave spectra can also be used to determine the net far-field structural intensity in the beam, which is given by:

$$p = \frac{2EIk^3}{\omega^3} (X_{AA} - X_{BB}) \tag{5.3.13}$$

For the connected beam structure considered here, each beam can be attributed with a pair of travelling wave amplitudes as shown in Fig.5.3.4. If it is assumed that the sand acts as a non-reflective termination and that damping in the beam is so low that it can be safely neglected, this technique can be used to determine the transmission efficiency across the flanged joint. For this purpose auto- and cross-spectral measurements were obtained over a 0-5 kHz frequency range using an accelerometer pair mounted at point 2 (Fig.5.3.4) on the steel beam. Decomposition of this data

using the matrix equation given in Appendix D provides the necessary auto-spectra X_{AA} and X_{BB} required to calculate the transmission efficiency, τ, using equations (5.3.11) and (5.3.12). For this calculation the origin x=0 was assumed to be at the flange so that the distances x_1 and x_2 represent the distance of the accelerometers from the joint.

Before looking at the transmission efficiency across the flange it would be useful to make a comparison between the structural intensity value calculated from the decomposed spectra using (5.3.13) and that obtained by processing the measured data directly using the more traditional structural intensity calculation provided by equation (4.3.12). This comparison is shown in Fig.5.3.5. It can be seen that the two spectra are almost indistinguishable, validating the relationships developed in Appendix D. Some difference between the two results can be detected above 3 kHz. This difference is probably due to finite difference errors which occur in the directly measured result and grow as frequency increases. The wave decomposition results are free from this effect because finite difference approximations are not used in the derivation of equation (5.3.13).

The measured transmission efficiency spectrum obtained using (5.3.11) and (5.3.12) is shown in Fig.5.3.6. It can be seen that the measured value remains between 70% and 95% over the majority of the frequency range. The very low values of τ below 300 Hz can be attributed to the influence of near-field effects which are not included in the theoretical development. Use of equation (3.4.5) shows that at 300 Hz the magnitude of the near-field component at this location is still at 17% of its maximum value at the flange.

The spike in the data around 1900 Hz coincides with the very low levels of energy flow along the beam indicated by the structural intensity measurements shown in Fig.5.3.5. It is likely that under these conditions of low energy flow the signal-to-noise ratio of the measured data is poor, leading to errors which have been carried through into the transmission efficiency calculation.

The exact reason for the reduction in energy flow around 1900 Hz cannot be established from these experimental results, although this phenomenon was also observed in other experiments involving sand terminated shaker driven beams. This observation suggests that this characteristic may be a result of shaker-structure interaction.

5.3.4 Model results

Having obtained the necessary parameters listed in section 5.3.1, the energy flow solution (5.3.2) can be employed to provide predicted power levels along the length of the beams. This modelling was limited to the 0-1.5 kHz frequency range because of unreliable power input data between 1.7 and 2.1 kHz. This frequency range corresponds to the region of the very low levels of energy flow indicated by the structural intensity measurements. Under these conditions poor signal-to-noise ratios are likely to have also degraded the power input measurement.

A comparison between model prediction and measured power level at location 2 is shown in Fig.5.3.7. Excellent agreement between the two spectra confirms the ability of this model to provide realistic predictions, given representative values for the modelling parameters. Some differences between the spectra are evident at lower frequencies due to the influence of near-field effects.

5.3.5 Discussion

Having established the transmission efficiency across the flange by measurement, it is interesting to compare these results with some theoretical values for arrangements of this type. Cremer (1973) provided analytical solutions for the reflection and transmission coefficients across a number of common structural discontinuities. These solutions are based on the boundary conditions present at the junction between two semi-infinite structures. Two cases are of particular interest here. The effect of a change in material properties at the junction and the blocking mass effect of a flange.

Cremer showed that the flexural transmission efficiency for the junction between two beams of identical cross-sectional dimensions, but dissimilar materials, is given by:

$$\tau = \left[\frac{2\sqrt{\kappa\xi}\ (1+\kappa)\ (1+\xi)}{\kappa(1+\xi)^2 + 2\xi(1+\kappa^2)} \right]^2 \qquad (5.3.14)$$

where

$$\xi = \left(\frac{\rho_2 E_2}{\rho_1 E_1} \right)^{\frac{1}{2}} \qquad \text{and} \qquad \kappa = \left(\frac{\rho_2 E_1}{\rho_1 E_2} \right)^{\frac{1}{2}}$$

The above expressions lead to a frequency independent value for τ, which in the case of the transition from steel to aluminium, has a value of 98%.

The second analysis of importance relates to the effect of a blocking mass between two beam sections. The inertial effect of the added mass results in an expression for transmission efficiency of the form:

$$\tau = \left| \frac{-i\,(4 + \mu - \theta^2\mu^3)}{(\mu + \theta^2\mu^3) - i\,(4 + \mu - \theta^2\mu^3 - \theta^2\mu^4/2)} \right|^2 \qquad (5.3.15)$$

where

$$\mu = \frac{k_b M}{\rho S} \qquad \text{and} \qquad \theta = \frac{\rho S}{M}\sqrt{R}$$

Here ρ, S and k_b represent the mass density, cross-sectional area and flexural wavenumber for the beam sections. M and R denote the total mass and the radius of gyration of the blocking mass. This expression yields a value for τ which is heavily frequency dependent. The general form of the characteristic is shown in Fig.5.3.8. The blocking mass effect is often likened to that of a "low pass filter". Initially the wave motion is transmitted relatively unhindered up to a frequency where total transmission occurs (ie. $\tau = 1$). Above this frequency the characteristic rapidly decays resulting in significant attenuation of the transmitted wave. The point at which this

total transmission condition occurs is heavily dependent on the inertial effect of the blocking mass. It is observed that as the inertia of the mass increases the "pass band" in the characteristic narrows and attenuation starts to occur at a lower frequency.

This analysis is not exactly suited to the real connected beam structure used in these experiments because it assumes that the beams on either side of the blocking mass have identical material properties. However, evaluation of (5.3.15) shows that the general characteristic is relatively insensitive to the difference in material properties relating to aluminium and steel, particularly below the total transmission frequency. Equation (5.3.15) can therefore be used to determine the theoretical blocking mass effect of a flange of this size, and in particular, a prediction for the frequency at which attenuation should start to occur. The results of this analysis are shown in Fig.5.3.9. It can be seen that the theoretical model predicts that for either material, the "pass band" extends to around 12 kHz and within this range the transmission efficiency remains above 95%.

Comparing this result with the measured characteristic shown in Fig.5.3.6 it can be seen that even with the combined effects of the change in material properties and the blocking mass effect of the flange, the measured transmission efficiency is significantly lower than the theoretical predictions. One possible reason for this is that some wave energy is being reflected back from the sand terminated end of the structure and passes through the joint to contribute to the amplitude of B_1, marked on Fig.5.3.4. This process would lead to a reduction in the effective transmission efficiency at the joint.

In order to confirm this idea it would be useful to be able to decompose the wave amplitudes at point 3 (Fig.5.3.1) to determine the relative amplitude of the reflected wave, B_2. Revisiting the theoretical development behind the wave decomposition technique given in Appendix D, it is evident that since in this case only the far-field wave amplitudes are required, the choice of the origin $x = 0$ is arbitrary. It is therefore possible to use the relationships developed by this analysis anywhere in the far-field of a beam structure, so long as appropriate values for x_1 and x_2 are used. For

general measurements on a beam a convenient origin for the calculation is the mid-point between the accelerometers, so that:

$$x_1 = -x_2 = \frac{\Delta}{2} \tag{5.3.16}$$

where Δ is the accelerometer spacing.

At the time of the experiments sufficient data was obtained to carry out this alternative form of the decomposition at points 1, 2 and 3 on the beam structure over a 0-2.5 kHz frequency range. A comparison between the measured ratio (X_{BB}/X_{AA}) for measurements at points 1 and 2 on the steel beam shows good agreement, see Fig.5.3.10. However, decomposition of the measured spectra at point 3 on the aluminium beam resulted in negative auto-spectral values being returned from the decomposition calculation, but by definition, auto-spectra must always be real and positive. Inspection of the raw data obtained at point 3 revealed some instability in the sign of the imaginary part of the cross-spectrum of the accelerometer outputs which could be the cause of the poor wave decomposition results obtained at this location. Unfortunately time constraints do not allow these measurements to be repeated before completion of this thesis. The consistency of the results obtained for the steel beam however, does show the ability of this technique to establish the relative magnitudes of the leftward and rightward travelling wave components in the far-field of a beam. For the case of this two beam structure, given reliable data at point 3 it should have been possible to determine whether a reflected component B_2 was responsible for the difference between the theoretically predicted and measured transmission efficiency values at the flange.

This investigation highlights the importance of reflections when building up a *global* model of a structure based on information concerning the transmission efficiency of its individual joints. In the case of the energy flow model for this connected beam structure, the measured result is the *effective* or *net* transmission efficiency across the joint, taking the downstream conditions into account. It therefore represents a better value for calculating the *global* energy flow through the structure than one obtained

from a calculation with no regard for effects downstream of the joint.

This exercise has also demonstrated that the wave decomposition technique has great potential for the study of transmission and reflection at structural discontinuities in beams. It is capable of providing far more information than a simple measurement of the net energy flow obtained by the direct application of structural intensity measurement techniques.

It is also worth noting that the far-field part of the solution to the wave equation for flexural motion in a beam, used as the starting point for this analysis, is identical in form to the solution for longitudinal wave motion. The matrix relationships between measured data and decomposed spectra given in Appendix D will therefore also hold for measurements made along the axis of a beam transmitting longitudinal waves. This observation highlights the potential for this technique in the study of wave transmission through angled or branched beam structures where conversion between flexural and axial wave motion occurs. In these cases knowledge of the relative amplitudes of each type of wave is potentially very useful in understanding the process of mode conversion.

5.4 Summary

This chapter describes the application of the energy flow approach to provide representative models of connected beam structures. The main points arising from this investigation are as follows:

1. It is difficult to select a boundary condition to model the power transmission across a structural discontinuity which is representative of true physical conditions and, at the same time, suitable for implementation using a finite element formulation. An expression which provides the best balance of these requirements has been obtained using an approach based on a model presented by Cho and Bernhard (1992). This expression includes the effects of partial reflection at the discontinuity via a transmission efficiency parameter and is suitable for implementation in a finite element form.

2. The energy flow approach has been used to develop a representative model of a structure consisting of two beams connected by a flanged joint. The majority of the parameters required by this model can be estimated using techniques described in Chapter 4. The evaluation of transmission efficiency at the joint is a new problem in the context of this work and is achieved experimentally using a wave decomposition approach.

3. Comparisons between model predictions for energy flow along the beam and measured values obtained by a structural intensity technique show that the model is capable of providing good predictions given realistic estimates of the modelling parameters.

4. Comparisons between measured transmission efficiency and those calculated using theoretical expressions indicate that reflection from downstream discontinuities may have a significant effect on the *net* transmission characteristics of the joint.

5. Reassessment of the theory relating to the wave decomposition approach shows that it can be used to separate far-field flexural *and* longitudinal wave components in beam structures. This indicates a potential for the technique to be applied to the analysis of more complicated beam structures containing bends and branches.

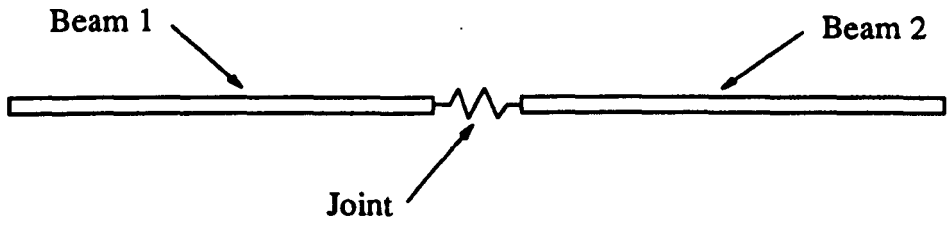

Fig.5.2.1 Two beam energy flow model

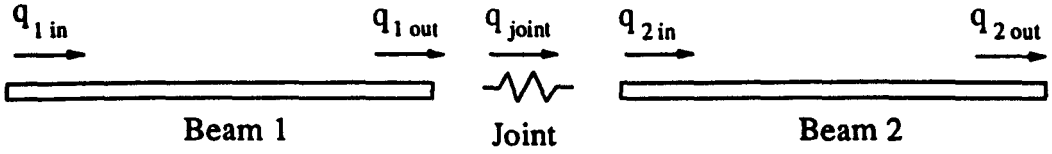

Fig.5.2.2 The power flux boundary conditions

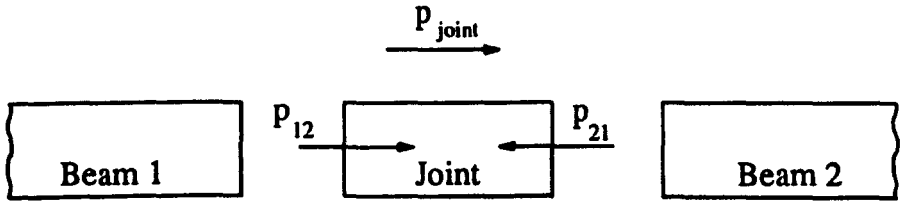

Fig.5.2.3 The Nefske and Sung joint model

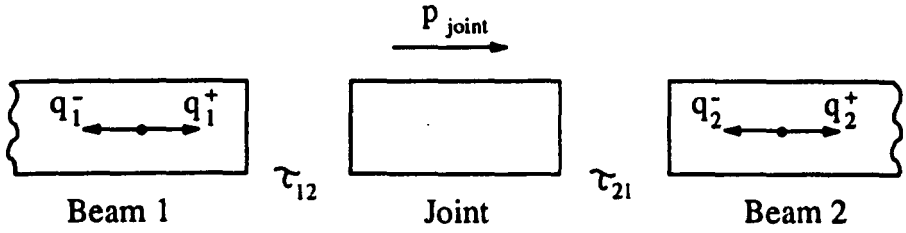

Fig.5.2.4 The Cho and Bernhard joint model

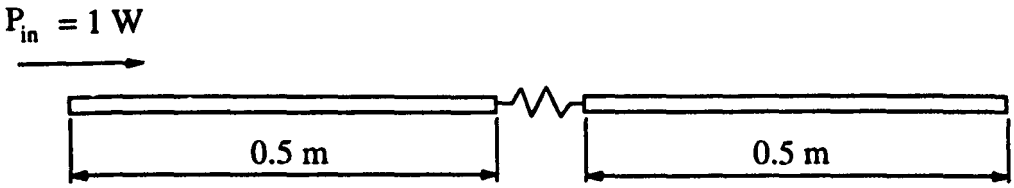

Beam section 10 mm x 10 mm

Young's modulus = 209 x 10^9 N/m^2

Density = 7800 kg/m^3

Fig.5.2.5 Connected beam example

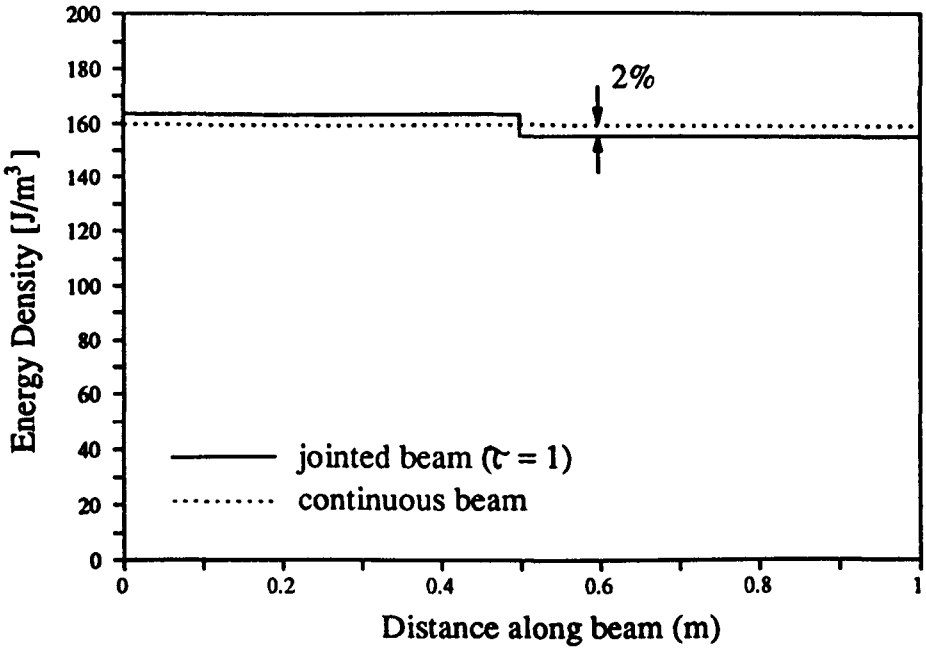

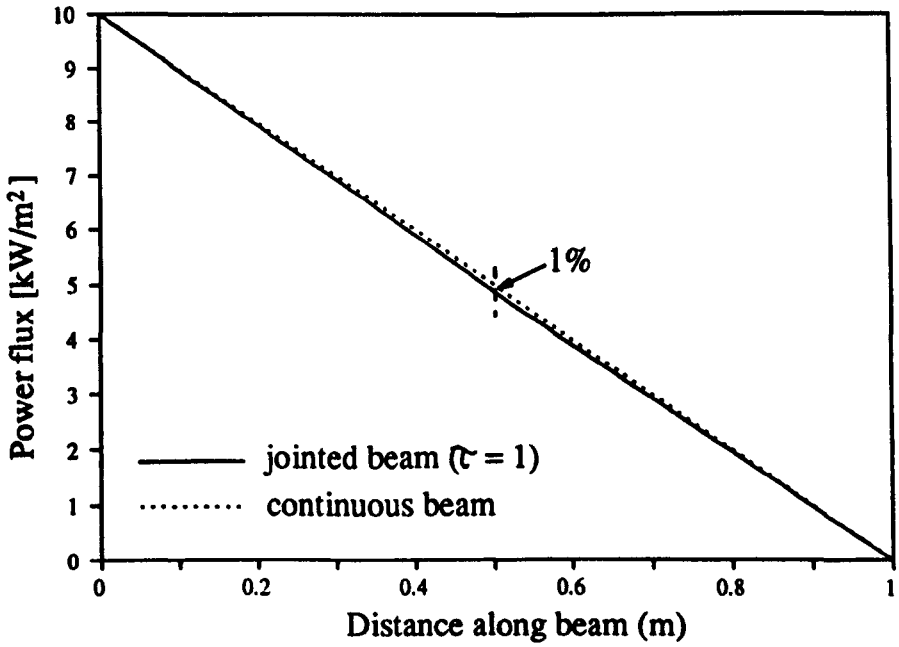

Fig.5.2.6 Effect of the Nefske and Sung boundary condition on the energy density and power profiles at 1000 Hz and with a damping factor of 0.01

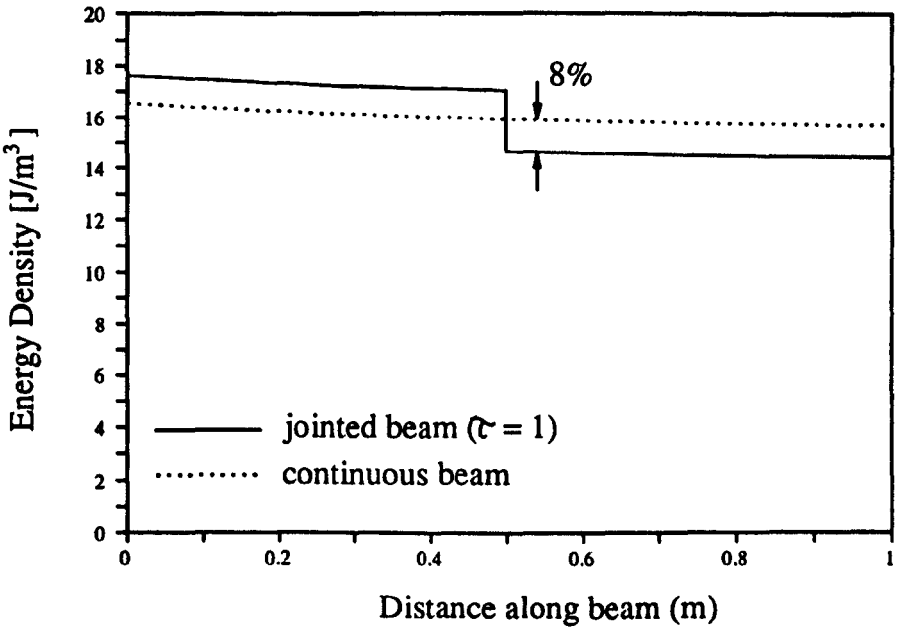

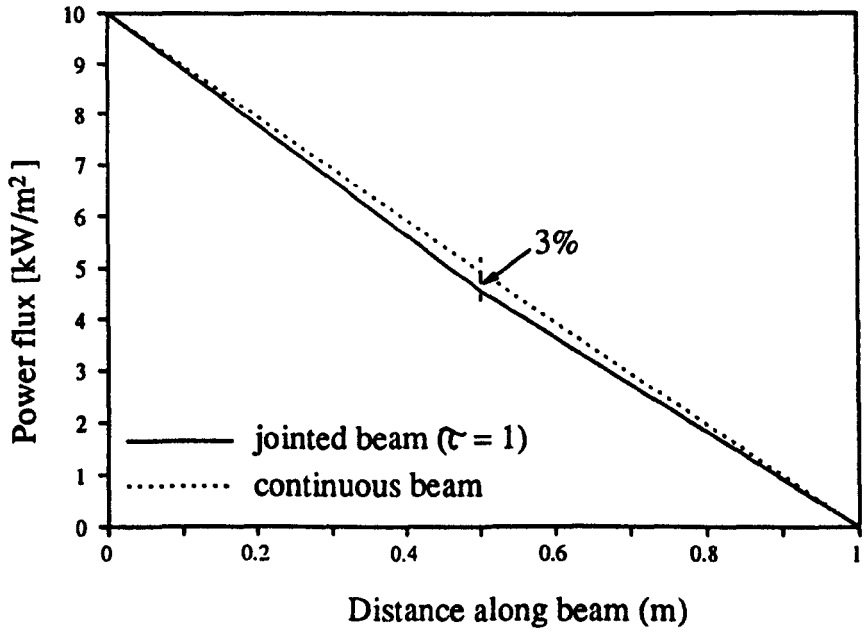

Fig.5.2.7 Effect of the Nefske and Sung boundary condition on the energy density and power profiles at 10000 Hz and with a damping factor of 0.01

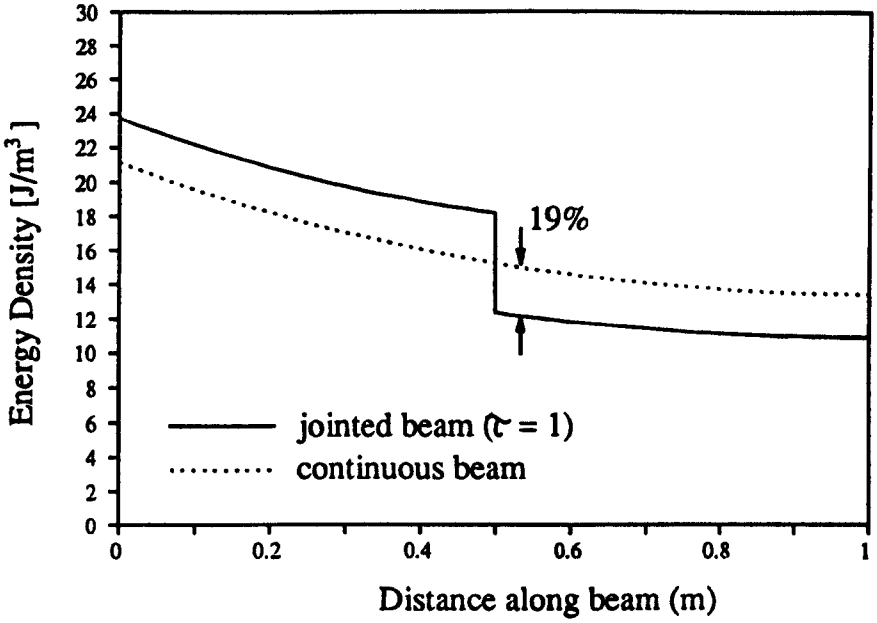

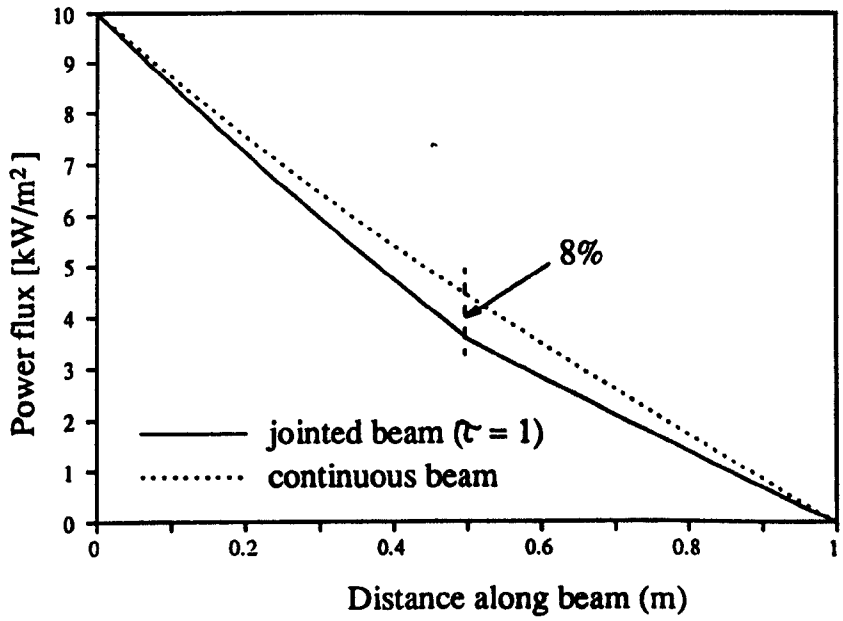

Fig.5.2.8 Effect of the Nefske and Sung boundary condition on the energy density and power profiles at 1000 Hz and with a damping factor of 0.10

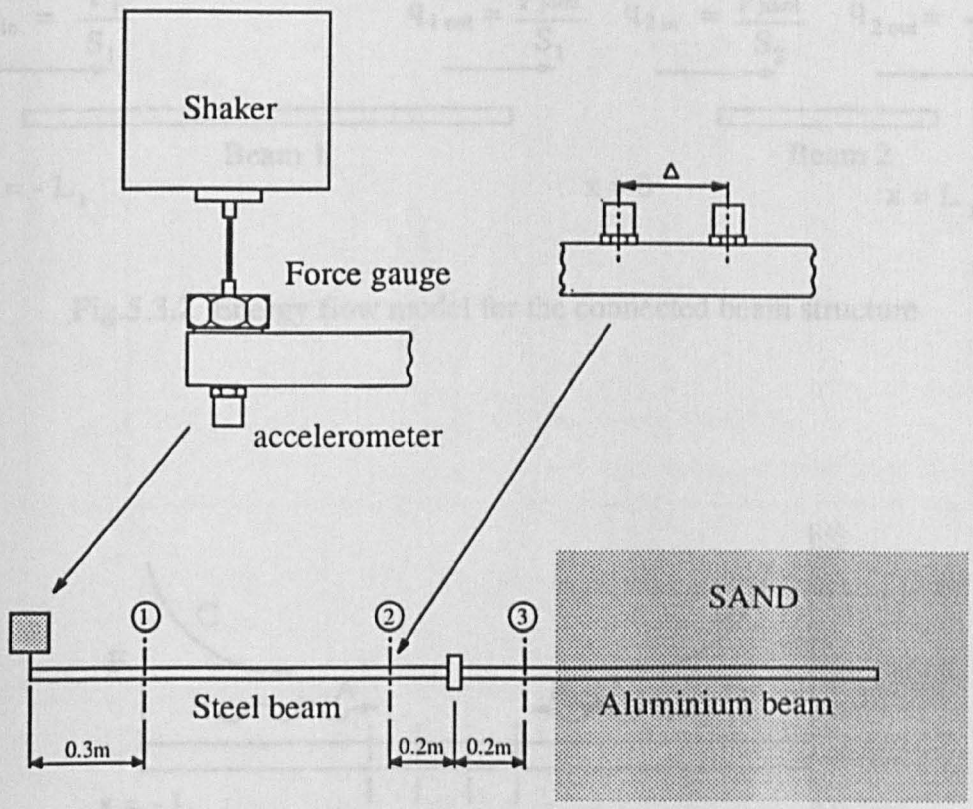

BEAM DIMENSIONS

Length = 1.5 m

Section = 16.5 mm x 16.5 mm

MATERIAL PROPERTIES

Steel: Density = 7800 kg/m ^{3}

E = 209 GN/m ^{2}

Aluminium: Density = 2700 kg/m ^{3}

E = 70 GN/m ^{2}

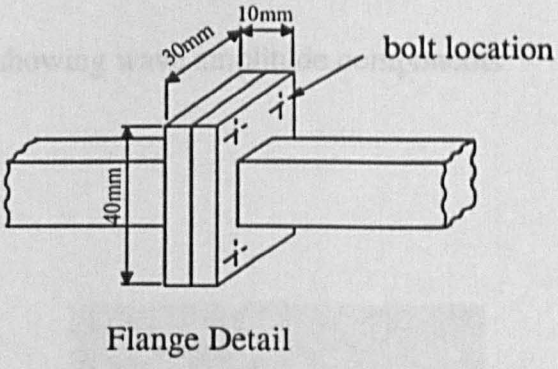

Flange Detail

Fig.5.3.1 Connected beam structure

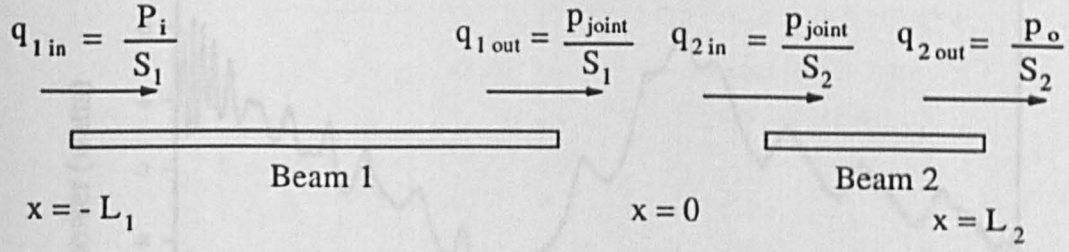

Fig.5.3.2 Energy flow model for the connected beam structure

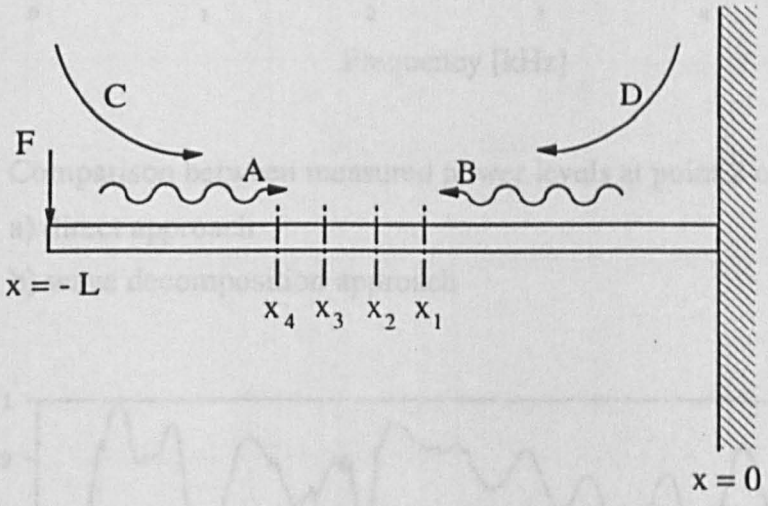

Fig.5.3.3 Terminated beam model showing wave amplitude components

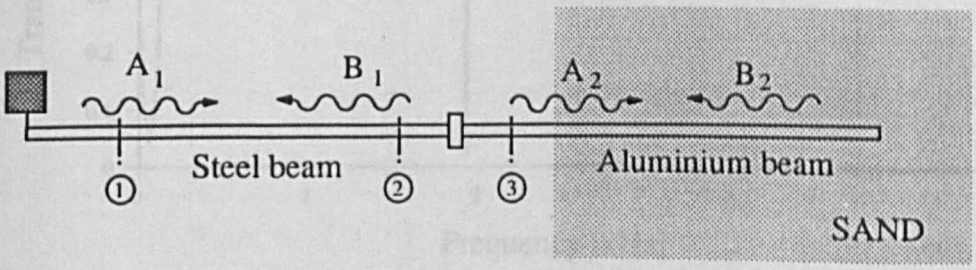

Fig.5.3.4 Travelling wave components in the real connected beam structure

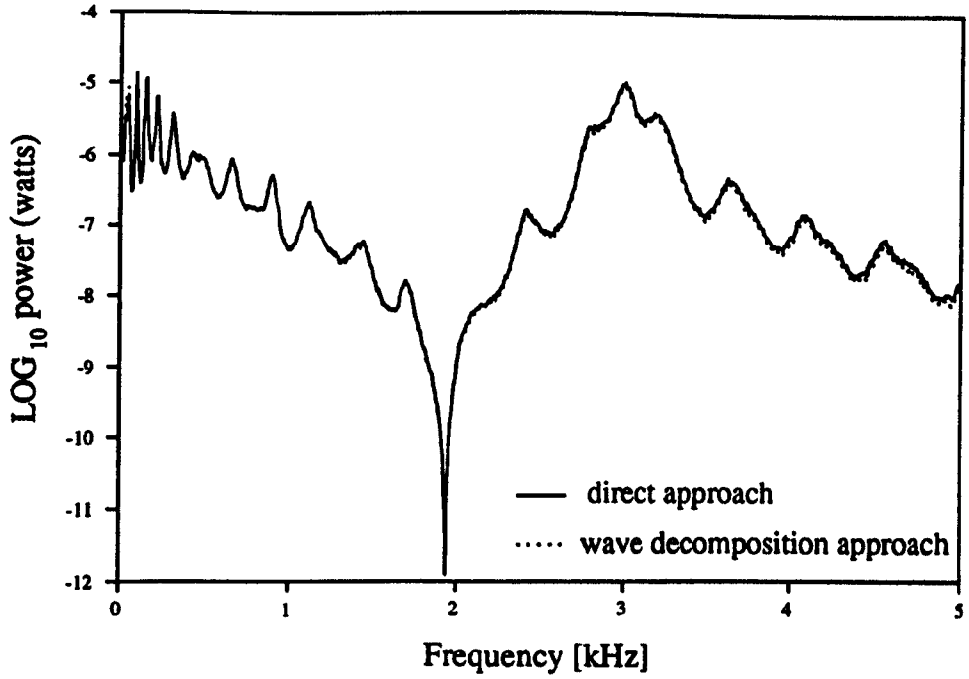

Fig.5.3.5 Comparison between measured power levels at point 2 obtained by:
a) direct approach
b) wave decomposition approach

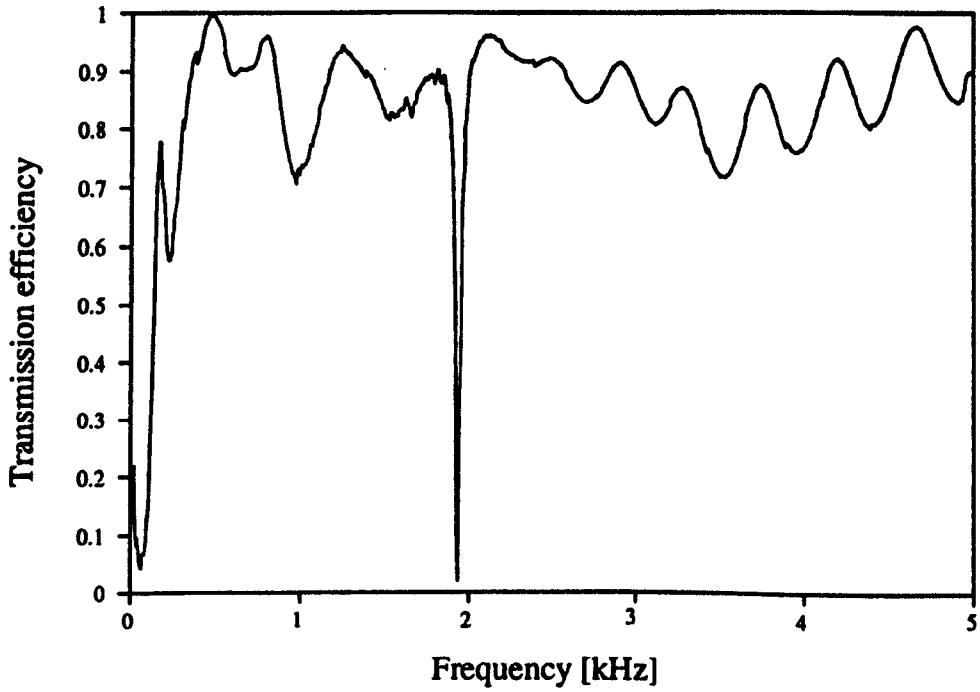

Fig.5.3.6 Transmission efficiency across the flanged joint obtained by the wave decomposition approach applied to data obtained at point 2

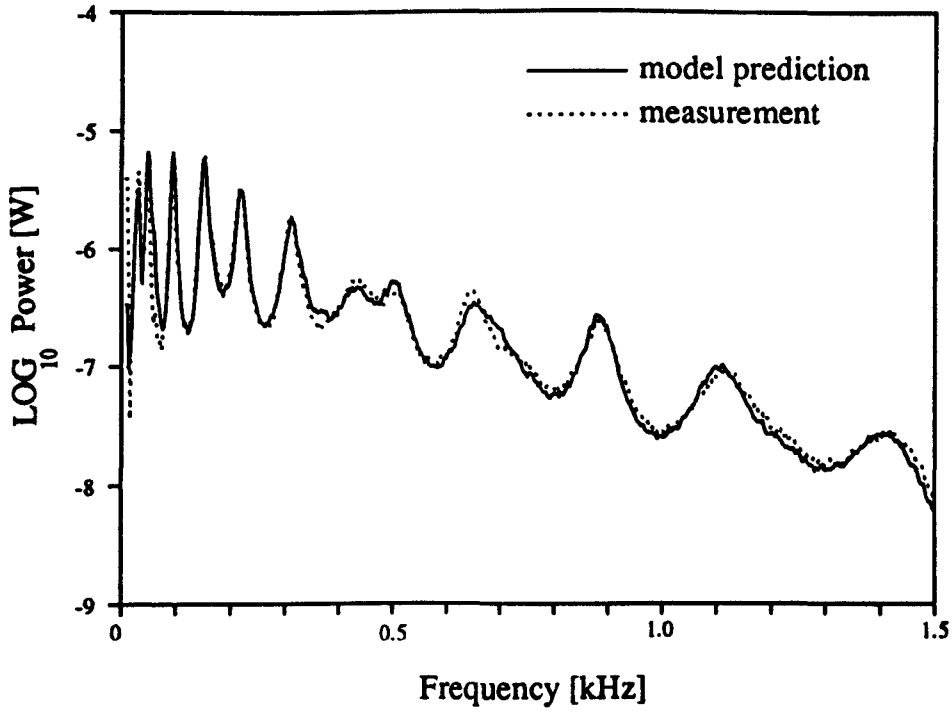

Fig.5.3.7 Comparison between predicted and measured power at point 2

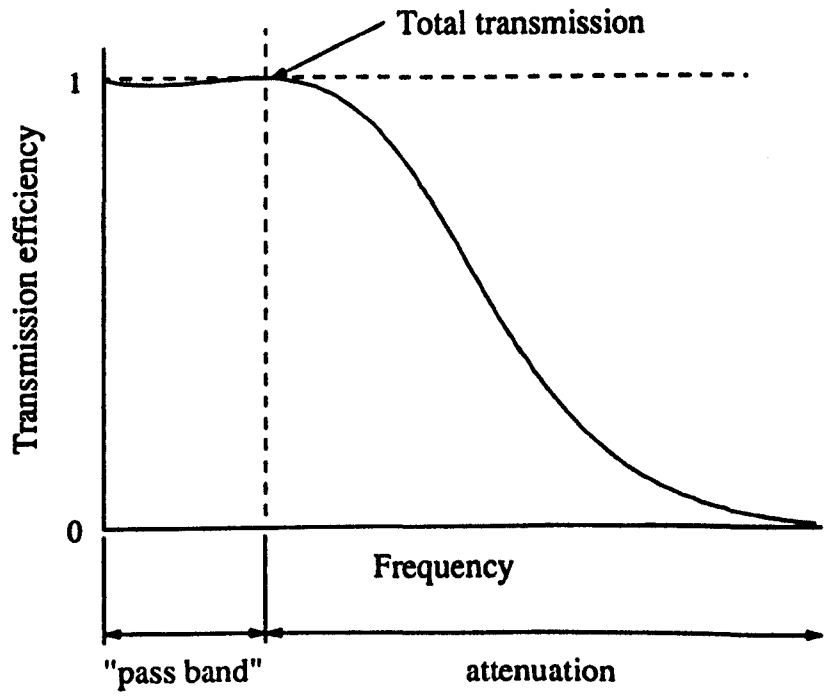

Fig.5.3.8 The general form of the transmission efficiency characteristic across a blocking mass

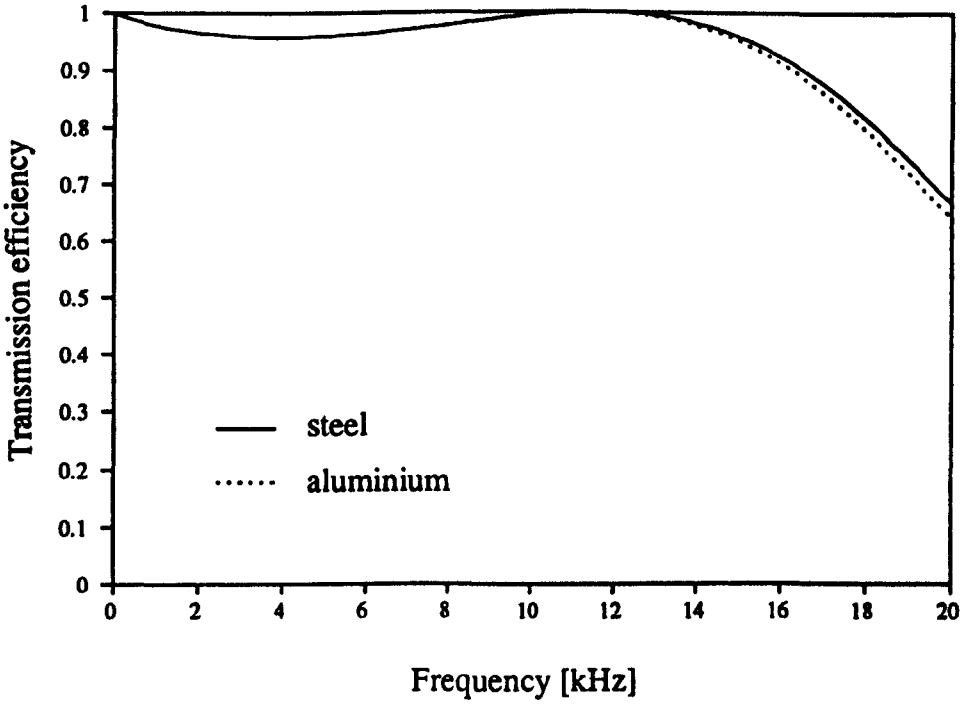

Fig.5.3.9 Theoretical predictions for transmission efficiency across the flange

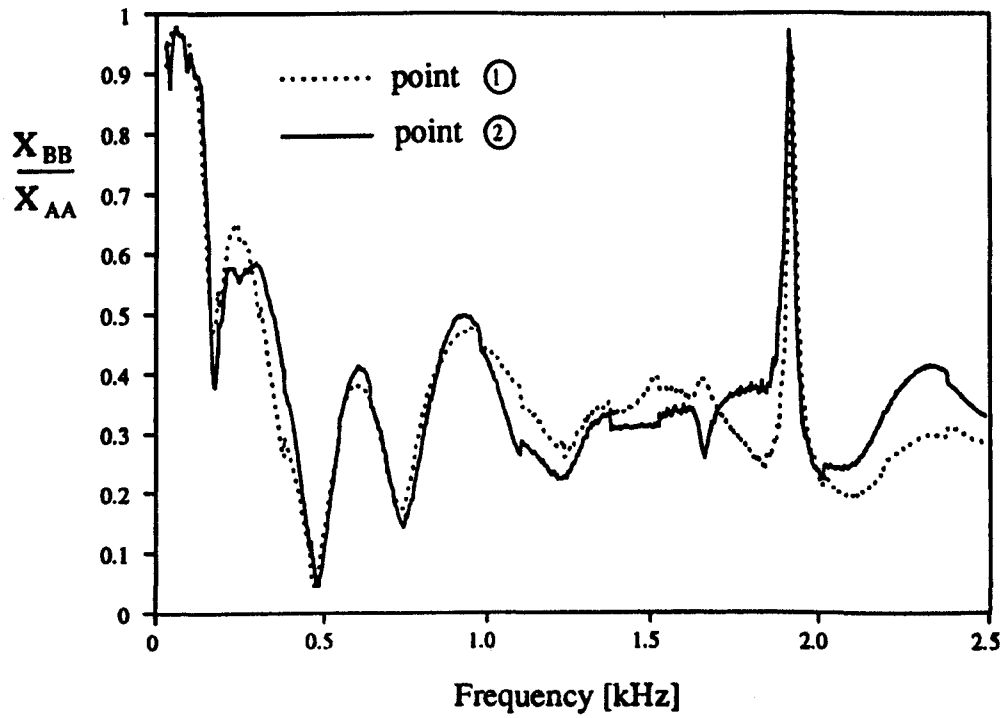

Fig.5.3.10 Ratio of wave amplitude auto-spectra obtained at points on the steel beam using the wave decomposition technique

Chapter 6

Finite element implementation of the energy flow approach

6.1 Introduction

From the outset of this work the potential to implement the energy flow analysis using finite elements has been regarded as a principal advantage of the approach. In previous chapters, examples of energy flow models for beam structures have been created using an analytical approach. For the case of two-dimensional or multiple component structures, this type of solution becomes much more difficult or even impossible to implement. In these cases, the use of a finite element approach to assemble and solve the equations relating to each section of the model provides a very attractive solution to this problem.

The use of finite elements also offers additional modelling capabilities which are not easily achievable using an analytical approach. These include the ability to investigate the effects of local variation of structural properties such as damping, and the ability to model a wide variety of structural configurations using the same computational framework.

For the purposes of this project, finite element energy flow models will be created by modifying a commercially available finite element package. The use of existing finite element software has a number of practical advantages over the development of a dedicated finite element solution aimed solely at implementing the energy flow approach. The major advantage of this technique is that it greatly reduces the time required for writing and testing what would become a rather extensive piece of software. Use of existing coding allows the principles and capabilities of the energy flow approach to be investigated without incurring high development overheads. It

also provides the possibility of using a number of pre- and post-processing packages designed for use with standard codes which make mesh generation and presentation of results less labour intensive.

Finally, it is important to note that finite element packages are already widely distributed amongst the engineering community so that the framework of the analysis is already in place. Adaptation of these existing tools to implement the energy flow approach allows the user to carry out additional analysis without an increase in capital costs.

In order to implement the analysis using existing finite element coding it is necessary to draw an analogy between the equations governing the energy flow approach and those relating to steady state heat conduction. This chapter describes this analogy and outlines the approach required to develop energy flow models using the ABAQUS™ finite element package. To illustrate the use of this technique as a quantitative transmission path ranking tool, the finite element approach is used to develop an energy flow model of a multiple transmission path structure. Although this work is carried out using the ABAQUS™ finite element suite, the principles involved should be generally applicable to most commercially available packages which cater for steady state thermal analysis.

6.2 Implementation of the energy flow approach using finite elements

In the context of the energy flow approach, the differential equation governing the flow of vibrational energy within a structural component is of the general form:

$$\nabla^2 Ce - p_{diss} = 0 \qquad (6.2.1)$$

This equation is of the same form as the equation governing temperature distribution in steady state heat conduction, often expressed as:

$$\nabla^2 KT + \theta = 0 \qquad (6.2.2)$$

where K represents the thermal conductivity of the material, T is temperature and θ represents heat generation or loss per unit volume of material. The above expression

forms the basis of the steady state thermal analysis provided by most commercially available finite element packages.

The technique developed here for the creation of finite element energy flow models is based on drawing an analogy between the vibrational energy density, e, in equation (6.2.1) and temperature, T, in equation (6.2.2). Having done this, the thermal parameters in the finite element package can be replaced by equivalent vibrational terms.

The first terms in equations (6.2.1) and (6.2.2) relate to the transport of energy through the system. Noting the analogy between T and e, it can be seen that the thermal conductivity parameter, K, is equivalent to the parameter C in the energy flow approach. The parameter C was introduced in Chapter 3 in the development of a relationship between the power flux and the gradient of the energy density. After a number of simplifications had been made and under space- and time-averaged conditions it was shown that:

$$C = \frac{c_g^2}{\omega\eta} \tag{6.2.3}$$

anywhere in a rod and in the far-field of a beam or a plate. This quantity must be used to replace K in the finite element analysis.

The second terms in equations (6.2.1) and (6.2.2) relate to a change of the internal energy of the system. In terms of the analogy, the loss of vibrational energy due to material damping can be modelled using convective heat transfer away from the system. In the thermal finite element analysis, convective heat transfer is governed by:

$$\Theta = h\, s_{el} \left(T - T_f \right) \tag{6.2.4}$$

where Θ is the rate of energy loss (in watts), h is the convective heat transfer coefficient, s_{el} is the surface area of the element in contact with the surrounding fluid, T is the temperature of the material and T_f is the temperature of the fluid.

The equivalent dissipation of vibrational energy within an element of material due to damping is:

$$P_{diss} = \omega \eta V_{el} e = \omega \eta d_{el} s_{el} e \qquad (6.2.5)$$

where V_{el} and d_{el} represent the volume and depth of the finite element respectively.

Comparing (6.2.4) and (6.2.5) it can be seen that the analogy can be maintained by setting:

$$h = \omega \eta d_{el} \qquad \text{and} \qquad T_f = 0 \qquad (6.2.6)$$

Finally, in order to build up connected structures using this approach, the joint boundary condition introduced in Chapter 5 must also be implemented within the finite element scheme. The joint boundary condition is of the form:

$$p_{joint} = \frac{\tau}{2(1-\tau)} \left(c_{g1} S_1 e_1 - c_{g2} S_2 e_2 \right) \qquad (6.2.7)$$

In the case of a one-dimensional two-noded thermal finite element, the transmission of thermal energy is based on the relationship:

$$Q = \frac{KS}{l_{el}} \left(T_1 - T_2 \right) \qquad (6.2.8)$$

where S and l_{el} are the cross-sectional area and length of the finite element, T_1 and T_2 are the temperatures at each node and K represents the thermal conductivity. The resulting conductivity matrix incorporated into the finite element calculation is always symmetrical and of the form:

$$[K] = \frac{KS}{l_{el}} \begin{bmatrix} 1 & -1 \\ -1 & 1 \end{bmatrix} \qquad (6.2.9)$$

Using (6.2.7) the equivalent "conductivity" matrix for a two-node "joint element" is:

$$[K_j] = \frac{\tau}{2(1-\tau)} \begin{bmatrix} c_{g1} S_1 & -c_{g2} S_2 \\ -c_{g1} S_1 & c_{g2} S_2 \end{bmatrix} \qquad (6.2.10)$$

If the structural components on either side of the joint are identical, the joint matrix will be symmetrical and can be created using a standard thermal finite element with a conductivity value set to:

$$K = \frac{\tau\, c_g\, l}{2(1-\tau)} \tag{6.2.11}$$

If however, the values of either c_g or S are not the same on either side of the joint, say for the case of two beams having different sections, a standard thermal finite element cannot be used. Within the ABAQUS™ finite element package this problem can be overcome by creating a "USER" element for which matrix members can be freely defined. In this way a general two-noded "joint finite element" can be created where the terms in the conductivity matrix are set individually according to equation (6.2.10).

To test the validity of this analogy the solutions to finite element energy flow models of single and connected beam structures, created using ABAQUS™, were compared with those obtained by the analytical models presented in Chapters 4 and 5. In all cases, the finite element results were within 0.2% of those provided by the analytical solutions.

6.3 Energy flow analysis of a multiple transmission path structure

The ability to implement the energy flow analysis using finite elements provides the opportunity to analyse more complex, multiple component structures which are more representative of those found in engineering applications. In the marine environment, transmission of vibrational energy along pipework systems is often difficult to assess because of their relatively complicated geometries and the complex dynamics of cylindrical shells which comes into play at higher frequencies. Although the complexity of pipe vibration is beyond the scope of the energy flow approach at this stage in its development, the finite element implementation of the approach is well suited to the treatment of multiple transmission path geometries typical of those found in pipes.

To illustrate this the finite element approach will be used to build a global energy flow model to represent the general transmission characteristics of the branched pipework system shown in Fig.6.3.1. The flow of vibrational energy through this system is divided between two paths. The first consists of a straight section of pipe containing a valve and the second is a section containing a number of 60° bends.

Because at this stage the energy flow approach is unable to accommodate pipe behaviour, the pipe sections will be represented by solid sections to make use of the expressions already developed for energy flow in rods and beams. This simplification should not detract from the main objective of this exercise which is to assess the ability of the energy flow approach to form a quantitative transmission path ranking tool for the analysis of multiple transmission path structures. Having made this simplification, the pipework system is effectively reduced to a framework structure shown in Fig.6.3.2.

The major influence on the global energy flow through the structure will be the partial transmission of wave energy across the joints and the valve. The valve represents a mass between two beam sections and will exhibit a blocking mass effect which is heavily dependent on frequency. This situation is rather like that of the flanged joint discussed in Chapter 5. The angled joints will also cause partial reflection of wave energy, which in this case, will also be accompanied by mode conversion between flexural and longitudinal motion. This is a new feature which has not yet been included in the energy flow modelling presented here.

6.3.1 The finite element energy flow model

The finite element energy flow model of this structure was created using the ABAQUS™ finite element package. The general form of this model is shown in Fig.6.3.3. Pipe sections are represented by one-dimensional thermal beam elements. It will be shown in the next section that the conductivity values for these elements are dependent on the proportions of flexural and longitudinal wave energy they possess. Because this will alter depending on the mode conversion and reflection characteristics at each joint, these values may not necessarily be the same on either side of the joint.

As a result, the joint elements must be created using the "USER" element facility which allows for non-symmetrical conductivity matrices defined according to equation (6.2.10).

In order to encourage a distinct flow of energy through the system an energy source and sink have been attached to the ends of the structure. The source consists of a beam, of identical dimensions to those of the other sections, with a concentrated power flux applied at its remote end. The sink is of a similar geometry but has a material damping factor set at ten times that of the sections representing the pipes. Both source and sink are joined directly to the ends of the pipework system giving 100% power transmission through the connections (ie. τ=1).

The finite element model requires a number of parameters to describe the transmission of vibrational energy through each modelling element. These parameters are as follows:

1. The *net* transmission efficiency value for each joint element which allows for partial transmission across the joint and conversion between wave types.
2. The "conductivity" value of each beam element dependent on the proportion of each wave type.
3. The convective heat transfer coefficient for each beam element to include the effects of damping.

The latter of these parameters is determined using equation (6.2.6). In the case of this illustrative example the value for the damping loss factor, η, was chosen as 0.01.

The first two parameters are directly related to the individual transmission efficiencies and the degree of mode conversion at the joints in this structure. In order to calculate these, it is first necessary to determine the transmissive characteristics of each joint in isolation from the rest of the structure and then assemble this information to establish their *net* effects. Having achieved this, a value for the conductivity of each section can be calculated based on the proportion of each wave type it transmits.

These calculations will be described in the following sections.

6.3.2 Wave transmission through angled and branched joints in beams

The initial stage in the development of this example consists of a study of the transmission properties of the joints in isolation from the rest of the structure to determine their individual transmission and mode conversion characteristics. In the case of the angled and branched joints contained in this model, the analysis is based on an approach described by Horner and White (1990). Here one considers the joint as a cylindrical mass connecting a number of semi-infinite beams which can be arranged at arbitrary angles. This configuration is shown in Fig.6.3.4. The incident wave approaching the joint along beam 1 is assumed to be either flexural or longitudinal in nature. As a result of the equilibrium and continuity conditions at the joint, part of this wave is reflected back along beam 1 and the remainder is transmitted into beams 2 and 3. This partial reflection is also accompanied by mode conversion, so that the incident wave can generate both flexural and longitudinal wave components in each of the three beam sections.

Assembly of the equilibrium and continuity expressions at the joint yields a 9 x 9 system of simultaneous equations which can be solved to provide values for the transmission efficiencies, τ, and reflection efficiencies, β, for each wave type, as shown in Fig.6.3.4. The suffices attached to these parameters distinguish between the various combinations of incident and resultant wave types. The first suffix relates to the nature of the incident wave and the second to the nature of the resulting wave after transmission or reflection. For example, τ_{lf} represents the transmission efficiency of a flexural wave resulting from an incident longitudinal wave at the joint.

Horner and White (1990) provided a full set of equilibrium and continuity expressions relating to this problem in the form of a 9 x 9 matrix equation. However, in working through their analysis as part of this study, some of the terms in their equilibrium and continuity equations differed from those developed here. This is probably due to differences in the conventions used in the two analyses, although this is difficult to establish because the conventions employed by Horner and White were not described

in detail in their publication.

For completeness, the solutions to the three-branched joint model developed as part of this study are provided in Appendix E. This is accompanied by similar solutions for the two-branched joint models shown in Fig.6.3.5, which are also required for the analysis of this structure. Beam dimensions and material properties chosen for this example are shown in the Figs.6.3.4 and 6.3.5.

6.3.3 Wave transmission across the valve

For the purposes of this example the valve is represented by a cylindrical mass with its polar axis in line with that of the beams, see Fig.6.3.6. The resulting solutions for the transmission efficiency of both flexural and longitudinal waves across this joint are similar to those developed for the two-branched joint model shown in Fig.6.3.5. In this case however, the angle θ is set to 0° and the term which includes the moment of inertia of the joint has been modified to take account of the change in orientation of the cylinder.

Once again, details of this solution are given in Appendix E. The dimensions and material properties chosen for the valve model are shown in Fig.6.3.6.

6.3.4 Net transmission efficiency and the effect of multiple reflections

The preceding sections deal with the transmission characteristics of the joints in isolation from the remainder of the structure. In finite structures the transmission characteristics across a joint are also affected by the reflective nature of other discontinuities downstream from it. This is because wave energy reflected by a downstream joint is partially transmitted back through the first, reducing its *net* or *effective* transmission efficiency. This effect was identified as a possible cause of the difference between measured and theoretical values for the transmission efficiency across the flanged joint discussed in Chapter 5. It follows that to representatively model the way in which vibrational energy flows through real structures, the effects of these multiple reflections between structural discontinuities must be taken into account.

Horner and White (1990) also addressed this problem and considered the *net* power transfer into a section bounded by two discontinuities, like the one shown in Fig.6.3.7. They showed that if the effects of damping were neglected, an expression for the *net* power transfer into the section could be obtained from the sum of an infinite series and the *net* transmission efficiency becomes:

$$\tau_{net} = \tau_1 \left(\frac{1 - \beta_2}{1 - \beta_2\beta_3} \right) \qquad (6.3.1)$$

where τ_1, β_2 and β_3 are defined in Fig.6.3.7.

To apply the above expression to the beam sections within this branched model, the calculation must be expanded to account for mode conversion and simultaneous transmission of flexural and longitudinal motion. In this case, each transmission and reflection efficiency value shown in Fig.6.3.7 must be broken down into four values to account for mode conversion at the discontinuities, see Fig.6.3.8.

The individual τ and β values required for this model can be obtained from the analytical solutions given in Appendix E, where the incident wave is of a single type. In order to combine these terms to calculate the *net* transmission efficiency, some knowledge of the ratio of flexural to longitudinal energy flow in the previous element must be assumed. For the purposes of this analysis ϕ will be used to represent the amount of flexural wave power as a proportion of the total transmitted wave power and ψ will represent the corresponding proportion of longitudinal wave power. Having defined these terms it is possible to obtain mixed mode values of τ_1, β_2 and β_3 used in equation (6.3.1), by superposition of the contribution from each wave type in the following way.

For the i^{th} element shown in Fig.6.3.8:

$$\tau_1 = \phi_{i-1}(\tau_{ff}+\tau_{fl}) + \psi_{i-1}(\tau_{lf}+\tau_{ll}) \qquad (6.3.2)$$

The nature of the wave now approaching discontinuity 2 will now be characterised by x_f and x_l which are given by:

$$x_f = \frac{\phi_{i-1}\tau_{ff} + \psi_{i-1}\tau_{lf}}{\tau_1} \qquad x_l = \frac{\psi_{i-1}\tau_{ll} + \phi_{i-1}\tau_{fl}}{\tau_1} \tag{6.3.3}$$

Using the above expressions, β_2 can be calculated from:

$$\beta_2 = x_f(\beta_{ff}+\beta_{fl}) + x_l(\beta_{lf}+\beta_{ll}) \tag{6.3.4}$$

and the resulting reflected wave approaching the first discontinuity will be characterised by:

$$x_f' = \frac{x_f\beta_{ff} + x_l\beta_{lf}}{\beta_2} \qquad x_l' = \frac{x_l\beta_{ll} + x_f\beta_{fl}}{\beta_2} \tag{6.3.5}$$

and finally:

$$\beta_3 = x_f'(\beta_{ff}+\beta_{fl}) + x_l'(\beta_{lf}+\beta_{ll}) \tag{6.3.6}$$

This provides the values for τ_1, β_2 and β_3, given by (6.3.2), (6.3.4) and (6.3.6), which can be inserted into (6.3.1) to obtain a value for τ_{net} into each section of the model.

6.3.5 Element conductivity

Previous models described here have only dealt with the transmission of vibrational energy by flexural waves. In the case of this branched system however, mode conversion at the joints makes it necessary to consider the simultaneous transmission of both flexural and longitudinal wave energy.

In the context of the energy flow approach the differential equation governing the steady state conduction and dissipation of flexural energy in a beam structure is:

$$\frac{4c_b^2}{\omega\eta}\frac{d^2e}{dx^2} - \omega\eta e = 0 \tag{6.3.7}$$

and the corresponding expression for longitudinal motion in a rod is:

$$\frac{c_L^2}{\eta\omega}\frac{d^2e}{dx^2} - \omega\eta e = 0 \qquad (6.3.8)$$

In order to model the simultaneous transmission of these two wave types it is necessary to incorporate the effects of the above governing equations in a single finite element form. Ideally this should be done in such a way that the flow of longitudinal energy is governed by the gradient of the longitudinal energy density and similarly for the flexural energy. To achieve this however, the model requires two independent primary variables to represent the individual energy components. This type of approach has been used by Cho and Bernhard (1992) to create an analytical model of an angled beam using the energy flow approach.

Within the context of the modelling work carried out here however, the use of an existing thermal finite element package means that only one primary variable is available. Given this limitation one approach is to combine the governing equations for the two energy components to form a "hybrid" expression, thus:

$$\left(\frac{\phi\ 4c_b^2 + \psi\ c_L^2}{\omega\eta}\right)\frac{d^2e}{dx^2} - \omega\eta e = 0 \qquad (6.3.9)$$

where ϕ and ψ denote the proportions of flexural and longitudinal wave power defined earlier.

The use of this modelling expression is not unreasonable within the context of the energy flow approach because the quantities involved are considered to be of a space- and time-averaged nature. However, because of the frequency dependence of c_b the use of the above expression should really be limited to frequency ranges where c_b and

c_L are of the same order of magnitude. It should also be noted that this rather simplified expression becomes more difficult to apply to structures which are more complex than the straight beams considered here, say for example the case of curved beams where the flexural and longitudinal wave quantities are coupled.

Using the analogy described in section 6.2 and the "hybrid" expression (6.3.9) above, the appropriate conductivity values for the thermal finite elements representing the i^{th} section of beam in this model are given by:

$$K = \frac{(\phi_i \, 4c_{b\,i}^2 + \psi_i \, c_{L\,i}^2)}{\omega \eta_i} \qquad (6.3.10)$$

where c_b, the bending wave speed for a beam, is given by:

$$c_b = \sqrt[4]{\frac{EI\omega^2}{\rho S}} \qquad (6.3.11)$$

and c_L is the longitudinal wave speed, obtained from:

$$c_L = \sqrt{\frac{E}{\rho}} \qquad (6.3.12)$$

The factors ϕ_i and ψ_i can be calculated given knowledge of the transmission and reflection efficiencies at the ends of each section. This calculation is based on determining the *net* transmission of each type of wave within the structure as a factor of the *total* transmission. Again some knowledge of the proportion of the power

carried by each wave type in the previous section, ϕ_{i-1} and ψ_{i-1}, must be assumed.

Using Fig.6.3.9, the flexural power transmitted into the i^{th} section is given by:

$$p_{f\,trans} = \left(\phi_{i-1}\tau_{ff} + \psi_{i-1}\tau_{lf} \right) P_{in} \qquad (6.3.13)$$

and the equivalent longitudinal power is:

$$p_{l\,trans} = \left(\phi_{i-1}\tau_{fl} + \psi_{i-1}\tau_{ll} \right) P_{in} \qquad (6.3.14)$$

In the absence of damping, a proportion of each of the above will be reflected by discontinuity 2 to form a reflected flexural power quantity given by:

$$p_{f\,ref\,1} = \beta_{ff1}\, p_{f\,trans} + \beta_{lf1}\, p_{l\,trans} \qquad (6.3.15)$$

and similarly, the reflected longitudinal power will be given by:

$$p_{l\,ref\,1} = \beta_{fl1}\, p_{f\,trans} + \beta_{ll1}\, p_{l\,trans} \qquad (6.3.16)$$

At the first discontinuity partial reflection will occur once again and the proportion of power reflected back will be:

$$p_{f\,ref\,2} = \beta_{ff2}\, p_{f\,ref\,1} + \beta_{lf2}\, p_{l\,ref\,1} \qquad (6.3.17)$$

and,

$$p_{l\,ref\,2} = \beta_{fl2}\, p_{f\,ref\,1} + \beta_{ll2}\, p_{l\,ref\,1} \qquad (6.3.18)$$

Since damping has been neglected, this process continues indefinitely and the *net* transmission of flexural power through the element is:

$$p_{f\,net} = p_{f\,trans} - p_{f\,ref\,1} + p_{f\,ref\,2} - \ldots\ldots \qquad (6.3.19)$$

and for longitudinal power,

$$p_{l\,net} = p_{l\,trans} - p_{l\,ref\,1} + p_{l\,ref\,2} - \ldots\ldots \qquad (6.3.20)$$

Investigation has shown that values of $p_{ref\,2}$ are much smaller than p_{trans} and subsequent terms in the above series can be neglected.

Thus, the proportion of the *net* flexural and longitudinal power transmitted through the i^{th} section of the structure can be obtained from:

$$\phi_i = \frac{P_{f\,net}}{P_{f\,net} + P_{l\,net}} \qquad \psi_i = \frac{P_{l\,net}}{P_{f\,net} + P_{l\,net}} \tag{6.3.21}$$

These values have been used to calculate the conductivity of the finite elements representing each beam section in the model.

They have also been used to obtain a value for the group velocity, c_g, required to calculate the elements of the joint conductivity matrix defined by equation (6.2.10). This value is given by:

$$c_g = \phi\ 2c_b + \psi\ c_L \tag{6.3.22}$$

Which, like (6.3.9), should only be used in frequency ranges where c_b and c_L are of the same order of magnitude.

6.3.6 Model results

Having established methods for determining the effective transmission characteristics of the joint and beam elements when they form part of the assembled structure, the finite element model described in section 6.3.1 can be used to provide a *global* energy flow model. The main objective of this exercise is to illustrate the use of this energy flow model as a quantitative transmission path ranking tool.

The main factor affecting the global transmission properties of this structure is the balance between the effective transmission efficiency values in each of the two possible transmission paths. Because the inertia of the valve is relatively high in comparison to the stiffness of the beams, its transmission characteristic is governed by a blocking mass effect which is heavily dependent on frequency. This characteristic, obtained by the analysis described in Appendix E, is shown in Fig.6.3.10. It can be seen from this figure that significant attenuation of both flexural and longitudinal wave power is predicted above 1 kHz. Conversely, the transmission characteristics of the branched and angled joints are relatively insensitive to changes in frequency because the cylinder used to model the joint has a much lower inertia than that used to represent the valve. In this case, the major factor affecting the

transmission characteristics across joints of this type is the angular displacement of the limbs, which are fixed for the purposes of this model.

In order to present two cases where the balance between the transmission efficiency values in the two transmission paths is very different, the analysis has been carried out at frequencies of 1000 Hz and 5000 Hz. Fig.6.3.10 shows that the τ values calculated for the valve model at the higher frequency are very much lower than those at the lower frequency. This result influences the *net* transmission efficiencies calculated for the seven joints in the energy flow model. These values, at the two frequencies studied, are presented in Table 6.3.1 below.

Joint Number	Net Transmission Efficiency	
	1000 Hz	5000 Hz
1	0.245	0.074
2	0.747	0.220
3	0.381	0.438
4	0.403	0.539
5	0.363	0.536
6	0.431	0.618
7	0.302	0.390

Table 6.3.1 Net transmission efficiency values for joint elements

It can be seen from the table, that the reduction in the individual τ values across the valve at 5 kHz results in a significant reduction in the net transmission efficiencies of joints 1 and 2 in the energy flow model. (These joint numbers are defined in Fig.6.3.3)

The results of the finite element analysis at the two frequencies are shown in Fig.6.3.11. The values shown represent the level of vibrational power transmitted through the element at the mid-point of each beam, as a percentage of the total power input at the source. At 1000 Hz transmission via the section containing the valve is

marginally higher than that through the section containing the bends. At 5000 Hz however, as a result of the reduction in transmission efficiency across the valve, there is a significant shift in energy flow towards the section containing the bends. Although this general effect might be predicted from inspection of the individual transmission characteristics of the joints, this model quantifies the relative transmission capabilities of each path, thus forming an effective transmission path ranking tool.

6.4 Discussion

This model represents the first application of this approach to provide a quantitative transmission path ranking tool. The energy flow theory forms the core of the analysis and acts to assemble the individual transmission characteristics of the component parts of the structure to provide a *global* picture of the energy transmission through the system. The creation of this type of model has been one of the fundamental aims of this work and has influenced certain aspects of the way that the approach has been developed. This is particularly true in relation to the boundary condition chosen in Chapter 5 to represent transmission across joints.

A common feature of the models described so far is that the form of the energy flow model has remained very general. The structural components are described only by a representative value of their "conductive" properties and a measure of their ability to dissipate energy by damping. Similarly, the joint elements are characterised only by a transmission efficiency value which governs the proportion of the incident energy that flows into subsequent sections of the structure. As a result of this, the modelling approach has the potential to be applied to any general assembly of components. This is made possible because the detailed characteristics of each particular structural feature are considered outside the realms of the energy flow model.

The form of this modelling approach can be illustrated using the schematic shown in Fig.6.4.1. It can be seen that the basic energy flow analysis developed by Wohlever (1988) and Bouthier (1992) forms the core of the model, whether it be implemented analytically or using finite elements. In order to use these relationships to provide a realistic model, representative values for the basic parameters must be established.

These parameters, which relate to the type of structure, the power input, the level of damping and the joint characteristics, are shown in the second level of this schematic.

The third level shows the techniques used within this work to establish values for these parameters. This level represents a methods library from which the best estimates of the modelling parameters can be obtained. There is no limit to the extent of this library since new methods must be added as new structural configurations are considered in the analysis. The information contained in this library will be essential for predicting vibrational energy transmission through structures which may still be at the very early stages of design.

The quality of the predictions obtained using this approach can, of course, only be as good as the estimates of the modelling parameters used in the model and will always be limited by the simplified nature of the energy flow analysis. The results of this modelling exercise do however, show that the approach does have the potential to provide a good indication of the energy flow characteristics within a complex structure at low computational cost. They also show that even if the absolute levels of vibrational energy in each section may not be determined exactly, this approach can provide a quantitative assessment of the relative efficiencies of various transmission paths in a complex structure. In this form, the model provides a very effective quantitative transmission path ranking tool.

6.5 Summary

This chapter describes the implementation of the energy flow approach using finite element analysis. The main points arising from this work are as follows:

1. The equations governing the energy flow approach are of a similar form to those relating to steady state heat conduction. This feature allows an analogy to be drawn between temperature and vibrational energy density which makes it possible to use an existing finite element package to model structures having complex geometries.

2. This approach is used to develop an energy flow finite element model of a multiple transmission path structure. The finite element model serves to assemble the information concerning the individual transmission characteristics of the components in the structure to provide a *global* picture of the energy flow through the system. This model is used to assess the global effect of variations in the transmission characteristics of the individual components of the structure. In doing this, the model acts as an effective transmission path ranking tool.

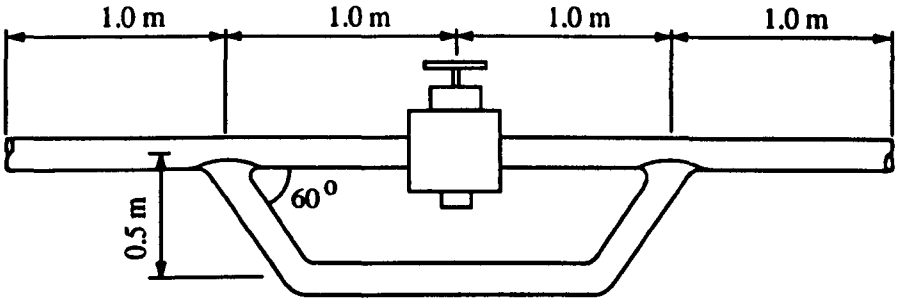

Fig.6.3.1 Pipework structure

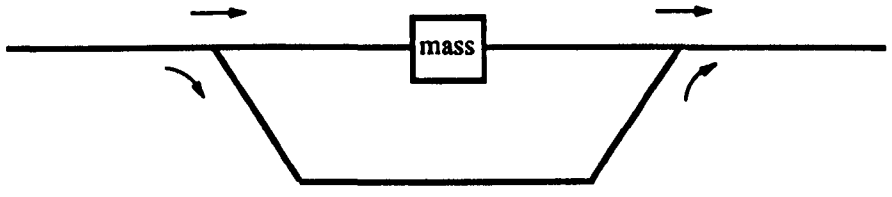

Beam section 20 mm x 20 mm

Young's modulus = 209 x 10^9 N/m^2

Density = 7800 kg/m^3

Fig.6.3.2 Simplified representation of the pipework structure

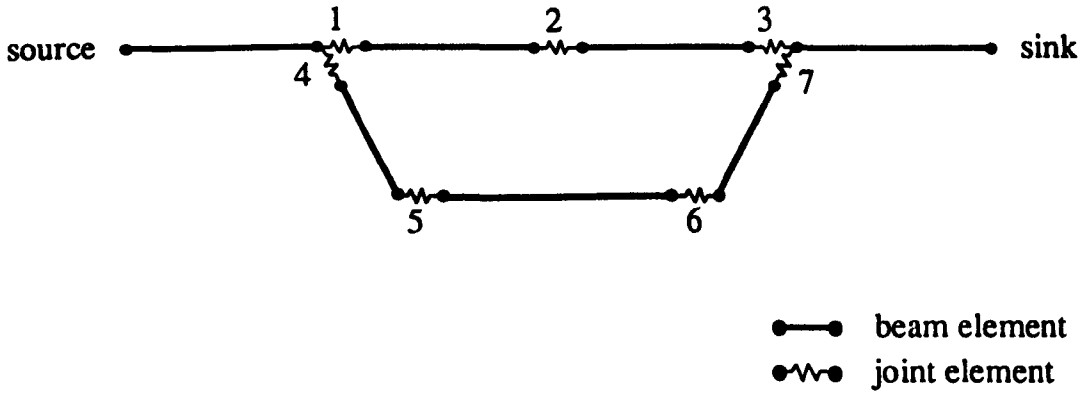

Fig.6.3.3 Finite element energy flow model

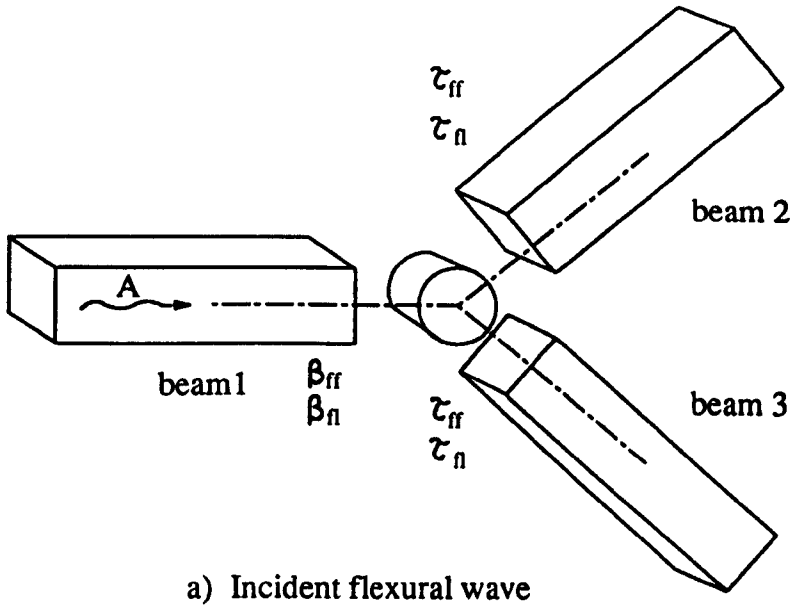

a) Incident flexural wave

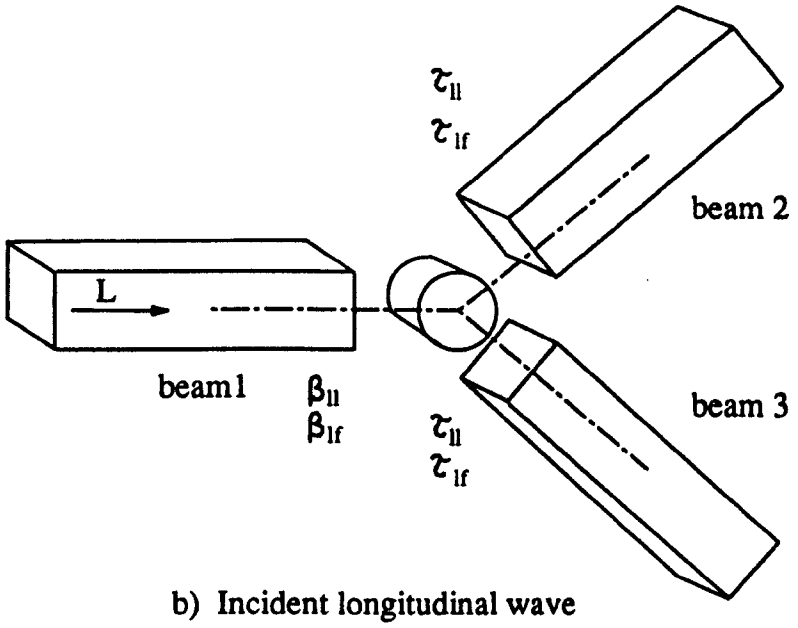

b) Incident longitudinal wave

Model properties

Beam section = 20mm x 20mm
Young's modulus = 209 x 10^9 N/m^2
Density = 7800 kg/m^3

Joint diameter = 20mm
Joint width = 20mm

Fig.6.3.4 Branched joint model

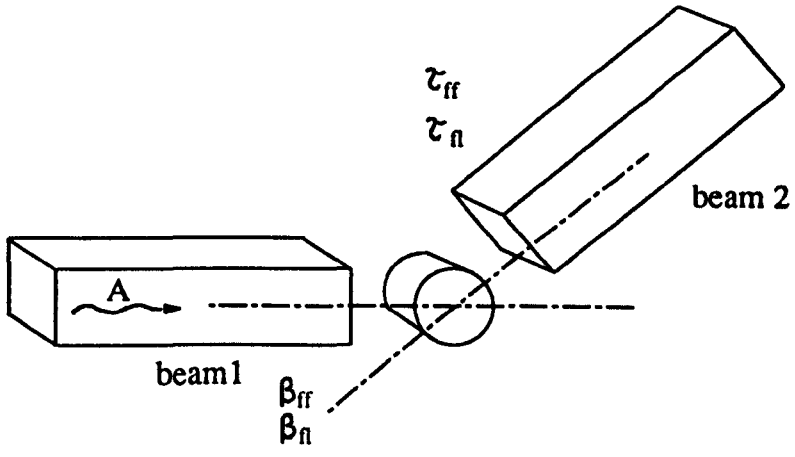

a) Incident flexural wave

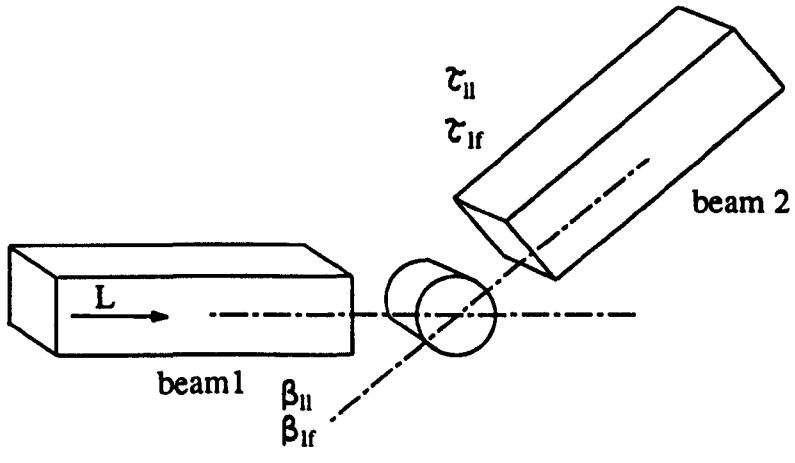

b) Incident longitudinal wave

Model properties

Beam section = 20mm x 20mm
Young's modulus = 209 x 10^9 N/m^2
Density = 7800 kg/m^3

Joint diameter = 20mm
Joint width = 20mm

Fig.6.3.5 Angled beam model

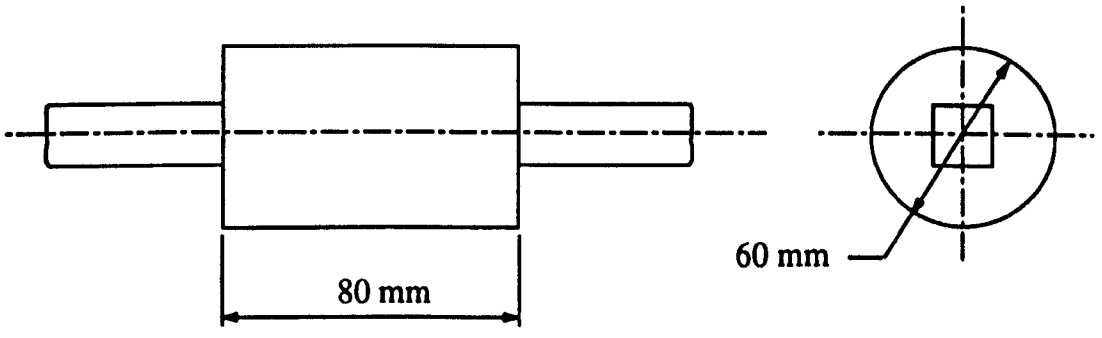

Beam section = 20mm x 20mm
Young's modulus = 209 x $10^9 N/m^2$
Density = 7800 kg/m^3

Fig.6.3.6 Valve representation

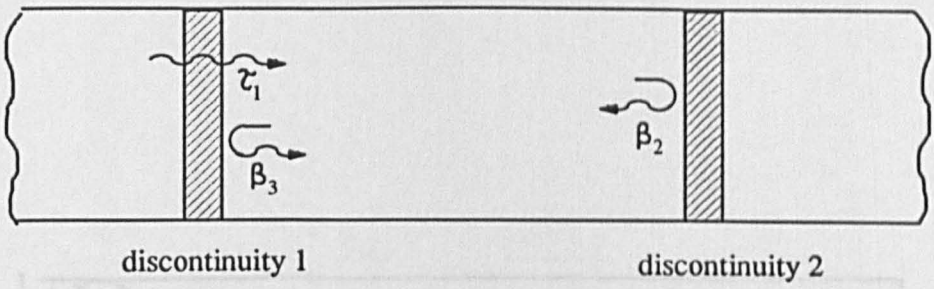

Fig.6.3.7 Beam section bounded by discontinuities

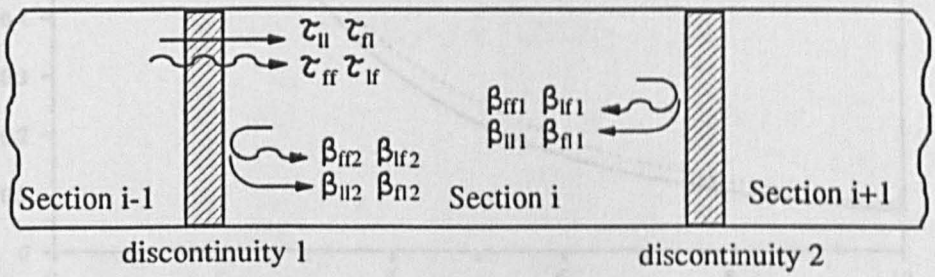

Fig.6.3.8 Transmission and reflection efficiencies under mixed mode conditions

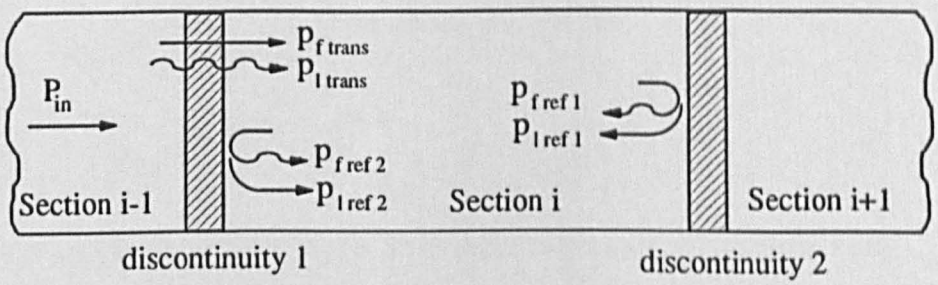

Fig.6.3.9 Multiple reflection in a finite structure

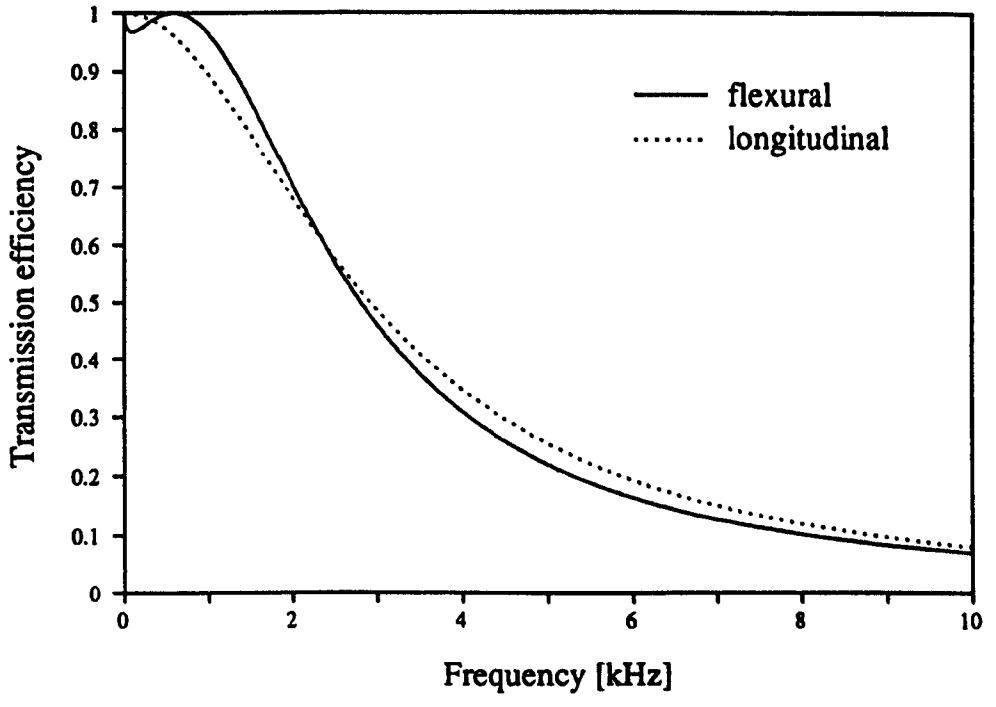

Fig.6.3.10 Transmission efficiencies for flexural and longitudinal waves across the valve model

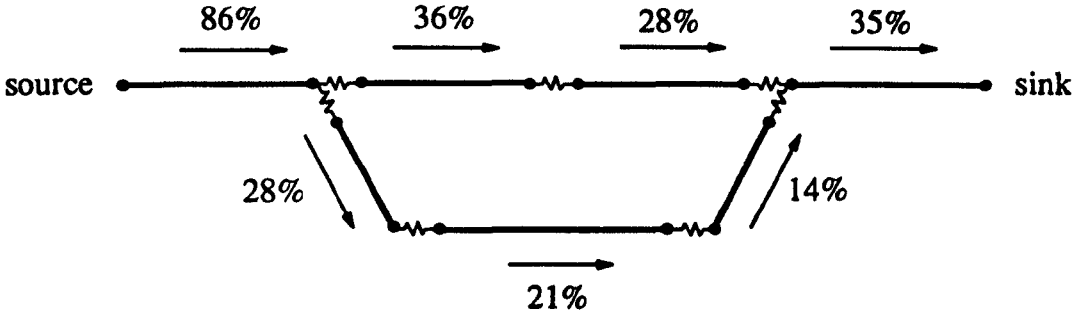

a) analysis at 1000 Hz

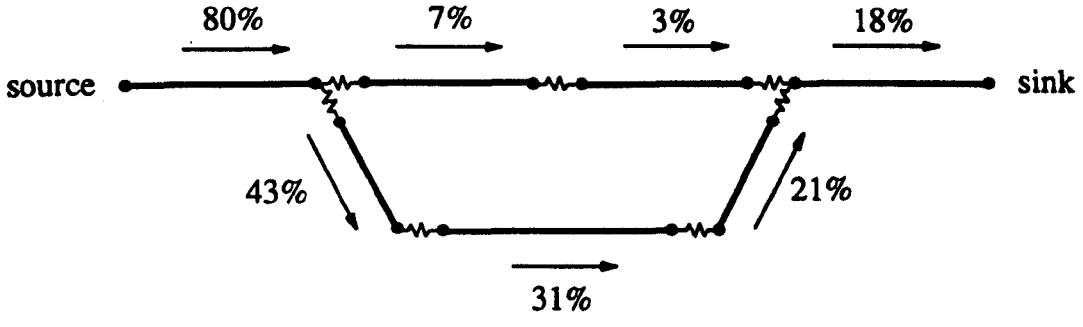

b) analysis at 5000 Hz

Fig.6.3.11 Energy flow predictions provided by the finite element energy flow model

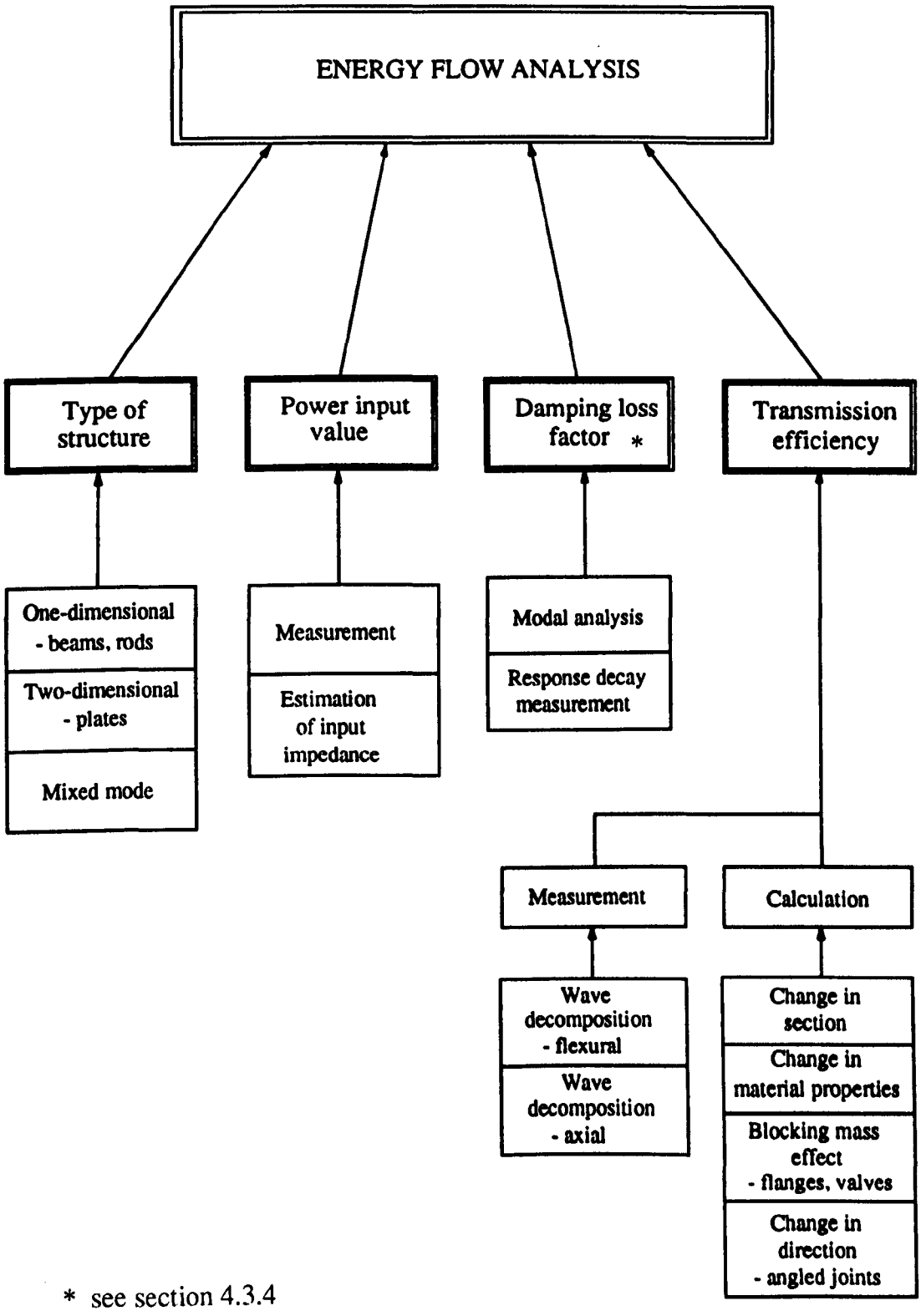

* see section 4.3.4

Fig.6.4.1 Schematic representation of the energy flow approach

Chapter 7

Experimental investigation into vibrational energy flow through a ribbed bulkhead structure

7.1 Introduction

This chapter describes a section of work aimed at assessing the vibrational energy flow characteristics of a ribbed bulkhead structure. This type of structure is a common feature of ship construction and normally consists of a section of plate, reinforced in one major direction by a number of parallel beam-like ribs. This configuration gives rise to rather complex wave transmission characteristics which have strong directional dependence.

The study of wave transmission through reinforced plate structures has been addressed in a number of ways. Belov et al (1977) and Nikiforov (1990) described simplified energy conduction models to predict the global transmission of vibrational energy through this type of structure at higher frequencies. Nikiforov's approach in particular, is aimed at assessing attenuating effects which result from partial reflection of wave energy at the ribs.

Lindqvist and Fahy (1976) and Nilsson (1976) approached this problem from a more analytical standpoint. These analyses are based on the conditions of equilibrium and continuity at the junction between the plate and the reinforcing ribs. This type of approach leads to a very detailed mathematical model of the structure which is able to account for flexural, longitudinal and torsional motion, but only in the direction parallel to the ribs.

The work described here consists of an experimental investigation into the vibration transmission characteristics of a section of ribbed plate which is representative of a

real marine bulkhead. The first part of the study involves experimental wavenumber measurement to determine the directionality of the structure's energy transmission characteristics. This is followed by a series of structural intensity measurements to provide an indication of the general pattern of vibrational energy flow through this rather complex structure.

A major incentive behind this experimental work is to obtain information on which to base the development of a two-dimensional energy flow model of the structure. It will also provide experimental results for comparison with model predictions. This modelling work will be described later in Chapter 8.

7.2 The test structure

The general form of the bulkhead structure is shown in Figs.7.2.1 and 7.2.2. These photographs are complemented by a schematic of the structure given in Fig.7.2.3. This schematic shows the major dimensions and certain features of the structure which will be referred to later in the text.

It can be seen from these figures that the bulkhead section is essentially a plate, stiffened in the vertical direction by a number of beam-like ribs. Extra localised stiffness has been introduced in the horizontal direction around a section which represents a machinery mounting platform. The lower portion of the structure is buried in sand to provide an energy sink.

For ease of reference throughout this chapter "the vertical direction" will be used to denote the direction parallel to the major ribs and "the horizontal direction" to denote that perpendicular to the major ribs. This notation is illustrated in Fig.7.2.3.

Excitation is provided by a shaker located towards one corner of the structure. This location has been chosen because it presents a clear energy flow path to the sand which is not interrupted by the machinery mounting platform. Because of this, the initial flow of vibrational energy away from the source should be influenced only by the presence of the ribs, rather than the machinery mounting platform which may have

more complicated effects.

The shaker is connected to the plate via a mounting block assembly shown in Fig.7.2.4 and in schematic form in Fig.7.2.5. This assembly was designed to allow a force gauge and accelerometer to be mounted back-to-back at the shaker connection to measure the mechanical power imparted to the block. Because of the geometry of the block this power is converted into a combination of force and moment components which excite flexural waves in the bulkhead plate. It should be noted that this arrangement is unable to detect components of power imparted to the block due to bending of the shaker push rod. An assessment of the likely influence of this effect based on the properties of the real structure has shown that the bending moment in the rod contributes less than 1% of the total moment exciting the plate in the frequency range considered here. It can therefore be safely neglected for the purposes of this study.

7.3 Modal analysis of the structure

Before studying energy flow in this bulkhead structure it is essential to develop an understanding of its general dynamic characteristics. Much of this can be achieved by studying the natural mode shapes of the structure provided by experimental modal analysis.

Response measurements made over the surface of the bulkhead plate were used to provide a modal analysis of the structure over a 0-2.5 kHz frequency range. This analysis gives natural frequencies, mode shapes and modal damping loss factors for the first 30 modes of vibration. Examination of this data shows that the mode shapes of the structure are predominantly flexural up to a frequency of about 1000 Hz. One strong torsional mode is evident around 750 Hz. Beyond 1000 Hz the mode shapes become more complex, but do exhibit strong components of flexural behaviour.

The dominance of flexural motion suggests that the behaviour of this structure can be approximated to an equivalent plate-like structure in flexure. Unlike a simple plate however, the bulkhead is greatly stiffened in one direction by the presence of the ribs. This means that the equivalent plate structure must possess orthotropic stiffness properties in order to properly represent the characteristics of the bulkhead plate.

The assumption of plate behaviour means that the level of vibrational energy flow through the structure can be measured using a structural intensity technique which has previously been applied to plates. The use of this technique will inevitably lead to some degree of error in the measured results because the motion of the bulkhead plate

is unlikely to be purely flexural, particularly at high frequencies. Nevertheless, the use of such an approach is necessitated because more exact techniques for the treatment of complicated structures do not yet exist. Despite the approximate nature of the measurement technique it should be able to provide an assessment of at least the general level of energy flow for comparison with model predictions.

7.4 Wave transmission characteristics of the structure

In the previous section it was suggested that the behaviour of the bulkhead section could be approximated to that of an equivalent orthotropic plate. The first part of this study is aimed at assessing the directionality of the global transmission properties of the structure by establishing its wavenumber characteristics in each of the major directions. This information will be generally useful in assessing the wave transmission characteristics of structures of this type and in particular, it should be able to provide some measure of the *effective* stiffness of the structure which is influenced by the presence of the stiffening ribs.

The determination of wavenumber will also have a role later in the development of a representative energy flow model of this structure. This is because wavenumber can be directly related to the group velocity, which is one of the parameters required to determine the "conductive" properties of the elements in the energy flow model.

7.4.1 Wavenumber for ribbed plates

Wavenumber, k, is a well established quantity used to characterise the transmission of harmonic wave energy through a structural or acoustic medium. Cremer (1973) provides expressions for calculating this quantity for simple beams and plates. In the case of this bulkhead however, which comprises a combination of beam and plate sections, the calculation of wavenumber is significantly more difficult.

Nilsson (1976) produced an analytical solution to determine the wavenumber for a structure of this type as part of an investigation into noise transmission in ships. In his analysis the bulkhead was broken down into a number of I-shaped sections consisting of a strip of hull plate with a central stiffening rib, illustrated in Fig.7.4.1.

The dimensions given in the figure correspond to the bulkhead used in the present study.

By considering equilibrium and continuity of a single beam-like section experiencing flexural and longitudinal motion, Nilsson was able to obtain the wavenumber characteristic for transmission in the direction parallel to the ribs. This analysis predicted that the wavenumber of the structure at lower frequencies remained very close to that for simple beam bending of the I-shaped section. At higher frequencies the wavenumber increased more rapidly with frequency and tended towards the value corresponding to flexure of the hull plate in isolation from the ribs.

This analysis gives some insight into the likely transmission characteristics of the bulkhead section in the direction of the ribs. It does not however, provide any information about the transmission of energy in the direction perpendicular to the ribs. For the purposes of this investigation it is convenient to obtain an estimate of wavenumber in each direction by a more general approach.

7.4.2 Flexural wavenumber measurements on beams and plates

The use of flexural wavenumber measurements on beam structures for the evaluation of structural intensity has been described by Meyer et al (1990) and Wagstaff et al (1990). These analyses rely on the assumption that the measurements are made in the far-field region where the acceleration, a, at any position, x, can be expressed as:

$$a(x,t) = \left(Ae^{-ikx} + Be^{ikx} \right) e^{i\omega t} \qquad (7.4.1)$$

differentiating (7.4.1) twice with respect to x, gives:

$$\frac{\partial^2 a}{\partial x^2} = - k^2 \left(Ae^{-ikx} + Be^{ikx} \right) e^{i\omega t} \qquad (7.4.2)$$

Substitution from (7.4.1) gives:

$$k^2 = - \frac{1}{a} \frac{\partial^2 a}{\partial x^2} \qquad (7.4.3)$$

The spatial derivative of the transverse acceleration at a point in the structure can be evaluated using a finite difference technique. In the case of a second-order derivative, the finite difference approximation is:

$$\frac{\partial^2 a}{\partial x^2} = \frac{1}{\Delta^2} \left(a_1 - 2a_2 + a_3 \right) \qquad (7.4.4)$$

where a_1, a_2 and a_3 are the outputs of a three accelerometers placed in a linear array at a small distance Δ apart, see Fig.7.4.2.

Substituting (7.4.4) into (7.4.3) and noting that the central acceleration a_2 coincides with the general value a, yields:

$$k^2 = \frac{2a_2 - a_1 - a_3}{\Delta^2 \, a_2} \qquad (7.4.5)$$

By multiplying top and bottom of (7.4.5) by the complex conjugate of a_2 it can be rewritten in terms of auto- and cross-spectral quantities, ie:

$$k^2 = \frac{2X_{22} - X_{12} - X_{32}}{\Delta^2 \, X_{22}} \qquad (7.4.6)$$

In general, the ratio (X_{nm} / X_{mm}) is the frequency response function, H_{nm}, between two dynamic signals. Hence (7.4.6) becomes:

$$k^2 = \frac{1}{\Delta^2} \left(2 - H_{12} - H_{32} \right) \qquad (7.4.7)$$

or,

$$k = \frac{1}{\Delta}\sqrt{2 - H_{12} - H_{32}} \qquad (7.4.8)$$

Meyer et al (1990) suggested that this approach could also be used for measuring flexural wavenumber in any given direction in a plate. Having established that the motion of the bulkhead can be approximated to that of a plate in flexure, this technique should be able to provide a measurement of wavenumber in its two major directions.

The results of these measurements will of course be affected by the fact that the motion of the bulkhead plate is not purely flexural, particularly at higher frequencies. It must also be remembered that the analysis assumes that measurements are made under far-field conditions, whereas the complicated nature of the present structure makes it difficult to identify areas where true far-field conditions exist. Despite these limitations, the technique should be able to capture at least the trend of the wavenumber characteristic from which a representative values can be estimated.

Wavenumber measurements were made at a number of locations across the bulkhead plate using the three-accelerometer technique described above. The axes of the arrays were aligned both vertically and horizontally to establish the wavenumber characteristics in each direction. Only a selection of these results will be presented here for discussion. These examples correspond to measurements made at six locations marked in Fig.7.4.3.

7.4.3 Results of the wavenumber measurements

The results of the wavenumber measurements made in the direction parallel to the ribs are shown in Figs.7.4.4 to 7.4.7. Also shown in these figures are the theoretical wavenumber values for beam flexure of the I-shaped section, shown in Fig.7.4.1, and flexure of the bulkhead plate in isolation from the ribs.

These values are denoted by k_b and k_p respectively and are given by:

$$k_b = \left(\frac{\rho S}{EI} \right)^{\frac{1}{4}} \omega^{\frac{1}{2}} \tag{7.4.9}$$

and

$$k_p = \left(\frac{12\rho(1-\nu^2)}{Eh^2} \right)^{\frac{1}{4}} \omega^{\frac{1}{2}} \tag{7.4.10}$$

where I and S correspond to the second moment of area and cross-sectional area of the I-shaped section shown in Fig.7.4.1, h represents the thickness of the bulkhead plate and ν is Poisson's ratio.

The measured results show some instability when compared to the theoretical values. This is probably due to the fact that the motion of the structure at the point of measurement is more complex than that of pure far-field flexural motion, on which the derivation of equation (7.4.8) was based. Despite this, trends in the data can be clearly identified from which an estimate of the wavenumber characteristic can be obtained.

Figs.7.4.4 and 7.4.5 show measurements obtained in the direction parallel to the ribs at locations 31 and 39, which are identified in Fig.7.4.3. These results show that at lower frequencies, in this case below about 2.5 kHz, the wavenumber of the structure remains close to the value corresponding to flexure of the I-shaped section shown in Fig.7.4.1. Above this frequency the measured characteristic moves towards the value which corresponds to flexure of the plate in isolation from the ribs. These observations are in line with those predicted by Nilsson (1976).

Figs.7.4.6 and 7.4.7 show measurements obtained in the same direction at locations 30 and 38. These results show a similar trend to the ones obtained at 31 and 39 although at higher frequencies, the characteristic remains closer to that of the I-shaped beam rather than tending towards that for the plate . This observation can be explained by the fact that these points correspond directly with the positions of

stiffening ribs. It is not surprising therefore, that the motion in these areas is strongly influenced by the ribs throughout the frequency range.

Although there is some difference in the characteristics obtained at these four points at higher frequencies, the measured results below 2.5 kHz compare well with the value calculated for flexure of the I-shaped beam section shown in Fig.7.4.1. This result will have a direct bearing on the development of the energy flow model which will be described in the next chapter. Firstly it implies that at lower frequencies, in this case below 2.5 kHz, the wave transmission characteristics in the vertical direction are approximately uniform across the width of the plate. Secondly, it shows that k_b is a good estimate of the wavenumber characteristic in this direction. This quantity will be used to calculate a representative value for the "conductive" properties of the elements in the energy flow model in the vertical direction.

Wavenumber measurements made in the direction perpendicular to the ribs are shown in Figs.7.4.8 and 7.4.9. These results show that throughout the frequency range, the measured wavenumber in this direction remains close to the value calculated for the flexure of the bulkhead plate in isolation from the ribs. This suggests that the ribs have little effect on the stiffness of the plate in the horizontal direction. They also show that k_p provides a good estimate of the wavenumber for motion across the bulkhead plate for use in the development of the energy flow model.

7.5 Structural intensity measurements on the bulkhead plate

The second part of this experimental study involves structural intensity measurements made at a number of locations over the surface of the bulkhead plate. The purpose of this exercise is two-fold: firstly, to attempt to build an experimental picture of the way in which vibrational energy is transmitted through this rather complex structure, secondly, to provide a datum against which model predictions can be compared.

7.5.1 The measurement approach

In attempting to make these measurements one immediately comes up against the problem of finding an appropriate measurement technique, given the complexity of

this structure. Techniques for measuring structural intensity in simple beam and plate structures are well established. In the case of more general structures however, such techniques do not yet exist. To assess the level of vibrational energy flow in this bulkhead it is once again necessary to assume that the motion of the bulkhead plate can be approximated to that of a simple plate in flexure. Earlier examination of the mode shapes of this structure showed that the validity of this assumption is good below a frequency of about 1000 Hz. Beyond this frequency the mode shapes become more complicated and the level of approximation increases. For this reason, structural intensity measurements made on the bulkhead plate will be limited to an upper frequency of 1250 Hz.

Linjama and Lahti (1989) showed that the measurement of far-field structural intensity in a plate experiencing flexure, in any chosen direction, can be achieved using a two-accelerometer technique similar to the one previously employed on beams. In this case however, the structural intensity is evaluated in terms of *power per unit width of plate* and given by:

$$p = \frac{2}{\Delta\omega^2}\left(\frac{EI'\rho h}{(1-\nu^2)}\right)^{\frac{1}{2}} \mathrm{Im}\,(X_{21}) \qquad (7.5.1)$$

where $\mathrm{Im}(X_{21})$ is the imaginary part of the cross-spectrum between the outputs of the two accelerometers placed a small distance, Δ, apart. I' represents the second moment of area of the plate section *per unit width.*

It is important to note that this expression is only strictly valid if measurements are made under far-field conditions. Given the complexity of this structure it is difficult to determine the extent of near-field effects. In the 0-1000 Hz frequency range however, the wavelength of flexural motion in this structure is generally significantly larger than the distance between the ribs. This suggests that any local effects of the ribs in disturbing the wave motion in this structure are not so important at these lower frequencies. Instead, their major effect can be considered as an increase in the global stiffness of the bulkhead in the vertical direction. This being the case, the major

discontinuities in the structure are likely to be limited to the site of the power input, the machinery mounting platform and the edges of the bulkhead plate. In regions away from these major discontinuities this far-field technique should be able to provide a good measure of the structural intensity in the plate. Elsewhere in the structure it should be possible to at least establish the general level of structural intensity, despite the influence of near-field effects.

The wavenumber measurements clearly indicate that at lower frequencies the bulkhead plate exhibits orthotropic wave transmission properties. This difference in properties is a result of the extra stiffness provided by the ribs, which acts predominantly in the vertical direction. In order to calculate structural intensity from cross-spectral measurements using equation (7.5.1), this difference in stiffness must be accounted for.

For the horizontal direction, the wavenumber measurements suggest that the *effective* stiffness of the bulkhead is comparable to that of the bulkhead plate in isolation from the ribs. This is given by:

$$\left(EI' \right)_{horiz} = \frac{Eh^3}{12} \tag{7.5.2}$$

where h represents the thickness of the plate.

In the vertical direction, the wavenumber characteristic of the plate/rib combination was found to be comparable with that of an I-shaped beam. It follows that the effective stiffness in this direction (per unit width of plate) is:

$$\left(EI' \right)_{vert} = \frac{EI_{beam}}{0.11} \tag{7.5.3}$$

where I_{beam} is the second moment of area of I-section shown in Fig 7.4.1 and 0.11 is the width (in metres) of the section of bulkhead that this strip represents.

Structural intensity measurements were made using accelerometer pairs mounted at 41 locations over the surface of the bulkhead plate. The position and orientation of these

measurements are shown in Fig.7.5.1.

In using equation (7.5.1) to evaluate structural intensity it is useful to assess the errors introduced by employing finite difference approximations. Equation (4.3.13) shows that finite difference errors are related to the quantity $k\Delta$. In this case, the accelerometer spacing Δ was nominally set at 20 mm. Using the wavenumber information obtained in section 7.4, the maximum expected finite difference errors are less than 10% at the upper frequency limit of these measurements. Phase mismatch errors were eliminated from these measurements using the switching technique, described in section 4.3.5.

7.5.2 Results of the structural intensity measurements

Having established the effective stiffness of the structure in each direction using equations (7.5.2) and (7.5.3), the structural intensity at points in the structure can be evaluated from cross-spectral measurements using equation (7.5.1). A number of these results will be used to provide an indication of the way in which vibrational energy flows through this structure from source to sink.

The structural intensity spectra presented here are not continuous. This is due to the presence of negative spikes in the measured cross-spectral data, which generally occurred away from the resonances of the structure where the level of energy flow is relatively low. At these low levels of energy flow, the signal-to-noise ratio of the measured data is poor and measurement errors are difficult to avoid. In calculating structural intensity, only the parts of the spectra which indicate energy flow away from the source were retained. This approach generally retained the peaks in the spectra which correspond to the natural frequencies of the structure. Despite the discontinuous nature of the spectra, the general level of energy flow at each point in the structure can still be clearly identified, particularly around resonances.

An indication of the energy flow characteristics of the structure can be obtained by making comparisons between the spectra obtained at various points around the shaker location. In making these comparisons the spectrum showing vertical energy flow

through point 6 will be used as a common datum.

Fig.7.5.2 shows that the energy flowing downwards from the source, measured at point 6, is generally much higher than that flowing upwards, through point 2. This result is to be expected since it indicates that the energy is predominantly flowing towards the sink. It is more surprising however, to compare the measured spectra at points 5 and 7, directly over the ribs, with that measured at point 6. Figs.7.5.3 and 7.5.4 clearly indicate that the energy flow at points 5 and 7 are very much lower than that measured at 6. This observation suggests that the energy in this area is concentrated in the section of plate between the two ribs. This suggestion is reinforced by the fact that the energy flow levels measured in the horizontal direction at locations 4 and 8 are also very much lower than that flowing vertically through 6. These comparisons are made in Figs.7.5.5 and 7.5.6.

At points in the structure closer to the sand there is evidence that the above effect diminishes. Fig.7.5.7 shows that the energy flow at location 31, directly below 6, is significantly lower than that closer to the shaker. This suggests that the energy contained between the ribs, measured at point 6, has spread across the plate as it progresses towards the sink. This suggestion is backed up by comparisons of the levels of energy flow at points 30, 31 and 32, shown in Figs.7.5.8 and 7.5.9. These figures show that there is only a relatively small difference between the levels of energy flow at adjacent points. Similar characteristics were exhibited by all the results obtained along this lower line of measurement points from 29 to 41, indicating that the energy flow becomes more evenly distributed across the structure in regions closer to the sand.

To check the quality of these structural intensity measurements it would be useful to be able to compare them to the power input measurement made at the shaker. Unfortunately, this is not immediately possible because of a disparity in the units, the power input being measured in units of *watts* whereas the structural intensity is evaluated in terms of *watts per unit width of plate.*

It is possible to make a direct comparison however, if one considers the total energy flow across a boundary around the shaker attachment. The boundary chosen for this calculation is shown in Fig.7.5.10, together with the locations and directions of four structural intensity measurements which were chosen as being representative of the level of energy flow across each edge of the boundary. Assuming that the flow of energy across the boundary is uniform along each edge, these four measurements can be used to calculate a value for the total vibrational power crossing the boundary. Because a "representative length" has been attached to each measurement, a value for the total power can be obtained in units of *watts* and compared directly to the power input measurement.

The comparison between the power input measurement and the calculated power crossing the boundary is shown in Fig.7.5.11. It can be seen that the general form of the two spectra compare very well, particularly above 300 Hz. This shows that there is good coherence between the structural intensity and power input measurements. Over the latter half of the spectrum however, the calculated power crossing the boundary is higher than the measured power input, which cannot realistically occur. One possible cause for this discrepancy could be linked to the neglect of near-field effects when making structural intensity measurements in this area. A more likely reason however, can be identified from the wavenumber measurement made in the vertical direction at point 31, shown in Fig.7.4.4. This plot indicates that below about 2.5 kHz, the measured wavenumber on the vertical line through point 6 is slightly higher than that calculated for the I-shaped beam section. This implies that the effective stiffness of the structure in this region is actually somewhat lower than the value used in the structural intensity calculation. Having adopted an over-estimate of the effective stiffness of the section at the point of measurement, an over-prediction of the structural intensity at this point will inevitably result.

It should be noted that this feature was not observed in measurements made in other regions of the structure. In most cases the measured results, although possessing scatter, correspond more closely to the value of k_b in the 0-2.5 kHz frequency range. This is illustrated in Figs.7.4.5 and 7.4.7. It is difficult to determine whether this

variation in the measured wavenumber characteristics is due to experimental problems, or actually reflects variations in the stiffness of different regions of the structure. The latter is certainly possible because of features like the machinery mounting platform and would explain the discrepancy observed in Fig.7.5.11.

This analysis shows that the two-accelerometer structural intensity technique does provide sensible measurements of the energy flow through the plate in this region and should therefore be able to reflect the general level of energy flow around the structure. It is also evident however, that some uncertainty in the absolute value of these measurements must be accepted due to the difficulty in establishing a representative value for the stiffness of the structure at the point of measurement.

7.6 Discussion

The work described in this chapter has shown that, given some sensible approximation, it has been possible to experimentally determine the general energy flow characteristics of this rather complex ribbed bulkhead structure.

These measurements have identified a means of obtaining a representative estimate of wavenumber for structures of this type which ties in well with earlier theoretical work. They also served to quantify the global stiffening effects of the ribs, which provided a measure of the effective stiffness of the structure for use in the structural intensity calculation. It will be shown later that this wavenumber information will also be useful in the development of an energy flow model of the structure.

It is clear from the quality of the structural intensity measurements that they are subject to some degree of uncertainty. This uncertainty is mainly due to:

a) the assumption of pure flexural motion at the point of measurement.
b) neglect of near-field effects.
c) likely variations in the effective stiffness of the structure.

These measurements do however, reflect the general level of energy flow around the

structure and although their absolute values may be subject to error, they are very useful in building up comparative observations concerning energy flow. These comparisons were able to identify an initial concentration of energy close to the source which spreads out more evenly as the energy flows towards the sink.

It should be remembered that the observations extracted from these results are subject to interpretation and cannot be considered as entirely conclusive. In attempting to clarify some of the uncertainties identified in the course of this work, it would be useful to apply these experimental techniques to a more uniform ribbed structure, where the effects of near-field contributions and variations in structural stiffness could be more easily assessed. Once the effects of these features are better understood attention could perhaps be turned to the study of the attenuating effects perpendicular to the ribs. This feature could not be included in this work due to the insensitivity of the measurement techniques.

7.7 Summary

This chapter described an experimental study to assess the way in which vibrational energy is transmitted around a ribbed bulkhead structure. The main points arising from this work are as follows:

1. The results of an experimental modal analysis showed that the behaviour of the structure could be approximated to that of an orthotropic plate in flexure. This approximation meant that existing measurement techniques could be used to make measurements of flexural wavenumber and structural intensity over the surface of the bulkhead plate.

2. A three-accelerometer technique was able to provide wavenumber measurements which agreed well with earlier theoretical work. They were also able to quantify the orthotropic wave transmission properties of the bulkhead and provide effective stiffness values for use in the structural intensity calculation.

3. The results of structural intensity measurements made over the surface of the bulkhead plate were subject to a significant amount of scatter due to the assumption of pure flexural motion and the neglect of near-field effects. Despite this scatter, it was possible to estimate the general level of energy flow at points in the structure which was used on a comparative basis to establish the general pattern of energy flow.

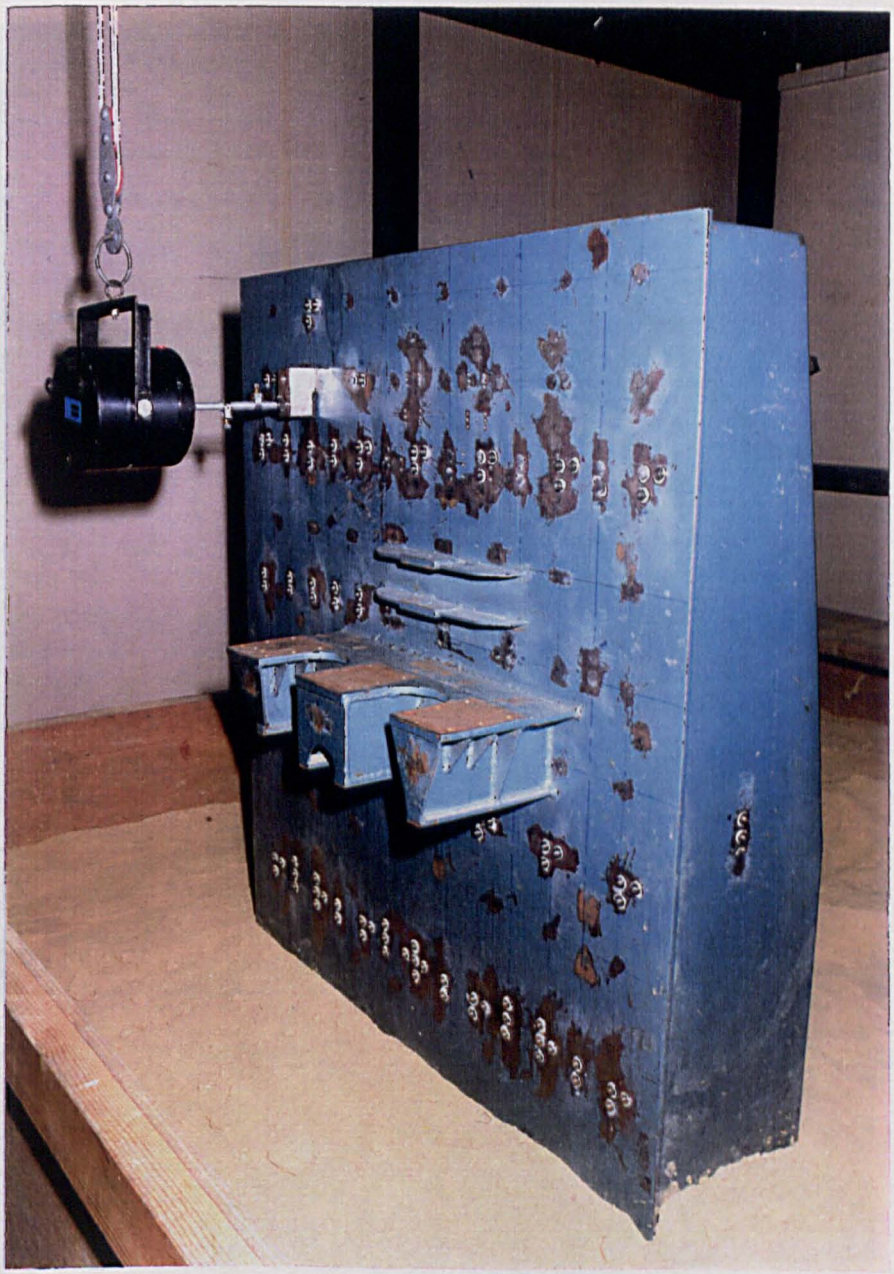

Fig.7.2.1 Front view of the bulkhead structure showing the location of the shaker and machinery mounting platform

Fig.7.2.2 Rear view of the bulkhead structure showing the rib pattern

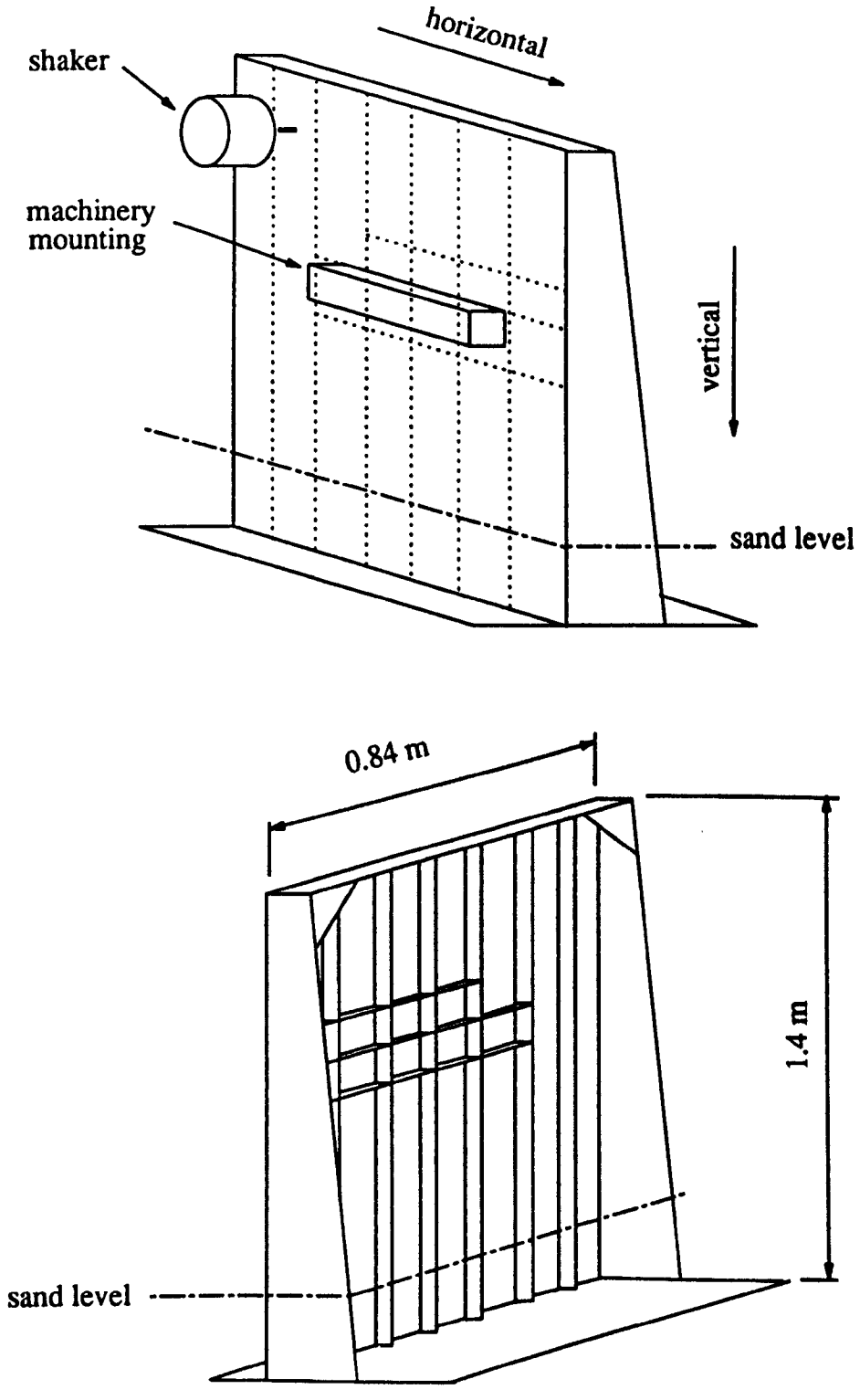

Fig.7.2.3 Schematic view of bulkhead section

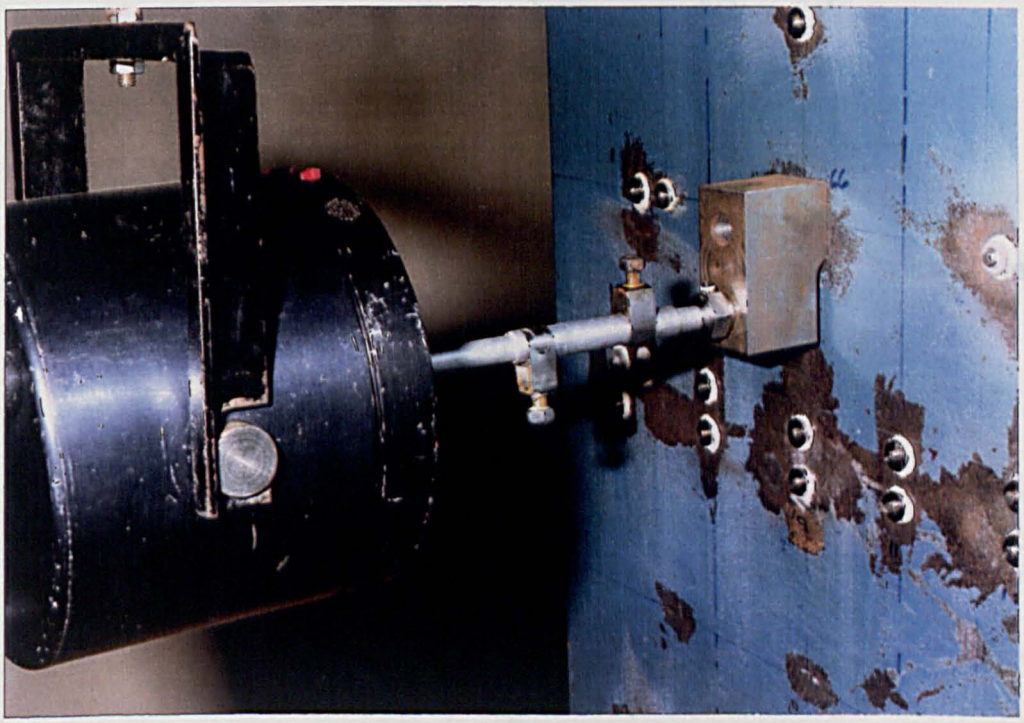

Fig.7.2.4 The shaker mounting arrangement

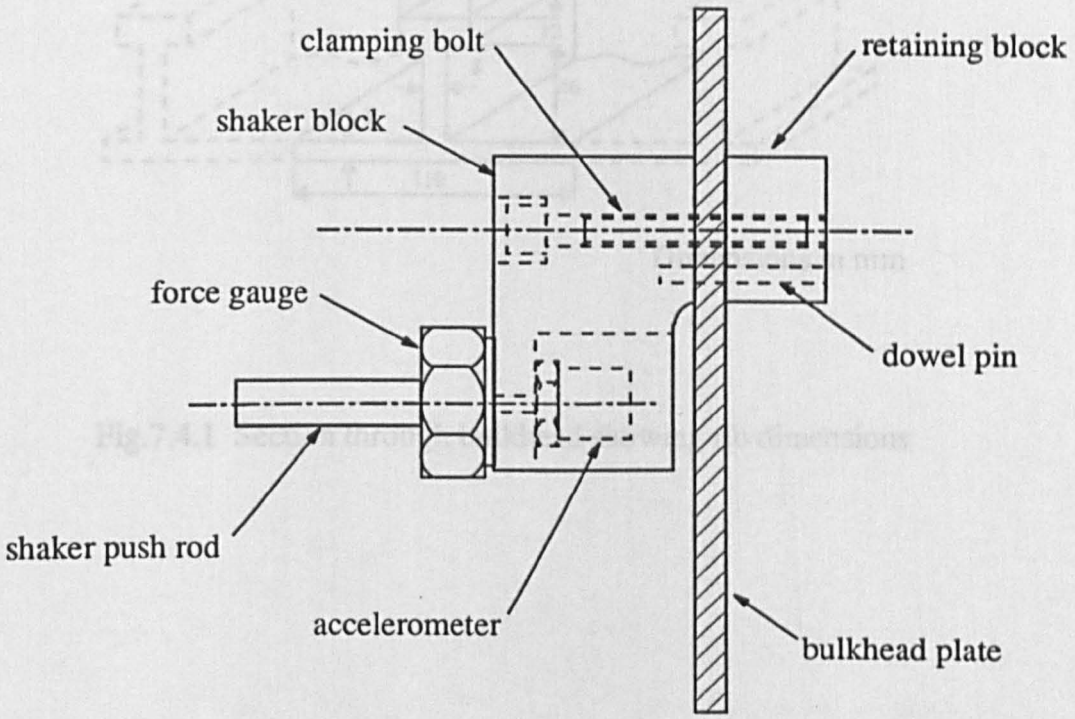

Fig.7.2.5 Shaker mounting block assembly

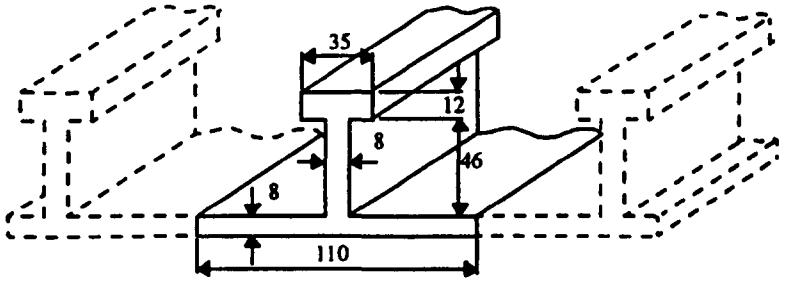

Dimensions in mm

Fig.7.4.1 Section through bulkhead showing rib dimensions

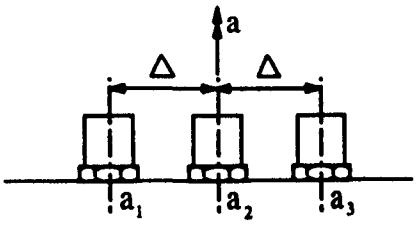

Fig.7.4.2 Three accelerometer array for flexural wavenumber measurement

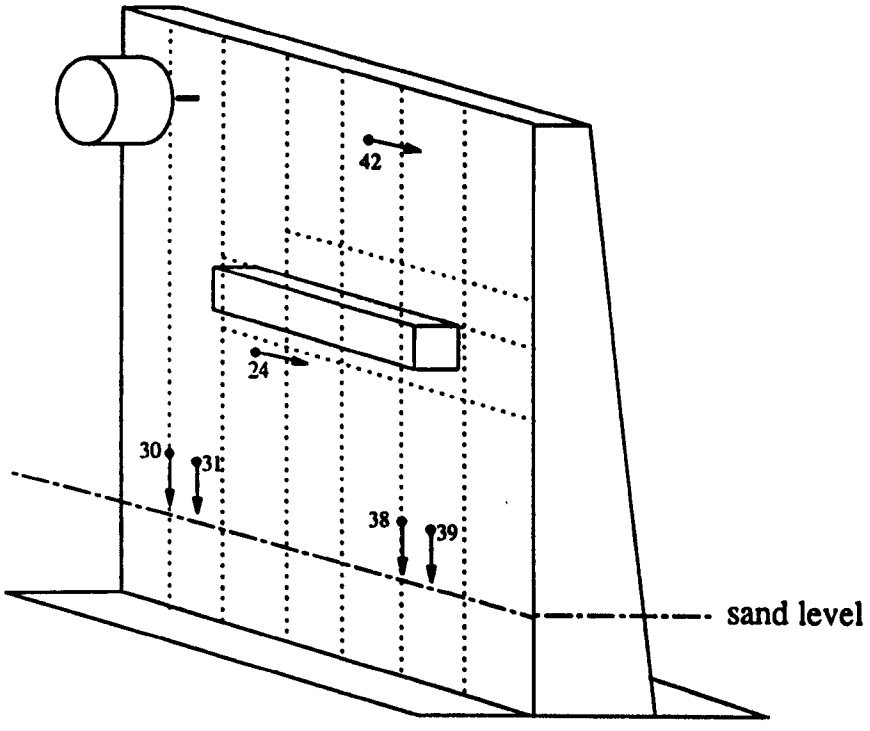

Fig.7.4.3 Location of wavenumber measurements on the bulkhead plate

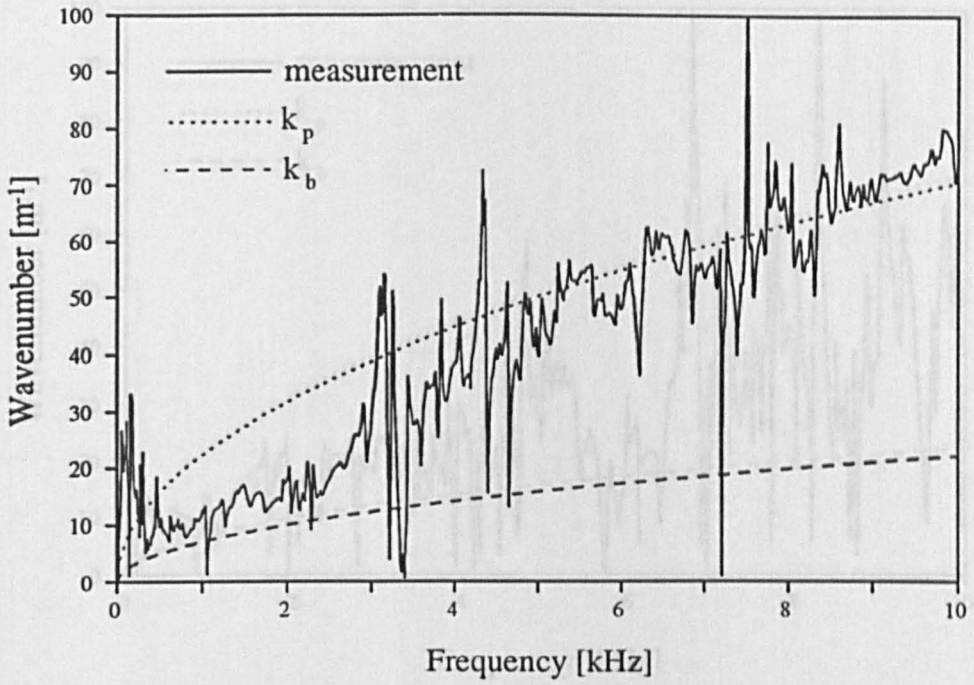

Fig.7.4.4 Measured wavenumber in the direction parallel to the ribs at location 31

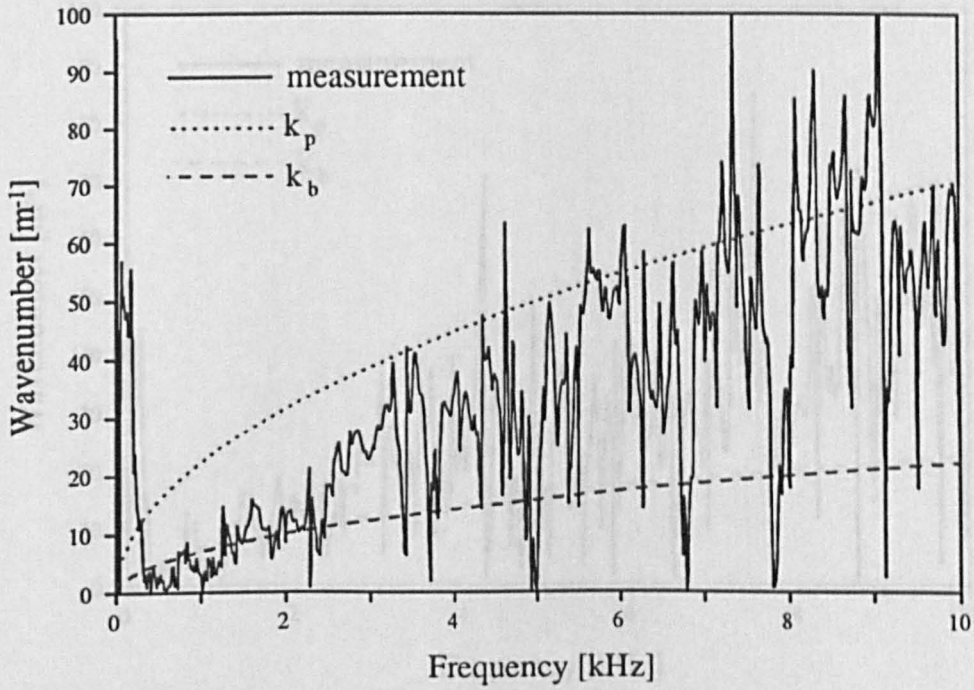

Fig.7.4.5 Measured wavenumber in the direction parallel to the ribs at location 39

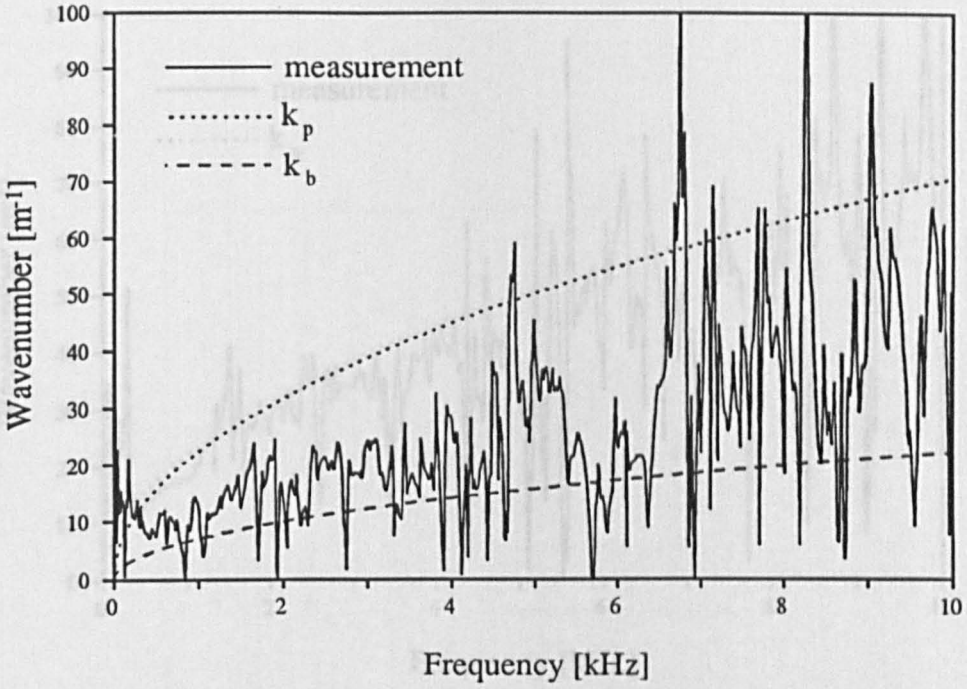

Fig.7.4.6 Measured wavenumber in the direction parallel to the ribs at location 30

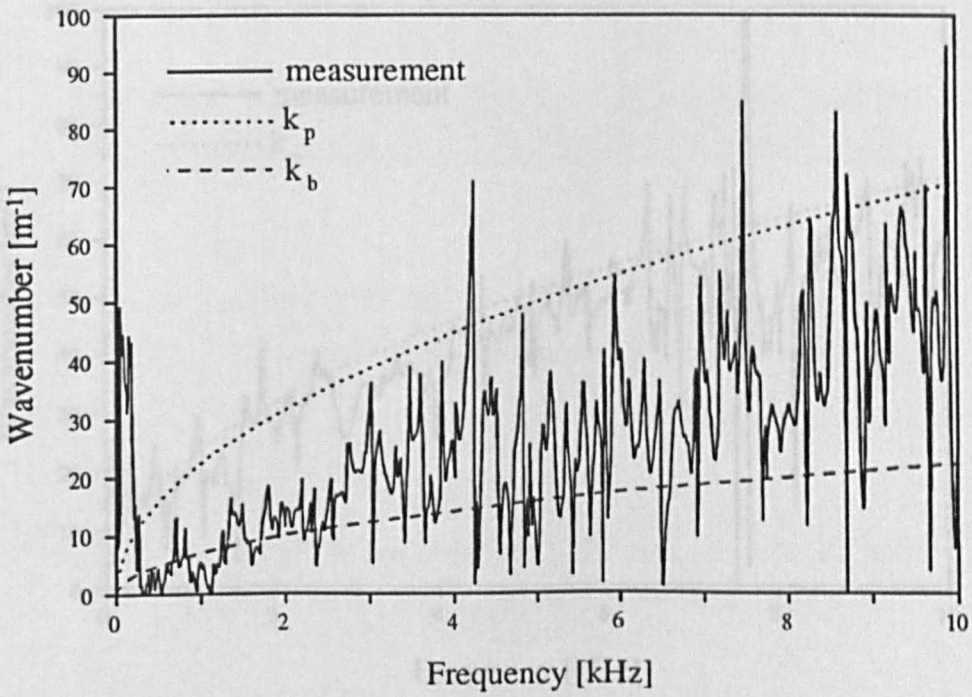

Fig.7.4.7 Measured wavenumber in the direction parallel to the ribs at location 38

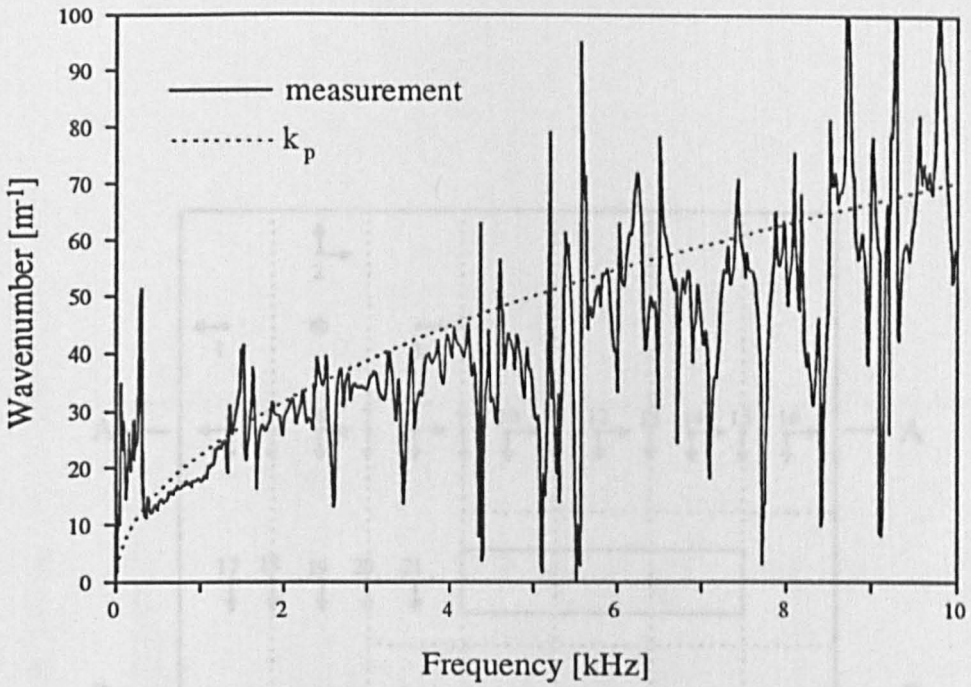

Fig.7.4.8 Measured wavenumber in the direction perpendicular to the ribs at location 42

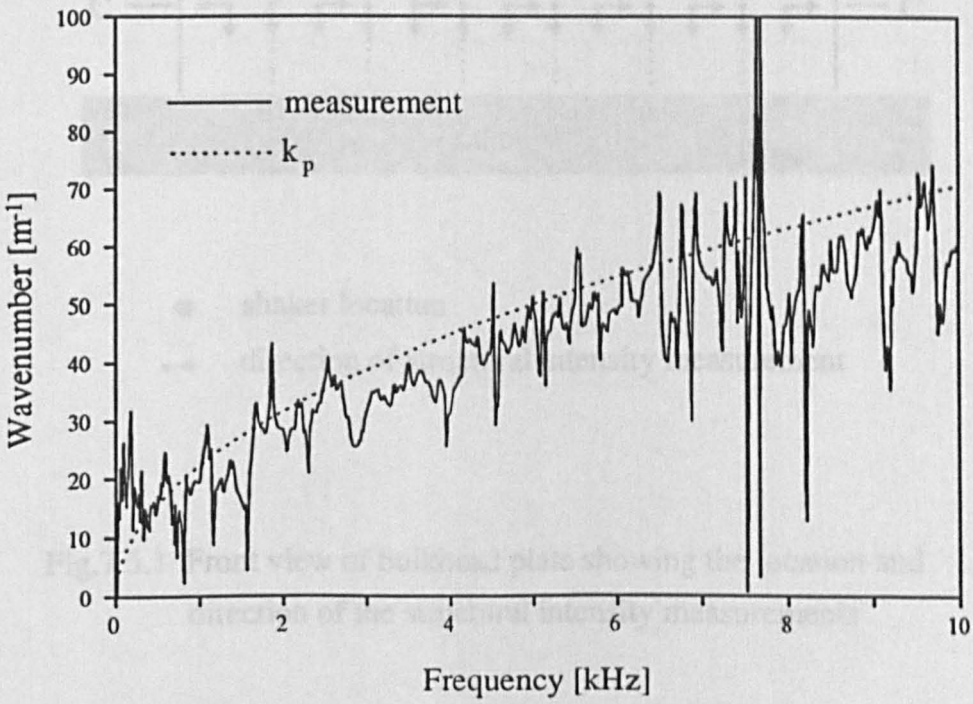

Fig.7.4.9 Measured wavenumber in the direction perpendicular to the ribs at location 24

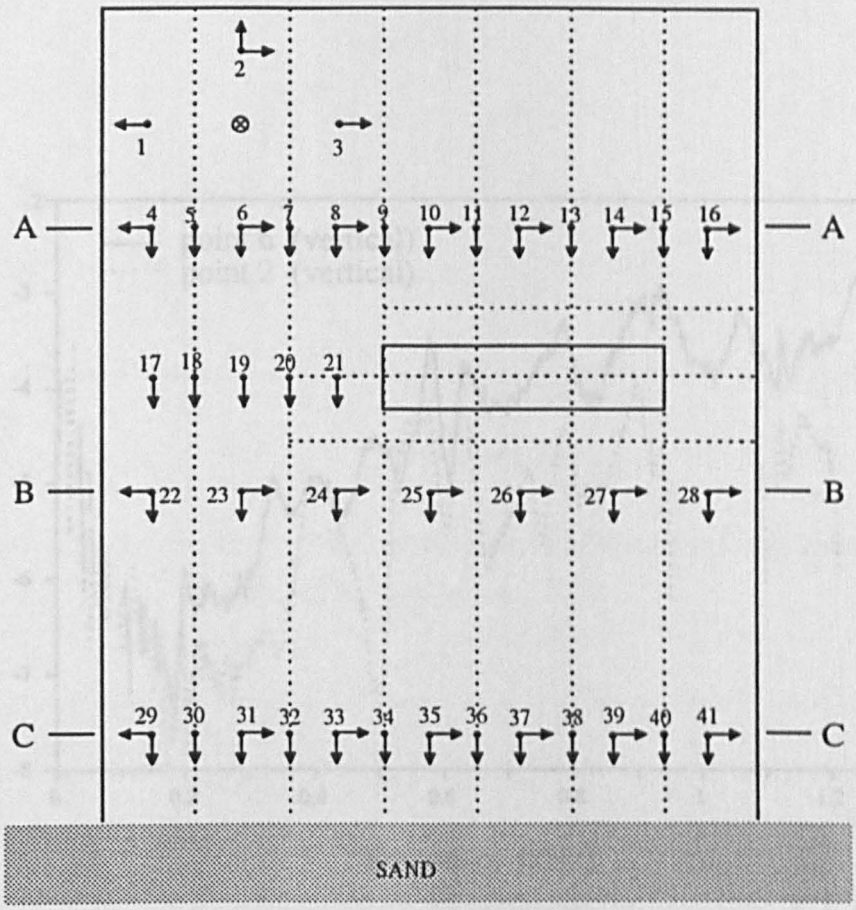

⊗ shaker location

→ direction of structural intensity measurement

Fig.7.5.1 Front view of bulkhead plate showing the location and direction of the structural intensity measurements

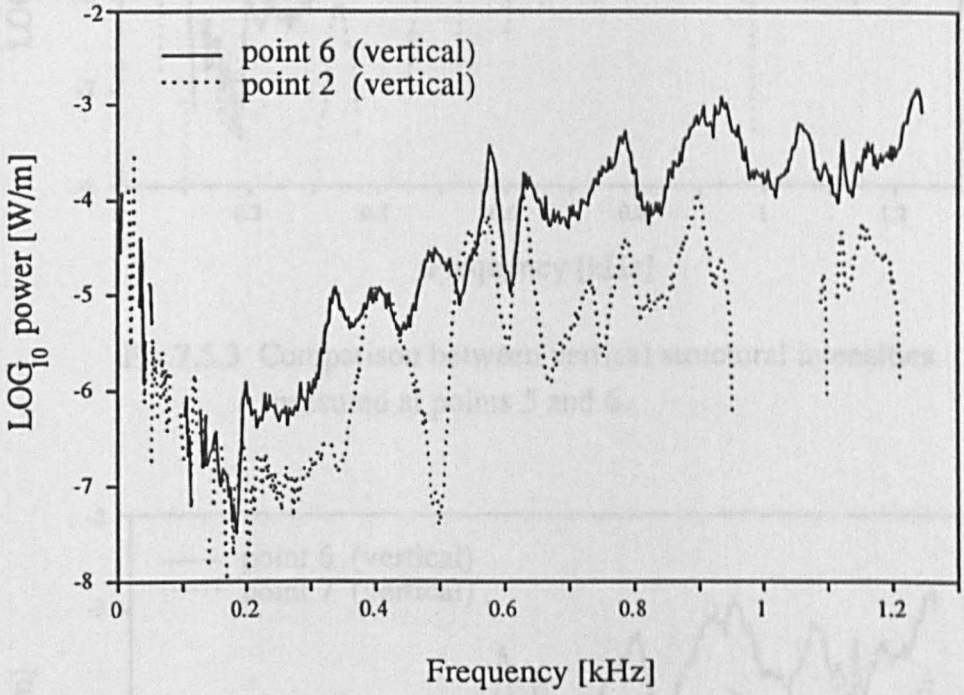

Fig.7.5.2 Comparison between vertical structural intensities measured at points 2 and 6

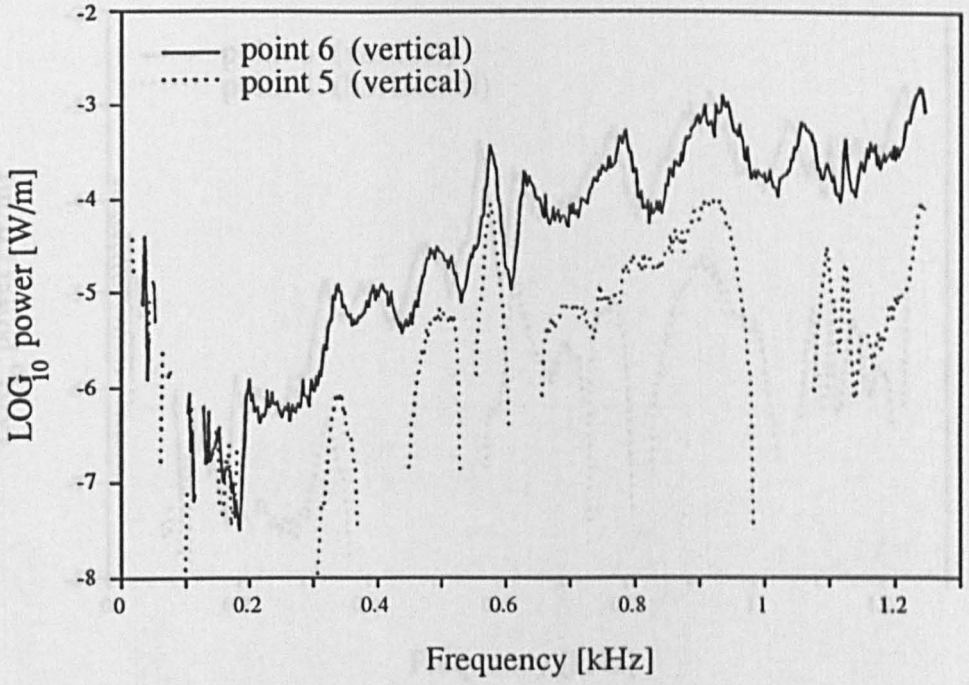

Fig.7.5.3 Comparison between vertical structural intensities measured at points 5 and 6

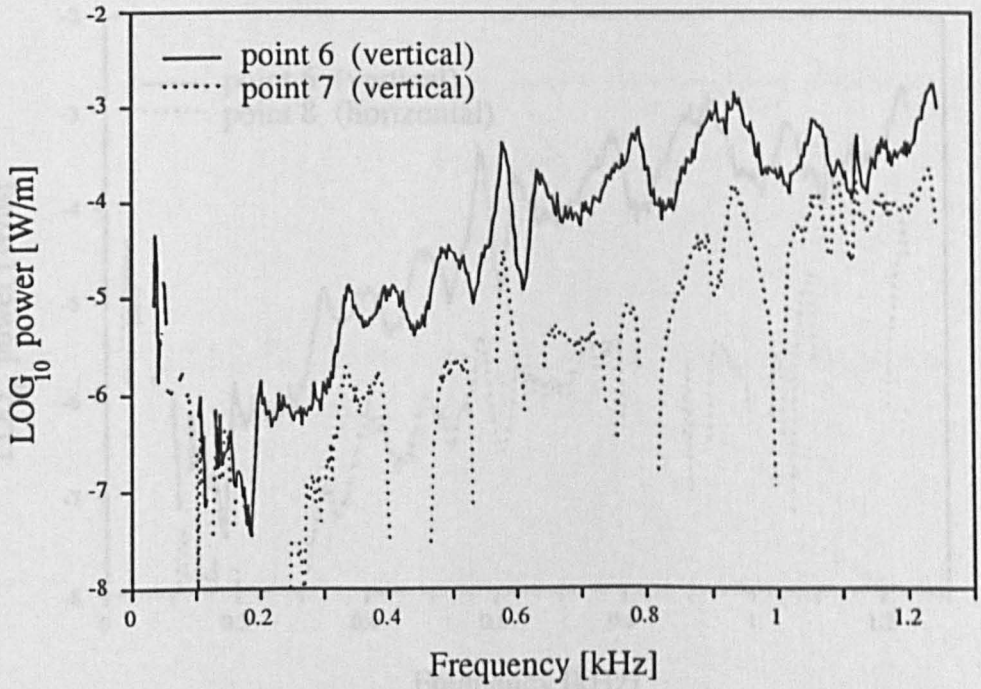

Fig.7.5.4 Comparison between vertical structural intensities measured at points 6 and 7

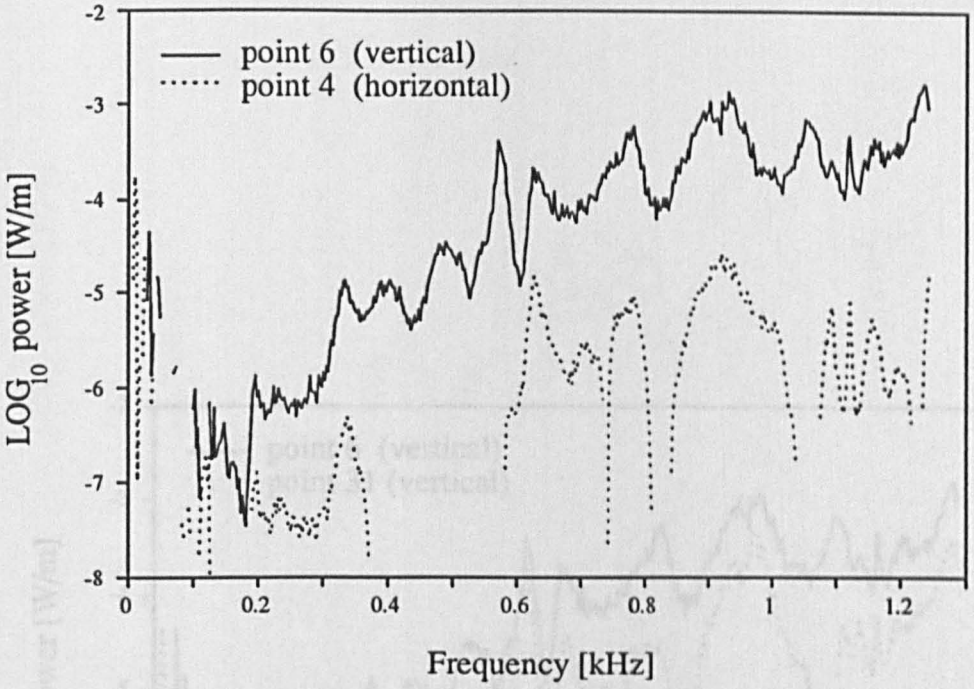

Fig.7.5.5 Comparison between vertical structural intensity measured at 6 and horizontal structural intensity measured at 4

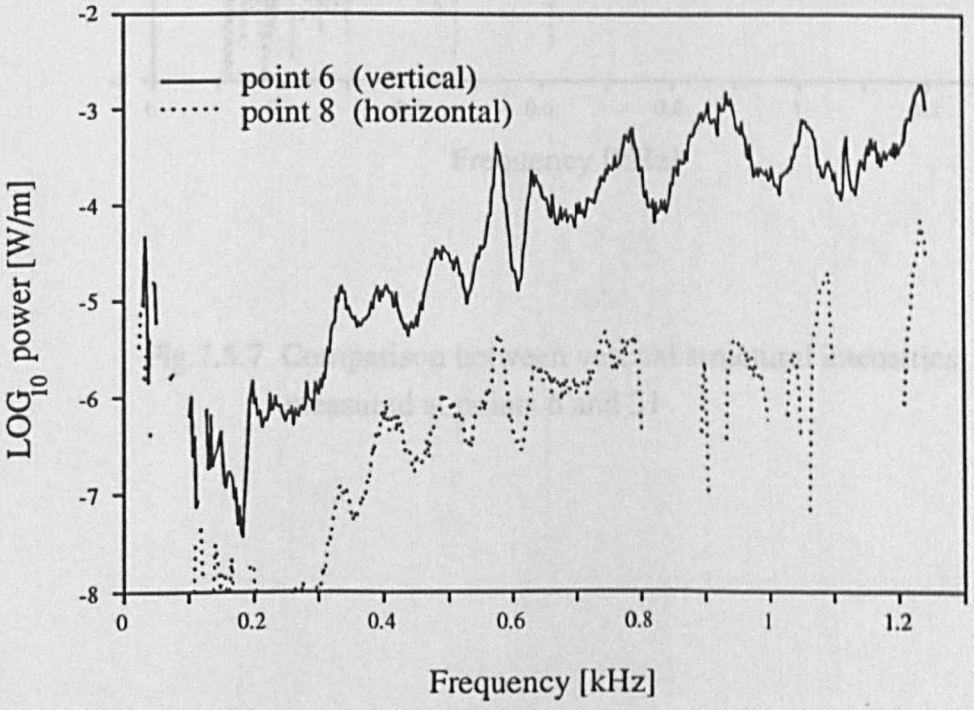

Fig.7.5.6 Comparison between vertical structural intensity measured at 6 and horizontal structural intensity measured at 8

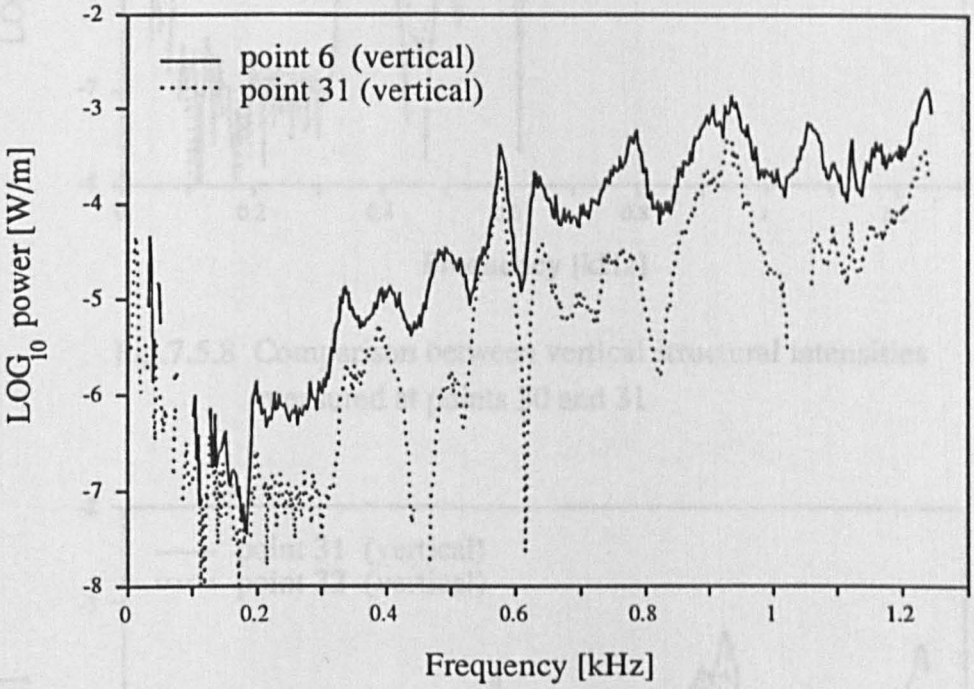

Fig.7.5.7 Comparison between vertical structural intensities measured at points 6 and 31

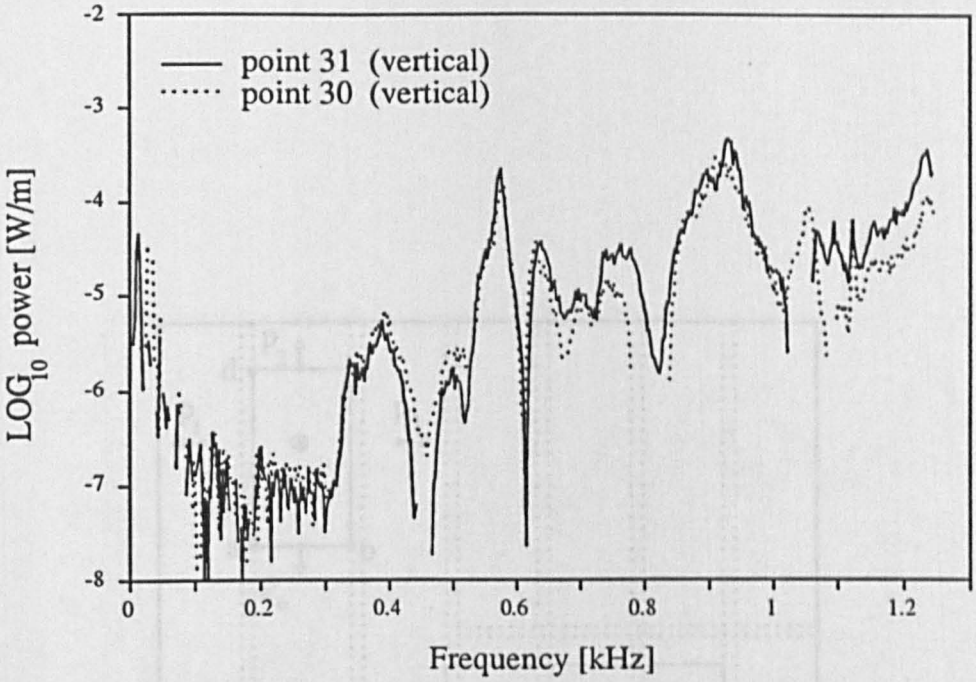

Fig.7.5.8 Comparison between vertical structural intensities measured at points 30 and 31

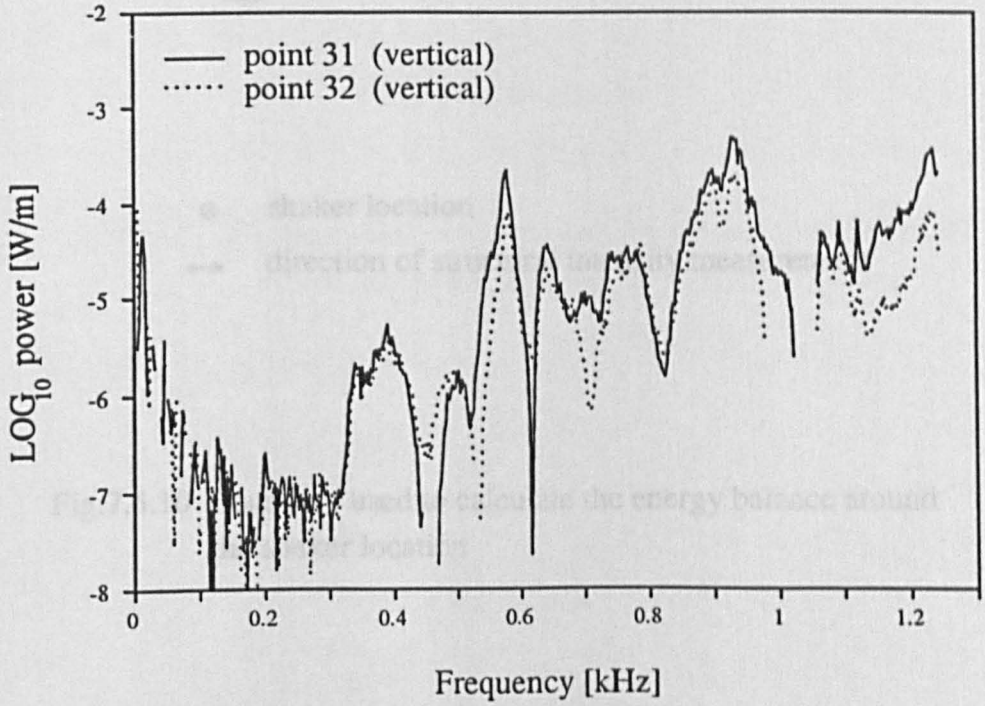

Fig.7.5.9 Comparison between vertical structural intensities measured at points 31 and 32

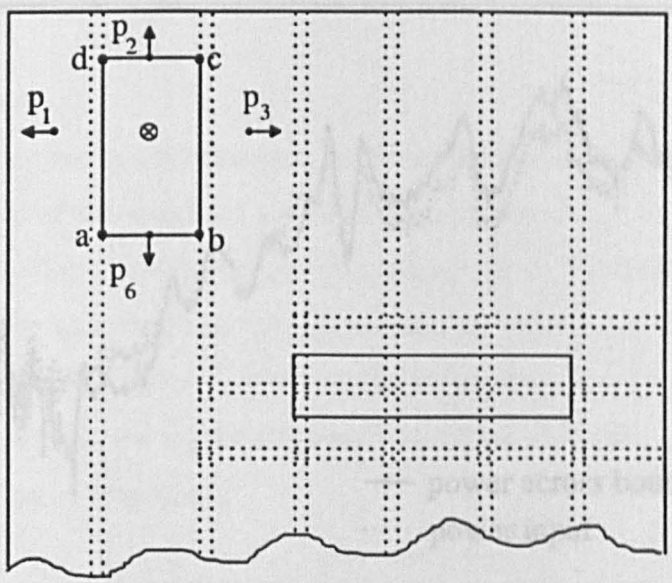

⊗ shaker location

→ direction of structural intensity measurement

Fig.7.5.10 Boundary used to calculate the energy balance around the shaker location

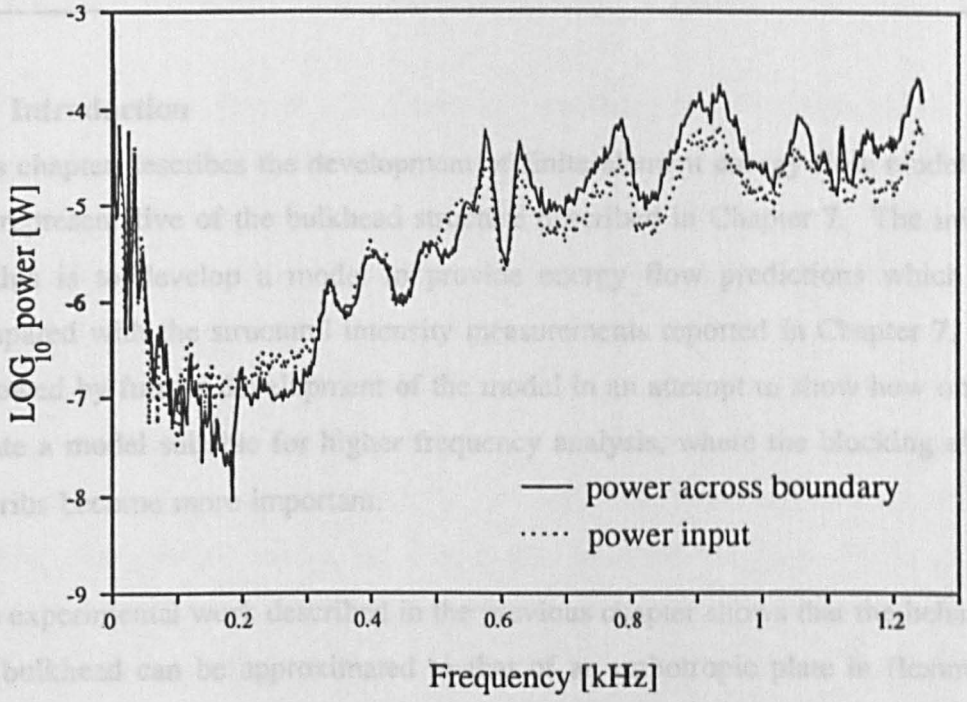

Fig.7.5.11 Comparison between power input and the calcluated vibrational power crossing the boundary a-b-c-d

Chapter 8

Energy flow modelling of a ribbed bulkhead structure

8.1 Introduction

This chapter describes the development of finite element energy flow models which are representative of the bulkhead structure described in Chapter 7. The initial aim of this is to develop a model to provide energy flow predictions which can be compared with the structural intensity measurements reported in Chapter 7. This is followed by further development of the model in an attempt to show how one might create a model suitable for higher frequency analysis, where the blocking effects of the ribs become more important.

The experimental work described in the previous chapter shows that the behaviour of the bulkhead can be approximated to that of an orthotropic plate in flexure. This assumption is carried through into this modelling work so that the plate formulations developed by Bouthier (1992) can be used to create the energy flow models.

8.2 Modelling at low frequencies

The aim of this first modelling exercise is to investigate the ability of the finite element implementation of the energy flow approach to create a representative two-dimensional model of the bulkhead structure described in Chapter 7. The quality of this model will be assessed by comparing its results with the structural intensity measurements made over the surface of the bulkhead plate. Limitations of the experimental techniques used to obtain these measurements meant that reliable results could only be obtained over a 0-1250 Hz frequency range. The properties of this initial model will therefore be chosen in accordance with experimental observations which are appropriate to this frequency range.

In creating a representative energy flow model of a complex structure it is important to identify the features of the structure which have the greatest influence on the energy flow in the frequency range of interest. In the case of this bulkhead structure, the wavenumber measurements indicate that below 2.5 kHz the bulkhead exhibits orthotropic wave transmission characteristics due to the global stiffening effects of the reinforcing ribs. This is an important feature of the structure at these lower frequencies and will be included in the energy flow model.

A second important feature which must be considered is the possible effects that the ribs may have in blocking the transmission of wave energy in the horizontal direction. Some judgement as to the importance of this effect can be obtained by considering the wavenumber characteristics of the structure reported in the previous chapter. These show that the motion of the structure in the horizontal direction has similar characteristics to that of the bulkhead plate in isolation from the ribs. Using this result it can be shown that the wavelength of flexural motion in a plate of this thickness, at a frequency of 1000 Hz, is more than twice the distance of the rib spacing. In general, one would expect that localised blocking effects caused by discontinuities like the ribs, would be significant only when the wavelength of the motion is much less than the distance between them. In the case of this structure, the experimental evidence suggests that this condition will only occur at frequencies much higher than 1000 Hz. For this reason, no attempt will be made to include any localised modelling features to represent the ribs in this lower frequency model.

8.2.1 The orthotropic plate model

The ABAQUS™ finite element model used to represent the bulkhead at lower frequencies is shown in Fig.8.2.1. The model takes the form of a plate consisting of a block of 14 x 28 four-noded, two-dimensional thermal finite elements.

To account for the difference in the transmission properties in the two directions, the "conductive" properties of the finite elements must be orthotropic. In accordance with

the analogy presented in Chapter 6 the conductive parameter is given by:

$$C = \frac{c_g^2}{\omega\eta} \tag{8.3.1}$$

This expression requires a value for the group velocity of waves travelling through the structure, which can be obtained given knowledge of its wavenumber characteristics. For flexural wave motion in a plate, the relationship between wavenumber and group velocity is:

$$c_g = \frac{2\omega}{k} \tag{8.2.2}$$

The wavenumber measurements described in the previous chapter provide representative estimates of the wavenumber characteristics of the bulkhead structure in both the vertical and horizontal directions. These values can be used to calculate the corresponding values of c_g from the equation above. In the case of this bulkhead model, the difference in the wavenumber characteristics in the two directions results in a conductivity value in the vertical direction which is about ten times greater than that in the horizontal direction.

Power input to the model is prescribed by a thermal flux value (in watts) applied at the node which corresponds to the shaker attachment position. This value was obtained using the force and acceleration measurements made at the shaker push rod.

Energy dissipation due to damping is modelled using convective heat loss from the finite elements. The dissipative properties of the elements can be calculated using equation (6.2.6). A damping loss factor of 0.01 was chosen as being representative of the plate material. Additional damping is included for those elements which are assumed to be immersed in the sand. This is achieved by increasing their loss factor to a value of 0.2.

The boundary conditions around the edges of the plate are shown in Fig.8.2.1. In general, the power flux values normal to the edges of the plate are zero. An

additional boundary condition is applied at nodes along the lower edge of the model to ensure that the energy level at the extremity of the sink is also zero.

8.2.2 Results and discussion

Comparisons between model predictions and the measured structural intensity results will be made at four frequencies (340 Hz, 580 Hz, 780 Hz and 930 Hz), over the measurement range. These frequencies were chosen because they correspond to peaks in the structural intensity spectra and generally avoid regions of poor data acquisition. Using these frequency values it was possible to obtain a value for structural intensity at the majority of the measurement locations across the bulkhead plate.

Measured structural intensity values are compared with model predictions in Figs.8.2.2 to 8.2.9. These comparisons are made along lines AA, BB and CC marked on the model shown in Fig.8.2.1. These lines incorporate the majority of the points where structural intensity measurements were obtained over the surface of the bulkhead plate, see Fig.7.5.1.

The model predictions for the energy flow in the vertical direction show similar characteristics at each of the four frequencies studied, see Figs.8.2.2 to 8.2.5. Along AA the predicted power is significantly higher in the region of the source than across the remainder of the plate. Further down the structure, along BB and CC, the energy becomes more evenly distributed across the plate and the power profile is almost flat. These figures also show the measured power levels at the appropriate points on the structure, obtained by the structural intensity technique. There is a significant amount of scatter associated with these measured results due to the approximate nature of the measurement approach. It can be seen however, that model predictions are generally representative of the level of energy flow obtained by measurement.

Similar comparisons for the levels of energy flow in the horizontal direction are shown in Figs.8.2.6 to 8.2.9. Along lines AA and BB the predicted power levels in the horizontal direction are generally higher than those obtained by measurement. Further down the structure the predictions along line CC are in much better agreement

with the measured results.

Now that the measured results have been shown for a single frequency value at neighbouring points in the structure, the degree of measurement scatter becomes more evident. The major source of this scatter is linked to the use of the two-accelerometer structural intensity technique on a structure of this complexity. The formulation behind this technique is only strictly valid if measurements are made on a plate experiencing pure flexural motion. It must also be assumed that near-field effects can be safely neglected in the region of the measurement. Because of the complexity of the structure is difficult to determine how well these assumptions are satisfied. The use of this measurement technique can however, be justified because more exact methods for the treatment of complicated structures do not yet exist. It should also be noted that before the two-accelerometer approach was employed, considerable effort was invested in establishing the general characteristics of the structure through modal analysis and the use of wavenumber measurement. As a result of these investigations, it was evident that the behaviour of the bulkhead structure could be approximated to that of an orthotropic plate and the use of plate formulations represents a good engineering solution to this problem.

A second area of uncertainty was highlighted while making a comparison between power input and structural intensity measurements. This comparison identified the problem of choosing a representative value for the effective stiffness of the structure at the point of measurement. Wavenumber measurements suggest that the characteristics of the structure may vary over the surface of the plate. This is not surprising when one considers the possible effects of the machinery mounting platform which were not included in this study.

Having accepted that there is some degree of uncertainty in the measured data, there are also a number of other factors which may lead to the differences between the measured and predicted results. The first of these is linked to the localised concentration of vertical energy flow detected by the measurements in the region of the shaker. It is clear from the vertical energy flow profiles shown in Figs.8.2.2 to

8.2.5, that the measured power levels directly below the shaker are generally higher than those predicted by the energy flow model. It is also evident that the model tends to over-estimate the horizontal flow of energy along lines AA and BB. These observations suggest that the model could be made more representative of the real structure if its properties were modified to encourage more energy to flow vertically downwards in the region of the energy source, so that less energy is allowed to flow across the upper part of the plate. This would certainly be more in keeping with the experimental observations reported earlier.

Further differences between measured and predicted results could stem from the fact that the power input value used in the model was measured at the shaker push rod. In doing this it is assumed that all the power fed into the structure by the shaker contributes to the flexural wave energy of the bulkhead plate. In reality however, some of this energy must be imparted to the panels on the top and at the sides of the plate which are not included in the energy flow model. It is also likely that some of this energy will be carried in other forms, eg. longitudinal and torsional wave motion, as a result of conversion at discontinuities.

Despite the limitations of the measurement technique and some areas where the details of the real structure have not been included in the model, the energy flow model has provided predictions which are generally comparable with the measured results. The general conclusion at this stage therefore, is that the idea of approximating the bulkhead to an orthotropic plate represents a reasonable engineering solution to the problem. In order to obtain this solution it is important to provide the model with representative values for the modelling parameters and ensure that the level of approximation involved in developing the model is well understood.

8.3 Modelling at higher frequencies

In the lower frequency model, aimed at the 0-1250 Hz frequency range, no attempt was made to account for the presence of the stiffening ribs explicitly, although their *global* effects naturally influenced the estimation of suitable conductivity values. At higher frequencies, where the wavelength of the motion is smaller, blocking mass

effects of the ribs may be expected to become more significant and perhaps to exert important *local* influences on the energy flow paths within the bulkhead structure. It is therefore appropriate to attempt to incorporate the blocking mass effect of the ribs into the energy flow model to more accurately represent the behaviour of the real structure at higher frequencies.

To include these effects in the model, it is necessary to develop a two-dimensional equivalent to the joint element introduced in Chapter 6. This is an important step in the development of the general modelling approach because it extends its applicability to include partial transmission across various types of joints in two-dimensional structures.

8.3.1 The two-dimensional joint element

A two-dimensional joint element can be developed by considering the joint between two plate sections shown in Fig.8.3.1. This joint takes the form of a strip of two-dimensional elements with conductivities K_1 and K_2 in each of the two major directions. In order to model the effect of the joint, the transmission of energy through this strip of elements must only take place in the direction of K_1.

The development of a one-dimensional joint element between two similar beams using standard thermal finite elements was described earlier in Chapter 6. It was shown that the appropriate value for the conductivity of these elements is:

$$K_j = \frac{\tau\, c_g\, l_{el}}{2(1-\tau)} \tag{8.3.1}$$

where l_{el} represents the length of the finite element in the direction of the energy flow.

To create the corresponding effect in a two-dimensional sense, the conductivity K_1 must be set to:

$$K_1 = \frac{\tau\, c_g\, l_{el}}{2(1-\tau)} \tag{8.3.2}$$

and the conductivity in the other direction, K_2, must be set to zero so that the presence of the joint element does not affect the energy flow in this direction.

8.3.2 The jointed plate model

To illustrate the use of these two-dimensional joint elements and to show how one might include the blocking mass effects of the ribs at higher frequencies, the energy flow model described earlier has been modified to include two-dimensional joint elements at the rib positions, see Fig.8.3.2.

It should be noted that the purpose of this analysis is purely illustrative and that the parameters used may not be entirely representative of the properties of the real structure at the frequencies considered. Where possible, the values of these parameters will be based on the findings of the experimental work described earlier. The remainder will be chosen arbitrarily, but sensibly, to complete the illustration.

The analysis will be carried out at a frequency of 10 kHz. The choice of the conductive properties of the plate elements at this frequency is based on the wavenumber measurements reported in section 7.4. These show that the wavenumber characteristics in both the horizontal and vertical directions are comparable to those calculated for the bulkhead plate in isolation from the ribs. This property is used to provide values for group velocity and element conductivity, using equations (8.2.1) and (8.2.2).

The value for transmission efficiency across the joint will be set arbitrarily to 0.5. In order to provide a more representative model at this frequency, further analysis would be required to estimate a value of τ based on the properties of the real structure.

In the absence of a power input measurement, the power flux applied to the node corresponding to the shaker position is set to 1 watt. The damping parameters remain the same as those for the lower frequency model described earlier.

8.3.3 Results and discussion

To show the effect of including these joint elements at the rib locations the predictions from the jointed model will be compared to those provided by a continuous plate model having the same parameters.

Vertical power profiles at points along lines AA and BB, marked on the model in Fig.8.3.2, are shown in Fig.8.3.3. It is clear from these profiles that the restriction to energy flow across the ribs imposed by the joint element introduces large differences between the vertical energy flow levels in adjacent plate sections across AA. This results in a concentration of energy flow parallel to the ribs close to the energy source. It can also be seen that this effect was less marked at points along BB.

These observations are complemented by the horizontal energy flow profiles shown in Fig.8.3.4. These show that along AA the energy flow across the jointed model is significantly less than that predicted for the continuous model, due to the restriction imposed by the joints. Along BB however, the reverse is true. This is because at this section in the continuous plate model, the energy is fairly evenly distributed across the width of the model leaving little difference to drive the flow. In the jointed model however, there remains a more significant energy gradient along BB to drive the flow across the joints.

The investigation using this jointed model has illustrated how the blocking effects of the ribs at higher frequencies can be incorporated into an energy flow model. The results suggest that the ribs might introduce significant differences in the vertical energy flow down adjacent sections of the structure due to the reduction of energy flow in the horizontal direction. Although these results have not been confirmed experimentally, they are nevertheless generally in accordance with intuition and indicate the potential for the application of the energy flow modelling approach to the analysis of two-dimensional jointed structures.

It should be noted that the jointed model does not include the transmission path provided by the panel running along the top of the bulkhead section. When the

blocking effects of the ribs become significant, in reality, this panel may act as an alternative flow path which could feed energy across the structure without it having to negotiate the ribs. This effect is likely to lead to a more even distribution of energy flow down the structure than the jointed energy flow model predicts.

8.4 Summary

This chapter described the development of two-dimensional energy flow models of the bulkhead structure to represent its behaviour under different frequency regimes. Where possible the parameters used in these models were based on the findings of the experimental investigation described in Chapter 7. The main points arising from this work are as follows:

1. From the information gained in the experimental investigation it was possible to calculate the necessary modelling parameters to create an energy flow model which is representative of the bulkhead structure at frequencies below about 2.5 kHz. This model consisted of a block of two-dimensional plate finite elements having orthotropic conductive properties. Predictions obtained from this model were generally comparable to the levels of energy flow obtained by measurement. Some differences between prediction and measurement were identified which are thought to be linked to localised features of the real structure which were not included in the energy flow model.

2. In the lower frequency model possible blocking effects which could reduce the flow of energy across the ribs were neglected. At higher frequencies however, these effects are likely to become more important and must be included in a representative energy flow model. To investigate this aspect, two-dimensional joint elements were developed and inserted into the existing model to introduce the effects of partial transmission across the ribs. The introduction of these joint elements resulted in a concentration of vertical energy flow in the elements close to the power source and a significant reduction of energy flow horizontally across the plate.

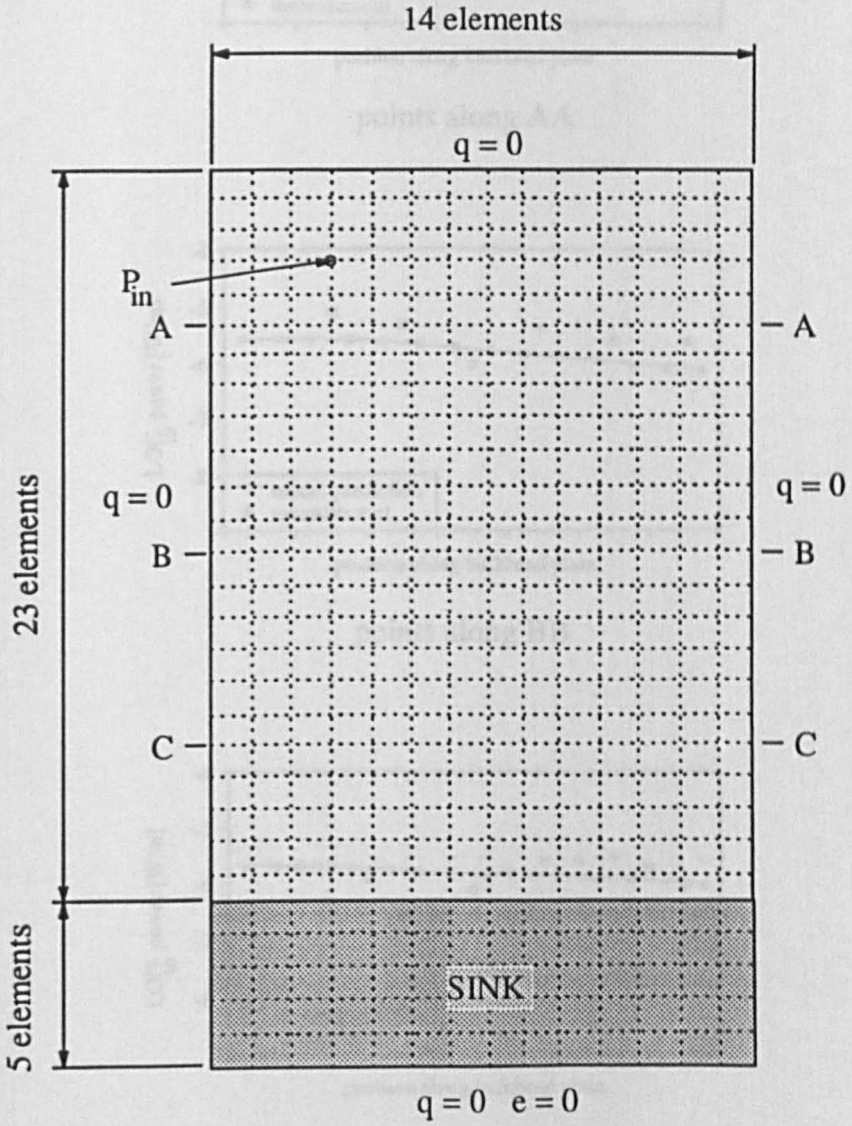

Fig.8.2.1 Orthotropic plate model

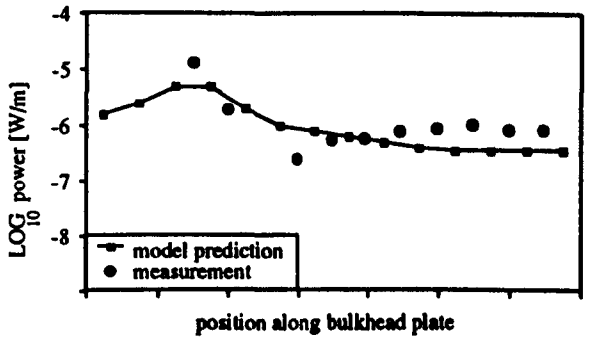

points along AA

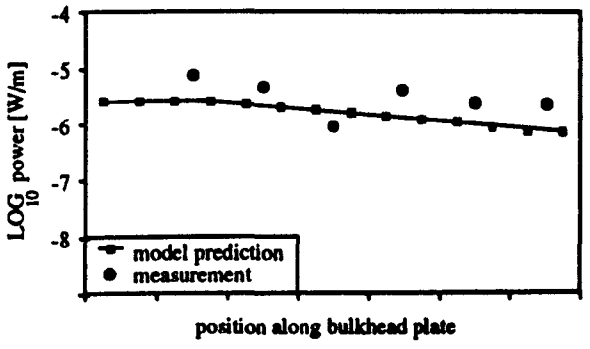

points along BB

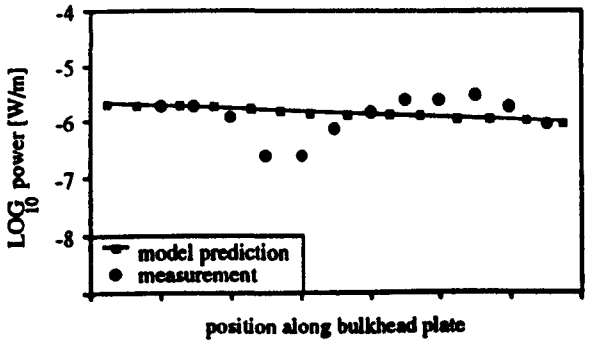

points along CC

Fig.8.2.2 Comparison between vertical structural intensity measurements and model predictions at 340 Hz

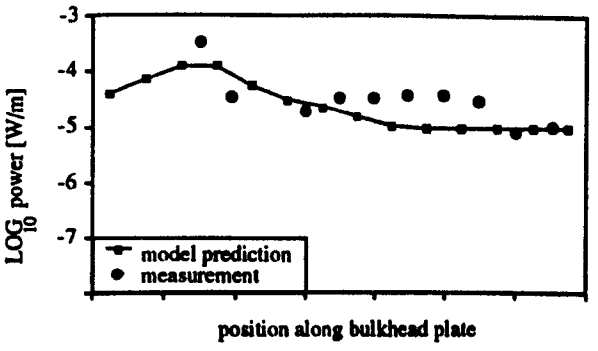

points along AA

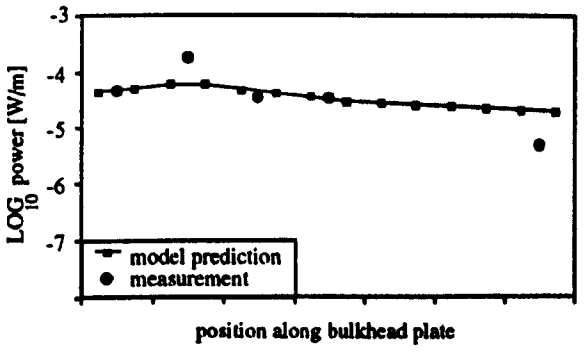

points along BB

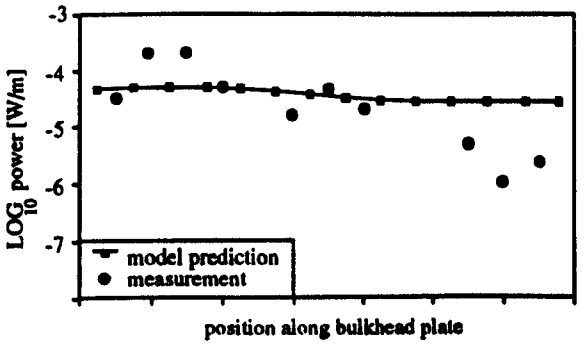

points along CC

Fig.8.2.3 Comparison between vertical structural intensity measurements and model predictions at 580 Hz

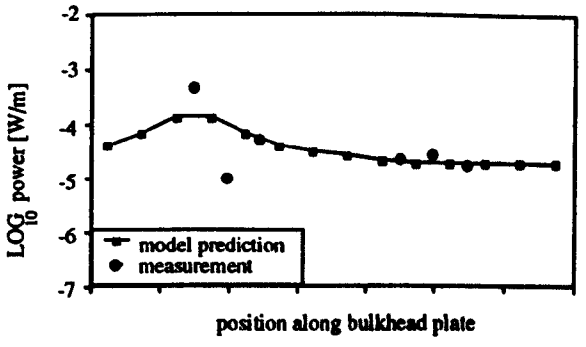

points along AA

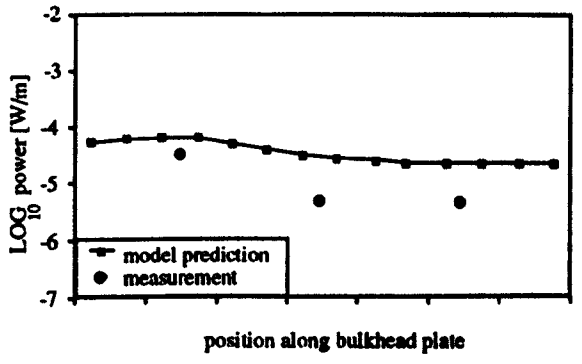

points along BB

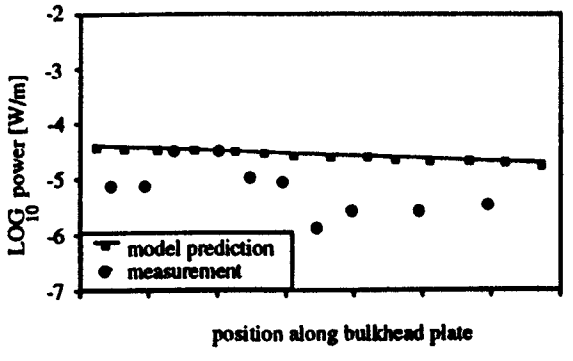

points along CC

Fig.8.2.4 Comparison between vertical structural intensity measurements and model predictions at 780 Hz

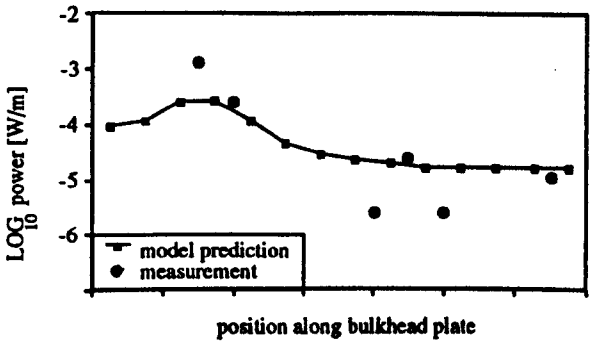

points along AA

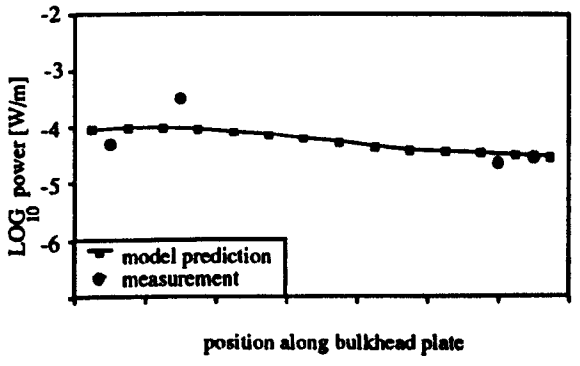

points along BB

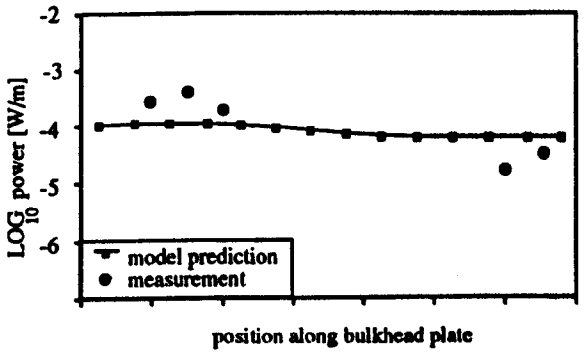

points along CC

Fig.8.2.5 Comparison between vertical structural intensity measurements and model predictions at 930 Hz

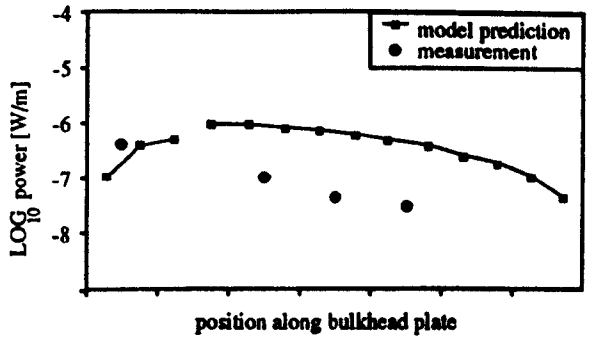

points along AA

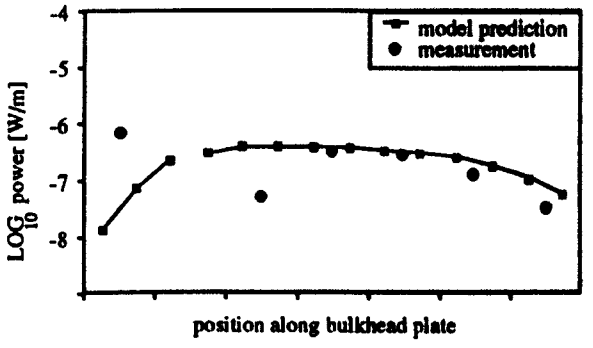

points along BB

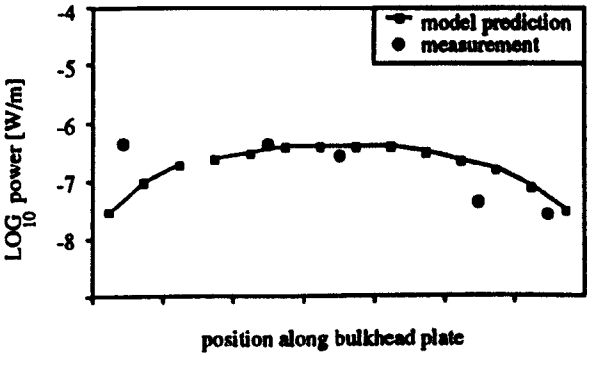

points along CC

Fig.8.2.6 Comparison between horizontal structural intensity measurements and model predictions at 340 Hz

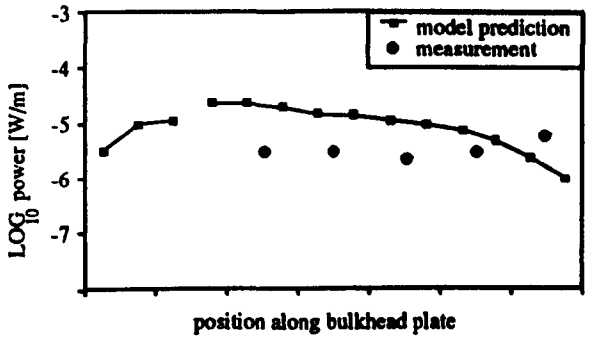

points along AA

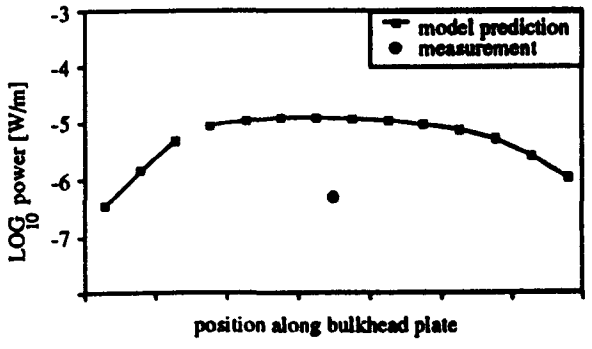

points along BB

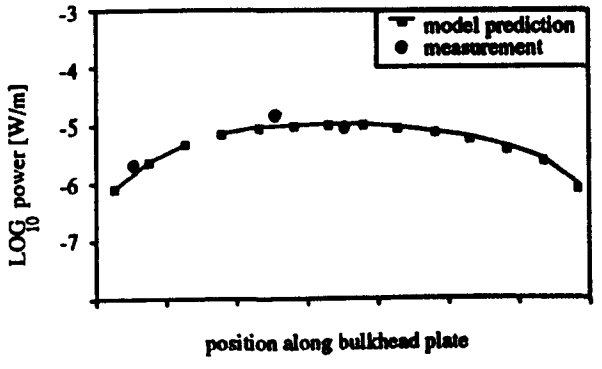

points along CC

Fig.8.2.7 Comparison between horizontal structural intensity measurements and model predictions at 580 Hz

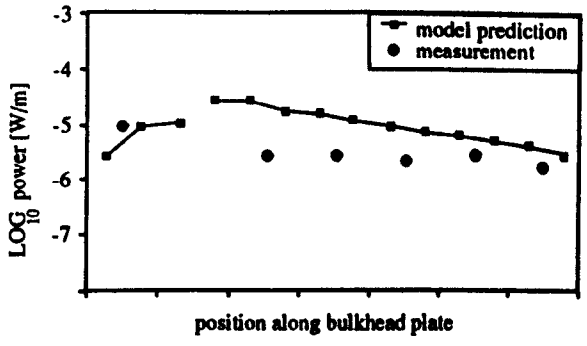

points along AA

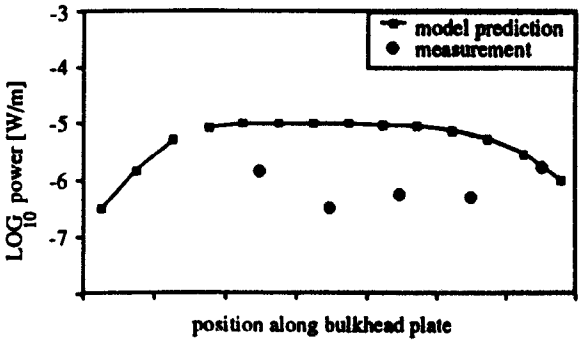

points along BB

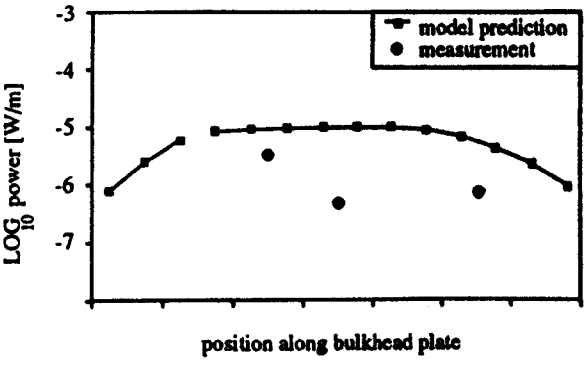

points along CC

Fig.8.2.8 Comparison between horizontal structural intensity measurements and model predictions at 780 Hz

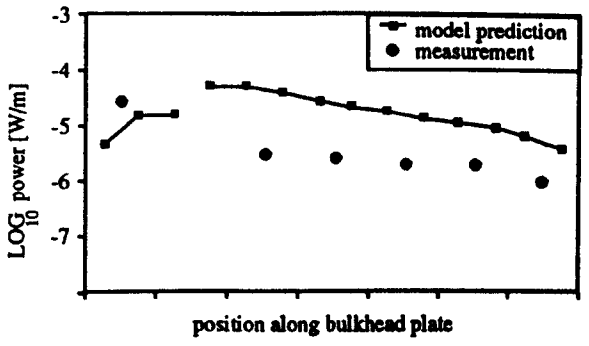

points along AA

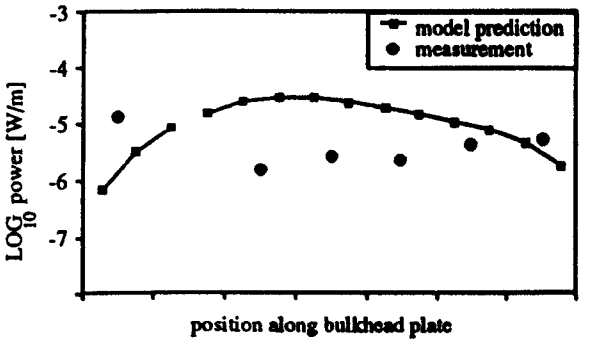

points along BB

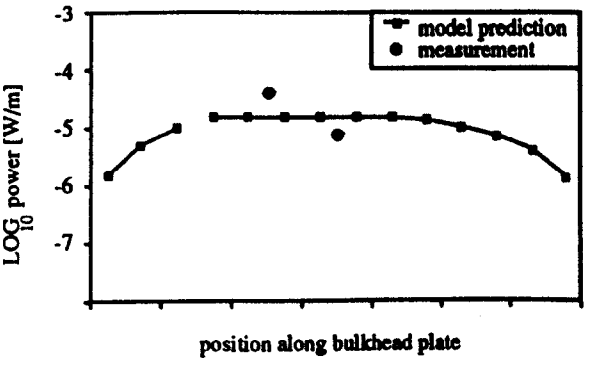

points along CC

Fig.8.2.9 Comparison between horizontal structural intensity measurements and model predictions at 930 Hz

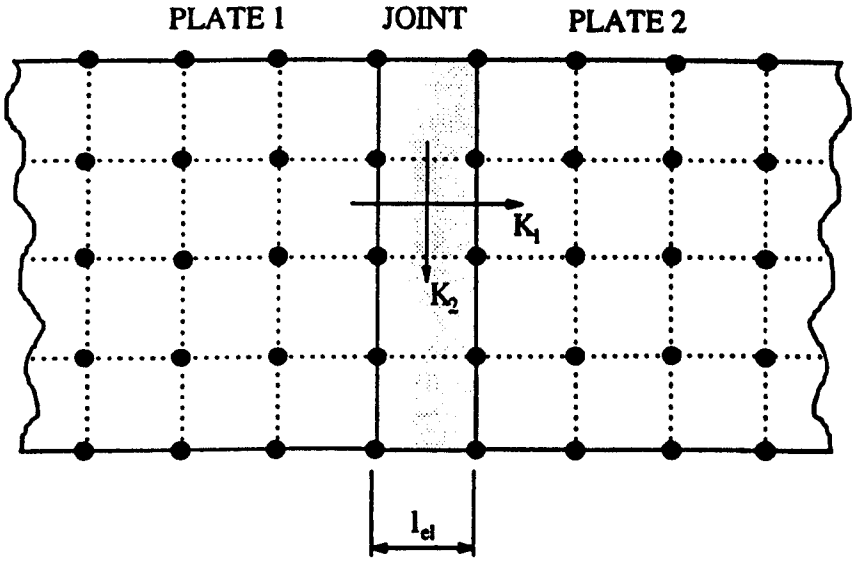

Fig.8.3.1 Two-dimensional joint configuration

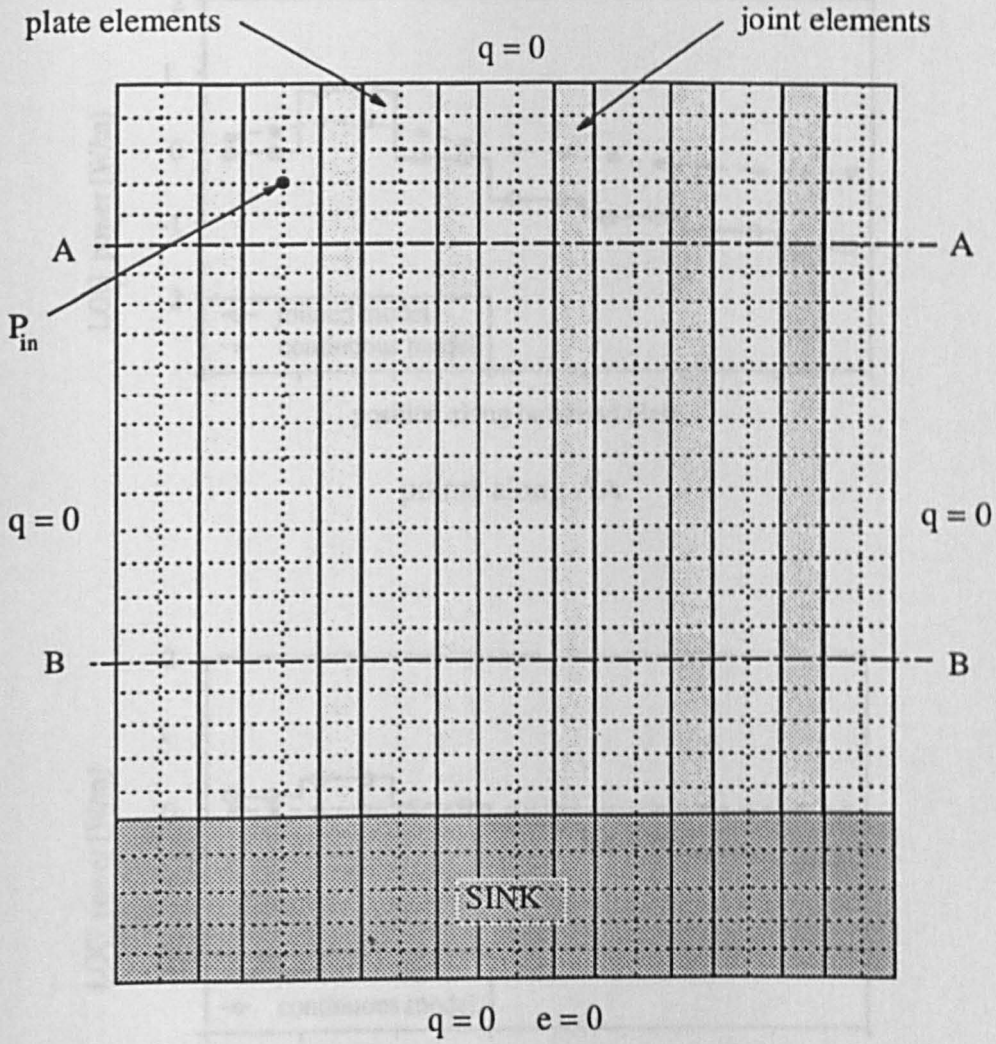

Fig.8.3.2 High frequency finite element model

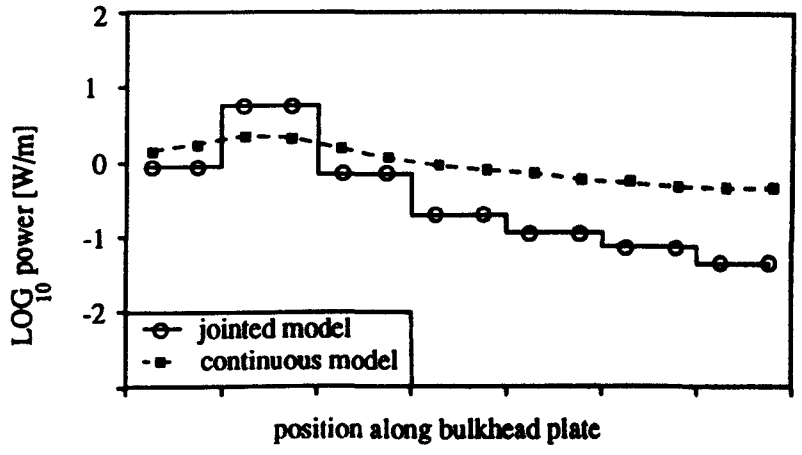

points along AA

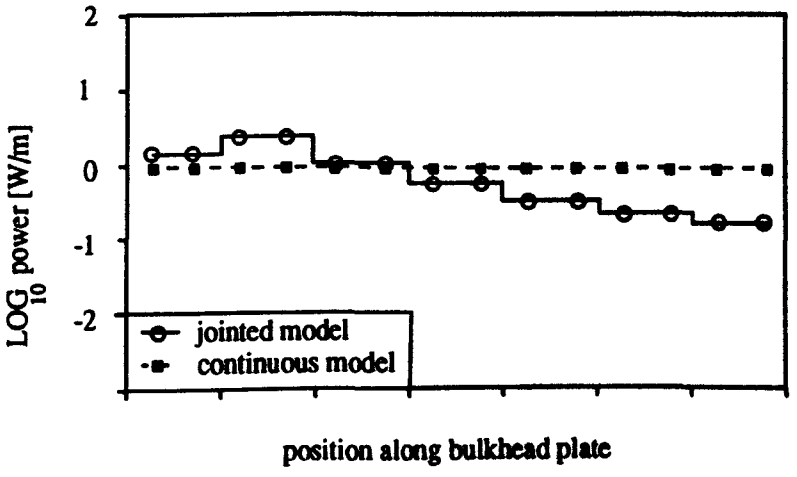

points along BB

Fig.8.3.3 Comparison between vertical power profiles obtained using the two finite element models at 10 kHz

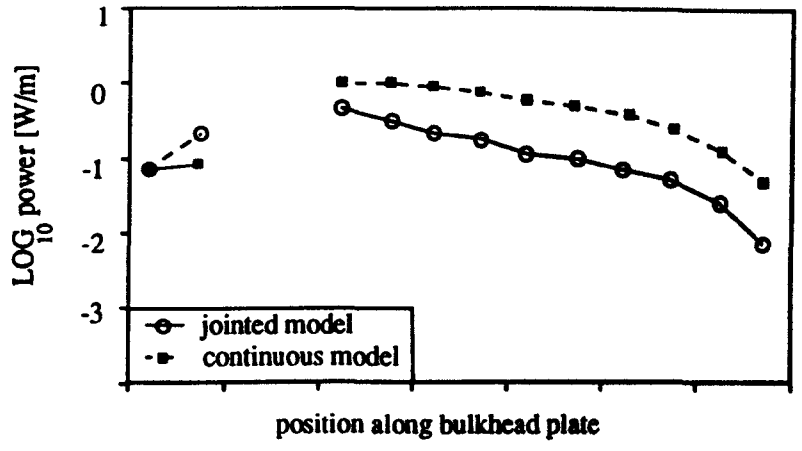

points along AA

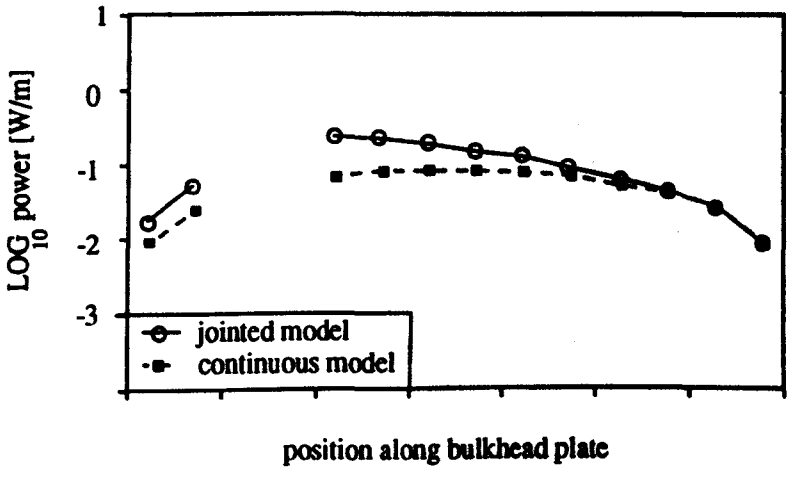

points along BB

Fig.8.3.4 Comparison between horizontal power profiles obtained using the two finite element models at 10 kHz

Chapter 9

Concluding discussion

9.1 Introduction

This final chapter summarises and discusses some of the more general aspects of the work carried out during the course of this project. The discussion also includes a description of some very recent research presented by other workers which provides further insight and possible improvement to the basic energy flow formulation. This is followed by some recommendations for further work which stem directly from the research documented here. Finally, the thesis is rounded off with some concluding remarks.

9.2 The modelling approach

The underlying objective of this work has been to develop a modelling tool which is capable of predicting the level of vibrational energy flow in relatively complex structures. It was envisaged that the primary task of this tool would be to quantitatively rank the ability of various paths to transmit vibrational energy through a structure. Such information is potentially useful during the design of a structure, or as a means of providing further insight into a structure's vibration transmission characteristics for development purposes. This task has been subject to a proviso that the analysis technique should be implemented at low computational cost in frequency ranges where traditional experimental and analytical modal analysis techniques have proved difficult or expensive to apply.

In developing a tool to meet these requirements a conflict exists between the desire to provide an analysis for a wide variety of structures at low cost and the need to ensure that the model is sufficiently representative of realistic structures for practical purposes. In this situation an increase in generality inevitably leads to higher levels

of approximation.

The philosophy behind the development of the modelling technique has been to maintain its generality by keeping the detailed characteristics of the structure outside the realms of the energy flow analysis. To achieve this, the properties of the energy flow model are entirely described by four general modelling parameters, namely power input, damping, group velocity and transmission efficiency, which are chosen in accordance with a detailed analysis of the individual components making up the structure. For example, the transmission characteristics of a joint are described only by a value for its transmission efficiency which defines the ratio of transmitted to incident wave power at the joint. This can be obtained from a detailed local analysis of the joint characteristics which is entirely separate from the energy flow model. The function of the energy flow model therefore, is to provide a framework within which all this localised information can be assembled to form a *global* description of the energy flow characteristics of the entire structure. This generalised type of approach is not dissimilar to that used in SEA.

Within this work, the field of application of the energy flow analysis has been greatly increased through the use of a finite element scheme, which allows the assembly of a number of beam, plate and joint elements to form a wide variety of structural configurations. For the models developed here, the analysis was carried out by adapting an existing finite element package. This approach was favoured because it eliminated the need to develop a dedicated computational framework within which to test the general modelling approach. It also meant that models could be created using software which is already accepted by and widely available to the engineering community.

In order to provide a tool for high frequency analysis at low computational cost it was necessary to employ an approach which describes the dynamics of the structure in a simplified manner. This is achieved by describing the energy flow within a structural component on a space- and time-averaged basis, neglecting near-field effects. As a result of these simplifications, the model is unable to provide a detailed description

of the energy distribution within a structure, but can provide a good indication of the general pattern and level of energy flow through it. This feature was particularly well illustrated using the multiple transmission path structure described in Chapter 6.

The computational efficiency of the approach stems from the second-order differential form of the simplified equations which have been used to describe the energy flow. In contrast to traditional modal solutions which take the form of a summation of frequency dependent modal contributions, the differential form of the energy flow expression is dependent on a single frequency term. If the behaviour of the structure at a particular frequency is required, the analysis incurs the same level of computational effort as that associated with "static" analysis, rather than that normally required for traditional "dynamic" techniques.

An important issue connected with the use of the energy flow approach is its range of application with respect to frequency. SEA has traditionally been limited to use at very high frequencies due to the difficulty in satisfying its rather rigorous assumptions in the lower frequency range. On the other hand traditional FEA, like all modal analysis techniques, is limited to the lower frequency range because of the need to model the structure using a fine mesh if many modes are involved. Although approximate, the energy flow approach is able to predict the general level of energy flow within a structure at low frequencies and, at higher frequencies the complexity of the calculation does not increase. This type of analysis therefore, has the potential to bridge the frequency gap between the more traditional analysis techniques.

In any modelling exercise the key to creating a realistic model of a structure is to provide representative values of the modelling parameters. This has been of primary concern throughout the course of this project and, where possible, a large proportion of these parameters have been obtained by experimental measurement. Within the SEA environment this part of the procedure is often considered the most difficult, mainly because the analysis is aimed at high frequencies where the measurement of the modelling parameters becomes difficult. The same difficulties also apply in the case of the energy flow approach, although during this project the task of parameter

estimation was made easier because the analyses were carried out over relatively low frequency ranges where reliable measurement techniques do exist.

At the outset of this project very little information existed concerning the quality of the predictions which could be obtained using the energy flow approach, particularly in relation to its application to real structures. Some example analyses did exist, but were provided only for very high frequency cases, where the approximations made in developing the approach have least impact on the quality of the results. During the course of this project it has been shown that the predictions obtained using the energy flow approach at lower frequencies are of a similar quality to those normally associated with SEA. It must be remembered however, that these predictions have been obtained at frequencies where SEA is considered very difficult to apply.

There are also some other features of this approach which can be considered as advantages over SEA. One of these is the way in which the model takes a form which is physically representative of the real structure, rather than an abstract assembly of sub-systems as used in SEA. This avoids the task of breaking down the structure into appropriate sub-systems which would be very difficult, for example in the case of the bulkhead structure studied here. Another feature of the approach is that it allows localised variation of the modelling parameters, like damping and power input, which cannot be accommodated in SEA.

9.3 Experimental work

Much of the experimental work undertaken during the course of this project was aimed at obtaining measurements of energy flow in real structures for validation of model results. This involved the use of existing frequency domain structural intensity approaches and the results of these measurements have been well documented in previous chapters.

Other phases of experimental work were carried out to obtain representative values for the parameters required by the model (eg. power input, damping, transmission efficiency and group velocity). During the course of these measurements two

techniques were used very effectively to provide an assessment of the wave transmission characteristics of real structures which might not have been so readily available through calculation.

In Chapter 5 the wave decomposition technique proposed by David-Taylor (1990) proved very successful in separating the leftward- and rightward-travelling flexural wave amplitudes in a beam. This enabled the effective transmission efficiency characteristic of a flanged joint to be obtained in a way which also took downstream effects into account. Following this work it was noted that with some adaptation the approach is also applicable to the analysis of longitudinal wave motion. This observation creates a potential for the application of this technique to the analysis of angled and branched one-dimensional structures which is an area where experimental evidence would be useful to validate a number of existing analytical solutions.

An example of a novel application of an existing technique appeared in Chapter 7. Here a wavenumber measurement technique originally proposed for simple plate structures was applied to the analysis of a section of ribbed bulkhead. These measurements were very effective in determining the directionality of the wave transmission characteristics of this rather complex structure and provided an indication of how these characteristics vary with frequency. This exercise showed that techniques developed for simple structures can be applied in more complicated situations providing the nature and level of the approximations involved are well understood. In many cases this type of approach is useful because more exact methods for the treatment of complicated structures do not yet exist.

9.4 Recent literature

The possibility of developing an approximate energy flow approach to bridge the gap between SEA and traditional FEA has attracted increasing attention over recent years. During the course of this project there has been a significant amount of new work carried out by other researchers in this area, much of which has already been summarised in Chapter 2.

Very recently however, two very important pieces of work have emerged which merit discussion before completion of this thesis. This is because they provide further insight into the interpretation of previous work and may also have a significant impact on the future development of techniques of this type.

Langley

The first piece of work is by Langley (1993), who has carried out an in-depth investigation into the fundamental validity and accuracy of the energy flow formulation for two-dimensional structures. Langley began his investigation by deriving the energy flow equation for a plate structure based on the assumption that its response can be described by a linear superposition of plane wave components. This represents a generalised form of the analysis presented by Bouthier (1992), outlined in section 3.5 of this thesis.

Having obtained the general solutions to this equation he showed that the energy flow approach does not properly describe the way in which vibrational energy flows through a plate. In particular, he highlighted the case of a damped point-excited plate where the energy flow solution predicts that far-field vibrational energy decays in proportion to $1/(r)^{1/2}$, where r is the radial distance from the point of excitation. This characteristic is in contradiction to the response profile given by an exact solution in which the energy level decays in proportion to $1/r$. As a result, the energy flow approach under-predicts the decay of vibrational energy away from the power input and can severely over-predict the level of energy density in the vicinity of the plate boundaries. It was pointed out that the latter could have a serious effect when modelling connected structures.

The effects of this were illustrated using an example based on a simply supported plate model with a damping factor of 0.3. Under these conditions there was clearly a significant difference between the energy density profiles provided by the energy flow analysis and those obtained by an exact modal calculation. It should be noted however, that such differences become less apparent in models possessing a much lower level of damping, which is more representative of that found in engineering

structures. Under these conditions there is very little appreciable decay in the response across the plate and the prediction provided by the energy flow approach represents a good average level of this response which is almost flat in nature.

Langley concluded that the response predictions provided by the energy flow approach do give a good estimate of the average energy density in the structure which, under certain conditions, may be in good agreement with exact results. The approach however, may not be robust under all conditions and some doubt must exist as to its general applicability to two-dimensional cases.

There is no doubt that this work raises important questions regarding the validity and applicability of the two-dimensional energy flow modelling expressions developed by Bouthier (1992). In particular, it shows that the problem stems from the use of the plane wave description of motion for a plate as the starting point of the analysis. The impact of the shortcomings identified by Langley will be dependent on the nature of the study being undertaken. Certainly, there is some doubt as to the accuracy of the approach when applied to the analysis of single well damped plate structures. As part of a global model however, with relatively low levels of damping these problems may not have such a dramatic effect, particularly when one considers the approximate nature of the overall approach.

For engineering purposes the suitability of the energy flow approach will be dependent on the type of information required from the model and the problem being considered. In the case of the modelling tool developed here, the use of the two-dimensional analysis developed by Bouthier (1992) could be considered as less than ideal because it does not properly deal with the "exact" form of the energy expressions governing plate structures. Alternatively the approach could be judged as adequate because of its ability to make predictions of the general level of energy flow in realistic structures with an accuracy that matches that of current measurement techniques.

Carcaterra and Sestieri

The second of these very recent studies was presented by Carcaterra and Sestieri (1993). In the quest for an approach to bridge the gap between SEA and FEA, they developed the theoretical basis for an approach which provides a space-averaged indication of the energy level along beam structures. The energy profile in this case is obtained through a quantity termed the "envelope energy".

This envelope energy is obtained using a smoothing function which incorporates the Hilbert transform. When this smoothing or "envelope" function is applied to the exact energy expressions describing flexure in a beam it provides a space-averaged trend of the energy level profile along it, similar in principle to that provided by the energy flow solution developed by Wohlever (1988). The important difference between this and Wohlever's approach however, is that Carcaterra and Sestieri were able to incorporate near-field terms within their energy flow solution.

The added complexity of retaining these near-field components in the envelope energy approach results in a fourth-order expression rather than the second-order relationship which forms the basis of the energy flow approach. This leads to some increase in mathematical complexity, although this is offset by improvements in the accuracy of the results close to discontinuities. An important feature of this envelope energy approach is that, like the energy flow approach, the dimension of the numerical problem is independent of frequency. The computational costs involved are therefore once again comparable with the "static" rather than the "dynamic" problem.

The characteristics of this novel approach were demonstrated by comparing energy level predictions along the length of simple beam models with those obtained using an "exact" modal solution and those provided by the energy flow approach. In regions away from discontinuities, the energy flow approach and the envelope energy approach provided identical results. Close to discontinuities however, the envelope energy solution gave a much better indication of the exact energy profile because it includes the near-field part of the exact solution.

There is little doubt that the envelope energy approach does provide a better indication of the level of vibrational energy along simple beam structures when compared to those obtained using the energy flow approach. This advantage is however, offset to some extent by an increase in mathematical complexity of the solution. Further potential advantages of this approach may become evident in the analysis of built up structures, where an improved estimate of the level of energy close to a joint will be of obvious benefit. This aspect, together with the application of the approach to plate structures, are current areas of research.

9.5 Further study

The use of approximate energy flow approaches to model discrete structural elements is still in a relatively early stage of development. Following its original proposal by Nefske and Sung over six years ago, there has been a rapid increase of interest in developing techniques of this type.

In the past three years research in this area has begun to move down a number of paths. Some studies, including this one, have concentrated on the application of the energy flow approach to provide a practical engineering tool. Others have taken a step back from these original formulations and considered the theoretical basis on which the approach is based. In some cases this has resulted in the proposal of improved approaches which are "less approximate" in nature. At this point in time it would be useful to make a careful assessment of the relative merits of various branches of the approach. In doing this one must not lose sight of the quest for a global modelling technique able to cope with one- and two-dimensional elements in a three-dimensional configuration. To achieve this it is inevitable that some degree of approximation will be necessary. An important aspect of future work should be an assessment of the level of approximation which can be tolerated from a practical point of view.

At present there is very little work linking the application of approximate energy flow analysis to other more established approaches like SEA and FEA. In future studies it will be important to include this type of comparison if the approach is to be shown

to be effective in bridging the gap between these more widely used techniques. It is also becoming apparent that examples of the application of the approach are not being provided in such a way that they can be compared with the results of alternative techniques. To do this one needs to adopt a non-dimensional frequency scale so that terms like "low, medium and high frequencies" become less ambiguous and comparisons can be made on a common basis. For this purpose a quantity like the "modal overlap factor" used widely in SEA would seem appropriate.

One of the major difficulties in developing a modelling approach is to decide on what basis one should judge its results. In the work carried out here, energy flow measurements obtained from real structures have been used successfully in lower frequency regions to provide a benchmark for comparison with model predictions. Having identified this energy flow modelling approach as one which is also very effective at higher frequencies, there is a need to establish measurement techniques which are better suited to the higher frequency ranges. The development of such techniques may be assisted by the increase in the use of laser-based measurement which promises better data acquisition capabilities.

An interesting area of study which stems directly from experimental work carried out here is the application of wave decomposition techniques to the analysis of jointed and branched framework structures. This would provide much needed validation of existing analytical models and supply a useful library of data for use with future energy flow modelling and SEA.

Finally, having studied energy flow in the ribbed bulkhead structure it is evident that there is a potential to obtain a considerable amount of insight into the characteristics of structures of this type through experimentation. A useful step in the further development of these experimental techniques would be to use a less complicated structure consisting of a section of plate reinforced in only one direction. This should allow clarification of some of the uncertainties which exist concerning the measured results presented within this work, which could be linked to localised features of the structure like the machinery mounting platform. Having established a firm basis for

these measurement approaches under controlled conditions, one would be in a good position to extend this work to the analysis of realistic engineering structures containing localised features which have the potential to disturb the pattern of energy flow.

9.6 Concluding remarks

This work set out to develop a general purpose analytical tool based on a simplified energy flow approach introduced originally by Nefske and Sung (1987). Considerable progress has been achieved during the period of this study and, although further research is still required, this work provides the framework for this modelling tool using an existing finite element technique.

A summary of the most important aspects of this work is as follows:

1. It provides a realistic assessment of the ability of the energy flow approach to predict the level of vibrational energy in a structural component under various conditions of damping and frequency.

2. It provides a significant contribution to current knowledge relating to the use of the simplified energy flow approach in relation to its ability to provide representative models of real structures, particularly in the area of parameter estimation.

3. It describes a technique which allows commercially available software to be used to implement the energy flow approach using finite elements.

4. It introduces the "joint finite element" for use with this approach which allows the partial reflection characteristics at structural connections to be represented within the energy flow model.

5. It illustrates the ability of the approach to provide an effective transmission path ranking tool for the analysis of multiple transmission path structures.

6. It describes the use of existing experimental techniques to estimate the wavenumber and energy flow characteristics of a marine bulkhead structure. This represents a good solution to the type of problem encountered in the real engineering environment.

In general, the approach developed here satisfies the requirements for the transmission path ranking tool laid down in Chapter 1. It provides a cost effective method for globally estimating the level of vibrational energy flow in a variety of structures which is not limited by frequency.

In order to carry out the analysis at low computational cost it was necessary to employ an energy flow formulation which describes the vibrational characteristics of the structure in a simplified manner. This means that the model is unable to provide a detailed description of response, but can provide a good estimate of the general pattern and level of energy flow within individual or assembled components.

The field of application of this modelling approach can be greatly increased through implementation by a finite element method. During the course of this work the use of existing finite element software has resulted in an enormous saving in the time required to develop a global modelling scheme. At the same time however, this has presented a problem in that only one primary variable is available for modelling purposes. This feature imposes constraints on the way in which the approach can be adapted to model some of the more complex wave transmission characteristics like the simultaneous transmission of two wave types. This problem was overcome to some extent for the case of straight beam assemblies, but will inevitably become an area of increasing difficulty when modelling general structures. In the light of these findings the development of a dedicated computational framework within which the different wave energy quantities can be represented independently is considered to be a worthwhile investment in order to increase the versatility of the approach for future development purposes.

In recent months some interesting work by Langley (1993) has identified shortcomings in the way in which the approach models energy flow in two-dimensional components. The impact of these shortcomings is likely to be dependent on the nature of the study being undertaken and the type of information required from the model. In order to realistically assess how these findings might affect future two-dimensional modelling using the energy flow approach further research is required to identify conditions under which the model provides an adequate representation of the energy flow characteristics of two-dimensional components when they form part of a complex structural assembly.

Although the concept of a global modelling scheme based on an approximate energy flow approach is still relatively new, there are already some good examples of the application of such techniques including those reported here. During the course of this work improvements to the formulations which form the basis of the analysis have been proposed elsewhere. These improved formulations provide a better indication of the variation of vibrational energy within individual components but it is still not known how well such approaches will lend themselves to the development of global modelling schemes.

In its current form, the modelling scheme described here might be considered as less than ideal because it is based on a simplified analysis which does not deal "properly" with near-field effects. It has also become evident that the use of existing finite element software may limit the versatility of the approach when dealing with the simultaneous transmission of more than one wave type. An alternative viewpoint is to judge the approach on its ability to make useful predictions for realistic structures with an accuracy which matches that of available measurement techniques. On this basis the work presented here shows considerable promise and it is believed that with some further detailed development the method has potential as a future engineering tool. It is also believed that continued work in this direction should lead to an optimised form of the energy flow approach which will be able to bridge the gap between SEA and traditional FEA.

References

Baker, J.R., Halliwell, N.A. and White, R.G., 1990
Proceedings of the International Congress on Intensity Techniques, Senlis, France, pp 167-172, "The application of laser technology to the measurement of structural intensity".

Belov, V.D., Rybak, S.A. and Tartakovski, B.D., 1977
Journal of Soviet Physics - Acoustics, vol 23, no 2, pp 115-118, "Propagation of vibrational energy in absorbing structures".

Bies, D.A. and Hamid, S.A., 1980
Journal of Sound and Vibration, vol 70, no 2, pp 187-204, "In-situ determination of loss factor and coupling loss factor by the power injection method".

Bishop, R.E.D. and Johnson, D.C., 1960
The mechanics of vibration, Cambridge University Press.

Bouthier, O.M., 1992
PhD Thesis, Purdue University, USA, "Energetics of vibrating systems".

Bouthier, O.M. and Bernhard, R.J., 1992
AIAA Journal, vol 30, no 3, pp 616-623, "Models of space-averaged energetics in plates".

Burrell, S.C., Warner, J.L. and Chernuka, M.W., 1990
ASME, Noise control and acoustics division (Publication), 90-WA/NCA-10, pp 1-7, "Power flow finite element analysis applied to a thin circular plate".

Buvailo, L.E. and Ionov, A.V., 1980
Journal of Soviet Physics - Acoustics, vol 26, no 4, pp 277-279, "Application of the finite element method to the investigation of the vibroacoustical characteristics of structures at high audio frequencies".

Carcaterra, A. and Sestieri, A., 1993
Proceedings of the 4th International Congress on Intensity Techniques, Senlis, France, pp 361-370, "An approximate power flow solution for one-dimensional dynamic structures".

Carrol, G.P. and Clark, J.A., 1989
Proceedings of the 8th IMAC Conference, USA, pp 958-964, "Power flow measurements on beams with small localized damping".

Cho, P.E. and Bernhard, R.J., 1990
ASME, Noise control and acoustics division (Publication), 90-WA/NCA-9, pp 1-4, "The energy finite element method for rod models".

Cho, P.E. and Bernhard, R.J., 1992
Proceedings of Inter-noise 92, Toronto, Canada, pp 487-491, " Coupling of continuous beam models".

Clarkson, B.L. and Pope, R.J., 1981
Journal of Sound and Vibration, vol 77, no 4, pp 535-549, "Experimental determination of modal densities and loss factors of flat plates and cylinders".

Clarkson, B.L. and Ranky, M.F., 1984
Journal of Sound and Vibration, vol 94, no 2, pp 249-261, "On the measurement of the coupling loss factor of structural connections".

Cremer, L., Heckl, M. and Ungar, E., 1973
Structure-borne sound, Berlin, Springer.

David-Taylor, P., 1990
Proceedings of the International Congress on Intensity Techniques, Senlis, France, pp 249-256, "Measurement of structural intensity, reflection coefficient and termination impedance for bending waves in beams".

De Clerk, J.P., Van Karsen, C., Evensen, H.A. and Rao, M., 1991
Proceedings of the 10th IMAC Conference, San Diego , USA, pp 841-844, "Using power flow to determine a frequency dependent loss factor".

Fahy, F.J. and Lindqvist, E., 1976
Journal of Sound and Vibration, vol 45, no 1, pp 115-138, "Wave propagation in damped, stiffened structures characteristic of ship construction".

Fahy, F.J., 1985
Sound and structural vibration, Academic press, London.

Garvic, L., Carniel, X. and Pavic, G., 1990a
Proceedings of the International Congress on Intensity Techniques, Senlis, France, pp 223-230, "Structure-borne intensity fields in plates, beams and plate-beam assemblies".

Garvic, L. and Pavic, G., 1990b
Proceedings of the International Congress on Intensity Techniques, Senlis, France, pp 207-213, "Computation of structural intensity in beam-plate structures by numerical modal analysis using FEM".

Ghering, W.L. and Raj, D., 1987
ASME, Noise control and acoustics division (Publication), NCA v3, pp 81-90, "Comparison of statistical energy analysis predictions with experimental results for cylinder-plate-beam structures".

Goyder, H. and White, R.G., 1980
Journal of Sound and Vibration, vol 68, no 1, pp 59-75, "Vibrational power flow from machines into built up structures, Part I: Introduction and approximate analysis of beam and plate-like foundations".

Hambric, S.A., 1990
Transactions of ASME Journal of vibration and acoustics, vol 112, pp 542-549, "Power flow and mechanical intensity calculations in structural finite element analysis".

Hayek, S.I., Pechersky, M.J. and Suen, B.C., 1990
Proceedings of the International Congress on Intensity Techniques, Senlis, France, pp 281-288, "Measurement and analysis of near- and far-field structural intensity by scanning laser vibrometry".

Horner, J.L. and White, R.G., 1990
International Journal of Mechanical Science, vol 32, no 3, pp 215-233, "Prediction of vibrational power transmission through jointed beams".

Langley, R.S., 1990
Journal of Sound and Vibration, vol 141, no 2, pp 207-219, "A derivation of the coupling loss factors used in statistical energy analysis".

Langley, R.S., 1993
Private communication.

Lase, Y. and Jezequel, L., 1990
Proceedings of the International Congress on Intensity Techniques, Senlis, France, pp 145-150, "Analysis of dynamic systems based on a new energetic formulation".

Linjama, J. and Lahti, T., 1989
Valtion Teknillinen Tutkimuskeskus, Tutkimuksia, n 583, 54 pages, "Measurement of bending wave power flow by the structural intensity technique".

Lyon, R.H., 1975
Statistical energy analysis of dynamical systems: theory and applications. Cambridge, Mass; MIT Press.

Meyer, B., Balannec, T.B., Sans, P. and Thomasson, D., 1990
Proceedings of the International Congress on Intensity Techniques, Senlis, France, pp 299-306, "Structural intensity in plates: formulation and experimental results".

Nefske, D.J. and Sung, S.H., 1987
Proceedings of the Winter Annual Meeting of ASME, Boston, USA, pp 277-279, "Power flow finite element analysis of dynamic systems: basic theory and application to beams".

Nikiforov, A.S., 1975
Sudostroieniye: Russian Academie of Science, "Vibration isolation in ship structures", (in Russian).

Nikiforov, A.S., 1990
Proceedings of the International Congress on Intensity Techniques, Senlis, France, pp 53-56, "Estimating the intensity of structure-borne noise in ribbed structures".

Nilsson, A.C., 1976
Journal of Sound and Vibration, vol 44, no 3, pp 393-405, "Wave propagation in simple hull-frame structures".

Noiseux, D.U., 1970
Journal of the Acoustical Society of America, vol 4, no 1, part 2, pp 238-247, "Measurement of power flow in uniform beams and plates".

Norton, M.P. and Greenhalgh, R., 1986
Journal of Sound and Vibration, vol 105, no 3, pp 397-423, "On the estimation of loss factors in lightly damped pipeline systems: some measurement techniques and their limitations".

Pavic, G., 1976
Journal of Sound and Vibration, vol 49, no 2, pp 221-230, "Measurement of structure borne wave intensity Part 1: Formulation of methods".

Pinnington, R.J.,and White, R.G, 1981
Journal of Sound and Vibration, vol 75, no 2, pp 179-197, "Power flow through machine isolators to resonant and non-resonant beams"

Pinnington, R.J., Redman-White, W. and Brown, K.T., 1981
Proceedings of the International Congress on recent developments in acoustic intensity measurement, Senlis, France, pp 229-236, "Methods for structural power transmission measurement".

Redman-White, W., 1984
Proceedings of the Second International Conference on Recent Advances in Structural Dynamics, Southampton, U.K, pp 1-7, "The experimental measurement of flexural wave power flow in structures".

Rockwood, W.B., Lu, L.K.H., Warner, P.C. and Dejong, R.G., 1987
ASME, Noise control and acoustics division (Publication), NCA v3, pp 73-79, "Statistical energy analysis applied to structure borne noise in marine structures".

Sato, K. and Honda, I., 1988
Proceedings of Inter-noise 88, pp 591-594, "Application of vibrational power measurement to the piping system in an air-conditioner".

Timoshenko, S. and Young, D.H., 1955
Vibration problems in engineering, New York, Van Nostrand.

Troshin, A.G., Popkov, V.I. and Popov, A.V., 1990
Proceedings of the International Congress on Intensity Techniques, Senlis, France, pp 265-272, "The measurement of vibrational power flux in rod structures".

Verheij, J.W., 1980
Journal of Sound and Vibration, vol 70, no 1, pp 133-139, "Cross spectral density methods for measuring structure borne power flow in beams and pipes".

Verheij, J.W., 1993a
Proceedings of the 4th International Congress on Intensity Techniques, Senlis, France, pp 415-422, "Using structural energy flow measurements to study sound transmission through a propeller shaft-bearing structure to underwater".

Verheij, J.W., Hopmans, L.J.M. and van Tol, F.H., 1993b
Proceedings of the 4th International Congress on Intensity Techniques, Senlis, France, pp 423-430, "Shipboard measurements of structural intensity on a rotating shaft and its use for sound path quantification".

Wagstaff, P.R., Bouzem, B. and Henrio, J.C., 1990
Proceedings of the International Congress on Intensity Techniques, Senlis, France, pp 257-264, "Optimisation of structural intensity measurements for lightly damped structures".

Wohlever, J.C, 1988
Masters Thesis, Purdue University, USA, "Vibrational power flow analysis of rods and beams".

Wohlever, J.C, Bernhard, R.J. and Bouthier, O.M, 1990
Proceedings of the International Congress on Intensity Techniques, Senlis, France, pp 37-44, "Energy and structural intensity formulations of beam and plate vibrations".

Wohlever, J.C and Bernhard, R.J., 1992
Journal of Sound and Vibration, vol 153, no 1, pp 1-19, "Mechanical energy flow models of rods and beams".

Zhao, Q., 1987
Proceedings of Inter-noise 87, Bejing, China, pp 1283-1286, "On the accuracy of bending wave power measurements in beams"

Appendix A

Modal response solution for a simply supported beam

The general equation of motion governing the forced vibration of a uniform beam, neglecting the effects of shear and rotary inertia, is:

$$\rho S \frac{\partial^2 w}{\partial t^2} + EI \frac{\partial^4 w}{\partial x^4} = F(x,t) \tag{A1}$$

where,

ρ = mass density

S = cross-sectional area

E = Young's modulus

I = second moment of area

The forcing term $F(x,t)$ can be expressed in the form:

$$F(x,t) = p(x) f(t) \tag{A2}$$

and for a continuous system, the displacement response $w(x,t)$ can be expressed as:

$$w(x,t) = \sum_r \phi_r(x)\, q_r(t) \tag{A3}$$

where $\phi_r(x)$ is a mode shape function of the r^{th} mode for a uniform beam, of the general form:

$$\begin{aligned} \phi_r(x) = {} & C_1 \sin \lambda_r x + C_2 \cos \lambda_r x \\ & + C_3 \sinh \lambda_r x + C_4 \cosh \lambda_r x \end{aligned} \tag{A4}$$

and

$$\lambda_r^4 = \frac{\rho S}{EI}\,\omega_r^2$$

The coefficients C_1, C_2, C_3 and C_4 are dependent on boundary conditions.

Substituting equations (A2) and (A3) into (A1) and carrying out the differentiation gives:

$$\rho S \sum_r \phi_r(x)\,\ddot{q}_r(t) + EI \sum_r \frac{d^4\phi_r(x)}{dx^4}\,q_r(t) = p(x)f(t) \tag{A5}$$

Pre-multiplying (A4) by another mode shape function $\phi_s(x)$ and integrating over the length of the beam gives:

$$\sum_r \left(\rho S \int_0^L \phi_s(x)\,\phi_r(x)\,dx\right)\ddot{q}_r(t) + \sum_r \left(EI \int_0^L \phi_s(x)\,\frac{d^4\phi_r}{dx^4}\,dx\right) q_r(t) = f(t)\int_0^L \phi_s(x)\,p(x)\,dx \tag{A6}$$

where L is the length of the beam.

It can be shown that mode shape functions are orthogonal, which means that:

$$\int_0^L \phi_s(x)\,\phi_r(x)\,dx = 0 \qquad \text{for } r \neq s \tag{A7}$$

It can also be shown that:

$$\frac{d^4\phi_r(x)}{dx^4} = \lambda_r^4\,\phi_r(x) \tag{A8}$$

Substituting these relationships into (A6) gives:

$$\sum_r \left(\rho S \int_0^L \phi_r^2(x)\,dx \right) \ddot{q}_r(t) + \sum_r \left(EI\lambda_r^4 \int_0^L \phi_r^2(x)\,dx \right) q_r(t) = f(t) \int_0^L \phi_r(x)\, p(x)\,dx \tag{A9}$$

Damping can be introduced into the beam model by replacing E by the complex modulus $E(1+i\eta)$, where η is the hysteretic damping factor.

For free vibration, the forcing term is zero and it can be shown that:

$$\ddot{q}_r(t) = -\omega_r^2 q(t) \tag{A10}$$

Applying the free vibration condition to one term of the summation (A9) and including the damping term gives:

$$-\omega_r^2 \rho S \int_0^L \phi_r^2(x)\,dx + E(1+i\eta) I \lambda_r^4 \int_0^L \phi_r^2\,dx = 0 \tag{A11}$$

or,

$$EI\lambda_r^4 \int_0^L \phi_r^2(x)\,dx = \frac{\omega_r^2}{(1+i\eta)} \rho S \int_0^L \phi_r^2(x)\,dx \tag{A12}$$

Substituting (A12) into (A9) gives:

$$\left(\rho S \int_0^L \phi_r^2(x)\,dx\right) \ddot{q}_r(t) + \frac{\omega_r^2}{(1+i\eta)} \left(\rho S \int_0^L \phi_r^2\,dx\right) q_r(t) = f(t) \int_0^L \phi_r(x)\, p(x)\,dx \tag{A13}$$

Rearranging gives:

$$\ddot{q}_r(t) + \frac{\omega_r^2}{(1+i\eta)}\, q_r(t) = \frac{\int_0^L \phi_r(x)\, p(x)\,dx}{\rho S \int_0^L \phi_r^2(x)\,dx}\, f(t) \tag{A14}$$

or

$$\ddot{q}_r(t) + \frac{\omega_r^2}{(1+i\eta)}\, q_r(t) = P_r\, f(t) \tag{A15}$$

For single frequency sinusoidal excitation:

$$f(t) = e^{i\omega t} \tag{A16}$$

and $q_r(t)$ will be of the form:

$$q_r(t) = Q_r^*\, e^{i\omega t} \tag{A17}$$

where Q^*_r is complex due to the presence of damping.

Using the (A16) and (A17), (A15) becomes:

$$-\omega^2 Q_r^* + \frac{\omega_r^2}{(1+i\eta)}\, Q_r^* = P_r \tag{A18}$$

which on rearrangement becomes:

$$Q_r^* = P_r \left(\frac{\omega_r^2 - \omega^2(1+\eta^2) + i\,\eta\,\omega_r^2}{(\omega_r^2-\omega^2)^2 + \eta^2\omega^4} \right) \tag{A19}$$

or

$$Q_r^* = P_r\, Z_r^* \tag{A20}$$

where

$$Z_r^* = \frac{\omega_r^2 - \omega^2(1+\eta^2) + i\,\eta\,\omega_r^2}{(\omega_r^2-\omega^2)^2 + \eta^2\omega^4} \tag{A21}$$

Equations (A14) and (A15) define P_r as:

$$P_r = \frac{\int_0^L \phi_r(x)\, p(x)\, \mathrm{d}x}{\rho S \int_0^L \phi_r^2(x)\, \mathrm{d}x} \tag{A22}$$

For a simply supported beam:

$$\phi_r(x) = \sin\left(\frac{r\pi x}{L}\right) \tag{A23}$$

which means that:

$$\int_0^L \phi_r^2(x)\, \mathrm{d}x = \frac{L}{2} \qquad \text{for all } r \tag{A24}$$

For point excitation of magnitude F applied at coordinate $x = a$:

$$\int_0^L \phi_r(x)\, p(x)\, \mathrm{d}x = \phi(a)\, F \tag{A25}$$

Substituting (A24) and (A25) into (A22) gives:

$$P_r = \frac{2\phi_r(a)F}{\rho SL} \tag{A26}$$

Thus, combining (A17), (A20) and (A26) gives:

$$q_r(t) = \frac{2\phi_r(a)F}{\rho SL} Z_r^* e^{i\omega t} \tag{A27}$$

which, when substituted into (A3) gives:

$$w(x,t) = \left(\frac{2F}{\rho SL} \sum_r \phi_r(x)\phi_r(a) Z_r^* \right) e^{i\omega t} \tag{A28}$$

For the sinusoidal quantity above, the rms value of displacement is given by:

$$w(x)_{rms} = \frac{1}{\sqrt{2}} \left| \frac{2F}{\rho SL} \sum_r \phi_r(a)\phi_r(x) Z_r^* \right| \tag{A29}$$

where $\phi_r(x)$ and Z^*_r are given by equations (A23) and (A21) respectively.

Appendix B

Energy flow solution for a connected beam model

The aim of this analysis is to provide an energy flow solution to describe the transmission of vibrational energy through a structure consisting of two beams connected by a joint having a transmission efficiency τ. The form of the energy flow model representing this structure is shown in Fig.B1.

It was shown in Chapter 4 that the general solution for the energy density profile along each beam is given by:

$$e = A_m \cosh(\alpha_m x) + B_m \sinh(\alpha_m x) \tag{B1}$$

where

$$\alpha_m = \frac{\omega \eta_m}{2c_{bm}} \tag{B2}$$

Here m = 1, 2 and refers to beams 1 and 2 respectively.

The boundary conditions in this problem relate to the power flux, q, at the ends of each beam, given by:

$$q = - \frac{4c_{bm}^2}{\eta_m \omega} \frac{de}{dx} \tag{B3}$$

Combining equations (B1) and (B3) and applying the boundary conditions shown in Fig.B1, results in the following relationships:

For beam 1, the condition that $q = P_i/S_1$ at $x = -L_1$ gives:

$$A_1 \sinh(-\alpha_1 L_1) + B_1 \cosh(-\alpha_1 L_1) = -\frac{P_i \eta_1 \omega}{4c_{b1}^2 \alpha_1 S_1} \tag{B4}$$

and if $q = q_1$ at $x = 0$:

$$q_1 + \frac{4c_{b1}^2 \alpha_1}{\eta_1 \omega} B_1 = 0 \tag{B5}$$

Similarly for section 2, $q = q_2$ at $x = 0$ gives:

$$q_2 + \frac{4c_{b2}^2 \alpha_2}{\eta_2 \omega} B_2 = 0 \tag{B6}$$

and if $q = 0$ at $x = L_2$:

$$A_2 \sinh(\alpha_2 L_2) + B_2 \cosh(\alpha_2 L_2) = 0 \tag{B7}$$

The remaining boundary conditions are related to the transmission characteristics of the connection. In this analysis the boundary condition will be expressed so that either the Nefske and Sung expression (5.2.6), or the improved relationship (5.2.19), can be included in the model by using the appropriate substitution for Γ. Noting that for flexural motion in a beam $c_g = 2c_{b2}$, the power flux leaving beam 1 is:

$$q_1 = \frac{p_{joint}}{S_1} = \Gamma \left\{ c_{b1} e_1 - \frac{c_{b2} S_2}{S_1} e_2 \right\} \tag{B8}$$

and similarly, the flux entering beam 2 is given by:

$$q_2 = \frac{p_{joint}}{S_2} = \Gamma \left\{ \frac{c_{b\,1}\, S_1}{S_2}\, e_1 - c_{b\,2}\, e_2 \right\} \tag{B9}$$

where

$$\Gamma = 2\,\tau \tag{B10}$$

when implementing the Nefske and Sung boundary condition (5.2.6), or

$$\Gamma = \frac{\tau}{(1-\tau)} \tag{B11}$$

when implementing the improved boundary condition (5.2.19).

Using (B8) and (B9) at $x = 0$ gives:

$$-\Gamma c_{b\,1}\, A_1 + \Gamma c_{b\,2} \frac{S_2}{S_1}\, A_2 + q_1 = 0 \tag{B12}$$

and

$$-\Gamma c_{b\,1} \frac{S_1}{S_2}\, A_1 + \Gamma c_{b\,2}\, A_2 + q_2 = 0 \tag{B13}$$

Assembling equations (B4), (B5), (B6), (B7), (B12) and (B13) to form a matrix equation gives:

$$[M]\begin{Bmatrix} A_1 \\ B_1 \\ A_2 \\ B_2 \\ q_1 \\ q_2 \end{Bmatrix} = \begin{Bmatrix} -\dfrac{P_i\eta_1\omega}{4c_{b\,1}^2\alpha_1 S_1} \\ 0 \\ 0 \\ 0 \\ 0 \\ 0 \end{Bmatrix} \qquad \text{(B14)}$$

where [M] is a 6 x 6 matrix of the form:

$$\begin{bmatrix} \sinh(-\alpha_1 L_1) & \cosh(-\alpha_1 L_1) & 0 & 0 & 0 & 0 \\ 0 & \dfrac{4c_{b\,1}^2\alpha_1}{\eta_1\omega} & 0 & 0 & 1 & 0 \\ 0 & 0 & 0 & \dfrac{4c_{b\,2}^2\alpha_2}{\eta_2\omega} & 0 & 1 \\ 0 & 0 & \sinh(\alpha_2 L_2) & \cosh(\alpha_2 L_2) & 0 & 0 \\ -\Gamma c_{b\,1} & 0 & \dfrac{\Gamma c_{b\,2} S_2}{S_1} & 0 & 1 & 0 \\ -\dfrac{\Gamma c_{b\,1} S_1}{S_2} & 0 & \Gamma c_{b\,2} & 0 & 0 & 1 \end{bmatrix}$$

Solving this matrix equation provides values for the unknown parameters A_1, B_1, A_2 and B_2. Substituting these values into equation (B1) provides the energy density profiles along each beam in the structure.

Combining equations (B1) and (B3) and noting that the vibrational power at any point in the structure is given by:

$$p_m(x) = q_m S_m \tag{B15}$$

gives:

$$p(x) = - \frac{4c_{b\,m}^2 S_m \alpha_m}{\eta_m \omega} \{ A_m \sinh(\alpha_m x) + B_m \cosh(\alpha_m x) \} \tag{B16}$$

which on substitution of A_1, B_1, A_2 and B_2, provides power profiles along each beam in the structure.

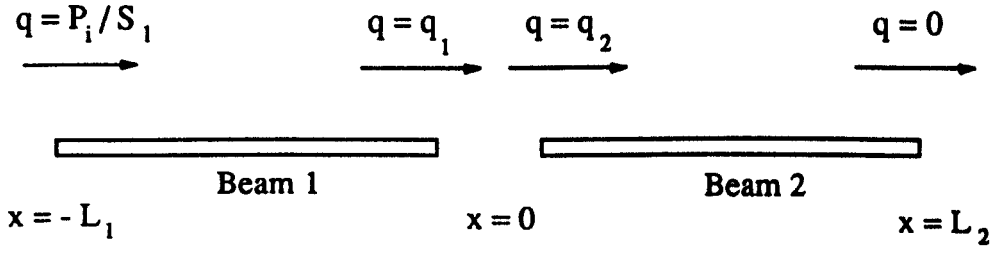

Fig.B1 Connected beam energy flow model

Appendix C

Energy flow model for the real connected beam structure

The energy flow model for the real connected beam structure described in section 5.3 is shown in Fig.C1. The energy flow solution for this model is identical to the one presented in Appendix B, except in relation to the boundary condition applied at the end of beam 2. In this case, Fig.C1 shows that when $x = L_2$, $q = p_o/S_2$. Applying this condition to the expression for the vibrational power profile along a beam yields:

$$A_2 \sinh(\alpha_2 L_2) + B_2 \cosh(\alpha_2 L_2) = - \frac{p_o \eta_2 \omega}{4 c_{b\,2}^2 \alpha_2 S_2} \qquad \text{(C1)}$$

Substituting this expression into the matrix solution given in Appendix B and using expression (5.3.19) to provide the boundary condition at the joint gives:

$$[M] \begin{Bmatrix} A_1 \\ B_1 \\ A_2 \\ B_2 \\ q_1 \\ q_2 \end{Bmatrix} = \begin{Bmatrix} - \dfrac{P_i \eta_1 \omega}{4 c_{b\,1}^2 \alpha_1 S_1} \\ 0 \\ 0 \\ - \dfrac{p_o \eta_2 \omega}{4 c_{b\,2}^2 \alpha_2 S_2} \\ 0 \\ 0 \end{Bmatrix} \qquad \text{(C2)}$$

where [M] is a 6 x 6 matrix of the form:

$$\begin{bmatrix} \sinh(-\alpha_1 L_1) & \cosh(-\alpha_1 L_1) & 0 & 0 & 0 & 0 \\ 0 & \dfrac{4c_{b1}^2\alpha_1}{\eta_1\omega} & 0 & 0 & 1 & 0 \\ 0 & 0 & 0 & \dfrac{4c_{b2}^2\alpha_2}{\eta_2\omega} & 0 & 1 \\ 0 & 0 & \sinh(\alpha_2 L_2) & \cosh(\alpha_2 L_2) & 0 & 0 \\ -\dfrac{\tau c_{b1}}{(1-\tau)} & 0 & \dfrac{\tau c_{b2} S_2}{(1-\tau)S_1} & 0 & 1 & 0 \\ -\dfrac{\tau c_{b1} S_1}{(1-\tau)S_2} & 0 & \dfrac{\tau c_{b2}}{(1-\tau)} & 0 & 0 & 1 \end{bmatrix}$$

Solution of this matrix equation provides the unknowns A_1, B_1, A_2 and B_2, which can be used to calculate the energy density and power profiles along the beam using the approach described in Appendix B.

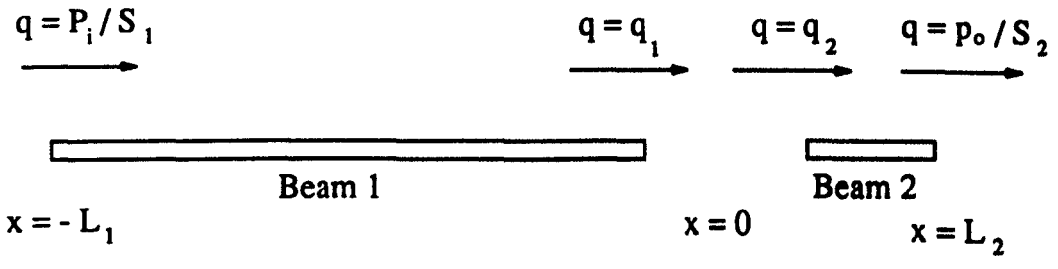

Fig.C1 Energy flow model for the real connected beam structure

Appendix D

The wave decomposition approach

The wave decomposition technique was introduced by David-Taylor (1990) as a means to determine the amplitudes of near- and far-field flexural wave components in a beam from measurements made using accelerometer arrays. The analysis presented here is limited only to the determination of the far-field wave components which can be used to calculate the reflection coefficient at a discontinuity.

Consider the beam shown in Fig.D1, terminated at x = 0 with a sinusoidal force input at x = - L. For harmonic flexural motion the acceleration at distance x_m from the termination can be expressed in terms of wave amplitude variables:

$$\ddot{u}_m = Ae^{-ikx_m} + Be^{ikx_m} + Ce^{-kx_m} + De^{kx_m} \qquad \text{(D1)}$$

where A and B are the leftward and rightward far-field travelling wave amplitudes, and C and D are the near-field wave amplitudes associated with the discontinuities. k is the bending wavenumber for the beam.

At points which are sufficiently far from the discontinuities for the near-field components to become negligible, (D1) reduces to:

$$\ddot{u}_m = Ae^{-ikx_m} + Be^{ikx_m} \qquad \text{(D2)}$$

In the frequency domain, the auto-spectrum of a Fourier transformed acceleration signal is defined as:

$$X_{mm} = (\ddot{u}_m \cdot \ddot{u}_m^*) \qquad \text{(D3)}$$

where the * indicates a complex conjugate quantity.

The cross-spectrum between two signals is defined as:

$$X_{mn} = (\ddot{u}_m \cdot \ddot{u}_n^*) \tag{D4}$$

which, being a complex quantity can be expressed in the form:

$$X_{mn} = C_{mn} + i\, Q_{mn} \tag{D5}$$

Using expressions (D2) and (D3), the auto-spectrum at position x_1 is given by:

$$X_{11} = (Ae^{-ikx_1} + Be^{ikx_1}) (Ae^{-ikx_1} + Be^{ikx_1})^* \tag{D6}$$

and by employing the following trigonometric identities:

$$\begin{aligned} e^{i\theta} &= \cos\theta + i \sin\theta \\ \cos(-\theta) &= \cos\theta \\ \sin(-\theta) &= -\sin\theta \end{aligned} \tag{D7}$$

equation (D6) reduces to:

$$\begin{aligned} X_{11} = AA^* + BB^* + BA^* \{ \cos(2kx_1) + i \sin(2kx_1) \} \\ + AB^* \{ \cos(2kx_1) - i \sin(2kx_1) \} \end{aligned} \tag{D8}$$

Using equations (D3) and (D5), it follows that:

$$AA^* = X_{AA} \tag{D9}$$

$$BB^* = X_{BB} \tag{D10}$$

and

$$AB^* = C_{AB} + i\, Q_{AB} \tag{D11}$$

It can also be shown that:

$$(BA^*) = (AB^*)^* \tag{D12}$$

Using (D9) to (D12) above, (D8) can be re-written as:

$$X_{11} = X_{AA} + X_{BB} + \{ 2 \cos (2kx_1) \} C_{AB} + \{ 2 \sin (2kx_1) \} Q_{AB} \quad \text{(D13)}$$

Similarly, the auto-spectrum at position x_2 is given by:

$$X_{22} = X_{AA} + X_{BB} + \{ 2 \cos (2kx_2) \} C_{AB} + \{ 2 \sin (2kx_2) \} Q_{AB} \quad \text{(D14)}$$

The same type of analysis can be used to determine the cross-spectrum between accelerations at x = x_1 and x = x_2. Using expressions (D2) and (D4),

$$X_{12} = (Ae^{-ikx_1} + Be^{ikx_1}) (Ae^{-ikx_2} + Be^{ikx_2})^* \quad \text{(D15)}$$

Employing the identities (D7) once again, and noting that:

$$\begin{aligned} \cos\theta \cos\phi \pm \sin\theta \sin\phi &= \cos (\theta \mp \phi) \\ \sin\theta \cos\phi \pm \cos\theta \sin\phi &= \sin (\theta \pm \phi) \end{aligned} \quad \text{(D16)}$$

equation (D15) reduces to:

$$\begin{aligned} X_{12} = {} & X_{AA} \{ \cos k(x_1-x_2) - i \sin k(x_1-x_2) \} \\ & + X_{BB} \{ \cos k(x_1-x_2) + i \sin k(x_1-x_2) \} \\ & + 2 C_{AB} \cos k(x_1+x_2) + 2 Q_{AB} \sin k(x_1+x_2) \end{aligned} \quad \text{(D17)}$$

Using expression (D5), (D17) can be separated into real and imaginary parts:

$$\begin{aligned} C_{12} = {} & \{ \cos k(x_1-x_2) \} X_{AA} + \{ \cos k(x_1-x_2) \} X_{BB} \\ & + \{ 2 \cos k(x_1+x_2) \} C_{AB} + \{ 2 \sin k(x_1+x_2) \} Q_{AB} \end{aligned} \quad \text{(D18)}$$

and

$$Q_{12} = \{ - \sin k(x_1-x_2) \} X_{AA} + \{ \sin k(x_1-x_2) \} X_{BB} \quad \text{(D19)}$$

Combining equations (D13), (D14), (D18) and (D19) in matrix form, the spectral components measured at two points on the beam can be expressed in terms of spectral combinations of the far-field wave amplitudes, ie.

$$[\,M\,] \begin{Bmatrix} X_{AA} \\ X_{BB} \\ C_{AB} \\ Q_{AB} \end{Bmatrix} = \begin{Bmatrix} X_{11} \\ X_{22} \\ C_{12} \\ Q_{12} \end{Bmatrix} \qquad \text{(D20)}$$

where $[M]$ is a 4 x 4 transfer function matrix of the form:

$$\begin{bmatrix} 1 & 1 & 2\cos(2kx_1) & 2\sin(2kx_1) \\ 1 & 1 & 2\cos(2kx_2) & 2\sin(2kx_2) \\ \cos k(x_1-x_2) & \cos k(x_1-x_2) & 2\cos k(x_1+x_2) & 2\sin k(x_1+x_2) \\ -\sin k(x_1-x_2) & \sin k(x_1-x_2) & 0 & 0 \end{bmatrix}$$

Structural intensity

Noiseux (1970) showed that the far-field structural intensity for a beam in flexure can be obtained from:

$$p = 2\,\mathrm{Re}\,\{X_{\Omega M}\} \qquad \text{(D21)}$$

where $X_{\Omega M}$ represents the cross-spectrum of angular velocity and bending moment.

Euler bending theory shows that:

$$\Omega = \frac{\partial \dot{u}}{\partial x} \tag{D22}$$

and

$$\frac{\partial M}{\partial t} = - EI \frac{\partial \Omega}{\partial x} \tag{D23}$$

Substituting (D22) into (D23) and transferring into the frequency domain, the bending moment can be expressed as:

$$M = - \frac{EI}{i\,\omega} \frac{\partial^2 \dot{u}}{\partial x^2} \tag{D24}$$

Now the transverse velocity at a point in the beam obtained by integrating (D2) is:

$$\dot{u}_m = \frac{1}{i\,\omega} \left(A e^{-ikx_m} + B e^{ikx_m} \right) \tag{D25}$$

Differentiating (D25) with respect to x and substituting into equation (D22) and (D24) respectively, gives:

$$\Omega = - \frac{k}{\omega} \left(A e^{-ikx_m} + B e^{ikx_m} \right) \tag{D26}$$

and

$$M = - \frac{EIk^2}{\omega^2} \left(A e^{-ikx_m} + B e^{ikx_m} \right) \tag{D27}$$

Substituting (D26) and (D27) into (D21) and employing (D7), (D9) and (D10), gives:

$$p = 2\ \mathrm{Re} \left\{ \frac{EIk^3}{\omega^3} \left(X_{AA} - X_{BB} \right) \right\} \tag{D28}$$

and since auto-spectra are always real quantities, the far-field structural intensity for a beam in flexure can be obtained from:

$$p = \frac{2EIk^3}{\omega^3} \left(X_{AA} - X_{BB} \right) \qquad \text{(D29)}$$

Reflection coefficient

For the case of the connected beam structure described in Chapter 5 the reflection coefficient, r, at the structural discontinuity is of primary interest. This quantity is defined as:

$$r = \frac{\text{reflected wave amplitude}}{\text{incident wave amplitude}} = \frac{B}{A} \qquad \text{(D30)}$$

It follows that:

$$| r | = \left| \frac{B}{A} \right| = \left(\frac{BB^*}{AA^*} \right)^{\frac{1}{2}} = \left(\frac{X_{BB}}{X_{AA}} \right)^{\frac{1}{2}} \qquad \text{(D31)}$$

Thus, having obtained the decomposed wave spectra it is also possible to determine the magnitude of the reflection coefficient at the discontinuity.

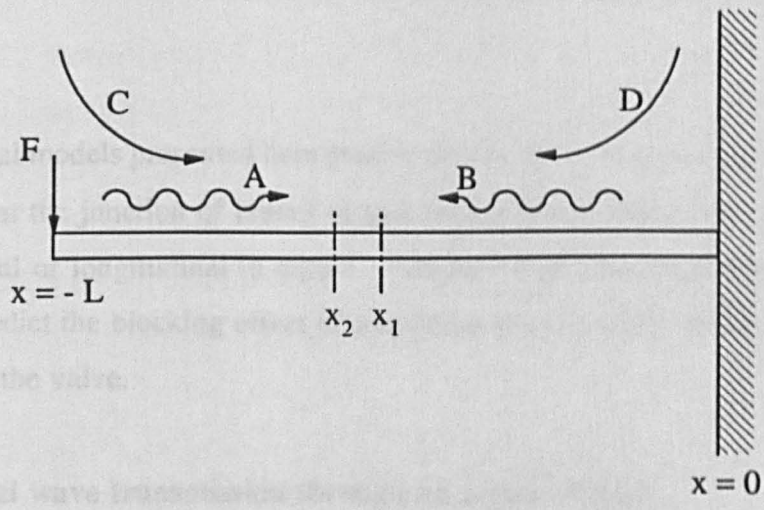

Fig.D1 Terminated beam model showing wave amplitude components

Appendix E

Wave transmission through joints in beams

To use the energy flow approach to create a global model of the multiple transmission path structure described in Chapter 6, it is first necessary to determine the individual wave transmission characteristics of each joint in isolation from the rest of the structure.

The analytical models presented here predict the necessary transmission and reflection efficiencies at the junction of branched and angled beams when the incident wave is either flexural or longitudinal in nature. Adaptation of this analysis also provides a model to predict the blocking effect of a cylindrical mass which is used in Chapter 6 to represent the valve.

E1. Flexural wave transmission through an angled T-joint

Consider the joint between three beams arranged at arbitrary angles as shown in Fig.E1. If a flexural wave having amplitude A_1 is incident at the joint, because of the angled nature of the beams this wave will be scattered into both flexural and longitudinal wave components in each of the three beam sections. In this situation the motion of each beam can be expressed in terms of the wave amplitude variables relating to it, ie:

Beam 1

$$\begin{aligned} w_1(x,t) &= \left(A_1 e^{-ik_f x} + C_1 e^{ik_f x} + D_1 e^{k_f x} \right) e^{i\omega t} \\ u_1(x,t) &= L_1 e^{ik_L x}\, e^{i\omega t} \end{aligned} \qquad \text{(E1.1)}$$

Beam 2

$$w_2(x,t) = \left(C_2 e^{-ik_f\Psi} + D_2 e^{-k_f\Psi} \right) e^{i\omega t}$$
$$u_2(x,t) = L_2 e^{-ik_L\Psi}\, e^{i\omega t} \qquad \text{(E1.2)}$$

Beam 3

$$w_3(x,t) = \left(C_3 e^{-ik_f\Theta} + D_3 e^{-k_f\Theta} \right) e^{i\omega t}$$
$$u_3(x,t) = L_3 e^{-ik_L\Theta}\, e^{i\omega t} \qquad \text{(E1.3)}$$

where A and C represent the amplitudes of propagating far-field flexural waves, D the amplitude of decaying near-field waves and L the amplitude of longitudinal waves. The suffices f and L refer to flexural and longitudinal motion respectively.

Assuming that the joint can be represented by a rigid cylinder, the equilibrium and continuity conditions relating to it are as follows:

Force equilibrium

$$-F_1 + F_2\cos\theta - V_2\sin\theta + F_3\cos\psi + V_3\sin\psi = m_j\ddot{u}_j \qquad \text{(E1.4)}$$

$$-V_1 + V_2\cos\theta + V_3\cos\psi + F_2\sin\theta - F_3\sin\psi = m_j\ddot{w}_j \qquad \text{(E1.5)}$$

Moment equilibrium

$$-M_1 + M_2 + M_3 + \frac{L}{2}\left(V_1 + V_2 + V_3 \right) = I_j\ddot{\phi}_j \qquad \text{(E1.6)}$$

Slope continuity

$$\frac{\partial w_1}{\partial x} = \frac{\partial w_2}{\partial \Psi} \qquad \text{(E1.7)}$$

$$\frac{\partial w_1}{\partial x} = \frac{\partial w_3}{\partial \Theta} \qquad \text{(E1.8)}$$

Displacement continuity

$$u_1 = u_2\cos\theta - w_2\sin\theta + \frac{L}{2}\frac{\partial w_2}{\partial \Psi}\sin\theta \qquad \text{(E1.9)}$$

$$w_1 = u_2\sin\theta + w_2\cos\theta - \frac{L}{2}(1+\cos\theta)\frac{\partial w_2}{\partial \Psi} \qquad \text{(E1.10)}$$

$$u_1 = u_3\cos\psi + w_3\sin\psi - \frac{L}{2}\frac{\partial w_3}{\partial \Theta}\sin\psi \qquad \text{(E1.11)}$$

$$w_1 = -u_3\sin\psi + w_3\cos\psi - \frac{L}{2}(1+\cos\psi)\frac{\partial w_3}{\partial \Theta} \qquad \text{(E1.12)}$$

m_j is the joint mass is given by:

$$m_j = \frac{\rho_j \pi L^2 W}{4} \qquad \text{(E1.13)}$$

where L represents the length of the joint and W represents its width, see Fig.E1. It follows that I_j, the moment of inertia of the joint, is given by:

$$I_j = \frac{m_j L^2}{8} \qquad \text{(E1.14)}$$

The displacement expressions (E1.1), (E1.2) and (E1.3) can be related to axial force, shear force and bending moment using Euler beam theory, which shows that:

$$F = EA\frac{\partial u}{\partial x} \qquad M = EI\frac{\partial^2 w}{\partial x^2} \qquad V = -EI\frac{\partial^3 w}{\partial x^3} \qquad \text{(E1.15)}$$

Using the displacement expressions (E1.1) to (E1.3) and the relationships given in (E1.15) above, the continuity and equilibrium conditions (E1.4) to (E1.12) can be re-written in terms of the wave amplitude variables. These equations can be assembled into a 9 x 9 matrix equation of the form:

$$[\,M\,]\{x\}_f = \{y\}_f \qquad \text{(E1.16)}$$

Assuming that the beams have identical cross-sectional dimensions and material properties, the non-zero members of matrix [M] are as follows:

$$M_{11} = k_f \qquad M_{13} = ik_f$$

$$M_{15} = k_f \qquad M_{16} = ik_f$$

$$M_{21} = k_f \qquad M_{22} = k_f$$

$$M_{23} = ik_f \qquad M_{24} = ik_f$$

$$M_{31} = EIk_f^3 + m_j\omega^2\left(1+\frac{Lk_f}{2}\right) \qquad M_{32} = EIk_f^3\cos\theta$$

$$M_{33} = m_j\omega^2 + i\left(\frac{m_j\omega^2 Lk_f}{2} - EIk_f^3\right) \qquad M_{34} = -\,i\,EIk_f^3\cos\theta$$

$$M_{35} = EIk_f^3\cos\psi \qquad M_{36} = -\,i\,EIk_f^3\cos\psi$$

$$M_{37} = i\,ESk_L\sin\psi \qquad M_{38} = -\,i\,ESk_L\sin\theta$$

$$M_{42} = \sin\theta\left(1+\frac{Lk_f}{2}\right) \qquad M_{44} = \sin\theta\left(1 + i\,\frac{Lk_f}{2}\right)$$

$$M_{48} = -\cos\theta \qquad M_{49} = 1$$

$$M_{51} = 1 \qquad M_{53} = 1$$

$$M_{55} = -\cos\psi - \frac{Lk_f}{2}(1+\cos\psi) \qquad M_{56} = -\cos\psi - i\,\frac{Lk_f}{2}(1+\cos\psi)$$

$$M_{57} = \sin\psi \qquad M_{61} = I_j\omega^2 k_f - EIk_f^2\left(1+\frac{Lk_f}{2}\right)$$

$$M_{62} = EIk_f^2\left(1+\frac{Lk_f}{2}\right) \qquad M_{63} = EIk_f^2 + i\left(\frac{EILk_f^3}{2} + I_j\omega^2 k_f\right)$$

$$M_{64} = -\,EIk_f^2\left(1 + i\,\frac{Lk_f}{2}\right) \qquad M_{65} = EIk_f^2\left(1+\frac{Lk_f}{2}\right)$$

$$M_{66} = -\,EIk_f^2\left(1 + i\,\frac{Lk_f}{2}\right) \qquad M_{75} = -\sin\psi\left(1+\frac{Lk_f}{2}\right)$$

$$M_{76} = -\sin\psi\left(1 + i\,\frac{Lk_f}{2}\right) \qquad M_{77} = -\cos\psi$$

$$M_{79} = 1 \qquad M_{81} = 1$$

$$M_{82} = -\cos\theta - \frac{Lk_f}{2}(1+\cos\theta) \qquad M_{83} = 1$$

$$M_{84} = -\cos\theta - i\frac{Lk_f}{2}(1+\cos\theta) \qquad M_{88} = -\sin\theta$$

$$M_{92} = -EIk_f^3\sin\theta \qquad M_{94} = iEIk_f^3\sin\theta$$

$$M_{95} = EIk_f^3\sin\psi \qquad M_{96} = -iEIk_f^3\sin\psi$$

$$M_{97} = -iESk_L\cos\psi \qquad M_{98} = -iESk_L\cos\theta$$

$$M_{99} = m_j\omega^2 - iESk_L$$

The values in column vector $\{x\}_f$, which represent the ratio of scattered wave amplitudes to the incident wave amplitude, are:

$$x_1 = \frac{D_1}{A_1} \quad x_2 = \frac{D_2}{A_1} \quad x_3 = \frac{C_1}{A_1} \quad x_4 = \frac{C_2}{A_1} \quad x_5 = \frac{D_3}{A_1}$$

$$x_6 = \frac{C_3}{A_1} \quad x_7 = \frac{L_3}{A_1} \quad x_8 = \frac{L_2}{A_1} \quad x_9 = \frac{L_1}{A_1}$$

and the non-zero terms of column vector $\{y\}_f$ are:

$$y_1 = ik_f \qquad y_2 = ik_f$$

$$y_3 = -m_j\omega^2 + i\left(\frac{m_j\omega^2Lk_f}{2} - EIk_f^3\right) \qquad y_5 = -1$$

$$y_6 = -EIk_f^2 + i\left(I_j\omega^2k_f + \frac{EILk_f^3}{2}\right) \qquad y_8 = -1$$

Transmission and reflection efficiencies are related to the power transmitted through the beam sections.

Flexural power can be obtained from:

$$p_f = EI\omega k_f^3 \ |A|^2 \tag{E1.16}$$

and longitudinal power is given by:

$$p_L = \frac{1}{2} ES\omega k_L \ |L|^2 \tag{E1.17}$$

where A and L represent amplitudes of the propagating flexural and axial waves respectively.

At this point it is necessary to define a convention to distinguish between various forms of transmission and reflection efficiencies. Each term will have two suffices. The first refers to the incident wave type and the second to the resultant wave type after transmission or reflection. As an example τ_{fl} represents the transmission efficiency of longitudinal motion resulting from an incident flexural wave at the joint.

Since the reflection efficiency is the ratio of reflected to incident wave power:

$$\beta_{ff} = | x_3 |^2 \tag{E1.18}$$

and using (E1.16) and (E1.17):

$$\beta_{fl} = \left\{ \frac{Sk_L}{2Ik_f^3} \right\} | x_9 |^2 \tag{E1.19}$$

Similarly transmission efficiency is the ratio of transmitted to incident wave power, hence for beam 2:

$$\tau_{ff} = | x_4 |^2 \qquad \tau_{fl} = \left\{ \frac{Sk_L}{2Ik_f^3} \right\} | x_8 |^2 \tag{E1.20}$$

and for beam 3:

$$\tau_{ff} = |x_6|^2 \qquad \tau_{fl} = \left\{ \frac{Sk_L}{2Ik_f^3} \right\} |x_7|^2 \tag{E1.21}$$

E2. Longitudinal wave transmission through an angled T-joint

Fig.E2 shows an identical joint to the one considered in section E1, except that the incident wave is now of a longitudinal nature having an amplitude L_0. The expressions for the motion of beam 1 are now of the form:

$$\begin{aligned} w_1(x,t) &= \left(C_1 e^{ik_f x} + D_1 e^{k_f x} \right) e^{i\omega t} \\ u_1(x,t) &= \left(L_0 e^{-ik_L x} + L_1 e^{ik_L x} \right) e^{i\omega t} \end{aligned} \tag{E2.1}$$

The remainder of the analysis is identical to the previous case and the expressions for the motion of beams 2 and 3 remain unchanged, as do the equilibrium and continuity equations (E1.4) to (E1.12).

The final 9 x 9 matrix solution can be expressed as:

$$[M] \{ x \}_L = \{ y \}_L \tag{E2.2}$$

where the matrix $[M]$ is identical to the one obtained for the case of an incident flexural wave.

In this case the terms in the column vector $\{x\}_L$ are:

$$x_1 = \frac{D_1}{L_0} \quad x_2 = \frac{D_2}{L_0} \quad x_3 = \frac{C_1}{L_0} \quad x_4 = \frac{C_2}{L_0} \quad x_5 = \frac{D_3}{L_0}$$

$$x_6 = \frac{C_3}{L_0} \quad x_7 = \frac{L_3}{L_0} \quad x_8 = \frac{L_2}{L_0} \quad x_9 = \frac{L_1}{L_0}$$

and the non-zero terms in $\{y\}_L$ are:

$$y_4 = -1 \quad y_7 = -1 \quad y_9 = -m_j\omega^2 - i\,EAk_L$$

Using the expressions for the power transmitted in the beams, (E1.16) and (E1.17), the reflection efficiencies in beam 1 are:

$$\beta_{ll} = |x_9|^2 \qquad \beta_{lf} = \left\{\frac{2Ik_f^3}{Sk_L}\right\} |x_4|^2 \tag{E2.3}$$

Similarly the transmission efficiencies in beam 2 are:

$$\tau_{ll} = |x_8|^2 \qquad \tau_{lf} = \left\{\frac{2Ik_f^3}{Sk_L}\right\} |x_4|^2 \tag{E2.4}$$

and for beam 3:

$$\tau_{ll} = |x_7|^2 \qquad \tau_{fl} = \left\{\frac{2Ik_f^3}{Sk_L}\right\} |x_6|^2 \tag{E2.5}$$

E3. Wave transmission through an angled joint

Analytical models which provide transmission and reflection efficiency values for angled joints in beams can be extracted from the more general solutions for the T-joints described in sections E1 and E2.

For the case of the angled joint between two beams shown in Figs.E3 and E4, with either flexural or longitudinal incident wave motion, the analytical model takes the form of a 6 x 6 matrix equation of the form:

$$[M]\{x\} = \{y\} \tag{E3.1}$$

The members of the 6 x 6 matrix $[M]$ can be obtained by removing rows 1, 5 and 7 and columns 5, 6 and 7 from the 9 x 9 matrix derived in section E1. The corresponding rows must also be removed from the column vectors $\{x\}$ and $\{y\}$.

E4. Wave transmission across the valve

For the purposes of the energy flow model described in Chapter 6 the valve is represented by a rigid cylinder with its polar axis in line with that of the beams, see Fig.E5. The analysis for this joint is however, almost identical to that for the angled joints described in section E3. The only differences are that the angle θ is always 0° and the expressions for the mass and moment of inertia of the joint must be replaced by:

$$m_j = \frac{\rho_j \pi W^2 L}{4} \tag{E4.1}$$

and

$$I_j = m_j \left(\frac{W^2}{16} + \frac{L^2}{12} \right) \tag{E4.2}$$

to take account of the orientation of the cylinder.

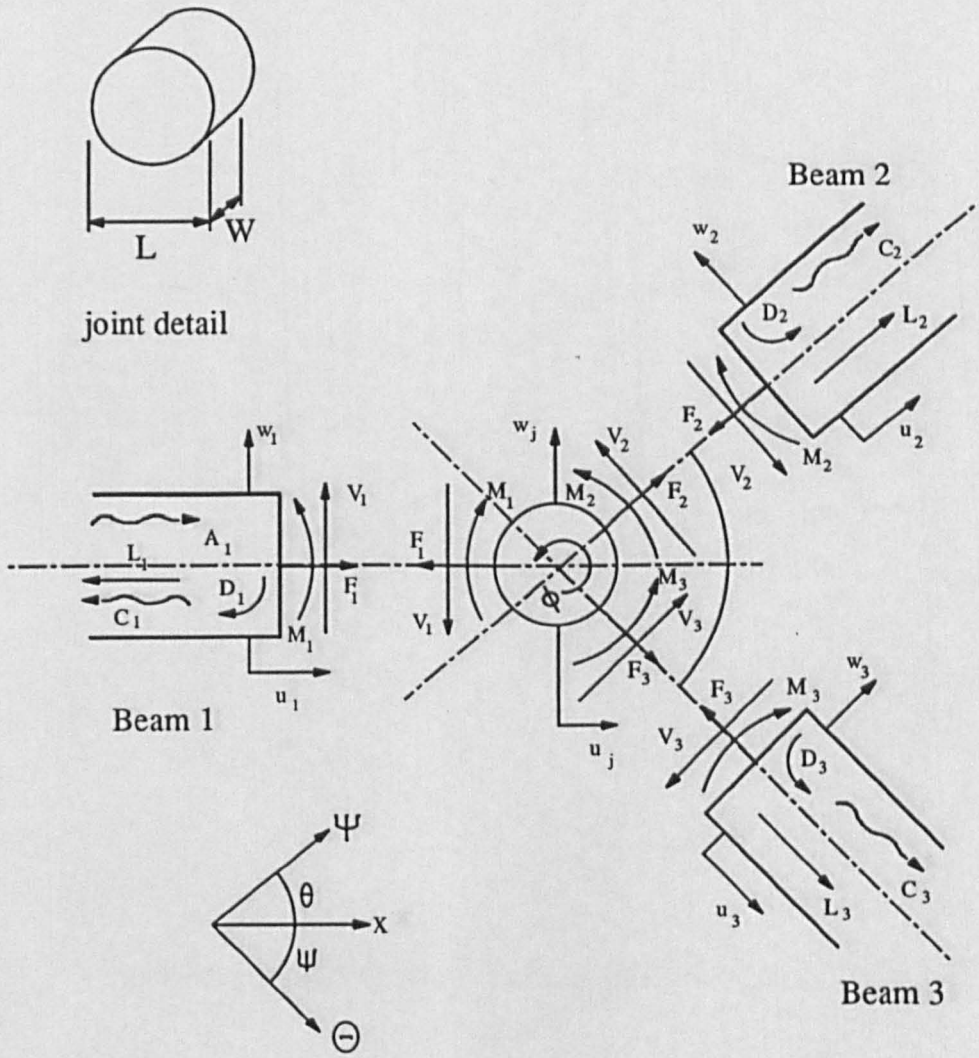

Fig.E1 Angled T-joint with incident flexural wave A_1

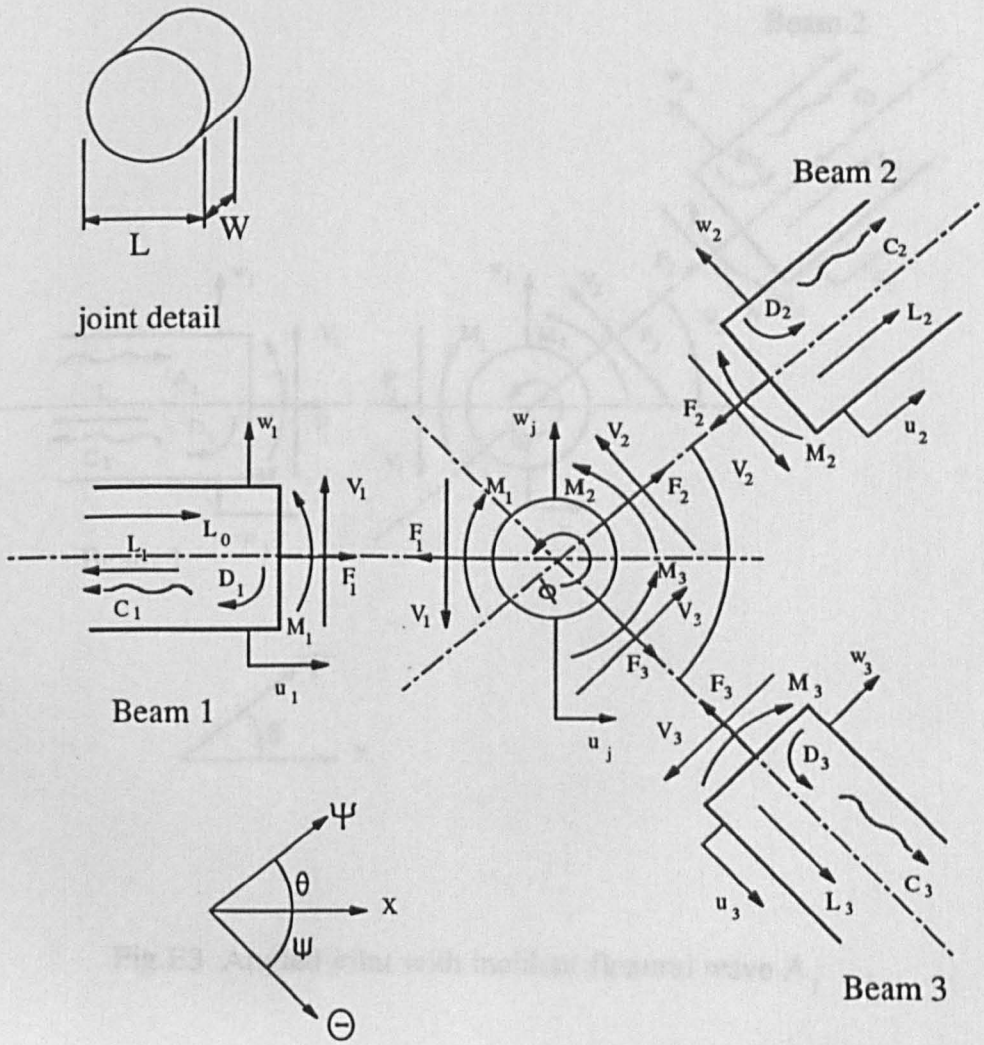

Fig.E2 Angled T-joint with incident longitudinal wave L_0

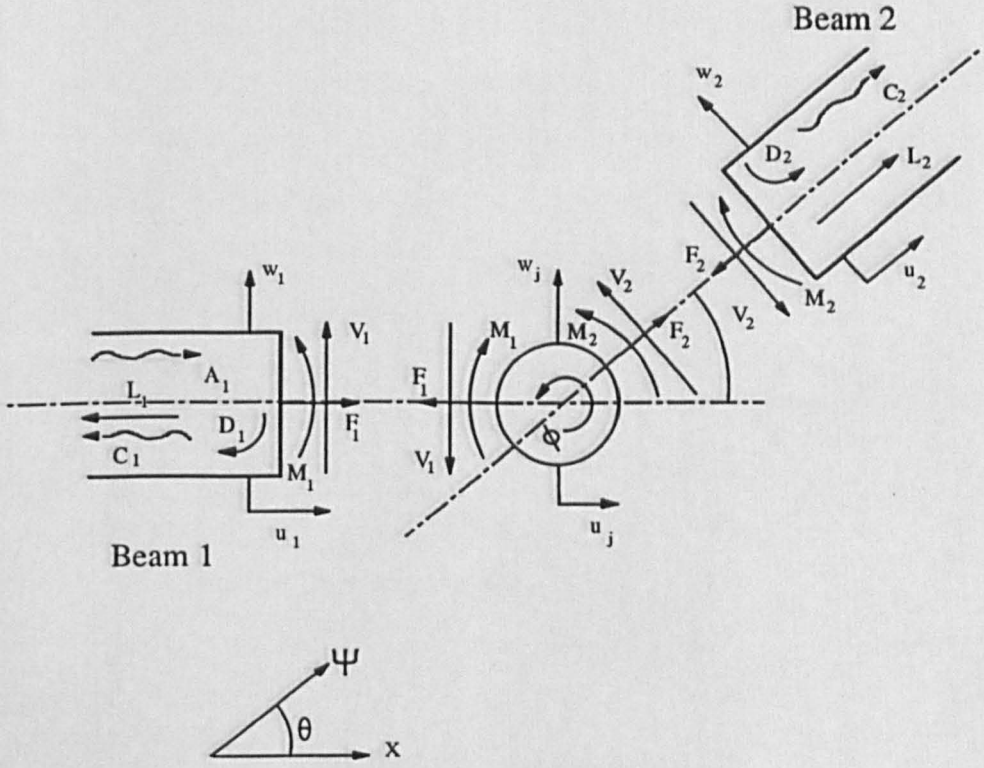

Fig.E3 Angled joint with incident flexural wave A_1

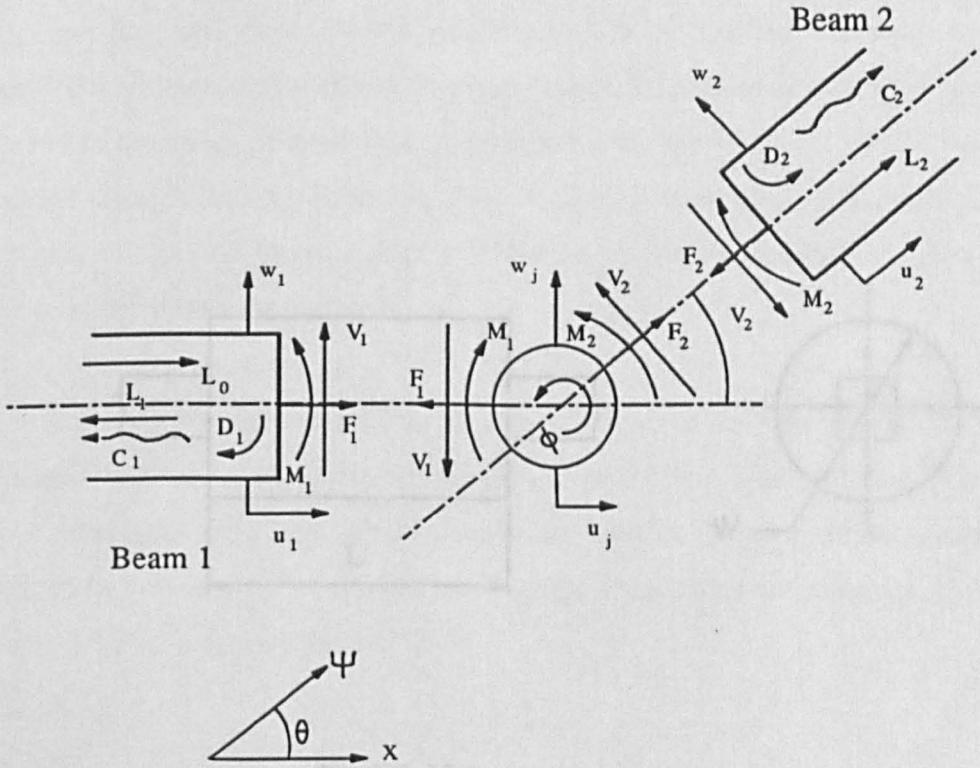

Fig.E4 Angled joint with incident longitudinal wave L_0

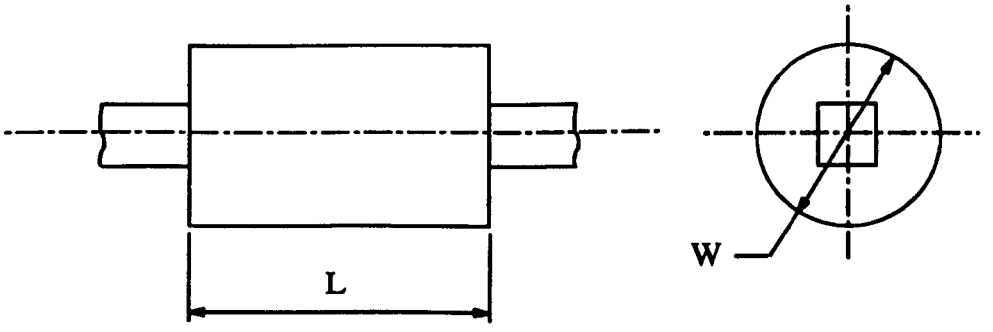

Fig.E5 Valve representation

Appendix F

Windowing effects on modal analysis results

When carrying out experimental modal analysis it is often necessary to apply exponential windowing to impact response data in order to avoid leakage error. This process has the effect of appearing to introduce extra damping into the system which is carried through into the modal analysis results. The purpose of this analysis is to show how modal loss factor values obtained under these conditions can be adjusted to account for windowing effects.

The modal analysis package used to provide estimates of the loss factors for the steel and aluminium beams described in Chapter 5 relies on a single degree of freedom curve fitting approach. The effect of the windowing on the analysis can therefore be examined by considering the response of a single degree of freedom system to impulse excitation. This response is given by:

$$y(t) = A \exp\left(-\gamma\omega_r t\right) \sin\left(\omega_r \sqrt{1-\gamma^2}\, t\right) \qquad \text{(F1)}$$

where ω_r is the undamped natural frequency of the system and γ is the damping ratio.

The exponential window function applied by the FFT analyzer is of the form:

$$W(t) = \exp\left(-\frac{t}{T}\right) \qquad \text{(F2)}$$

where T is the time constant defined by the operator.

When the window is applied to the response data the resulting captured response is of the form:

$$y'(t) = A \exp\left(-\gamma\omega_n t - \frac{t}{T}\right) \sin\left(\omega_n \sqrt{1-\gamma^2}\, t\right) \tag{F3}$$

and the apparent system damping is:

$$\left(\gamma\omega_n + \frac{1}{T}\right) \tag{F4}$$

If damping is low, the loss factor, η, is related to the damping ratio, γ, by:

$$\eta = 2\gamma \tag{F5}$$

Hence, the relationship between measured and actual loss factors is:

$$\frac{\eta_{actual}}{2}\omega_r + \frac{1}{T} = \frac{\eta_{meas}}{2}\omega_r \tag{F6}$$

or rearranging:

$$\eta_{actual} = \eta_{meas} - \frac{2}{T\,\omega_r} \tag{F7}$$

This expression can be used to correct the damping loss factor values obtained by the modal analysis to remove the artificial effects of the windowing.